GEOTILL Inc.

Geotechnical Engineering • Subsurface Exploration • Environmental Services • Construction Testing and Material Engineering

GEOTECHNICAL ENGINEERING LIBRARY

GEOTILL

USA

GEOTILL

ENGINEERING, INC.

Phone 317-449-0033 Fax 317- 285-0609

info@geotill.com

Toll Free: 844-GEOTILL

Geotechnical, Environmental and Construction Materials Testing Professionals

www.geotill.com

Offices Covering all USA

School of Civil and Environmental Engineering

Penetrometers for Soil Permeability and Chemical Detection

Susan E. Burns, PhD, P.E.

Paul W. Mayne, PhD, P.E.

National Science Foundation and
U.S. Army Research Office

July 1998

Georgia Institute of Technology

Penetrometers for Soil Permeability and Chemical Detection

prepared by

Susan E. Burns, PhD, P.E.

and

Paul W. Mayne, PhD, P.E.

Geosystems Engineering Group
School of Civil and Environmental Engineering
Georgia Institute of Technology
Atlanta, Georgia 30332-0355

Funding provided by
National Science Foundation
Arlington, Virginia

Army Research Office
Raleigh, North Carolina

July 1998

Penetrometers for Soil Permeability and Chemical Detection

By Susan E. Burns and Paul W. Mayne

Funding provided by NSF and ARO
Issued by Georgia Institute of Technology
Report No. GIT-CEEGEO-98-1, July 1998

Executive Summary

Cone penetration soundings are an expedient and efficient means of geoenvironmental site characterization for delineating site stratigraphy. Standard piezocone penetrometers provide continuous measurements of point resistance (q_c), sleeve friction (f_s), and shoulder porewater pressures (u_b). Several specialized penetrometers are available with additional sensor capabilities, notably the seismic cone outfitted with a velocity geophone to allow downhole measurements of shear wave velocity (V_s) with depth.

The importance of soil permeability (k) is recognized as a commonly-sought parameter in the varied disciplines of water resources, environmental sciences, geotechnical engineering, groundwater systems, and waste management. Permeability is a fundamental characteristic parameter reflecting the ease through which fluids flow through porous media. The permeability (or hydraulic conductivity) relates directly to the coefficient of consolidation (c_h) and constrained modulus ($D=1/m_v$). An analytical solution is presented for interpreting the coefficient of consolidation from piezocone dissipation tests in clayey and silty soils, based on principles of cavity expansion theory and critical-state soil mechanics. This solution accommodates the routine monotonic decay of porewater pressures with time associated with soft to firm to stiff silts and clays, as well as the noted dilatory responses (increase then decrease with time) observed in overconsolidated fissured materials.

A new integrated optics (IO) chemical sensor is introduced for realtime assessments of subsurface pore fluid chemistry. This sensor is compact, economical, reversible, and based on the principles of wave-interference patterns to distinguish fluid types. It is novel in that it is essentially "tuneable" to a wide variety of different chemistries. In trial laboratory tests, the BTEX (benzene-related) group of fuel contaminants was assessed in small-scale chamber tests of quartzitic sand.

ACKNOWLEDGEMENTS

The authors extend their gratitude to Dr. Priscilla P. Nelson who served as the program director for the Geomechanical, Geotechnical, and Geoenvironmental Engineering Division at the National Science Foundation (NSF) that provided the primary funding support for these efforts. In particular, the NSF program permitted the opportunities to develop field testing skills related to cone, piezocone, and seismic cone penetration sounding, as well as the academic freedom to conduct both analytical and numerical evaluations of the piezocone dissipation problem.

Additional funds for research were allocated by a separate source within NSF and by the US Army Research Office (ARO). An NSF Traineeship in Sensors Development in the Chemistry Department at Georgia Tech was issued from a program administered by Prof. Rick Browner at Georgia Tech. A small technology transfer research (STTR) program was funded by ARO specifically for the work on the integrated opto-electronic (IO) chemical sensor. This aspect of the research program involved an interdisciplinary team comprised of Nile Hartman, Dan Campbell, and Jim Suggs of the Electro0Optics, Environment, and Materials Laboratory (EOEML) within the Georgia Tech Research Institute (GTRI), John Edwards of Photonics Sensor Systems (PSS), and Dr. Guangxuan Zhu and Mark Prytula of the Daniel Environmental Laboratory at Georgia Tech.

During these studies, guidance and technical committees assisted the first author, Dr. Susan E. Burns on her residency as both a graduate research assistant and graduate teaching assistant. The committees consisted of Dr. Paul W. Mayne, Dr. Patricia M. Dove, Dr. J. David Frost, Dr. Glenn J. Rix, and Dr. J. Carlos Santamarina. Technical assistance on certain aspects of the work were provided by Ken Thomas and Seth Scott in the Geosystems Laboratory at Georgia Tech. Additional help was given by several graduate students including Dr. Barry Shiyo Chen and Dr. Yasser A. Hegazy.

Appreciation is also due to several individuals who assisted our research program over the past several years. Dr. Jean-Lou Chameau (currently Dean of the GT College of Engineering) provided the funds to purchase our first seismic cone penetrometer. Equipment donations were provided by Tom Nolan and Jay Auxt of Hogentogler & Company, Columbia, Maryland. Partners from industry also aided in securing outside funding and actual field experiences for testing and operation of the seismic piezocone equipment, including: Dr. Stevan Vidic of AGRA Earth & Environmental, Phoenix; Danny Brahana of Law/Gibb Group, Atlanta; Kevin McLain of the Missouri DOT; and Mike Palmer of Law Engineering, Houston.

TABLE OF CONTENTS

Executive Summary i
Acknowledgements ii
Table of Contents iii
List of Symbols vi
Mathcad Symbols Used viii

CHAPTER 1 INTRODUCTION

Cone Penetration Testing 1
Tip Resistance and Sleeve Friction Measurements 3
Porewater Pressure Measurements 3
Sensor Technology for Geoenvironmental Site Investigation 7
Geotechnical Sensor Technology 7
Inclinometer 8
Resistivity 8
Vibratory Module 8
Accelerometer/Geophone 8
Neutron/Gamma Radiation 9
Lateral Stress 9
Acoustic Emissions 9
Pressuremeter Module 9
Time Domain Reflectometry 9
Video Cone 10
Environmental Sensor Technology 10
Resistivity 10
pH 10
Redox Potential 10
Temperature 10
Dielectric Constant 10
Site Characterization and Analysis Penetrometer System (SCAPS) 11
Gamma Radiation 11
Integrated Opto-Electronic Sensors 12
Sampling Technology 12
BAT Enviroprobe 12
Hydropunch 12
Envirocone® 12
Cone Sipper™ 13
Summary of Cone Sensor and Sampling Technology 13
Maintaining Integrity in the Sampling of Contaminated Fluids 16
Chemical Compatibility 16
Filter and Sampling Materials 17
Filters Used in Cone Penetration Testing 19
Summary of Chemical Compatibility Issues During Sampling 20
Experiments and Modeling in Geoenvironmental Cone Penetration Testing 20

CHAPTER 2 LITERATURE REVIEW

Introduction 22
Evaluation of the Coefficient of Consolidation From Piezocone Dissipation Data....22
Generation of Excess Porewater Pressures 22
Pore Pressure Dissipation Behavior 24
Radial versus Vertical Drainage 27
Type 1 versus Type 2 Dissipation 27
Existing Soil Models For Pore Pressure Dissipation 28
Dissipation in Normally- and Lightly-Overconsolidated Clays 29
Dissipation in Heavily-Overconsolidated Clays 40
Chronological Development of Pore Pressure Dissipation Modeling 42
Summary 42
Evaluation of Soil Permeability 44
Coefficient of Permeability 44
Influence of Soil Parameters 45
Measurement of the Permeability of Soils 45
Laboratory Measurement of Permeability 45
Field Measurement of Permeability 46
Piezocone Testing Evaluation of Permeability 47
Summary 51

CHAPTER 3 INTEGRATED OPTO-ELECTRONIC CHEMICAL SENSOR FOR BTEX DETECTION IN CONE PENETRATION TESTING

Introduction 53
Sensor Operation 53
Sensor Housing 55
Fluid Sampling System 55
Geochemical Behavior of the BTEX Chemicals 57
Laboratory Testing Program 57
Experimental Results 61
Discussion 66
Conclusions 67

CHAPTER 4 PIEZOCONE MODEL FOR EVALUATING THE COEFFICIENT OF CONSOLIDATION IN SOFT TO HARD CLAYS

Introduction 68
Components of Porewater Pressure 68
Shoulder Position Dissipation Model 69
Normal-Induced Pore Pressures From Cavity Expansion Theory 69
Shear-Induced Pore Pressures From Modified Cam Clay 73
Derivation of the Analytical Solution to the Consolidation Equation 74
Model Parameters 79
Evaluated Results From Test Sites 82
Reference Values of the Coefficient of Consolidation 82
Dissipation Sites 83

Soft Clay Sites 84
Stiff Clay Sites 88
Error Surfaces for Model Parameters 93
Comparison With Existing Solutions 99
Normalized Dissipation Data 99
Discussion 104
Conclusions 104

CHAPTER 5 INTERPRETATION OF SEISMIC PIEZOCONE RESULTS FOR THE EVALUATION OF SOIL PERMEABILITY IN CLAYS

Introduction 106
Seismic Cone Penetration Test 106
V_s-q_T Relationships in Soils 110
Geotechnical Estimation of Mass Density 113
Methodologies for Evaluating Permeability from Piezocone Data 115
Evaluation of the Constrained Modulus from Piezocone Data 116
Cone Tip Resistance Correlation 116
Janbu's Method 118
Shear Wave Velocity Correlation 120
Evaluation of Permeability 122
Estimated Permeability Comparison with Existing Methods 125
Conclusions 126

CHAPTER 6 CONCLUSIONS AND RECOMMENDATIONS

Conclusions 128
Recommendations 129

BIBLIOGRAPHY 131

LIST OF SYMBOLS

A_f = Skempton's pore pressure parameter at failure.
B_q = penetration pore pressure ratio = $\Delta u/(q_T-\sigma_{vo})$.
D = constrained modulus = $1/m_v$.
D_r = relative density.
E = Young's modulus.
G = shear modulus.
G_{max} = maximum shear modulus = small strain shear modulus.
G_s = specific gravity.
I_r = rigidity index = G/τ_{max}.
J0 = Bessel function of the first kind of order 0.
J1 = Bessel function of the first kind of order 1.
K = hydraulic conductivity.
K_{ow} = octanol-water partition coefficient.
LL = liquid limit.
M = slope of the critical state line = $6\sin\phi'/(3-\sin\phi')$ in triaxial compression.
N_f = bearing capacity factor.
N_k = cone bearing factor.
N_m = cone resistance number.
N_q = bearing capacity factor for deep failure.
N_u = bearing capacity factor for porewater pressure.
OCR = overconsolidation ratio = σ_p'/σ_{vo}'.
PL = plastic limit.
R = radius.
S = saturation.
T = time factor.
T* = modified time factor.
V_s = shear wave velocity.
Y0 = Bessel function of the second kind of order 0.
Y1 = Bessel function of the second kind of order 1.
a' = attraction = $c' \cot\phi'$.
a_n = net area ratio for unequal cone end areas.
a_v = coefficient of compressibility.
c' = effective cohesion intercept.
c = coefficient of consolidation.
c_h = coefficient of consolidation in the horizontal direction.
c_v = coefficient of consolidation in the vertical direction.
e_o = void ratio.
f = modified hyperbola parameter.
f_s = cone sleeve friction.
g = modified hyperbola parameter.
g = gravitational constant = 9.81 m/s^2.
h_w = height of water table.
k = coefficient of permeability (hydraulic conductivity) = $k^*\rho g/\mu$.
k* = intrinsic permeability.
m = modulus number.

m_v = coefficient of volumetric compressibility = $a_v/(1+e_o)$.
n = porosity.
q_c = measured cone tip resistance.
q_T = corrected cone tip resistance = $q_c + (1-u_2)a_n$.
r = radius.
r_o = radius of cone or probe.
r_p = radius of plasticized zone.
r_{shear} = radius of shear zone.
s_u = undrained shear strength.
t = time.
t_o = initial time.
t_{100} = time at which excess pore pressure = 0 (end of primary consolidation).
u_o = hydrostatic pore pressure.
u_1 = pore pressure measured on the face of a cone penetrometer.
u_2 = pore pressure measured behind the tip of a cone penetrometer.
u_3 = pore pressure measured behind the sleeve of a cone penetrometer.
u_m = measured pore pressure.
u_{max} = maximum measured pore pressure.
Δu = excess pore pressure = $u_m - u_o$.
Δu_m = pore pressure generated in excess of hydrostatic.
Δu_{oct} = excess pore pressure due to changes in mean octahedral stress.
Δu_s = excess pore pressure due to changes in mean octahedral shear stress.
w_n = water content.
x = distance.
α = Henkel's pore pressure parameter associated with $\Delta\tau_{oct}$.
β = Henkel's pore pressure parameter associated with $\Delta\sigma_{oct}$.
γ_s = shear strain.
γ_{sat} = saturated unit weight.
γ_t = total unit weight.
γ_w = unit weight of water.
ε_a = axial strain.
ϕ' = effective stress friction angle.
ρ = mass density of the material = γ_t/g.
ρ_w = mass density of water = γ_w/g.
σ_a' = 100 kPa (reference stress = 1 atm).
$\Delta\sigma_{oct}$ = change in octahedral normal stress.
σ_p' = preconsolidation stress.
σ_{vo} = total overburden stress.
σ_{vo}' = effective overburden stress.
$\Delta\tau_{oct}$ = change in octahedral shear stress.
τ = shear stress.
τ_{max} = shear strength.
ν = Poisson’s ratio.

MATHCAD SYMBOLS

a	=	cone radius.
b	=	radius of the plasticized zone.
c	=	radius of shear zone.
σ_{vo}	=	total overburden stress.
$e\sigma_{vo}$	=	effective overburden stress.
u_o	=	hydrostatic pore pressure.
u_2	=	pore pressure measured behind cone tip.
q_T	=	corrected cone tip resistance.
r_{cone}	=	cone or probe radius.
$r_{plastic}$	=	radius of the plasticized zone.
ϕ	=	effective stress friction angle.
c_h	=	coefficient of consolidation (radial).
I_r	=	rigidity index.
M	=	slope of the critical state line.
s_u	=	undrained shear strength.

CHAPTER 1

INTRODUCTION

Cone Penetration Testing

Cone and piezocone penetration tests are a widely utilized technology for the in-situ investigation of soil deposits, and are primarily used for profiling soil stratigraphy and for distinguishing fine-grained clayey soils from coarse-grained sandy soils. In addition to stratigraphy, cone tests yield information about soil strength, soil stress history, and the hydrogeologic conditions at a site, all of which provide valuable information for site characterization. More recently, specialized sensors have been incorporated within the cone body to detect and measure geoenvironmental properties in order to broaden the usefulness of the cone penetrometer. Cone testing is ideal for environmental site characterization because it generates no cuttings, uses no drilling fluids, minimizes the potential for aquifer cross-contamination through the use of grouting, and reduces the chances of hazardous exposure for operating personnel.

A standard cone penetrometer has a diameter of 3.57 cm, a tip angle of 60 degrees, a projected tip area of 10 cm^2, and a friction sleeve with an area of 150 cm^2 (Figure 1.1 and Figure 1.2). Established standards (ASTM D5778-95) allow for the design of larger penetrometers in order to include additional sensors or to increase the robustness of the device. The geometry of the larger penetrometer is: 4.37 cm diameter, a tip angle of 60 degrees, a projected tip area of 15 cm^2, and a friction sleeve area of 200 to 300 cm^2. The penetrometers are hydraulically pushed from the soil surface at a rate of 20 mm/s during a cone sounding using either a conventional drill rig or a cone truck (Figure 1.3). Both the tip and the sleeve of the penetrometer are instrumented with strain gauges to measure stresses exerted on the soil during penetration (q_c = tip resistance

Figure 1.1. View of Miniature, Four Standard-Size, and Large Penetrometers

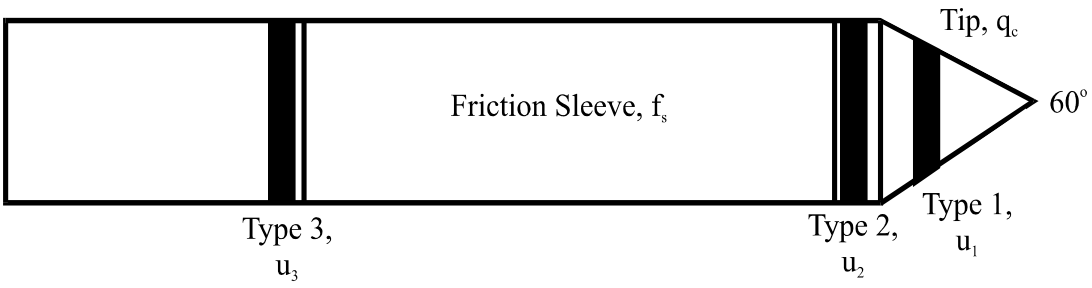

Figure 1.2. Diagram of Piezocone Sensing Elements

Figure 1.3. Fugro Cone Truck During Cone Penetration Testing

= stress exerted on cone tip and f_s = sleeve friction = stress exerted on cone sleeve), while pore pressure transducers are included in the cone to measure the pore pressure generated on the cone tip (u_1 or Type 1 pore pressure), on the cone shoulder (u_2 or Type 2 pore pressure), or behind the friction sleeve (u_3 or Type 3 pore pressure). Figure 1.1 shows a photograph of a variety of piezocone penetrometers used for site investigation. The figure shows, from left to right, a miniaturized half-scale cone penetrometer (4.2 cm^2), a Type 2 electric piezocone (10 cm^2), a Type 1 electric piezocone (10 cm^2), a Type 2 seismic electronic piezocone (10 cm^2), a dual-element (Types 1 and 2) seismic electronic piezocone (10 cm^2), and a triple-element (Types 1, 2, and 3) electronic piezocone (15 cm^2).

Tip Resistance and Sleeve Friction Measurements

The tip and sleeve readings of a cone penetrometer are used in combination with the magnitude of the excess pore water pressure for determining soil stratigraphy and for the evaluation of soil properties. Many classification methods exist for the determination of soil types, and the methods most commonly use a combination of the measured tip resistance and sleeve friction (Robertson and Campanella, 1983; Olsen, 1994); however, methods that utilize the reading of pore pressure are also available (Senneset et al., 1989; Robertson, 1990).

The readings from a cone are semi-continuous, performed every two centimeters of push, and are rapid, economical, and reproducible. The readings in a cone penetration test are actually averaged values measured over the cone's effective zone of influence, which is a function of the soil type being penetrated. Soil parameters derived from cone penetration data include the stress history of clays (Chen and Mayne, 1994), unit weight of clays (Larsson and Mulabdic, 1993), relative density of sands (Jamiolkowski et al., 1985), and the effective friction angle of sands (Robertson and Campanella, 1983) and clays (Senneset et al., 1989). A detailed listing of the parameters derived from piezocone testing is presented in Mayne et al. (1995).

Porewater Pressure Measurements

As discussed earlier, piezocone penetrometers are instrumented with at least one pressure transducer to measure the penetration pore water pressures (u_m) generated during a sounding. This allows for the calculation of excess pore pressure, $\Delta u = u_m - u_o$ (Janbu and Senneset, 1974; Baligh et al., 1981), where Δu is the difference between the generated pore pressure and the hydrostatic pressure (u_o). The inclusion of the pore pressure reading was a significant improvement in cone technology because the generated excess pore pressure measurements provide important insight into the type of soil being penetrated. Soundings in fine-grained soils, which have a characteristic low hydraulic conductivity, generate large pore pressures in excess of hydrostatic values because the displaced water cannot move freely throughout the soil column; consequently, the sounding occurs under undrained conditions. The interpretation of the data gathered from pore pressure measurements is also useful for the evaluation of geoenvironmental parameters including the coefficient of consolidation and the permeability of a soil deposit. These properties give information about the flow of pore fluid in a soil matrix and are important in applications such as consolidation of clay landfill liners and contaminant transport.

Coarse-grained soils which have high hydraulic conductivity do not generate large excess pore pressures because the displaced water can easily dissipate to other parts of the soil column as shown in Figure 1.4 and Figure 1.5. This sounding was performed in Po River sand in Italy, and the penetration pore pressure essentially matches hydrostatic pressure throughout the profile.

In contrast, Figure 1.6 shows an example piezocone record a soft insensitive lacustrine clay where significant excess pore pressures were generated (pore pressures measured in both the u_1 and u_2 positions, with u_1 always greater than u_2). Figure 1.7 shows similar behavior in a soft sensitive clay from St. Alban, Quebec; note that increasing the sensitivity of the clay decreases the difference between the pore pressures measured in the Type 1 and 2 positions (Mayne et al., 1990). Finally, Figure 1.8 shows the pore pressure behavior in the heavily-overconsolidated Gault clay.

In lightly-overconsolidated clays, the measured penetration pore pressures are always positive, regardless of the location of the pore pressure transducer (Figure 1.6 and Figure 1.7). However, in heavily-overconsolidated clays, the penetration pore pressures measured in the Type 2 or Type 3 locations can either be positive or lower than hydrostatic, or even negative, while the penetration pore pressures measured in the Type 1 position will always remain positive. shows the results of a dual element piezocone sounding in the heavily-overconsolidated and fissured Gault clay

where the measured Type 1 pore pressure is always positive, while the Type 2 pore pressure goes lower than hydrostatic and negative during the sounding.

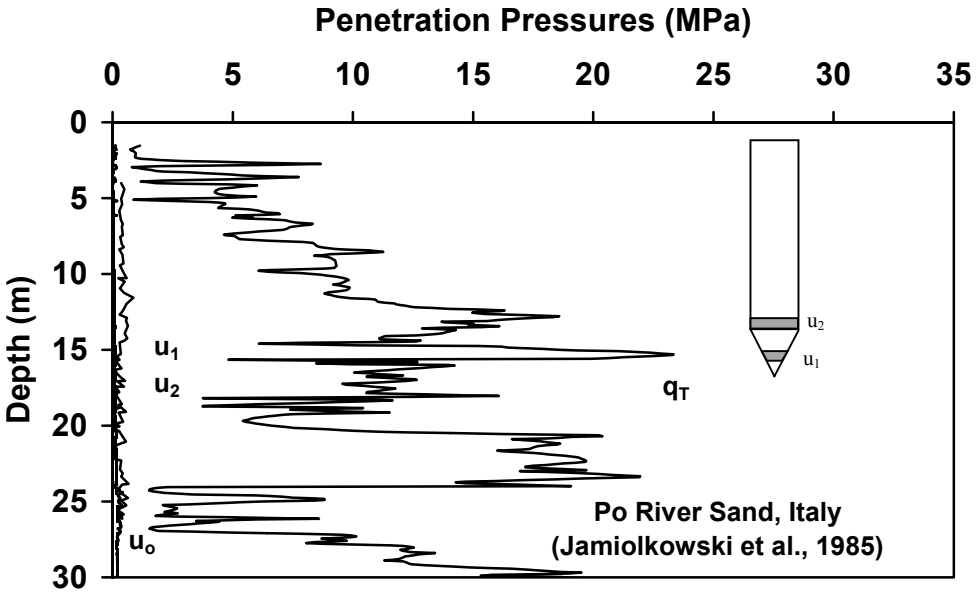

Figure 1.4. Penetration Pressures in Medium to Dense Sand, Drained Conditions

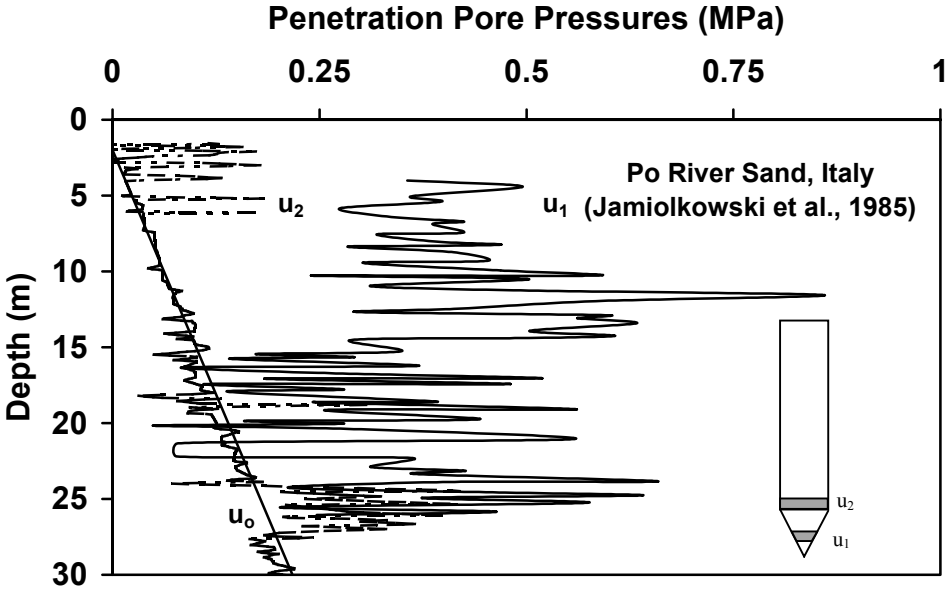

Figure 1.5. Penetration Pore Pressures in Medium to Dense Sand, Drained Conditions

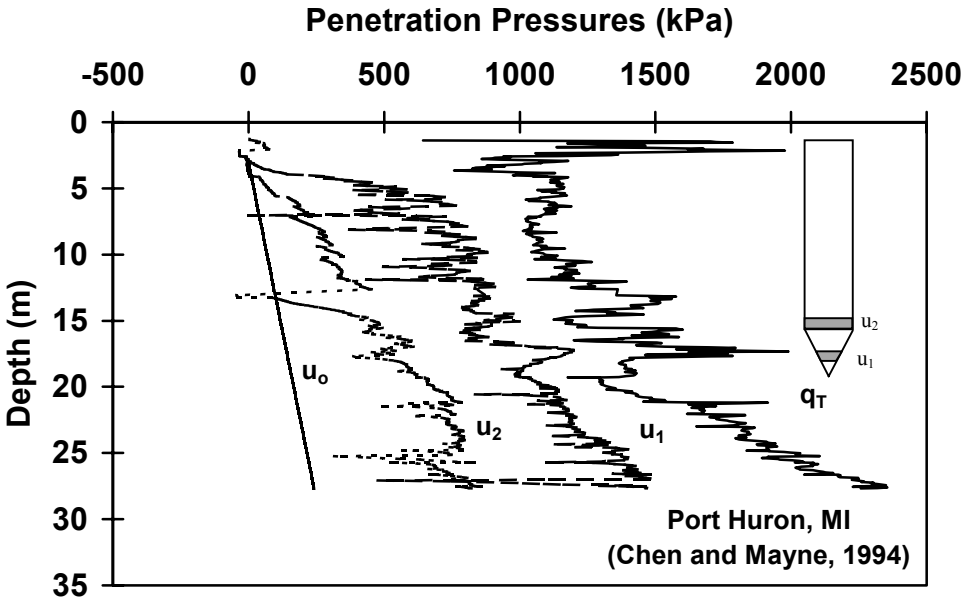

Figure 1.6. Penetration Pressures at Port Huron, MI in a Soft Insensitive Clay

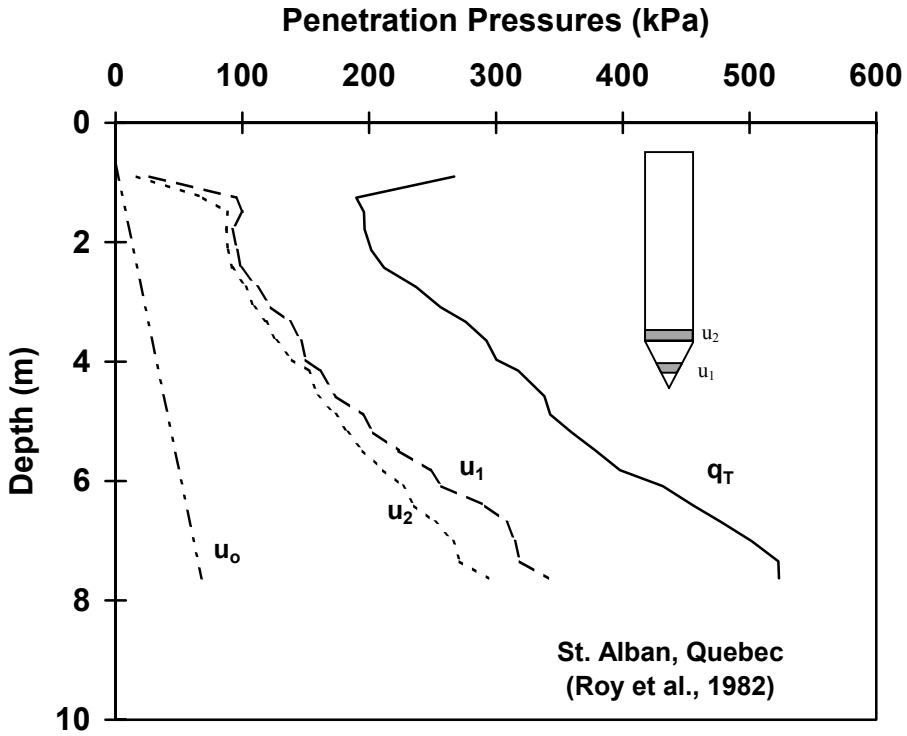

Figure 1.7. Penetration Pressures in a Soft Sensitive Clay

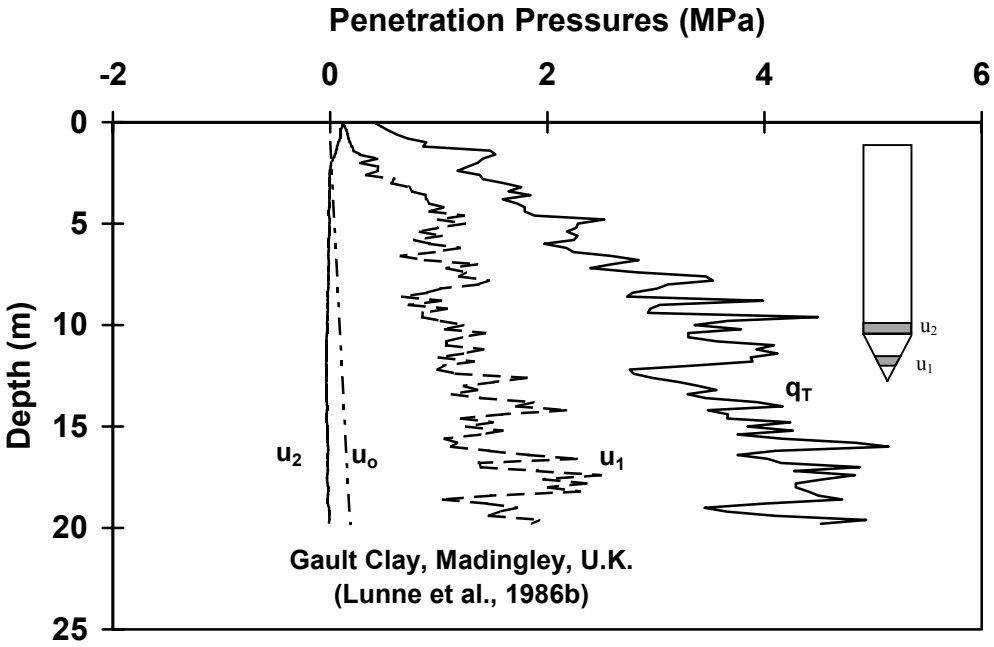

Figure 1.8. Penetration Pressures in Heavily-Overconsolidated Gault Clay

The pore pressure transducer in the piezocone is in contact with a cavity within the cone body, and pore water is brought into the cavity through a filter which is most commonly made of polypropylene, stainless steel, or a ceramic. Before a sounding is performed, the cavity is saturated with water and the pore pressure filter is saturated with either water, a water/glycerin mixture, or in some cases, a heavy oil. During the initial development of the piezocone, the location of the pore pressure filter was not standardized; early versions of the piezocone had filter locations ranging from the apex to various positions on the shaft. Most filter positions today occur either on the penetrometer tip or midface (Wissa et al., 1975), behind the shoulder (Jamiolkowski et al., 1985), or behind the friction sleeve (Campanella and Robertson, 1988) (Figure 1.2). The location of the filter element is an important consideration because the magnitude of the measured pore pressure has been shown to decrease as the filter location is moved up the cone body, away from the cone tip (Campanella et al., 1986a; Brown, 1993); that is, $u_1 > u_2 > u_3$.

The Type 1 filter location is advantageous because the measured pore pressures are always positive at this location which gives excellent profiling detail (Mayne et al., 1990). However, the Type 2 position is necessary for the correction of tip resistance measured with pore pressure acting on unequal end areas of the cone tip (Jamiolkowski et al., 1985; Lunne et al., 1986a). The correction is given as follows:

$$q_T = q_c + (1 - a_n)u_2 \qquad \textbf{Equation 1.1}$$

where q_T = corrected tip resistance, q_c = measured cone tip resistance, a_n = net area ratio determined in a calibration chamber, and u_2 = Type 2 pore pressure measured at the shoulder position. The net area ratio is a function of the cone geometry and must be measured using a pressurized triaxial

chamber. The reported values of a_n for commercially built cone penetrometers range from $a_n = 0.38$ to 0.85. It is preferable to design cones with values of a_n as large as possible ($a_n \geq 0.8$) because the cone tip resistance correction is smaller. The correction factor is especially important in soundings in soft to firm fine-grained soils due to the large excess pore pressures which can develop, and in deep soundings where hydrostatic readings are large.

Sensor Technology for Geoenvironmental Site Investigation

While the traditional measuring capabilities of a cone penetrometer include tip resistance, sleeve friction, and pore pressure, the cone makes an excellent vehicle for transporting other measuring devices into the subsurface, with less disturbance when compared to traditional boring methods like auger drilling which create large diameter holes and soil cuttings. Consequently, additional sensors have been incorporated into cone penetrometers in order to measure soil properties or geoenvironmental characteristics of a soil deposit. These sensors are most commonly included in either the portion of the cone which is directly behind the friction sleeve, or in a separate module which trails directly behind the cone body. An overview of the sensor technology in use today is presented in the following paragraphs.

The main goals of a geoenvironmental site characterization include the delineation of soil stratigraphy and hydrogeologic conditions, and the detection of the extent and magnitude of chemical contamination. Because the investigations are complicated by the presence of hazardous chemicals which can harm operating personnel, recent emphasis has been placed on developing investigation techniques which perform the measurements and sampling either below the soil surface, or within a completely contained sampling module which transfers liquid and vapor to the surface for analysis.

Site investigation practice is beginning to de-emphasize the use of traditional boring and sampling techniques and has begun to rely on the use of either semi-invasive techniques like cone penetration testing, or on non-invasive techniques like seismic investigations. However, quantitative evaluation of contaminant characteristics as a function of depth requires some minimum degree of invasion; consequently, the use of the cone penetration test as a vehicle for the transport of specialized sensors into the subsurface has become a common approach to site characterization. These sensors commonly take one of two forms: either a direct non-sampling sensor which performs measurements on the probe surface, or an indirect sampling sensor which draws an amount of pore fluid or gas into the cone body or through transmission lines to the soil surface for analysis. Sensor technology which does not require drawing pore fluid into the cone typically cannot provide quantitative measurements, it can only map the relative qualitative differences in soil properties, for example changes in bulk resistivity. To date, the quantitative measurement of chemical concentrations in-situ can be performed only through sampling of the soil, pore fluid, or vapor. The following section provides a review of both the sensor and sampling technology available for use in geoenvironmental site investigation. For the purpose of review, the available sensor technologies have been divided into applications used mainly for geotechnical or for environmental purposes; however, the technology may be applicable to both cases in some instances.

Geotechnical Sensor Technology

One group of sensors focuses on the measurement of mechanical soil properties used in geotechnical site characterization and design, including measurements of strength, deformability, in-situ states of stress, and moisture content. These are discussed in the following paragraphs.

Inclinometer

Inclinometers have been included in cone penetrometers in order to monitor the verticality of the cone during a sounding (Campanella and Robertson, 1988). A cone can deviate from verticality due to misalignment, bent push rods, soil layering, or be pushed off a vertical course during penetration if it encounters an obstacle such as a large rock. A large deviation from the initial alignment can cause breakage of the cone rods and loss of the cone down the hole; consequently, many penetrometer systems are equipped with an automatic shutoff if the cone exceeds an inclination of 9^{o}. While the sensor measures the inclination of the cone, the data are not used to evaluated soil parameters.

Resistivity

The resistivity cone was developed to detect changes in the electrical conductance properties of a soil pore fluid (Horsnell, 1988; Campanella and Weemees, 1989). Resistivity, the reciprocal of conductivity, is a measure of the mobility of ions through a medium; in general, sands exhibit high resistivity (low conductivity), while clays, which are relatively electrically active, exhibit low resistivity (high conductivity). Resistivity cones operate under the same principle as in surface geophysics: four electrically-isolated electrodes are built into a module which trails the cone penetrometer and a current is applied across the two outer electrodes, while the voltage drop across the two inner electrodes is measured. The measured property is the resistance, which is a function of probe geometry, and the resistivity, which is a material property, is calculated from the measured resistance. Measurements from soil resistivity probes have been used to estimate the porosity and formation factor of sands through use of the empirical relationship known as Archie's Law (Bellotti et al., 1994).

Vibratory Module

Cone penetrometers have been designed with a trailing vibratory module for use in the identification of zones of loose sands which are susceptible to liquefaction during an earthquake (Sasaki and Koga, 1982; Sasaki et al., 1985; Koga et al., 1986; Teparaksa, 1987, 1990; Mitchell, 1988; Tokimatsu, 1988; Jamiolkowski and Robertson, 1988; Du and Wu, 1992). The method of evaluation requires one cone sounding without the use of vibration during penetration (static sounding), and a second cone sounding with the use of vibration (dynamic sounding). The two soundings, one prior to vibratory densification and one after vibratory densification, are then compared, and the liquefiable sand zones are identified by a significant increase in measured cone tip resistance in the areas which were densified by vibration.

Accelerometer/Geophone

One of the most commonly used sensors for geotechnical site investigation is the accelerometer or geophone, which is included in the cone for measurement of the shear wave velocity (V_s) or corresponding small strain properties of a soil deposit (Robertson et al., 1986). These sensors can also measure vibration and damping characteristics of a soil deposit, and the compression wave velocity (V_p). The seismic cone test is most commonly performed as a downhole test with a mechanical source placed at the surface to generate shear waves which propagate through the soil deposit. The travel time from source to receiver is monitored through the detection of the arrival time at the sensor within the cone body, and the shear wave velocity can be calculated by division of the travel distance by the travel time. These seismic measurements are also used for environmental applications including waste detection and landfill delineation.

Neutron/Gamma Radiation

Neutron and gamma radiation sensors have been included in cone penetrometers in order to evaluate the moisture content and relative density of a soil deposit (Marton et al., 1988; Mitchell, 1988; Sully and Echezuria, 1988; Shibata et al., 1992). Neutron sensors rely on the interaction of the neutrons with the hydrogen present in the pore fluid, while gamma-radiation sensors rely on the interaction of gamma rays with soil particles. These sensors are most commonly used to measure the pore fluid and density characteristics of a soil deposit; however, studies have also been performed which relate the natural water content measured with the radiation sensors to the relative density and liquefaction potential of a soil deposit (Mimura et al., 1995).

Lateral Stress

Lateral stress cells have been developed in order to evaluate the in-situ state of horizontal stress (σ_h) of a soil deposit (Mitchell, 1988; Sully, 1991). Lateral stress cone designs typically place the measurement module behind the cone body in order to remove it from the variable stress regime which occurs at the cone tip during penetration. The cell is designed for freedom of radial movement and is instrumented with strain gauges in order to monitor the lateral stress exerted on the cone body. The lateral stress cone provides a direct measurement of the total horizontal stress during penetration, a property which is a function of the strength and stress history of a soil deposit and is difficult to quantify through laboratory experimental methods.

Acoustic Emissions

Monitoring of the acoustic emissions produced during a cone sounding has been performed using microphones included within the cone body (Villet et al., 1981; Tringale and Mitchell, 1982) and by inclusion of a piezoelectric acoustic emission transducer located directly behind the cone tip (Massarsch, 1986). Penetration of a cone into soil produces audible emissions due to the interaction of the soil with the probe body and push rods. Testing using the acoustic emission sensor has shown that layering of different soil types (sand, silt, or clay), changes in relative density, and changes in fabric can be identified (Menge and Van Impe, 1995).

Pressuremeter Module

Pressuremeter modules have been added as components of cone penetrometers in order to facilitate full-displacement pressuremeter testing procedures. Cone pressuremeters combine the traditionally measured cone parameters with measurements of strength, deformation, and horizontal stress measurements from the pressuremeter module (Houlsby and Withers, 1988; Houlsby and Hitchman, 1988; Ghionna et al., 1995). The pressuremeter module trails the cone penetrometer and is an inflatable probe which is expanded into the soil in a radial direction. Results from the pressuremeter test can also be used to evaluate the complete stress-strain-strength behavior curve for soils.

Time Domain Reflectometry

Time domain reflectometry sensors have been included in cone penetrometers for the measurement of soil/pore fluid dielectric constant (Lightner and Purdy, 1995). The sensor operates by monitoring the response from a pulsed electromagnetic wave sent through the surrounding soil. The dielectric constant is then correlated to moisture content in terms of volumetric water content. Research at Sandia National Laboratory measured moisture by volume to within $\pm$ 1% when compared to laboratory measurements.

Video Cone

Video Cones have been developed which record the soil images along the edge of a cone during a sounding (Hryciw and Raschke, 1996; Raschke and Hryciw, 1997). The imaging is performed through a sapphire window on the body of the cone, and grain size analysis can subsequently be performed on the recorded data using digital image analysis.

Environmental Sensor Technology

This group of sensors focuses on the evaluation of soil properties or contaminant characteristics used in environmental site investigations. These sensors most commonly infer the location of contamination through measurement of a property of the bulk soil/pore fluid matrix, for example bulk resistivity. No sensor technology exists today which can provide quantitative measurements of chemical concentration without sampling of contaminated media.

Resistivity

The resistivity cone is used in environmental investigations to delineate soil contamination through changes in the measured bulk resistivity (Horsnell, 1988; Campanella and Weemees, 1989; Strutynsky et al., 1991; Woeller et al., 1991a). The resistivity cone has been used to detect acidic spills, which produce highly conductive conditions, and to detect organic non-aqueous phase liquid (NAPL) spills, which are highly resistive contaminants. Use of the resistivity cone requires a site-specific calibration because it is used to detect relative differences in magnitude, rather than absolute values.

pH

Cone penetrometers have been designed with pH sensors to identify areas of acidic or basic contamination (Olie et al., 1992). The sensor has a small flow cell within the cone body in order to bring fluid into contact with the miniaturized glass, gel-filled Ag/AgCl pH electrode. Use of the pH sensor has enabled mapping of pH as a function of depth, and monitoring of the progress of the remediation of acidic waste sites.

Redox Potential

Redox potential sensors have been included in cone penetrometers to measure the reduction-oxidation potential of a site (Olie et al., 1992). The redox potential of the bulk soil/pore fluid matrix is useful for the monitoring of hazardous waste sites under bio-remediation because it is a measure of the state of electron donors and acceptors, a critical control on biological activity (Pluimgraaf et al., 1995).

Temperature

Thermocouples have been included to monitor the temperature of the cone body during a sounding (Horsnell, 1988; Mitchell, 1988). Applications of the temperature sensor include the mapping of zones of endothermic or exothermic temperature changes, due either to chemical reaction such as methane generation in landfills, or to biological activity. Depth of permafrost has also been mapped using the temperature sensor (Woeller et al., 1991b).

Dielectric Constant

Robertson et al. (1996) give details of a cone penetration device developed to measure the dielectric constant of a soil pore fluid mixture. The dielectric constant is a measure of a molecule's interaction with an electromagnetic field, and is a function of the applied frequency. A retractable cone has been developed by Delft Geotechnics which operates by pushing to the depth of interest,

opening a soil sample chamber and pushing until the chamber is filled (Stienstra and van Deen, 1994). An electromagnetic field pulse is generated at the soil surface and transmitted through a coaxial cable to a pin in the middle of the chamber which is the antenna; the chamber rim is the receiver. Subsequently, the dielectric constant can be measured as a function of frequency to help identify areas contaminated with NAPLs which have a characteristic low dielectric constant (~3 to 8), when compared to water which has a dielectric constant of 80.

Site Characterization and Analysis Penetrometer System (SCAPS)

One of the most promising cone penetration tools currently in use is the Site Characterization and Analysis Penetrometer System (SCAPS) developed by the US Department of Defense (Lieberman et al., 1991; Apitz et al., 1992a, 1992b; Theriault et al., 1992). The SCAPS cone was developed as a field screening tool for the detection of the constituents of fuel products and oils. It is also known as the laser-induced fluorescence cone (LIF-CPT). The basic operation of the cone relies on the monitoring of a fluorescence response of aromatic hydrocarbons in aqueous solutions. Fluorescence is a property of a group of molecules which sorb a quantum of light when exposed to an energy source. This forces the molecules into a higher, or activated energy state, as long as the external excitation is present. When the source is removed, the molecule returns to its normal energy level and releases the quantum of energy as light. This release can be detected, and the phenomenon is known as fluorescence. The cone penetrometer used with the SCAPS system is built with a sapphire window in a slight recess on the cone body; transmission and receiving fiber optic cables are strung down the cone rods to the window and light from an N_2 laser is pulsed down the transmission cable. When the excitation is removed, the fluorescent chemicals will emit light, which is transmitted to the surface using the receiving fiber optic cables. Because chemicals fluoresce at different wavelengths, the frequency of the laser light is adjustable in order to optimize detection.

While the SCAPS cone is a valuable tool for the screening of fuel contamination, it has several limitations. These include the fact that background sources, including natural organic matter can also fluoresce, making it necessary to acquire a site specific baseline at each testing location. The measurement is limited to qualitative data; estimations of concentration are performed only through correlations with measured concentrations in given soil conditions. Finally, the sensor operation is limited to the group of compounds which fluoresce, and is not capable of detecting many chemicals of environmental concern, including the chlorinated hydrocarbons like trichloroethylene or perchloroethylene.

Another sensor, known as the Rapid Optical Screening Tool (ROST™) system relies on the same concept of fluorescence but uses a neodymium-doped yttrium aluminum garnet laser operating at wavelengths of 280 to 300 nm, instead of the N_2 laser used by the SCAPS cone (Lightner and Purdy, 1995).

Additionally, a Raman spectrograph sensor has been included in a cone and also operates under conditions similar to the SCAPS and ROST™ cones. Use of the Raman spectrograph enables the detection of chlorinated hydrocarbons in addition to fluorescence.

Gamma Radiation

The gamma radiation sensor was developed to identify radioactive contaminants in-situ (Brodzinski, 1995). The sensor uses a sodium iodide crystal (NaI) in combination with spectral analysis for the detection of radioactive ^{238}U daughter products; however, initial trials with the sensor indicated high detection limits (Lightner and Purdy, 1995).

Integrated Opto-Electronic Sensors

A new class of sensor technology has been developed in order to quantitatively measure chemical concentrations in-situ. These sensors rely on chemical reaction of the contaminant of interest with a polymeric coating on an optically transparent waveguide (Hartman et al., 1988; Hartman, 1990). This interaction produces a change in the refractive index and alters the travel of a beam of light through the waveguide; the alteration can be measured and correlated linearly with chemical concentration. The sensor has been laboratory tested for the measurement of pH (hydrogen ion concentration) and ammonia, and is currently under development for the detection of the BTEX and other chemicals. A more detailed explanation of the operation of this sensor will be presented in Chapter 3.

Sampling Technology

Current site investigation practice requires either the drilling of a monitoring well or the use of a discrete water sampler for the quantitative evaluation of groundwater. A monitoring well is typically five centimeters (two inches) or larger in diameter, and requires screening at the depth from which the sample is to be taken. While monitoring wells are the most common method for analyzing groundwater, there are several drawbacks to their use, including expense, limited sampling depths, generation of soil cuttings which may be contaminated, and venting of groundwater to the atmosphere, which is especially detrimental in the detection of volatile chemicals. In addition, sampling of monitoring wells is most commonly performed using a bailer which further increases exposure to atmospheric oxygen. Discrete water samplers were developed in order to address some of the problems seen in monitoring wells. The following section reviews the direct push technology (DPT) samplers which are in use today.

BAT Enviroprobe

The BAT Enviroprobe was developed by Torstensson (1984) for the sampling of contaminated groundwater. The push-in sampler has a similar outer configuration to a cone penetrometer; however, glass sample vials which are sterilized and under vacuum are stored inside the probe body. When the depth of interest is reached, an outer sleeve is retracted to expose a filter. A double-ended hypodermic needle is then pushed through two septums which connect the filter to the sampling vial, and pore fluid is drawn into the chamber. The BAT Enviroprobe is best suited for taking small volume fluid samples of less than 150 mL.

Hydropunch

The Hydropunch is a liquid sampler which also has the outer form of a cone penetrometer. This sampler is pushed to the desired sampling depth, and an outer sleeve is retracted to expose a stainless steel filter and a miniaturized bailer is lowered through the push rods and probe body in order to take a sample (Robertson et al., 1996). A significant difficulty associated with the use of the Hydropunch is the high sample turbidity due to incomplete screening of fines.

Envirocone®

The Envirocone® was developed by ISMES for characterization of groundwater and vapor at contaminated sites (O'Neill et al., 1996; Piccoli and Benoit, 1995). The device is pushed to the sampling depth of interest and pore fluid is drawn in through either stainless steel or sintered steel filters located above the probe tip. The device uses a positive displacement pump, contained in the probe body, to transfer the samples through Teflon sampling lines (2 mm diameter) to the soil surface for analysis. At the surface, the sample is analyzed for pH, redox potential, dissolved oxygen, electrical conductivity, and temperature. Vapor samples are analyzed for dissolved oxygen,

total volatile organics, combustible gas, H_2S, and CO_2. Flushing of the system in order to minimize the possibility of sample cross-contamination is performed using a pressurized air/water flushing system.

Cone Sipper™

The Cone Sipper™ was developed as a mechanism to rapidly transfer ground water samples to the soil surface (Lightner and Purdy, 1995). The probe uses a gas lift pump in combination with a series of check valves, vacuum lines, and pressure lines to pump pore fluid from the probe intake to analytical equipment above ground. Samples up to 100 mL in volume are obtained with the system.

Summary of Cone Sensor and Sampling Technology

The review presented here has divided the cone technology available for geoenvironmental site investigation into two general categories: sensor equipment and sampling equipment. For the most part, sensor technology is taken as that which can perform measurements on the sensor surface, without bringing a sample into the probe body, while a sampling technology requires a mechanism to draw the specimen in to the cone body.

In terms of sensors available for site investigation, the resistivity cone and the SCAPS cone have proven to be the most viable and useful of the environmental characterization tools at the present time. Resistivity is commonly used for the investigation of inorganic, ionic contaminants, while the SCAPS cone is used for identification of fluorescent organic contaminants. In practice, both of the sensors yield measurements which are qualitative indicators of the presence of contaminants, and so are most useful as screening tools for initial phase investigations. A summary of the available sensor technology for both geotechnical and environmental applications is presented in Table 1.1 and Table 1.2 (modified after Bowders and Daniel, 1994).

Sampling tools have been developed in order to obtain quantitative measurements of contaminant concentrations which can be used as the basis for remedial design. The use of in-situ samplers tends to be slow and requires chemical analysis by laboratory instrumentation such as a gas chromatograph, either at the soil surface, or in an off-site laboratory location. The other main concern associated with sampling technology is the preservation of sample integrity during acquisition. Probes which use sample transfer lines, or the same filter to obtain a series of samples must be equipped with flushing systems and constructed of materials which are resistant to cross-contamination. Because the issue of cross-contamination is of concern for the operation of the BTEX sensor used in this study, a review of the materials most suited to sampling of environmental contaminants follows.

Table 1.1. Review of Geotechnical Sensors Used in Piezocone Testing

Sensor	Measurement	Applications	Reference
Inclinometer	Cone verticality	• Prevent damage of cone	Campanella et al. (1986b)
Resistivity	Mobility of ions in pore fluid using electrically isolated electrodes	• Porosity of sands • Fabric of sands • Conductivity = 1/Resistivity	Bellotti et al. (1994); Campanella and Weemees (1989)
Vibratory Module	Vibration of cone during push	• Assessment of soil liquefaction potential	Sasaki and Koga (1982); Sasaki et al. (1985); Mitchell (1988)
Accelerometer/ Geophone	Shear wave velocity	• Measurement of small strain properties of a soil • Site specific G_{max} • Particle velocity for damping ratio	Robertson et al. (1986)
Neutron/ Gamma Radiation	Moisture content	• Soil density • Moisture content • Correlation with liquefaction potential	Marton et al. (1988); Mitchell (1988); Sully and Echezuria (1988); Mimura et al. (1995)
Lateral Stress	Lateral stress on cone shaft	• Evaluation of in-situ states of stress	Mitchell (1988); Sully (1991)
Acoustic	Acoustic emissions	• Soil type • Soil compressibility • Soil fabric	Villet et al. (1981); Tringale and Mitchell (1982); Menge and Van Impe (1995)
Pressuremeter Module (Full displacement)	Radial deformation	• Shear strength • Horizontal stresses • Deformability	Houlsby and Withers (1988); Houlsby and Hitchman (1988); Ghionna et al. (1995)
Time Domain Reflectometry	Dielectric constant through pulsed electromagnetic wave	• Correlated with moisture content	Lightner and Purdy (1995)
Video	Video images of soil during penetration	• Grain size quantification • Soil stratigraphy	Hryciw and Raschke (1996); Raschke and Hryciw (1997)

Table 1.2. Review of Geoenvironmental Sensors Used in Piezocone Testing

Sensor	Measurement	Applications	Reference
Resistivity	Mobility of ions in pore fluid using electrically isolated electrodes	• Salt water intrusion • Acid spills • Detection of water table in mine tailings	Horsnell (1988); Campanella and Weemees (1989); Strutynsky et al. (1991); Woeller et al. (1991a); Malone et al. (1992)
Temperature	Temperature of cone body	• Endothermic/ exothermic activity	Horsnell (1988); Mitchell (1988); Woeller et al. (1991b)
SCAPS	Laser-induced fluorescence of fuel contaminants; N_2 laser at λ = 337 nm	• Fuel, oil, and lubricant contamination capable of fluorescing	Lieberman et al. (1991); Apitz et al. (1992a); Apitz et al. (1992b); Theriault et al. (1992); Lambson and Jacobs (1995)
Redox Potential	Reduction-Oxidation Potential	• Monitoring of conditions during bio-remediation	Olie et al. (1992); Pluimgraaf et al. (1995)
pH	Hydrogen ion concentration	• Acid spills • Base spills	Brylawski (1994)
Dielectric Constant	Dielectric constant of soil/pore fluid mixture as a function of frequency	• NAPL contamination	Arulmoli (1994); Stienstra and van Deen (1994)
Raman Spectroscopy	Raman spectrograph to measure argon ion laser induced fluorescence	• NAPL contamination • Chlorinated hydrocarbons	Carrabba (1995) Bratton and Timian (1995)
ROST™	Laser-induced fluorescence of fuel contaminants; neodymium-doped yttrium aluminum garnet laser at λ = 280 - 300 nm	• Fuel, oil, and lubricant contamination capable of fluorescing	Naval Command (1995)
Gamma Radiation Probe	Detection of Uranium by-products using a NaI(Tl) crystal detector	• Identification of radioactive contaminants	Brodzinski (1995); Lightner and Purdy (1995)
Integrated Optoelectronics	Measurement of in-situ chemical concentration by wave interference	• Ammonia • pH • BTEX	Hartman et al. (1988); Hartman (1990) This study

Maintaining Integrity in the Sampling of Contaminated Fluids

Sampling of contaminated fluids for chemical analysis requires careful consideration of the process and materials used in order to maintain specimen integrity. In order to draw ambient pore water vapors and fluids from the soil environment into the probe chamber, it is important to have a porous filter stone that allows the transmission of gases and fluids, yet prevents the influx of soil particles. These aspects are complex within the scope of soil and fluid mechanics because of the vast range in particle sizes encountered in natural geomaterials. The size classification of particles ranges several orders of magnitude from gravel to sand (4.75 mm to 0.075 mm), to silt (0.075 mm to 2 μm), to clay (< 2 μm), as shown in Figure 1.9. The porous filter must also have a permeability high enough as to not inhibit flow and volume of fluids for testing. Finally, the porous filter must be constructed of a material that does not interact with the groundwater chemistry and taint the desired measurements.

Sampling of contaminated groundwaters is also complicated by the complex aqueous chemistry often found at hazardous sites. One of the main difficulties in working with contaminated materials is the extreme variability of chemical conditions that exist in practice. Conditions range from low to high pH, from oxidizing to reducing conditions, and from contamination by metals to contamination by organics; consequently, the materials used in the investigation and characterization of a site must be suitable to resist the contaminates of concern at a particular site in order to maintain integrity in the monitoring process.

All direct push groundwater and vapor samplers require filtering mechanisms in order to draw a fluid sample into the probe body. Because the filter is in direct contact with the soil during push, it must resist abrasion and clogging, and must be chemically compatible with the surrounding groundwater. Filter materials commonly used in direct push applications in non-contaminated soils include high density polyethylene, ceramic, brass, polyvinyl chloride, and sintered stainless steel (Marsland and Quarterman, 1982; Campanella and Robertson, 1988; Bratton and Timian, 1995; O'Neill et al. 1996). However, of additional concern to the issue of sampling for chemical analysis at contaminated sites is the material or materials which will come into contact with the given sample through filter inlets, sampling lines, or storage vials. Not only must these materials be physically durable in order to withstand the abrasion and high pressures generated during DPT penetration, but they must also be chemically resistant and non-reactive with the target chemicals of interest.

Chemical Compatibility

The materials most commonly used in the sampling of groundwater include stainless steel, polytetrafluoroethylene (PTFE, Teflon®), and polyvinyl chloride (PVC). Each of these materials possesses advantages and disadvantages and none is suited to sampling in all conditions, because the physical and chemical properties of contaminants of concern cover a range of diverse behaviors. In general, however, metals like stainless steel are most applicable for the sampling of organics, while organic materials like Teflon® or rigid PVC are most applicable for the sampling of metals.

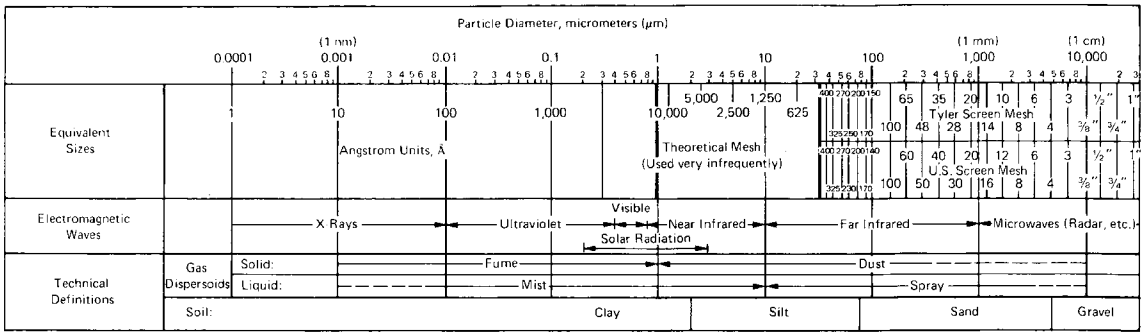

Figure 1.9. Range of Particle Sizes in Nature (Mitchell, 1993)

Parker (1992) developed suggested guidelines for the use of stainless steel, PVC, and Teflon® for the sampling of groundwater, with a focus on chemical and physical durability, and on material effects on sample integrity. Of the three materials, stainless steel has the greatest physical strength, with corrosion resistance which is generally quite good, except in the long-term exposure to highly corrosive environments with low pH, high dissolved oxygen contents, hydrogen sulfide, carbonic acid, or high chloride concentrations. In terms of sample integrity, Parker (1992) notes that stainless steel casing can react with or sorb metals from solution or can leach metals into solution, especially from the weld joints. However, stainless steel shows little interaction with organic contaminants, either in terms of sorption or outgassing into solution. These properties suggest that stainless steel provides a better filtration and sampling material for organic contaminants than for metallic contaminants.

Teflon® is used extensively in environmental sampling, mainly due to its corrosion and dissolution resistance. Parker (1992) reports that Teflon® shows little interaction with metals in solution, either in terms of sorption onto the Teflon® surface, or in terms of leaching metals into solution. While it is known to sorb/partition some organics from solution into its matrix, Teflon® does so at much lower concentrations than seen in flexible PVC (Tygon). Leaching of organics from Teflon® into solution is negligible. In contrast to Teflon®, Tygon will dissolve or swell when exposed to highly concentrated solvents. It also has a tendency to sorb metals from solution and to leach metals from its stabilizers into solution. Tygon also sorbs/partitions organics from solution into its matrix and can release organics from its plasticizers into solution. However, Parker (1992) notes that rigid PVC, which is often used for well casings, shows little leaching of metals or organics into solution and little sorption/partitioning of organics into its matrix.

Filter and Sampling Materials

A review was performed in order to evaluate the porous filters and sampling materials which are commonly used in practice today, with references from this review compiled in Table 1.3 and Table 1.4. The material most commonly used in DPT for filtration of both liquid and vapor samples is stainless steel. Undoubtedly, this is due to its high abrasion resistance which is required during push penetration of the cone penetrometer or sampling probe. While stainless steel has been shown capable of adsorbing metals from or leaching metals into solution, depending on the geochemistry of the strata being sampled, transfer of metal ions is strongly dependent on contact time; longer contact

Table 1.3. Metallic Filter Elements for Direct Push Technology

Material and Application	Reference
Stainless Steel 304/316; Argonne National Laboratory performed study of transfer lines made of stainless steel, nickel, aluminum, and Teflon® to quantify interaction with samples in terms of outgassing and transfer loss of VOCs. Temperature, flow rate and latent moisture content were varied; stainless steel, type 304 and 316, yielded the most accurate results.	Lightner and Purdy (1995)
Stainless Steel; Batch water sampler; uses stainless steel wire filter screen and all stainless steel construction for the body of the sampler.	Auxt and Wright (1995)
Stainless Steel; Soil sampler; uses stainless steel 316 sample tubes with caps and all stainless steel construction for the body of the sampler.	Auxt and Wright (1995)
Stainless Steel; Envirocone uses stainless steel filter with thin, open ridges when taking liquid and vapor samples in sand; used in highly abrasive soils. Sample is pumped to the surface for analysis (Teflon transfer line).	Piccoli and Benoit (1995); O'Neill et al. (1996)
Stainless Steel; Fine mesh stainless steel screen surrounded by perforated stainless steel screen for filtration of fluid used in the assessment of hydraulic conductivity.	Konrad and Frechette (1995)
Stainless Steel; Hydropunch discrete water sampler. Stainless steel construction.	Strutynsky and Sainey (1992)
Stainless Steel; Monitoring well filter pack of rounded silica sand surrounded by two stainless steel wire wrapped screens. Developed to limit migration of fines into water samples.	Strutynsky and Sainey (1992)
Stainless Steel; Filter rings on Envirocone®; used to sample both liquid and vapor.	O'Neill et al. (1996)
Stainless Steel; Filter material used for discrete water samplers like the BAT Enviroprobe and the Hydropunch	Robertson et al. (1996)
Stainless Steel; Filter elements used in piezocone penetration testing	Campanella and Robertson (1988)
Sintered Steel; Filter collars on Envirocone®; used to sample both liquid and vapor.	O'Neill et al. (1996)
Sintered Steel; Envirocone uses sintered steel filter when taking liquid and vapor samples in clay; used only in soils with low abrasion. Sample is pumped to the surface for analysis (Teflon transfer line).	Piccoli and Benoit (1995); O'Neill et al. (1996)
Sintered Bronze; Filter element used in piezocone penetration testing	Campanella and Robertson (1988)
Carborundum; Filter element used in piezocone penetration testing	Campanella and Robertson (1988)
Aerolith-10; Filter element used in piezocone penetration testing	Campanella and Robertson (1988)
Splinted Metal Filters; Filter for vapor entry to soil gas sampling tube; tendency to clog in fine-grained soils.	Bratton et al. (1995)

Table 1.4. Non-Metallic Filter Elements for Direct Push Technology

Material and Application	Reference
Teflon®; Soil gas transfer line from cone penetrometer to gas sampling manifold at surface for VOC analysis. Cone push demonstration, April 1993, at DOE Hanford Site in Washington.	Lightner and Purdy (1995)
Teflon®; Soil gas sampling tubing to bring soil gas from cone penetrometer to analysis equipment at surface.	Bratton et al. (1995)
Teflon®; Sampling and flushing lines in Envirocone®.	O'Neill et al. (1996)
Teflon®; Filter elements used in piezocone penetration testing	Campanella and Robertson (1988)
PVC*; Direct push monitoring well placement; PVC used for casing and well screen.	Auxt and Wright (1995); Bratton and Timian (1995)
PVC; Direct push discrete water sampler; PVC filter screen used.	Bratton and Timian (1995)
PVC; Direct push monitoring well placement; PVC used for screen and casing.	Bratton et al. (1995)
HDPE**; Soil gas sampling tubing to bring soil gas from cone penetrometer to analysis equipment at surface.	Bratton et al. (1995)
Polypropylene; Filter elements used in piezocone penetration testing	Campanella and Robertson (1988)
Plastic; Filter for vapor entry to soil gas sampling tube; tendency to clog in moist clays.	Bratton et al. (1995)
Ceramic; Cemented Quartz Sand; Stone; Filter elements used in piezocone penetration testing (1988)	Campanella and Robertson (1988)

Note: *Polyvinylchloride
**High-density polyethylene

times lead to greater risk of contamination. In situations where contact time between the sampler filter and the fluid being sampled is short, the risk of sample contamination is minimized. Alternately, polymeric materials were most commonly used for the transfer of liquid and vapor from the sampler to the ground surface. The flexibility of polymeric tubing makes it ideal for sample transfer from depth to chemical analysis equipment located at the soil surface. As was the case with metals, sorption/partitioning of organics into polymeric materials is a function of contact time, so contact times between the sample and the polymeric sampling lines should be minimized in order to preserve sample integrity.

Filters Used in Cone Penetration Testing

The filter materials used in cone penetration testing have been optimized in terms of mechanical parameters, rather than in terms of chemical behavior. The hydraulic push of a cone into

the soil during piezocone penetration testing requires a filter that can withstand extreme physical abrasion from the adjacent soil, and pore fluid pressures as high as 50 atmospheres. In addition, piezocones measure pore pressures by filtering the fluid into a small cavity in the cone body which houses a pore pressure transducer. In this configuration, where a pressure is measured rather than a sample being taken, there is no concern about chemical contamination or fluid transfer, as is the case in environmental sampling. The main purpose of the filter in the measurement of pore pressures is the separation of fines from the fluid being measured, so the filter must efficiently separate solids from the fluid while retaining a permeability which is high enough to not interfere with fluid flow into and out of the cavity.

The materials used commonly as filter materials for the measurement of pore fluid pressures in cone penetration testing include stainless steel, high density polypropylene, and ceramic. In addition, sintered brass, aerolith-10, Carborundum, cemented quartz sand, stone, and Teflon® have also been used (Campanella and Robertson, 1988). Smits (1982) investigated the properties of both ceramic and sintered stainless steel filters for the measurement of dynamic pore pressures. He reported that ceramic filters suffered from abrasion in quartz sands and also experienced pore pressure noise in dense sands due to their low rigidity. Ceramic was also more brittle than other materials used for filter elements and could crack during penetration in dense soil deposits. In terms of sintered stainless steel, Smits (1982) reported that the filter surface was subject to smearing when pushed through sands and could also clog when pushed through fine-grained soils. However, Campanella and Robertson (1988) stated that many of the problems of abrasion and smearing have been overcome through improvements in the material properties of both stainless steel and ceramic. High-density plastics are commonly used because they are inexpensive and disposal, allowing change of the filter between soundings.

Summary of Chemical Compatibility Issues During Sampling

As applications for cone penetrometry and direct push technology become more wide-ranging, it is increasingly important to evaluate the filter and sample transfer line materials chosen for use in a specific tool. While materials like stainless steel, ceramic, Teflon®, and polypropylene have become standards in the industry, it is clear that both the mechanical and geochemical properties of the site being tested must be taken into consideration. For example, Teflon® would be the material of choice in environmental sampling for metal contamination at a site, while stainless steel is superior for the sampling of organics. In cases where filter exchange is not possible, the sampling contact time should be reduced to a minimum in order to limit the transfer of contaminants into or out of the sample solution. Filter materials used during DPT or CPT penetration are also constrained in terms of abrasion resistance, pore pressure resistance, and permeability considerations. In summary, filters used in cone penetration testing must withstand physical abuse without sacrificing permeability into the pore pressure transducer cavity, while filters used in geo-environmental sampling must withstand physical abuse, must be permeable, and must be chemically compatible with the site conditions.

Experiments and Modeling in Geoenvironmental Cone Penetration Testing

The work in this study examines two major issues in cone penetration testing, particularly for improved site characterization in geoenvironmental engineering, through the introduction of a new chemical sensor, and a more versatile approach to evaluating porewater dissipation tests in clays. Specifically, the work examines the development and laboratory testing of a new class of chemical detection sensors designed to measure the aqueous concentrations of aromatic hydrocarbons in-situ. The device which was tested is a miniaturized integrated optoelectronics sensor developed to detect

the BTEX chemicals (benzene, toluene, ethylbenzene, and xylene) during cone penetration testing. In addition, the response and interpretation of geoenvironmental data gathered from the cone pore pressure sensor are examined. The study develops a methodology to interpret the dissipation of piezocone pore pressure transducer measurements for the evaluation of the horizontal coefficient of consolidation (c_h) and permeability (k_h) of a soil deposit, both of which are geoenvironmental parameters important to the flow of water and transport of contaminants within the subsurface.

Chapter 2 provides a review of literature related to the dissipation behavior of the penetration pore water pressures that are generated during cone soundings in fine-grained soils. Additionally, current methods for the evaluation of the coefficient of consolidation and the permeability from porewater pressure decay are reviewed.

Chapter 3 examines the behavior of a miniaturized version of an integrated opto-electronic BTEX sensor tested in a silica sand soil/water matrix using a bench-top configuration. The sensor was initially enclosed in a prototype module which was compatible with soil testing and was evaluated using BTEX contaminants at a variety of concentrations. Related issues in the adaptation of the sensor to full-scale field cone penetration testing and environmental site characterization are discussed.

Chapter 4 focuses on the interpretation of pore pressure sensor data. It outlines the development of a dissipation model which uses a hybrid cavity expansion and critical state soil mechanics approach, combined with an analytical solution to the partial differential equation which governs radial consolidation around a cone penetrometer, in order to evaluate the coefficient of consolidation of normally-consolidated or heavily-overconsolidated clay soil deposits. The method evaluates the monotonically decreasing porewater pressure decay with time in soft clays and silts, as well as the dilatory dissipation behavior (an increase in pore pressure followed by a subsequent decrease as a function of time) which has been observed in heavily-overconsolidated clays.

Chapter 5 integrates shear wave velocity measurements gathered with the seismic cone penetrometer in order to make approximate evaluations of the in-situ void ratio of a clay deposit, and develops a methodology that combines data from the seismic piezocone penetration test with porewater pressure dissipation measurements to obtain estimates of the in-situ permeability. Here, the shear wave velocity is used to evaluate the constrained modulus ($D = 1/m_v$) and relates the coefficient of consolidation to the permeability ($k = c_h \gamma_w / D$). The estimation is verified by comparison with data collected at well-documented test sites.

It is hoped that the introduction of a new chemical-detection module and the improved interpretation of porewater pressure dissipation data will further promote the utilization and application of cone penetration testing in geoenvironmental practice.

CHAPTER 2

LITERATURE REVIEW

Introduction

In addition to the direct measurement of properties, the interpretation of data gathered from piezocone testing provides important information about the geoenvironmental properties of a soil deposit. In particular, evaluation of the properties which control the movement of pore fluid through a soil deposit can be performed through analysis of piezocone dissipation tests. This chapter provides a review of the methodologies available for the evaluation of the coefficient of consolidation and soil permeability from piezocone dissipation tests.

Evaluation of the Coefficient of Consolidation From Piezocone Dissipation Data

During a piezocone penetration test in fine-grained soils, significant pore pressures are generated in excess of the hydrostatic pore pressure. When the piezocone test is halted during penetration in clays, these pressures dissipate, and the measured variation of pressure with time relates to the coefficient of consolidation and the permeability of the deposit.

The coefficient of consolidation is an important parameter in both geotechnical and geoenvironmental engineering because it is a measure of the time-rate of response and flow characteristics of soils. In environmental applications, the coefficient of consolidation controls the dissipation of excess pore pressures generated in clay landfill liners when they are subjected to repetitive overburden loading through the application of waste materials, and is also directly related to the permeability and flow of fluid through the pore space of a soil. Consequently, it influences the advective transport of groundwater and contaminating chemical species through the subsurface. In traditional geotechnical applications, the coefficient of consolidation is an important parameter for estimating rates of settlement in foundation loading (Lutenegger et al. 1988), embankment construction (Hansbo et al. 1981), and for the design of wick drains to dewater a site (Robertson et al. 1988a). The permeability of a soil is paramount in groundwater flow applications and mass transport studies in geoenvironmental engineering. Because of this importance, this section reviews the relevant literature regarding existing methodologies for the evaluation of the coefficient of consolidation from piezocone dissipation tests.

Generation of Excess Porewater Pressures

Traditional analyses of penetration problems have been divided into the two general categories of shallow and deep penetration problems. Shallow penetration differs from deep penetration because the displaced volume of soil has more freedom of movement and is able to move out and up to the soil surface, similar to a footing bearing capacity failure. However, in deep penetration problems like cone testing, constraints on the displaced volume force deformation of the surrounding soil in mainly lateral directions (Houlsby and Teh, 1988). Researchers have noted that surface heave occurs in the initial driving of piles, but ceases to occur at large depths of pile penetration below the surface (Randolph and Wroth, 1979a). Consequently, at great depths, the soil surrounding a piezocone or a driven pile during deep penetration problems is forced to deform within a constrained volume surrounding the penetrometer. While the complete mechanism of failure surrounding a penetrating piezocone is not fully understood, it is generally accepted that cone soundings produce failure under the cone tip which is similar to the expansion of a spherical cavity in an elasto-plastic medium, and failure around the body of the cone which is similar to the expansion of a cylindrical cavity in an elasto-plastic medium (Torstensson, 1975; 1977; Battaglio et al., 1981).

Cone penetration also induces changes in the pore fluid conditions surrounding the penetrometer, especially in clayey soils which have a characteristic low hydraulic conductivity. For soundings which occur under undrained conditions, the change in pore pressure is a combination of changes in the mean octahedral normal stress, $\Delta\sigma_{oct}$, and octahedral shear stress, $\Delta\tau_{oct}$. The change in pore pressure due to the change in octahedral normal stress results from the displacement of soil and fluid by the penetrating cone, while the change in pore pressure due to the change in octahedral shear stress is due to the shear deformation of the soil adjacent to the cone body. Initial attempts to estimate the magnitude of pore pressure changes from the individual components were based on the approximate expression introduced by Henkel (1959):

$$\Delta u = \beta\Delta\sigma_{oct} + \alpha\Delta\tau_{oct} \qquad \textbf{Equation 2.1}$$

where Δu = change in pore pressure, $\Delta\sigma_{oct}$ = change in octahedral normal stress, $\Delta\tau_{oct}$ = change in octahedral shear stress, and α and β are Henkel's empirical pore pressure parameters, with β typically assumed equal to 1.0 in saturated clays (Roy et al., 1981). Under the cone tip, the largest change in magnitude of pore water pressure is due to the changes in mean normal stress and the relative changes in shear stress are small (<20%) in comparison (Baligh, 1986). However, along the shaft of the cone body, the shear stresses become a significant portion of the excess pore pressure change because the large octahedral stresses acting on the cone tip undergo stress relief at this location. Evidence suggests that the stress regime directly behind the cone tip is more significantly affected by the shear stress than the area located directly beneath the cone tip (Wroth, 1984; Campanella et al., 1986a).

The total magnitude of pore pressure measured in the piezocone test includes not only the excess pore pressure generated due to changes in the mean octahedral normal stress and in the octahedral shear stress, but also the hydrostatic pore pressure in the soil profile, and can be represented as follows:

$$u_m = u_o + \Delta u_{oct} + \Delta u_{shear} \qquad \textbf{Equation 2.2}$$

where u_m = the magnitude of pore pressure measured by the cone penetration test, u_o = hydrostatic pore pressure, Δu_{oct} = excess pore pressure due to changes in the mean octahedral stress, and Δu_{shear} = excess pore pressure due to changes in the octahedral shear stress (Figure 2.1). If the prevailing groundwater conditions are known, the hydrostatic pore pressure term can be calculated as $u_o = \gamma_w h_w$, where γ_w = the unit weight of water and h_w = the height to the water table above the reference depth z. This yields the following equation for excess pore pressure:

$$\Delta u_m = \Delta u_{oct} + \Delta u_{shear} \qquad \textbf{Equation 2.3}$$

where $\Delta u_m = u_m - u_o$ = the pore pressure generated in excess of hydrostatic pressure during a cone sounding. It is important to note that the penetration pore pressure is a total magnitude measurement and the contributions of the individual components (Δu_{oct} or Δu_{shear}) cannot be measured separately.

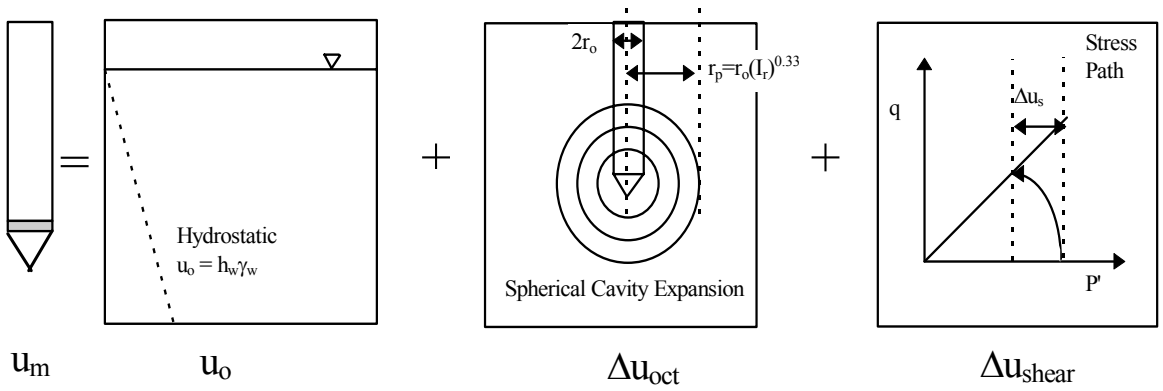

Figure 2.1. Components of Measured Pore Water Pressure During Cone Penetration
Note: $q = (\sigma_1-\sigma_3)$ and $p' = 1/3(\sigma_1'+\sigma_2'+\sigma_3')$

Pore Pressure Dissipation Behavior

When cone penetration is halted, the induced excess pore pressure will dissipate to the hydrostatic value in time. A typical pore pressure dissipation record shows magnitudes of porewater pressure monotonically decreasing with time from the initial reading, similar to the behavior seen during one-dimensional consolidation tests. This behavior is observed in normally- to lightly-overconsolidated clays (note: OCR = overconsolidation ratio = preconsolidation stress / effective vertical overburden stress = σ_p'/σ_{vo}'), regardless of the location of the pore pressure filter element on the penetrometer (Figure 2.2). The same behavior is observed in heavily-overconsolidated clays when the pore pressure filter element is located on the cone tip or face position (u_1). However, when measuring pore pressure dissipation in heavily-overconsolidated clays with the filter element located behind the cone shoulder (u_2), the pore pressures often exhibit dilatory behavior, by first increasing in magnitude, and then subsequently decreasing with time to hydrostatic values (Figure 2.3).

Dissipation curves from piezocone testing can be modeled to predict the coefficient of consolidation of the surrounding medium. The coefficient of consolidation incorporates the material properties which influence the rate of consolidation in a soil deposit, where the end of primary consolidation is defined as the dissipation of excess pore pressures to zero, or the decay of measured pore pressures to the hydrostatic value. Consequently, the coefficient of consolidation can be used as an indicator of soil behavior.

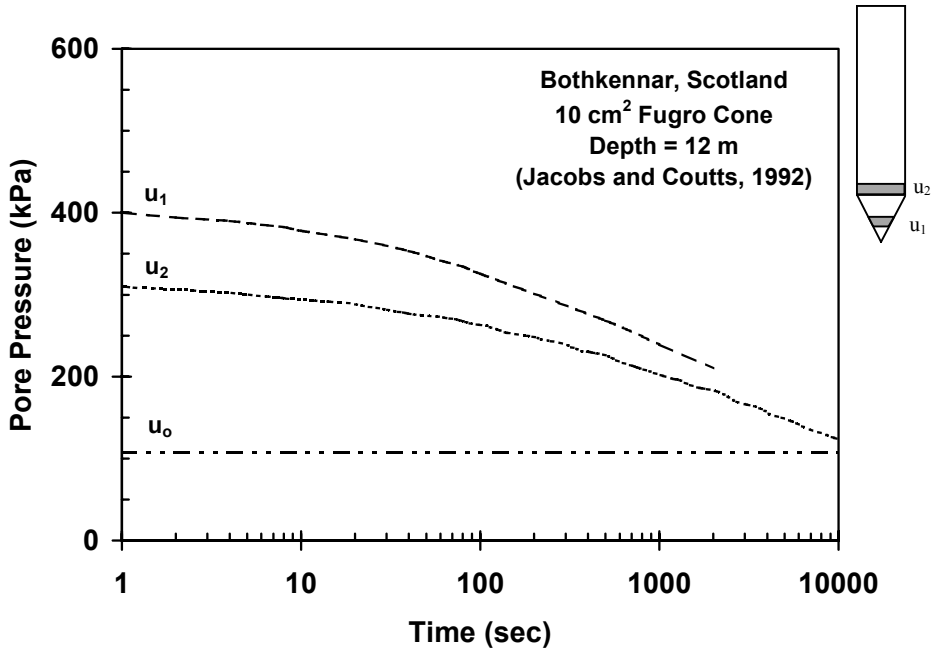

Figure 2.2. Dissipation in a Lightly-Overconsolidated Clay

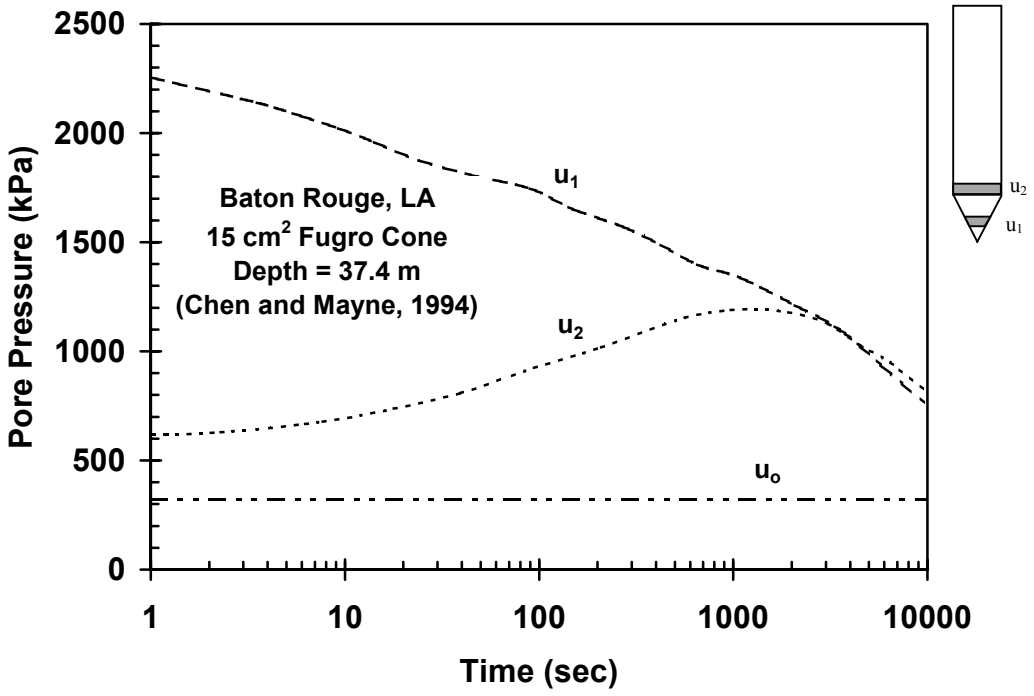

Figure 2.3. Dissipation in a Heavily-Overconsolidated Clay

An important difference to note in the comparison of piezocone-determined and laboratory-measured values of the coefficient of consolidation is that the process of cone testing significantly remolds the soil surrounding the cone. Consequently, during a piezocone dissipation test, consolidation takes place in a partially remolded soil, which differs from the laboratory case where consolidation takes place in a sampled, but not remolded soil specimen (Gillespie and Campanella, 1981). Additionally, the one-dimensional consolidation test, which is used to provide reference measurements of the coefficient of consolidation, restricts the deformation of the soil skeleton and the movement of pore fluid to the vertical direction, while experimental evidence in pile driving, wick drains, and cone testing shows that the movement of pore fluid corresponding to drainage tends to flow out radially (Randolph and Wroth, 1979a), rather than the vertical movement mandated in the Terzaghi consolidation test.

If the soil fabric is arranged isotropically, the horizontal and vertical values of the coefficient of consolidation will be the same; however, if the soil fabric is anisotropic, as is most commonly the case for platy clay particles, the two values will differ somewhat. In natural clays, however, the difference between horizontal permeability (k_h) and vertical permeability (k_v) is typically small (Tavenas et al., 1983b) as shown by Figure 2.4. Exceptions would be highly-stratified deposits and varved silts and clays where $k_h > k_v$. Another important difference between the methods of evaluation is that the one-dimensional consolidation test utilizes a very small sample of soil, while the cone test is performed in-situ in the deposit and is affected by a large volume of soil surrounding the cone. Finally, the one-dimensional consolidation test begins with a homogeneous initial distribution of excess pore pressure throughout the soil specimen, while the pore pressures resulting from a piezocone test have a radial gradient.

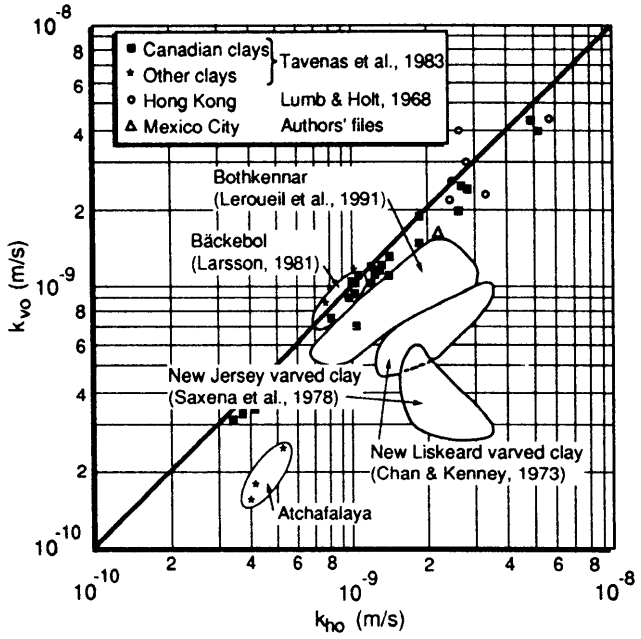

Figure 2.4. Relationship Between Horizontal and Vertical Permeability Measured on Natural Marine Clays in Constant Head Laboratory Tests (Leroueil and Jamiolkowski, 1991)

Radial versus Vertical Drainage

The drainage characteristics of a soil are an important component of the consolidation behavior which occurs during a pause in cone penetration. Clearly, in an unbounded soil medium, drainage will occur in all directions, away from the gradients induced by the piezocone or driven pile. Consolidation results from drainage in both the horizontal and vertical directions, and the coefficient of consolidation can vary significantly depending on the direction of flow. Previous studies of instrumented piles driven into soft clays showed that the major pore pressure gradients developed along the pile shaft in the radial direction rather than in the vertical direction (Bjerrum and Johannessen, 1961; Koizumi and Ito, 1967; Lo and Stermac, 1965; Randolph and Wroth, 1979a). Additionally, the carefully-instrumented St. Alban site has shown an increase in pore pressure at large radial distances away from a driven pile, which has been taken as further evidence of radial consolidation (Roy et al., 1981).

Levadoux and Baligh (1986) noted that results from the strain path method show that c_h controls the drainage behavior surrounding a cone penetrometer in all but the most extreme cases. Houlsby and Teh (1988) performed a sensitivity analysis using the strain path method in combination with a large strain finite element model and found that for $c_h \geq c_v$, the consolidation behavior is dominated by c_h, or radial drainage. Gillespie and Campanella (1981) investigated experimentally the influence of filter location on the consolidation characteristics surrounding the cone penetrometer. Their results showed that the dissipation around a cone with the filter located in the Type 2 position, shoulder location, was only slightly faster than dissipation when the filter was located 12.5, 25, or 38 cm behind the tip. This indicated that the horizontal component of drainage contributed strongly to consolidation around the penetrometer because the Type 2 position would be more strongly influenced by spherical drainage than would the other positions. Other authors have also noted that radial drainage is the controlling mechanism when the pore pressure filter was located on the shoulder (Kabir and Lutenegger, 1990; Teh and Houlsby, 1989). Consequently, the majority of solutions for consolidation around a penetrometer or a pile assume radial drainage dominates the dissipation behavior.

Type 1 versus Type 2 Dissipation

While dissipation curves can be recorded for pore pressure transducers located at both the Type 1 and Type 2 positions, the recorded Type 1 profiles are not always reliable due to stress relief on the tip during a halt in the cone sounding. A dissipation test is most commonly performed when the sounding is paused in order to add another rod for pushing. Typically, when the sounding is stopped, the drill rods lift slightly as the pressure from the drill rig is released. In the case of the Type 1 pore pressure transducer, the induced pressures show a discontinuous step (Figure 2.5), leading to inaccurate values for the induced pore pressure and dissipation profile. It is possible to procedurally lock the rods in place; however, a standard method of performing this for dissipation testing has not been established. The Type 2 readings are not affected by the stress release (Figure 2.5). In this study, the focus is on the pore pressure profiles obtained with Type 2 pore pressure transducers, which are insensitive to stress relief due to rod uplift, and because the shoulder pore pressure reading is necessary for the cone tip resistance correction.

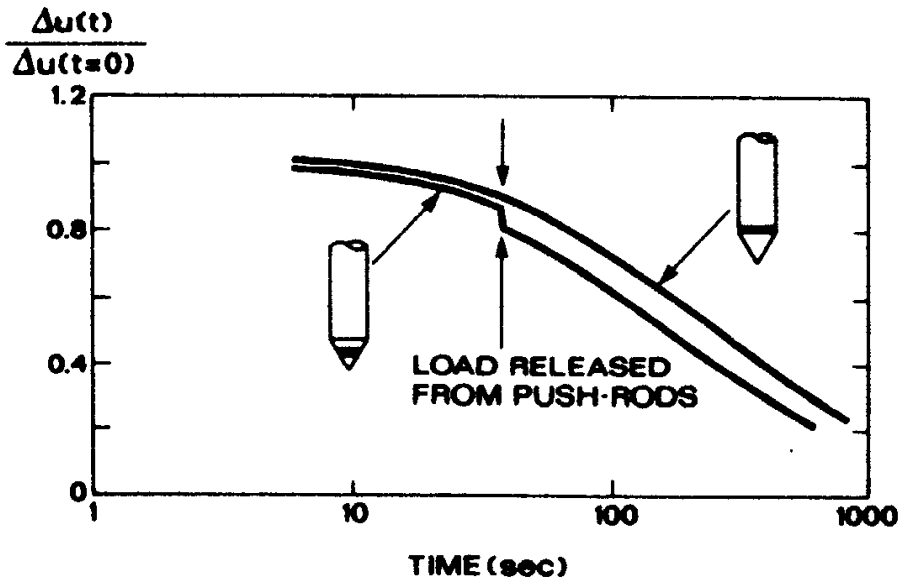

Figure 2.5. Load Release Behavior (Campanella and Robertson, 1988)

Existing Soil Models For Pore Pressure Dissipation

Excess pore pressures produced by the insertion of a cone penetrometer, or any penetrating probe, will in time reach equilibrium conditions, corresponding to hydrostatic pore pressure (u_o) when $\Delta u = 0$ (Figure 2.6). Many attempts have been made to model the change in pore pressure with time in order to obtain an in-situ estimate of the coefficient of consolidation. While the models have varied in their degree of complexity, ranging from the simple cavity expansion theory to the relatively complex strain path method, the predictive capabilities of the models are not significantly different. In all cases, the soil conditions which occur during cone penetration are extremely complicated; too complex to be modeled without significant simplifying assumptions.

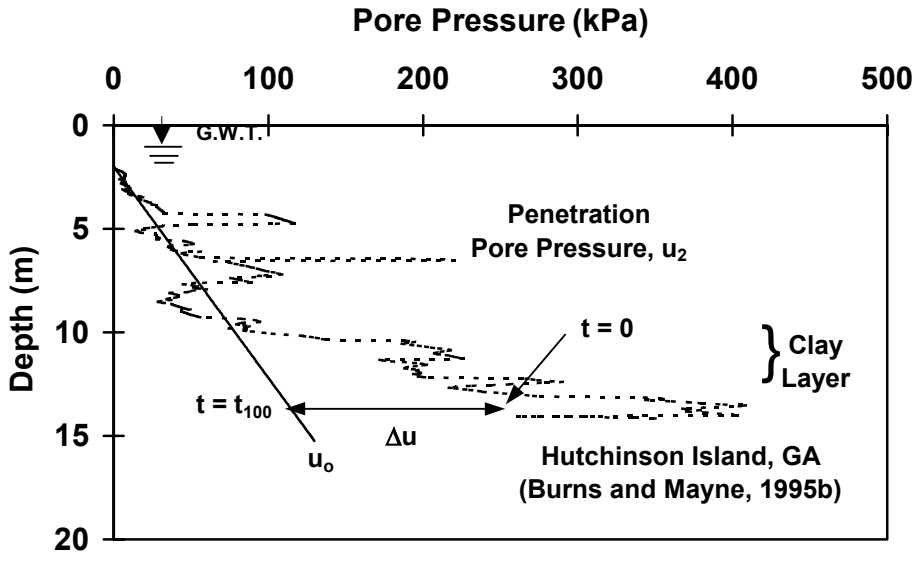

Figure 2.6. Dissipation of Excess Pore Pressures

Dissipation in Normally- and Lightly-Overconsolidated Clays

The first attempt to model the dissipation of excess pore pressures in fine-grained soils was made by Torstensson (1977) using cavity expansion theory (Hill, 1950; Vesic, 1972). (A more detailed review of cavity expansion theory is provided in Chapter 4.) The problem was represented as the expansion of either a cylindrical or spherical cavity in an elastic-perfectly plastic medium. By assuming that the soil failed in undrained shear and neglecting the volume change in the plastic zone, the radius of the plastic zone was calculated as follows:

$$r_p = r_0\left[\frac{E}{2(1+\nu)s_u}\right]^{\frac{1}{3}} = r_o\left[\frac{G}{s_u}\right]^{\frac{1}{3}} \qquad \textit{Spherical cavity} \qquad \textbf{Equation 2.4}$$

$$r_p = r_0\left[\frac{E}{2(1+\nu)s_u}\right]^{\frac{1}{2}} = r_o\left[\frac{G}{s_u}\right]^{\frac{1}{2}} \qquad \textit{Cylindrical cavity} \qquad \textbf{Equation 2.5}$$

where r_p = radius of the plastic zone, r_o = radius of the pore pressure probe, s_u = undrained shear strength, E = Young's modulus, ν = Poisson's ratio, and G = shear modulus. Assuming an isotropic and homogeneous soil, an impermeable cone/soil interface boundary, and no excess pore pressure change outside the plastic zone, the maximum excess pore pressure was calculated as follows:

$$\Delta u = \frac{4}{3}s_u \ln\left[\frac{E}{2s_u(1+\nu)}\right] = \frac{4}{3}s_u \ln\frac{G}{s_u} \qquad \textit{Spherical cavity} \qquad \textbf{Equation 2.6}$$

$$\Delta u = s_u \ln[\frac{E}{2s_u(1+\nu)}] = s_u \ln\frac{G}{s_u} \qquad \textit{Cylindrical cavity} \qquad \textbf{Equation 2.7}$$

In Torstensson's representation, the magnitude of pore pressures generated by insertion of the piezoprobe into the clay deposit was calculated as the value predicted by cavity expansion theory. This magnitude was then used as the initial condition for the solution of the consolidation equation. Boundary conditions included: 1) the cone is an impermeable boundary and 2) there is no increase in pore pressure outside the plasticized zone.

$$\frac{\partial u}{\partial t} = c_i \frac{2}{r}\frac{\partial u}{\partial r} + c_i \frac{\partial^2 u}{\partial r^2} \qquad \textit{Spherical Cavity} \qquad \textbf{Equation 2.8}$$

$$\frac{\partial u}{\partial t} = c_h \frac{1}{r}\frac{\partial u}{\partial r} + c_h \frac{\partial^2 u}{\partial r^2} \qquad \textit{Cylindrical Cavity} \qquad \textbf{Equation 2.9}$$

where c_i = coefficient for isotropic drainage and c_h = coefficient for radial drainage. Torstensson solved the Terzaghi consolidation equation using the method of finite differences. The solution was a one-dimensional, linear uncoupled analysis which predicted c_h by matching field dissipation curves with predicted dissipation curves. Linear analysis assumed that the value of the coefficient of consolidation did not change during consolidation, and the uncoupled model assumed that during consolidation the total stresses remained constant and the strains that occurred resulted from the change in pore water pressure only. The value of c_h was determined by matching the predicted dissipation with the measured dissipation at 50% consolidation, or t_{50} which is the time at which 50% of the excess pore pressures have dissipated. Torstensson stated that his method overestimated field values by a factor of approximately 2 for the normally-consolidated clay dissipation records which were used to verify the model; the number of sites modeled was not reported. Sample dissipation curves presented by Torstensson are shown in Figure 2.7; note that τ_f = the maximum undrained shear strength.

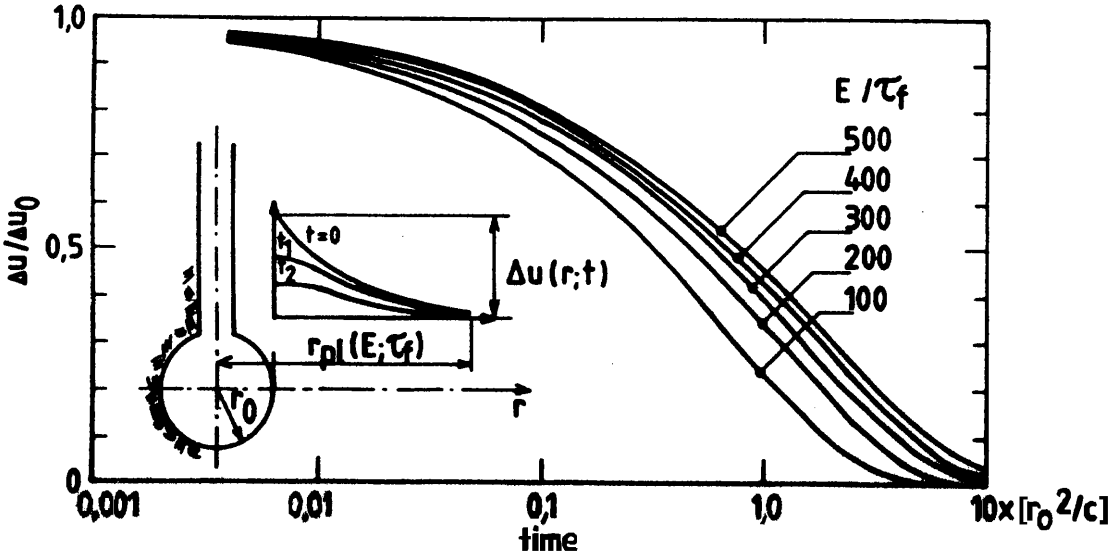

Figure 2.7. Spherical Cavity Dissipation Prediction (Torstensson, 1977)

Baligh and Levadoux (1980; 1986), Baligh (1985), and Levadoux and Baligh (1986) used the strain path method to predict the initial excess pore pressure distribution generated in normally- to lightly-overconsolidated insensitive clays by cone soundings, in combination with a two-dimensional linear uncoupled consolidation analysis. The strain path method was developed to model cone penetration because cavity expansion did not consider the strain paths followed by the soil elements surrounding the cone (Baligh, 1986). In this method, the cone was taken as a static penetrometer with soil flowing around it like a viscous fluid. Excess pore pressures generated by cone penetration were calculated by predicting soil velocities and strain rates using potential theory (assuming an ideal incompressible fluid flow and neglecting shearing resistance), integrating the strain rates along the stream lines to determine the strain history of the soil elements, and computing the deviatoric and shear-induced pore pressures using a total stress model (Levadoux and Baligh, 1986). While the strain path method was an approximate solution, it more accurately modeled the strain history of the soil elements surrounding the penetrometer than did cavity expansion; however, in the solution, an inequilibrium in stresses developed near the cone tip and the cone shoulder, making it necessary to correct the results using finite element methods (Houlsby and Teh, 1988). The two-dimensional uncoupled consolidation solution was performed using a finite element program. Sample dissipation curves presented by Levadoux and Baligh are shown in Figure 2.8. The model results were verified using dissipation test results in resedimented Boston Blue Clay. Comparisons were performed for dissipation surrounding cones with 60° and 18° tips, with pore pressure filters on the face and shoulder of the cone, and dissipation of the normalized excess pore pressure was determined to be a function of the time factor, $T \cong c_h(t/r^2)$, where r = cone radius.

Levadoux and Baligh (1986) also performed a finite element study which examined the effects of using a coupled solution to the consolidation equation rather than the uncoupled solution used in the one-dimensional consolidation tests. This solution accounted for the coupling between pore pressures and total stresses during consolidation. Results showed that the effect was significant for measurements made on the tip of an 18° piezocone, but as the location for measuring pore pressure was moved up the cone body away from the tip, the effect of coupling became negligible.

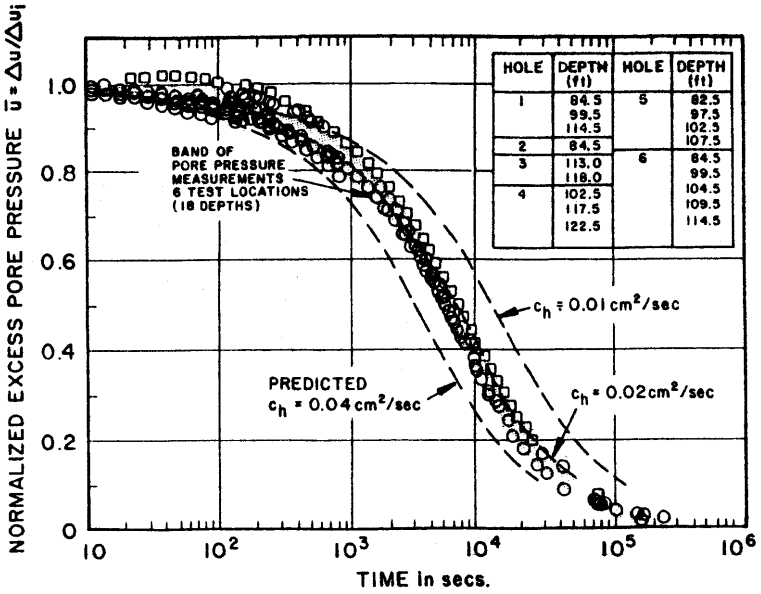

Figure 2.8. Strain Path Method Dissipation Prediction (Baligh and Levadoux, 1986)

While the current study is concerned with the excess pore pressure behavior surrounding piezocones, similar behavior has been observed in clay soils surrounding driven piles. The act of driving a pile into soil creates much the same type of failure as has been seen in the cone penetration test. Additionally, when driving piles in clays, excess pore pressures are generated which dissipate as the pore water migrates away from the pile. Randolph and Wroth (1979b) developed an analytical solution to the consolidation equation in order to model the effect of pore pressure dissipation behavior on the pile driving process. The solution was based on cavity expansion theory (elastic-plastic soil) and assumed that consolidation was governed by radial drainage away from the pile. The estimated decay was compared with data from two different pile sites from the literature and gave agreement within 10% of the measured values.

Gillespie and Campanella (1981) compared existing models from the literature with field data obtained at two different sites in British Columbia. Their comparisons showed that the cylindrical solution by Torstensson (1977), the analytical solution by Randolph and Wroth (1979b), and the two dimensional solution by Baligh and Levadoux (1980) provided reasonable predictions of c_h in lightly-overconsolidated clays when compared with laboratory values. However, the spherical solution by Torstensson was found to somewhat underpredict the value for the two sites examined which is in disagreement with the finding of Torstensson (1977).

Battaglio et al. (1981) modeled dissipation behavior around piezocone penetrometers by combining cavity expansion theory with Skempton's and Henkel's empirical pore pressure equations. Initial magnitudes of pore pressure were predicted using the following formulations:

$$\Delta u = s_u[\ln(I_r) + 0.577(3A_f - 1)] \qquad \textit{Cylindrical Cavity} \qquad \textbf{Equation 2.10}$$

$$\Delta u = s_u[\frac{4}{3}\ln(I_r) + 0.667(3A_f - 1)] \qquad \textit{Spherical Cavity} \qquad \textbf{Equation 2.11}$$

where A_f = Skempton's pore pressure parameter at failure and I_r = the rigidity index = G/s_u. The linear uncoupled consolidation equation was then solved using the method of finite differences until the predicted curve reached a minimum deviation from the measured field curve. The model was validated with data from two soft clays (Porto Tolle and Trieste) in Italy.

Jones and Van Zyl (1981) presented an empirical method for the evaluation of the coefficient of consolidation. The value of t_{50} obtained from dissipation tests was plotted versus the value of c_h measured in laboratory oedometer testing. Linear regression of the data yielded the following empirical relationship:

$$c_v = \frac{50}{t_{50}} \qquad \textbf{Equation 2.12}$$

where c_v is in (m^2/yr), and t_{50} is in (min). The authors noted that more data were needed to improve the relationship shown in Figure 2.9.

Senneset et al. (1982) assessed the coefficient of consolidation from piezocone dissipation tests using a logarithmic distribution of the initial excess pore pressure which was dissipated using a solution to the one-dimensional consolidation equation. The coefficient of consolidation was defined as:

$$c_h = \lambda_c r_o^{\,2} \left| \frac{\Delta u}{\Delta u_i} \right| \qquad \textbf{Equation 2.13}$$

where λ_c = pore pressure dissipation rate factor, r_o = filter radius, $\Delta u = du/dt$ = measured rate of dissipation, and Δu_i = initial excess pore pressure minus hydrostatic excess pore pressure = u_i - u_o. The solution was presented as normalized pore pressure curves which were a function of the rate factor for soft, medium, and stiff clays (Figure 2.10). The authors stated that the values estimated using this method gave best agreement when measured at stresses greater than the preconsolidation stress.

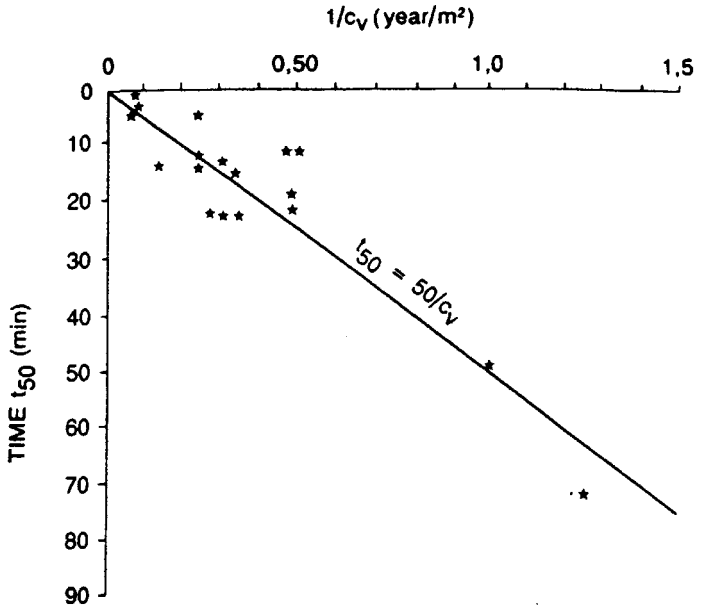

Figure 2.9. c_v - t_{50} Correlation (Jones and Van Zyl, 1981)

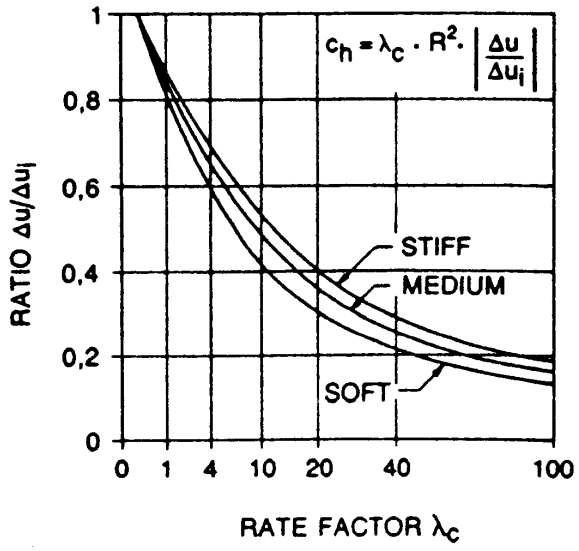

Figure 2.10. Pore Pressure Dissipation Rate Curves (Senneset et al., 1982)

Tavenas et al. (1982) drew on the relationship between c_h, k, and the modulus of deformability by developing an empirical correlation in order to evaluate t_{50} in Champlain Sea Clays. The proposed method measured the permeability from permeability tests and the preconsolidation pressure (σ_p') from oedometer tests. Then t_{50} was plotted versus $k\sigma_p'/\gamma_w$ in order to generate the correlation shown in Figure 2.11.

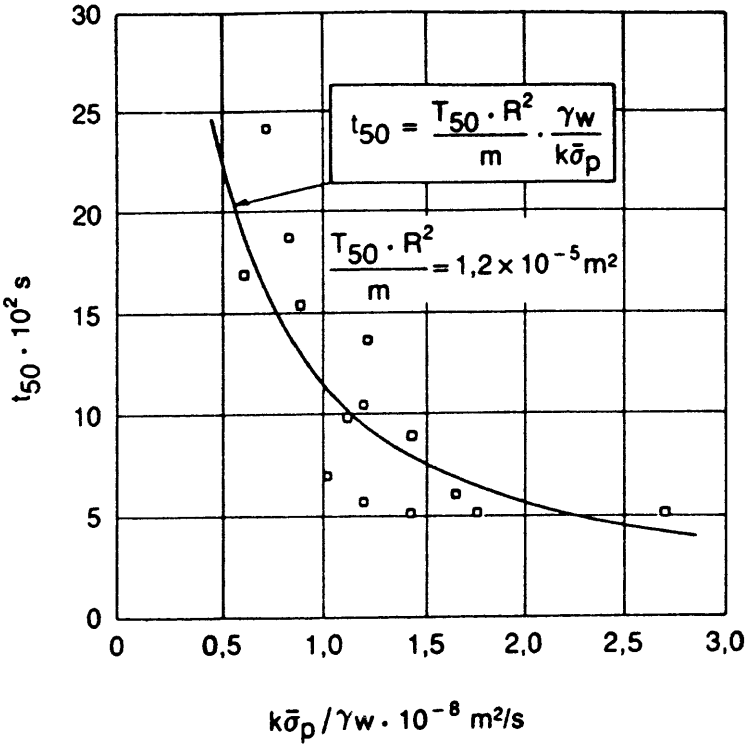

Figure 2.11. t_{50} Correlation in Champlain Sea Clays (Tavenas et al., 1982)

Tumay et al. (1982) evaluated the coefficient of consolidation from dissipation tests using a combination of theoretical values and experimental measurements. The authors used the strain path method (Levadoux and Baligh, 1980) together with experimental measurements obtained by Roy et al. (1979) to predict the initial pore pressure distribution generated due to cone penetration. Dissipation of these pore pressures was then performed using linear uncoupled finite element analysis. Evaluation of c_h for the soil deposit was performed using values obtained for t_{90}, rather than the more commonly used t_{50}. This was because the disturbance effects, anisotropy effects, and filter element location effects were less significant in the later consolidation phases. The influence of anisotropy was also taken into account. The method required estimation of two factors: first T_{90}, the point to which the dissipation curves converge, and second, T_{90}', the point to which straight line portions of the dissipation curves converge as shown in Figure 2.12. The authors stated that the ratio of the logarithms of these parameters equals a constant, A:

$$\frac{\log T_{90}}{\log T_{90}'} = A \qquad \textbf{Equation 2.14}$$

The time for 90% consolidation was estimated by:

$$t_{90} = 10 \exp A \log t_{90}' \qquad \textbf{Equation 2.15}$$

where t_{90} = time for 90% consolidation, and t_{90}' = time for 90% dissipation of straight line portion. Finally, the coefficient of consolidation was calculated by:

$$c_h = \frac{T_{90}}{t_{90}} r^2 \qquad \textbf{Equation 2.16}$$

where r = probe radius. Values evaluated by this method were within ten to twenty times the values measured in laboratory consolidation testing.

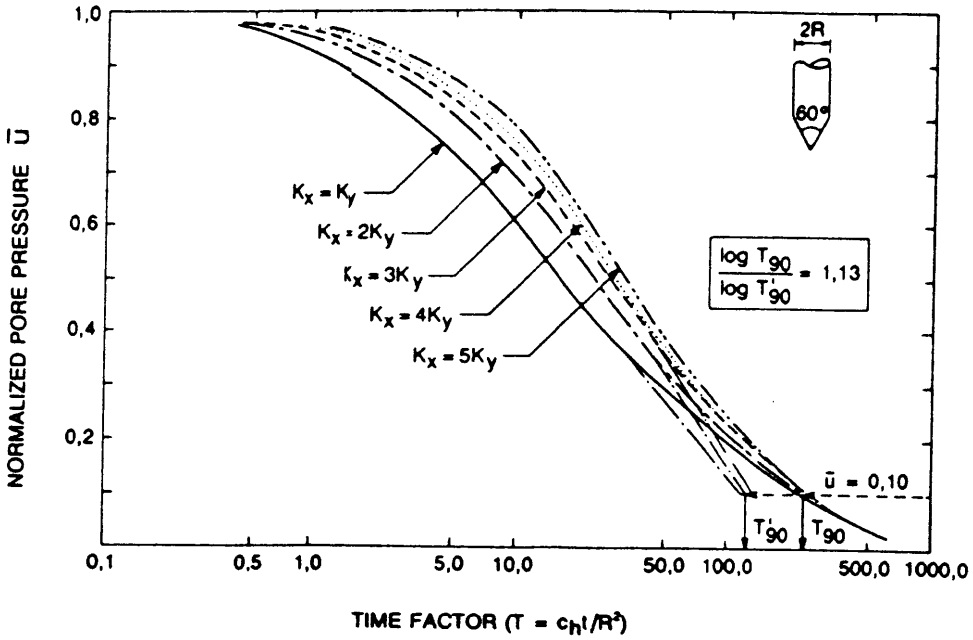

Figure 2.12. Pore Pressure Dissipation With Anisotropy (Tumay et al., 1982)

Tumay et al. (1985) and Acar and Tumay (1986) performed an assessment of the steady-state penetration of a cone penetrometer. The soil was treated as a non-compressible, inviscid fluid, and the solution analytically modeled the strain rate field, and the strain rates, surrounding the cone during penetration in very soft fine-grained soils. When combined with the time history of strains, the method could be used to predict the pore pressures generated by cone penetration, although that was not done in the study presented.

Gupta (1983) and Gupta and Davidson (1986) predicted the initial pore pressure developed around a cone penetrometer by modeling a series of spherical cavity expansions which propagated as the cone was advanced into the soil. Excess pore pressure was calculated using Vesic's logarithmic distribution (Vesic, 1972) which was given as follows:

$$\Delta u_B = \frac{(u_A - u_{oA})[0.943\alpha_f + 4\ln(\frac{r_{plastic}}{r_B})}{[0.943\alpha_f + 4\ln(\frac{r_{plastic}}{r_A})]}$$ **Equation 2.17**

where Δu_B was the excess pore pressure at any point B within the spherical cavity, u_A = the pore pressure measured at point A, u_{oA} = the hydrostatic pore pressure at point A, $r_{plastic}$ = the radius of the plastic zone = $(G/s_u)^{0.333}$, α_f = Henkel's pore pressure parameter at failure (= 0.707[3A_f - 1]), and A_f = Skempton's pore pressure parameter at failure. Additionally, they accounted for the fact that dissipation began to occur before the cone reached the location where the dissipation test was performed. Dissipation was modeled using an alternating direction implicit finite difference solution to the linear uncoupled consolidation equation with both radial and vertical drainage components. The initial variables for the prediction, G/s_u and A_f, were determined from field and lab tests, and the dissipation curves were plotted as a function of the time factor, $T_{50} = c_h t_{50}/R^2$, where t_{50} = the time to achieve 50% consolidation and R = the expanded cavity radius. The model was calibrated using data from three sites and their predicted results were within approximately two to five times the laboratory results. Sample dissipation curves presented by Gupta and Davidson are shown in Figure 2.13.

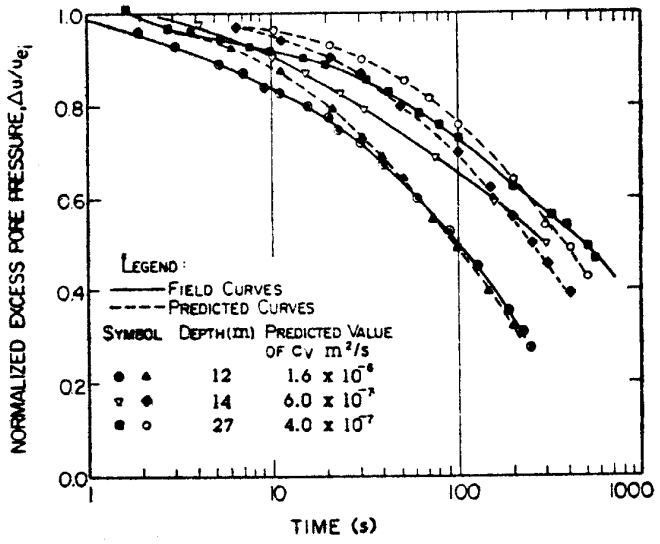

Figure 2.13. Successive Spherical Cavity Formation Dissipation Prediction (Gupta and Davidson, 1986)

Kabir and Lutenegger (1987; 1990) performed a comparison of oedometer-measured values of the horizontal and vertical coefficient of consolidation with piezocone predicted values using solutions proposed by Torstensson (1977), Baligh and Levadoux (1986), and Gupta and Davidson (1986) at two medium stiff clays sites: a soft Leda clay deposit in New York, and a soft alluvial deposit in Nebraska. Their results showed that the two former solutions agreed well with the laboratory values at low percentages of consolidation only, the third method gave agreement in both cases.

Houlsby and Teh (1988) modeled the dissipation of excess pore pressures around a piezocone using the strain path method combined with a large strain finite element analysis. Their analysis modeled the clay deposit as an incompressible elastic-perfectly plastic material and used uncoupled consolidation theory to model pore pressure dissipation around the cone. The finite element model was performed in order to account for the lack of stress equilibrium generated in the strain path method; the solution from the strain path method was taken as the initial state of stress in the model, the cone was held static and forces were applied incrementally in order to balance the forces, and then the cone was penetrated using a large strain finite element simulation.

Results from the method were combined with Henkel's estimate of pore pressure (Equation 2.1) in order to estimate the magnitudes of pore pressure during cone penetration. The linear uncoupled consolidation equation was then solved using an alternating direction implicit finite difference method. They found that the shear stress contribution was minimal to the overall magnitude of pore pressure surrounding the cone due to the fact that overconsolidation was not taken into account. Results showed that the consolidation rate predicted at the cone shoulder was similar to the consolidation rate predicted by cylindrical cavity expansion theory. However, at the tip, the predicted rate was faster than cylindrical theory and along the shaft, the predicted rate was slower than cylindrical theory due to differences in prediction of the mean stress gradients along the length of the cone (Houlsby and Teh, 1988). Because the time factor is a function of rigidity index, the authors chose to present the dissipation of pore pressure as a function of a modified time factor, T^*:

$$T^* = \frac{c_h t}{r^2 \sqrt{I_r}} \qquad \textbf{Equation 2.18}$$

where r = the cone radius.

Teh and Houlsby (1991) performed a combined strain path finite element method analysis of pore pressure dissipation based on dissipation data in sensitive marine clay in Quebec reported by Roy et al. (1981). The predicted rate of dissipation agreed quite closely with the field values for both the tip and shaft locations. The method closely predicted the magnitude of pore pressure developed along the shaft of the penetrometer, but underpredicted the magnitude of pore pressure acting at the cone tip by approximately 20%.

Teh and Houlsby (1991) also analyzed cone penetration using the strain path method alone. This analysis showed that the strain path method predictions of soil straining at large radial distances away from the cone tip were qualitatively similar to those predicted by cylindrical cavity expansion; however, neither method could fully represent the complex conditions at the tip of the cone. Sample dissipation curves presented by Teh and Houlsby are shown in Figure 2.14 for a rigidity index of equal to 100. These curves are plotted as a function of the dimensionless Time Factor, $T = c_h t/r^2$, where r = cone radius. Dissipation curves specific to a Type 2 cone are shown in Figure 2.15 where the results are plotted against the dimensionless Time Factor, T^*, where $T^* = T(I_r)^{-0.5}$. Incorporating the influence of the rigidity index unified the dissipation curves for values of I_r ranging from 25 to 500 into essentially a single relationship. The proposed solution was used to evaluate the coefficient of consolidation as a function of the time factor, the filter element location, the time needed to reach the given level of dissipation, the cone radius, and the rigidity index of the soil.

The solution proposed by Teh and Houlsby (1991) was evaluated by Robertson et al. (1992) through a comparison of the estimated values of coefficient of consolidation with lab measured values at many sites throughout the world. Additionally, Schnaid et al. (1997) used the method to

evaluate the coefficient of consolidation at two sites in South America and in calibration chamber results obtained at the University of Oxford. Both studies found that the most reliable predictions resulted from pore pressure data gathered at the cone shoulder.

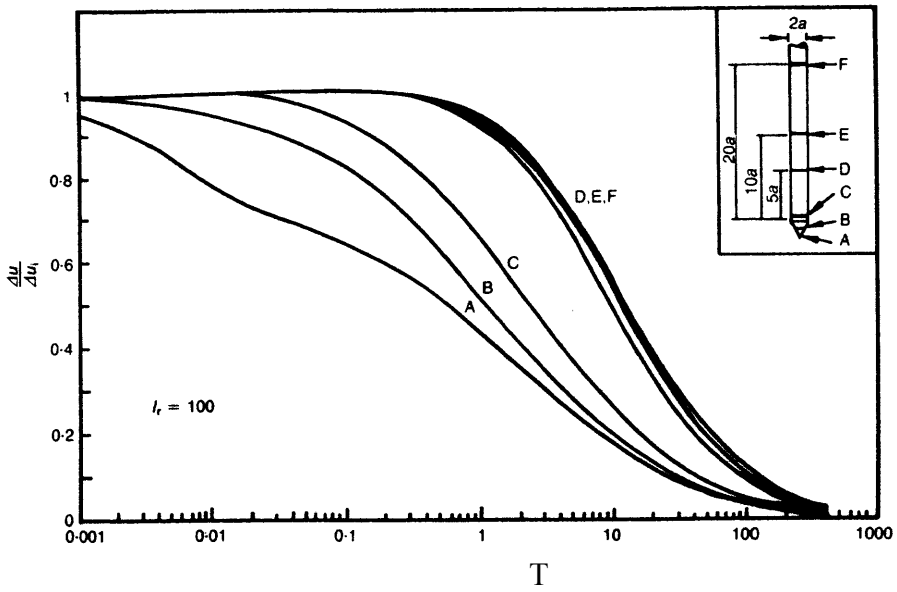

Figure 2.14. Dissipation Prediction at Multiple Locations (Teh and Houlsby, 1988)

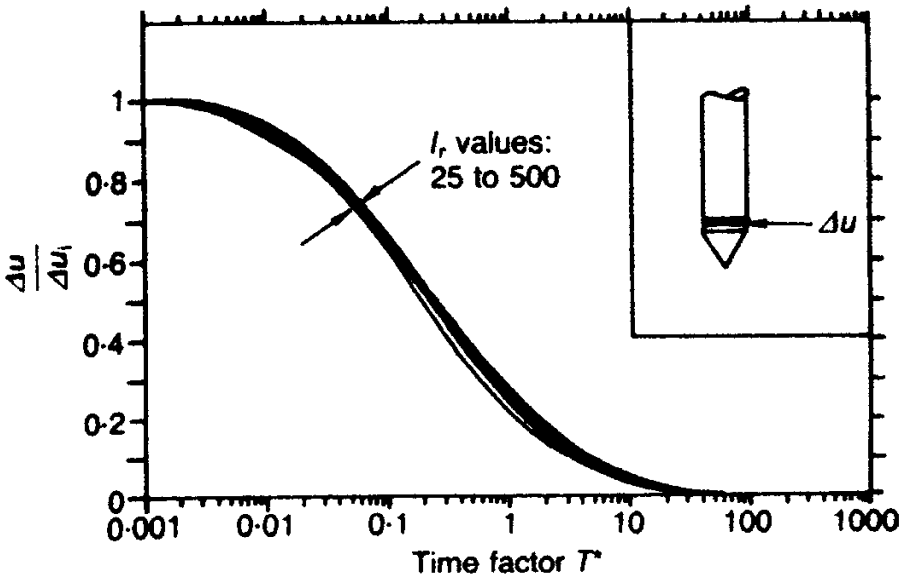

Figure 2.15. Dissipation Prediction for Type 2 Cone (Teh and Houlsby, 1991)

Dislocation theory has also been proposed for evaluating piezocone dissipation data (Elsworth, 1990; 1993). In this method, cone penetration was modeled as a moving volumetric dislocation. The advancement of the cone was treated as a point dislocation of equivalent volume which generated accompanying pore pressure increase and the soil was modeled as a linear elastic material. In dislocation theory, the rate of pore pressure build up at the tip was a function of the penetration rate of the cone, and the coefficient of consolidation and soil permeability were evaluated from the predicted pore pressure buildup and subsequent dissipation. However, the theory was not able to predict the coefficient of consolidation for pore pressures measured on the shaft because it predicted that the dissipation along the shaft was controlled, not by the material parameters surrounding the cone, but by the cone penetration rate and the distance the filter was located up the shaft from the tip. The solution was verified at two normally- to lightly-overconsolidated clay sites and gave general agreement within a factor of four for the coefficient of consolidation. The method overestimated the in-situ permeability by approximately two orders of magnitude.

Dissipation in Heavily-Overconsolidated Clays

If the porewater filter elements are properly saturated, dissipation curves in normally-consolidated or lightly-overconsolidated clays always exhibit a monotonic dissipation behavior: that is, magnitude always decreasing with time, when the pore pressure filter is located in either the Type 1 or Type 2 location. Additionally, heavily-overconsolidated clays exhibit standard monotonic dissipation curves when the filter is in the Type 1 location. Sully and Campanella (1994) designate these curves as Type I curves (Figure 2.16). However, in a heavily-overconsolidated clay when the filter is in the Type 2 location, the dissipation curves can be dilatory, showing an initial increase in magnitude followed by a subsequent decrease in magnitude with time (Davidson, 1985; Lutenegger and Kabir, 1988; Sully and Campanella, 1994; Campanella et al., 1986a; Chen and Mayne, 1994). Sully and Campanella (1994) designate these curves as Type II (initially above hydrostatic, increases, then decreases to hydrostatic); Type III (initially below hydrostatic, increases above hydrostatic, then decreases to hydrostatic); or Type IV (initially below hydrostatic, increases to hydrostatic) as illustrated by Figure 2.17. Assuming that the pore pressure filter was properly saturated before the test was begun, the dilatory dissipation behavior appears to be characteristic of dissipation behavior in heavily overconsolidated and fissured clays. Previous solutions based on cavity expansion, strain path, and finite element methods only provide solutions for the monotonic decay, not for the observed dilatory behavior.

Davidson (1985) reported the results of nine piezocone soundings performed in a heavily overconsolidated clay in Florida. All of the profiles showed an increase in pore pressure, followed by a decrease with time. Davidson attributed the phenomenon to the fact that the large normal stresses which were developed during cone penetration were relieved behind the tip of the cone where large shear stresses also developed. These large shear stresses forced the excess pore pressure negative during penetration; however, when penetration was stopped, the negative values were consumed by the inflow from the higher pressure zone developed at the tip of the cone.

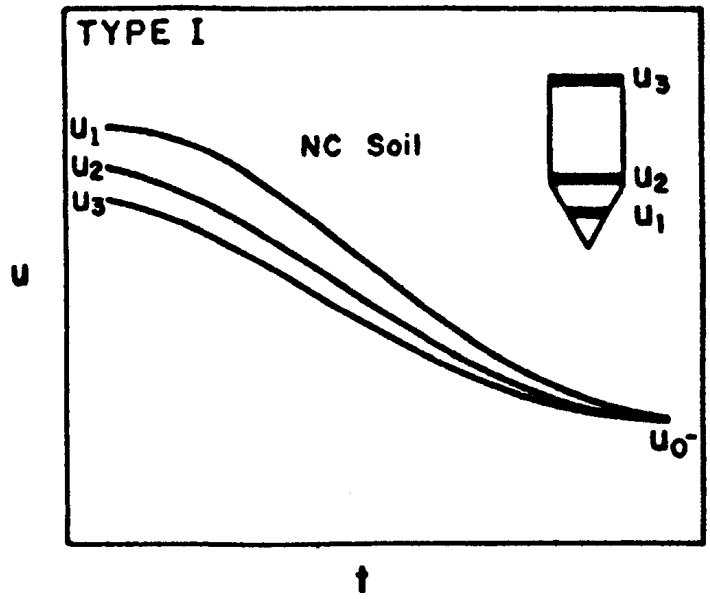

Figure 2.16. Pore Pressure Dissipation in Normally Consolidated Clays (Sully and Campanella, 1994)

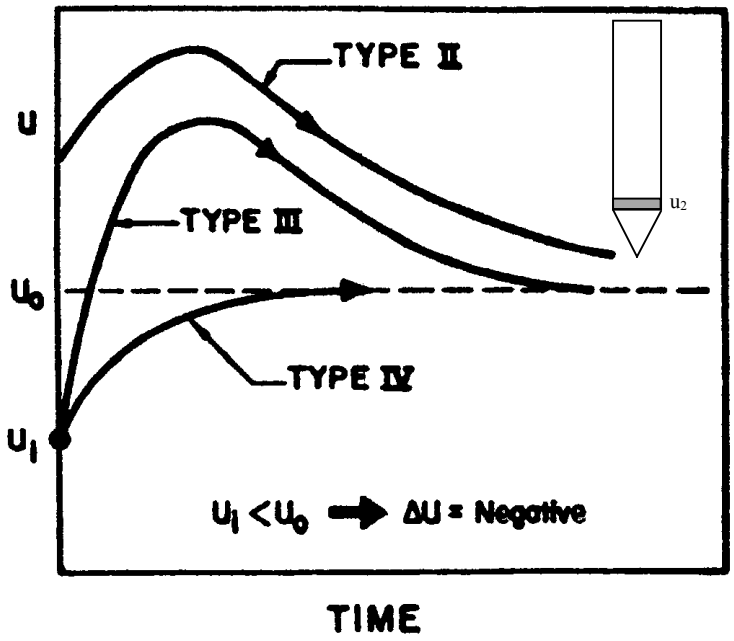

Figure 2.17. Pore Pressure Dissipation for Shoulder Piezocone Elements in Heavily Overconsolidated Clays (Sully and Campanella, 1994)

Sully and Campanella (1994) reported the results of dissipation tests at one stiff overconsolidated clay site where non-standard dissipation behavior was observed. The authors stated that the dilatory behavior was the result of pore pressure redistribution resulting from the large gradients induced in overconsolidated soils. For the dissipation curves in which pore pressures first increased and then decreased, they suggested an empirical offset procedure by taking the maximum pore pressure value reached during the dissipation test as the peak value, adjusting this value to time

zero, and adjusting all other time values on this basis. Subsequent evaluation of c_h for the remaining monotonic decay was performed using the method proposed by Teh (1987).

Similar dilatory dissipation behavior has been observed at clays sites during the driving of piles in clays. Coop and Wroth (1989) document pore pressures which increase and then decrease after the driving of cylindrical steel piles in the heavily overconsolidated Gault clay deposit at Madingley, England. The site was instrumented with a series of piezometers which recorded negative pore pressures in addition to the overconsolidated dissipation behavior. Likewise, the dilatory behavior during pile driving was observed by Lehane and Jardine (1994) in the stiff glacial clay deposit at Cowden, England.

Chronological Development of Pore Pressure Dissipation Modeling

A listing of the historical developments in pore pressure dissipation modeling to date is given in Table 2.1. In summary, numerous methods exist to evaluate the coefficient of consolidation from piezocone dissipation data. All prior methods only address dissipation tests exhibiting the monotonic decrease of porewater pressure with time. For the most part, the solutions can be divided into two categories: those which use cavity expansion to predict the initial pore pressure distribution and those which use the strain path method to predict the initial pore pressure distribution. All solutions then dissipate the excess pore pressures using consolidation theory, either in one or two dimensions. The strain path method was developed in order to accurately model the strain paths which the soil elements surrounding the cone penetrometer follow; however, the method incurred an inequilibrium of stresses at the cone tip which must be corrected. Alternately, cavity expansion models the advance of a cone penetrometer as the expansion of either a sphere or cylinder from zero radius to the radius of the probe. Neither the strain path method nor cavity expansion theory are capable of completely modeling the soil conditions during cone penetration, and in reality, the two methods yield similar results for the prediction of the coefficient of consolidation. The solution proposed by Houlsby and Teh is the most commonly used, most likely due to the ease of use of the normalized chart solution presented for the evaluation of c_h.

The method of Sully and Campanella (1994) addressed the dilatory pore pressure profiles by suggesting an empirical offset procedure for the evaluation of c_h. The proposed method is not supported on a theoretical basis, and has not been extensively tested in order to verify its applicability.

Summary

This section provided a review of the current methodologies available to evaluate the coefficient of consolidation from piezocone dissipation tests. Dissipation data recorded surrounding driven piles in clay were also included in the review because the soil behavior in pile tests is quite similar to that seen during the cone penetration test. While the available models differ significantly in their level of complexity, there are no models available which incorporate all aspects of soil behavior during a cone sounding due to the complex nature of penetration.

Table 2.1. Historical Development of Piezocone Dissipation Modeling*

Reference	Cavity Type	Soil Model	Initial Pore Pressure, Δu_i	Consoli-dation	Comments
Soderburg (1962)	Cylindrical, radius R	Elasto-plastic	$\Delta u/\Delta u_i = R/r$	1-D	Consolidation surrounding driven piles; Finite Difference
Torstensson (1975, 1977)	Cylindrical Spherical	Elasto-plastic	$\Delta u_i = 2s_u \ln(r_p/r)$ $\Delta u_i = 4s_u \ln(r_p/r)$	1-D	No shear stresses; Finite Difference
Randolph and Wroth (1979b)	Cylindrical	Elasto-plastic	$\Delta u_i = 2s_u \ln(r_p/r)$	1-D	Consolidation surrounding driven piles; Analytical
Baligh and Levadoux (1980); Levadoux and Baligh (1986)	Piezocone Model	Non-linear	From strain path method; Total stresss soil model	2-D	
Battaglio et al. (1981)	Cylindrical Spherical	Elasto-plastic	$\Delta u_i = 2s_u \ln(r_p/r)$ $\Delta u_i = 4s_u \ln(r_p/r)$	1-D	Shear by empirical method; Finite Difference
Jones and Van Zyl (1981)	n/a	Empirical approach	n/a	n/a	Correlation between measured t_{50} and oedometer measured values of c_h
Kavvadas (1982)	Piezocone Model	Non-linear	From strain-path method; Effective stress-strain model	1-D	
Senneset et al. (1982)	Cylindrical	Elasto-plastic	$\Delta u_i = 2s_u \ln(r_p/r)$	1-D	
Tumay et al. (1982)	Piezocone Model	Linear	From strain path method; Experimental data	1-D	
Gupta and Davidson (1986)	Piezocone Model	Elasto-plastic	Modified cavity expansion; dissipation as cone penetrates	1-D	Isotropic and anisotropic
Soares et al. (1987)	Piezocone Model	Non-linear	Corrected by visual examination and regression analysis	2-D	
Whittle (1987)	Piezocone Model	Non-linear	From strain-path method; Effective stress-strain model	1-D	
Houlsby and Teh (1988); Teh and Houlsby (1991)	Piezocone Model	Non-linear	Predicted by large strain finite element analysis and strain path method	1-D	Finite Difference
Elsworth (1990; 1993)	Point Dislocation Theory	Elasto-plastic	From point dislocation theory	2-D	Not applicable for u_2 measurements
Aubeny (1992)	Piezocone Model	Non-linear	From strain path method; Effective stress-strain model	2-D	Coupled consolidation
Sully and Campanella (1994)	Piezocone Model	Non-linear	Predicted by large strain finite element analysis and strain path method	1-D	Empirical time shift to u_{max} for OC dissipation
Burns and Mayne (1995a)	Spherical	Elasto-plastic	$\Delta u_{oct}=4s_u \ln(r_p/r)$ $\Delta u_{shear}=\sigma_{vo}'[1-(OCR/2)^{0.8}]$	1 D	Incorporates shear stresses; models OC dissipation; Finite Difference
Burns (1997) This Study	Spherical	Elasto-plastic	$\Delta u_{oct}=4s_u \ln(r_p/r)$ $\Delta u_{shear}=\sigma_{vo}'[1-(OCR/2)^{0.8}]$	1 D	Incorporates shear stresses; models OC dissipation; Analytical

*Modified after Lunne et al. (1992) and Jamiolkowski (1995)

Evaluation of Soil Permeability

In addition to the coefficient of consolidation, soil permeability is another important factor in both geotechnical and environmental engineering which can be obtained through the interpretation of piezocone test data. In geotechnical engineering, the permeability of the soil is used in earth dam design, dewatering considerations, and in seepage and slope stability problems. Additionally, the permeability controls soil behavior, in terms of drained versus undrained response with respect to rate of loading, during in-situ and laboratory testing. In environmental applications, the permeability of a soil controls the advective transport of both groundwater and contaminating chemicals in the subsurface environment. Consequently, it is a critical factor in many design instances. The permeability of a soil is commonly measured both in the laboratory using small-scale specimens, and in the field using borehole techniques, such as pumping tests.

There are several advantages to measuring the permeability of a soil in-situ, including the fact that testing is performed on large quantities of soil, the geochemical regime is not disturbed, the temperature is the same, and there is no disturbance due to sampling and transportation. In-situ devices test a large portion of the subsurface soils during measurement, as opposed to laboratory testing methods which rely on small, high-quality specimens. There are also a number of disadvantages to in-situ testing methods, the most significant of which include uncontrolled boundary conditions and disturbance due to probe penetration. However, the advantages to in-situ measurement of permeability are significant enough to warrant the use of field testing methods. This section focuses on the review of methods to evaluate the value of the coefficient of permeability using laboratory methods, field methods, and piezocone testing.

Coefficient of Permeability

In geotechnical engineering, the term permeability (k) has the units of (L/T) and is used to represent the ease with which water flows through a porous medium. The coefficient of permeability assumes that the permeant fluid is water. However, other disciplines, including hydrogeology and environmental engineering, use the term hydraulic conductivity to refer to this property. The term intrinsic permeability, k^*, is then used to refer to the properties of the soil alone by factoring out the effect of fluid viscosity; this term has units of (L^2). The permeability is defined as:

$$k = \frac{q}{Ai} \qquad \textbf{Equation 2.19}$$

where k = the coefficient of permeability in geotechnical engineering terminology and q = flow rate (L^3/T), A = cross-sectional area (L^2), and i= hydraulic gradient. The permeability and the hydraulic conductivity are related by the following:

$$K = \frac{k^* \rho g}{\mu} = k \qquad \textbf{Equation 2.20}$$

where K = the hydraulic conductivity (L/T) in hydrogeology and environmental engineering and k^* = intrinsic permeability (L^2), ρ = fluid mass density (MT^2/L^4), μ = dynamic viscosity (MT/L^2), and g = the acceleration due to gravity (L/T^2). Throughout this chapter, the term permeability (k) will be used and is assumed equivalent to the term hydraulic conductivity.

Influence of Soil Parameters

The permeability of a soil is dependent on a variety of soil characteristics including particle size, void ratio, mineralogy (in clays), fabric, and saturation. Additionally, the diameter of soil particles has been related to the permeability of a soil deposit. In particular, the permeability has been linked proportionally to the square of D_{10}, where D_{10} is the equivalent diameter at which 10% of the soil particles are finer. For sands, Hazen developed the following relationship relating the permeability to D_{10} (Lambe and Whitman, 1969):

$$k = 100 D_{10}^{\,2} \qquad \textbf{Equation 2.21}$$

where k is in cm/s and D_{10} is in cm. Soils with a wide gradation of particle sizes can pack more efficiently, leading to smaller diameter pore sizes which reduce the flow of fluid.

The void ratio, e, is another parameter which affects the permeability of a given soil. The void ratio is defined as the ratio of the volume of the voids to the volume of the solids; consequently, an increase in the void ratio, or void space, will lead to an increase in the permeability of a given soil (Lambe, 1951).

The mineralogy and fabric of a soil deposit are most important in the behavior of clay soils. In general, clay minerals with sodium as the exchangeable cation tend to have lower permeabilities than other clay minerals (Lambe and Whitman, 1969). Particle size is also important for clays, with montmorillonite showing a much lower permeability than kaolinite. Additionally, the fabric affects the behavior, with clays which are in a flocculated state having much higher permeability values than do clays in a dispersed state.

The other major parameter which influences the measured permeability of a soil is the degree of saturation. In geotechnical engineering, the saturation is defined as the ratio of the volume of the water to the volume of the voids, $S = V_w/V_v$. Permeability is a direct function of the degree of saturation, with an increase in saturation causing an increase in permeability (Lambe, 1951).

Measurement of the Permeability of Soils

Many different methods, both laboratory and field, exist for the determination of the permeability of a soil. Additionally, the permeability will vary when measured using different testing devices or different boundary conditions. A brief review of the methods currently used to evaluate the permeability of a soil deposit follows.

Laboratory Measurement of Permeability

Laboratory permeability testing can take many forms including testing in fixed-wall or flexible-wall chambers, constant head or variable head testing, and oedometer or triaxial chamber testing. Daniel et al. (1985) performed an experimental comparison between fixed-wall and flexible-wall permeameters. It was concluded that rigid-wall permeameters were inexpensive, simple, compatible with organic liquids, and did not need high confining stresses; however, the rigid-wall devices did not allow complete control over stresses, did not allow measurements of deformability, were difficult to use in terms of soil placement, and had a potential for sidewall leakage. In contrast, flexible-wall permeameters which conform to the soil specimen minimized sidewall leakage, allowed control of applied stresses, allowed measurements of deformation, allowed sample backpressuring, and could test a range of sample diameters. Disadvantages to the flexible wall permeameters included a higher cost, membrane incompatibility with organic liquids, and the need for high confining pressures at large hydraulic gradients.

Another variation in laboratory testing is the choice between falling head or constant head testing. Falling head tests are performed with a variable pressure head exerted on the soil sample, while constant head tests maintain the pressure head at a constant value.

Field Measurement of Permeability

Field permeability tests were developed because the soil tested in laboratory permeability devices were conducted on small specimens. Field tests fall into four general categories: borehole, porous probe, infiltrometer, and underdrain (Daniel, 1989). Borehole methods drill a hole from the soil surface and measure soil permeability either by the rate of flow into or out of the borehole. Porous probe measurements are performed by penetrating a probe to the depth of interest and measuring the rate of flow into a sampling chamber within the device. Infiltrometer tests are performed by placing a sealed hydraulic source at the surface and measuring the flow into the subsurface. Finally, underdrain tests are performed by placing a hydraulic source at the surface and measuring the rate of flow through the layer being investigated into a porous underlayer. Field methods are advantageous over laboratory methods because they utilize a large portion of the soil being tested; however, homogeneous conditions are assumed in the test, and the boundary conditions cannot be controlled.

Leroueil et al. (1992) performed a comparison of three field and three laboratory techniques to measure the value of the permeability of the clay at the Bothkennar site in Scotland. In-situ investigation techniques used push-in piezometers (constant head), a self-boring permeameter (constant head), and the BAT system (variable head) (Torstensson, 1984). The results from the in-situ tests showed that the push-in piezometer and BAT system evaluated consistently lower magnitudes of the permeability than did the self-boring permeameter. Laboratory tests performed included measurement of the vertical permeability in oedometer (variable head) and triaxial cells (constant head), and measurement of the horizontal permeability in oedometer (variable head) and radial flow cells (constant head). The tests performed in the triaxial cell consistently measured higher values of permeability than the tests performed in the oedometer, which Leroueil et al. (1992) attributed to the fact that more coarse grained particles were contained in the triaxial specimens. The horizontal permeabilities measured in the oedometer were also consistently lower than those measured in the radial flow cell which the authors also attributed to differences in specimen sample size. Values of the permeability back-calculated from settlement and pore pressure dissipation data show that the self-boring permeameter and the radial flow cell gave the magnitudes which most closely agreed with the actual values. However, in general, the in-situ measured values were 30% smaller than the laboratory measured values. Leroueil et al. (1992) stated that the difference was because the in-situ sand and silt lenses were discontinuous, while in a laboratory specimen, those lenses could extend to the imposed drainage boundaries of the test, which would give rise to a higher measured permeability.

Because permeability is a difficult parameter to measure accurately, many different test configurations have been developed in order quantify the value. However, the differences in the testing methodologies, in both the laboratory and the field, yield large variations in the measured value of soil permeability. Figure 2.18 shows a comparison of data gathered using two field methods and one laboratory method where the difference in the measured permeability is as large as an order of magnitude (Leroueil and Jamiolkowski, 1991). The variability is not restricted to differences between laboratory and field methods of measurement. Figure 2.19 shows permeability values evaluated in the laboratory using fixed-wall and flexible-wall permeameters, and the measured difference is again as large as an order of magnitude (Daniel, 1994).

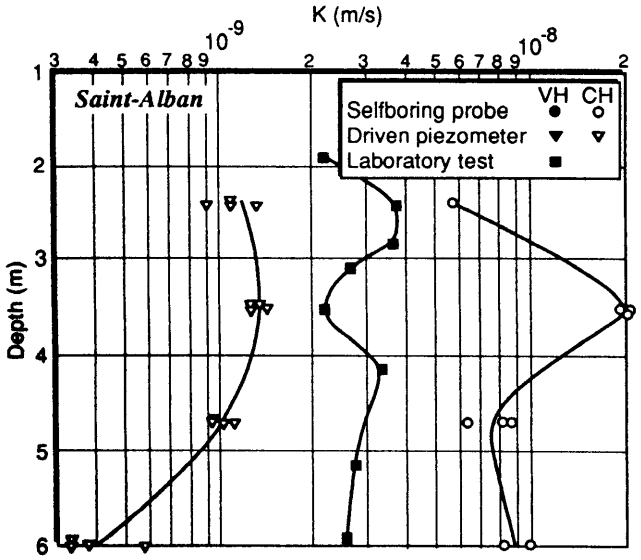

Figure 2.18. Comparison of Lab and Field Measured Permeabilities (Leroueil and Jamiolkowski, 1991)

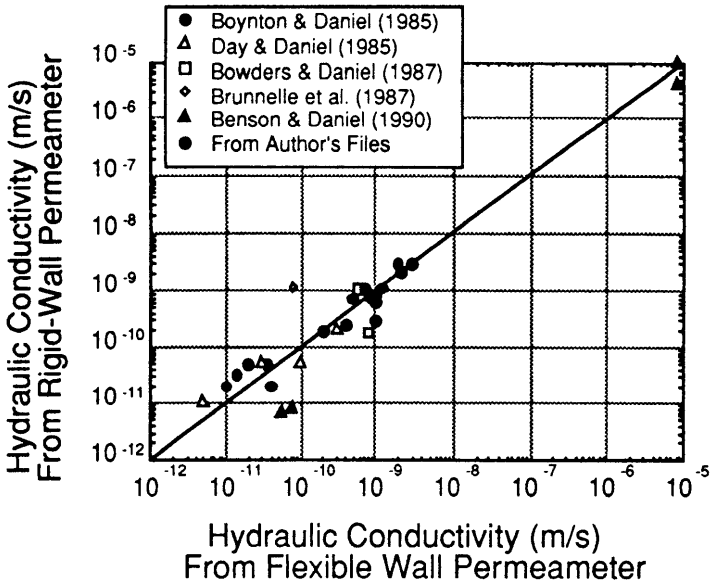

Figure 2.19. Comparison of Permeability Measured in Fixed versus Flexible Wall Permeameters (Daniel, 1994)

Piezocone Testing Evaluation of Permeability

In addition to laboratory and field methods for the measurement of soil permeability, it can also be evaluated from piezocone penetration data. To date, the methods rely either on empirical correlations, or on the estimation of the coefficient of consolidation and evaluation of permeability using one-dimensional consolidation theory.

Schmertmann (1978) proposed an empirical correlation of permeability with piezocone dissipation data. The correlation was based on the time for 50% and 90% dissipation of excess pore water pressure with his proposed relationship shown in Figure 2.20. Comparison with field and laboratory measured data was not presented; therefore, the accuracy and reliability of the approach is uncertain.

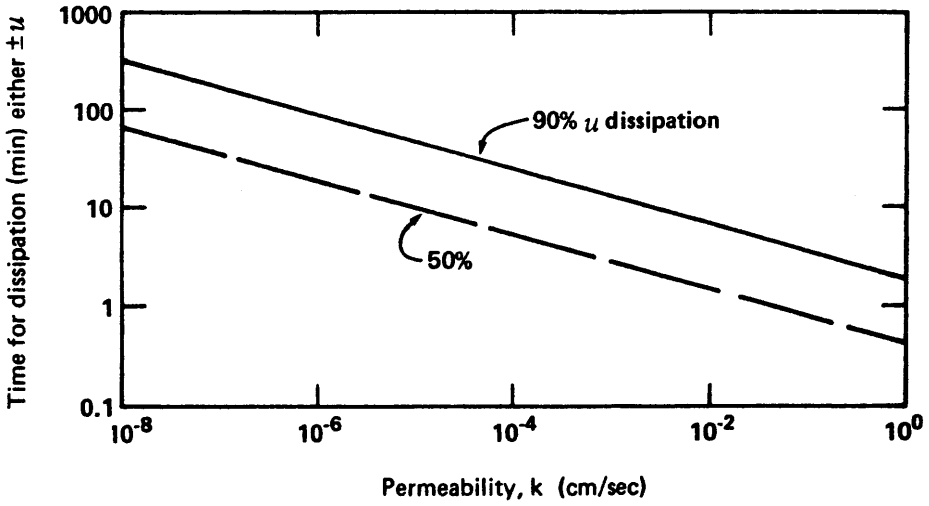

Figure 2.20. Schmertmann's Empirical Permeability Correlation (Schmertmann, 1978)

Baligh and Levadoux (1980, 1986) proposed the following equation for evaluating the horizontal permeability of a soil deposit from dissipation test data:

$$k_h(piezocone) = \frac{\gamma_w}{2.3\sigma_{vo}'} RR(piezocone) c_h(piezocone) \qquad \textbf{Equation 2.22}$$

where *RR(piezocone)* = the recompression ratio = $C_r/(1+e_o)$ = strain per log cycle of effective stress during recompression evaluated in the laboratory. Recompression was assumed because the increase in pore pressure caused a decrease in the mean effective stress, or contributed to an artificial overconsolidation of the initially normally-consolidated clay. Consequently, consolidation occurred in a recompression mode as the excess pore pressures dissipated. The approach was verified using data from Boston Blue Clay and showed that the permeability was overpredicted by approximately one order of magnitude in the upper 20 m, and predicted within one to two times in the lower 20 m of the deposit. Battaglio et al. (1986) applied this method to data gathered at the Porto Tolle site and found that the permeability evaluated for normally consolidated soil was comparable to laboratory data.

Gupta (1983) evaluated the in-situ permeability of Gainesville, Florida clays using a site specific correlation developed through cone penetration testing and laboratory consolidation testing. The following correlation for Lake Alice Clay in Gainesville was given:

$$D = 4q_c \qquad \textbf{Equation 2.23}$$

where $D = 1/m_v$ = constrained modulus, and the permeability was evaluated by:

$$k = \frac{c_h \gamma_w}{D} \qquad \textbf{Equation 2.24}$$

where the coefficient of consolidation was evaluated using the method of Gupta and Davidson (1986). This was a site specific correlation for the Lake Alice clay which was based on uncorrected tip resistance. The field predicted values were within one order of magnitude of the lab measured values; however, because the correction (Equation 1.1) can be significant in soundings performed in clays, correlations based on uncorrected tip readings are not reliable.

Wroth (1984) presented the following methodology for evaluating the permeability from self-boring pressuremeter holding tests. After evaluation of the coefficient of consolidation, the horizontal permeability was estimated by the following relationship:

$$k_h = \frac{c_h \gamma_w}{2G[\frac{1-\nu}{1-2\nu}]} \qquad \textbf{Equation 2.25}$$

where through elastic theory, the shear modulus, G, and the constrained modulus, D, are defined as follows:

$$G = \frac{E}{2(1+\nu)} \qquad \textbf{Equation 2.26}$$

$$D = \frac{E(1-\nu)}{(1+\nu)(1-2\nu)} \qquad \textbf{Equation 2.27}$$

and can be related:

$$G = \frac{D(1-2\nu)}{2(1-\nu)} \qquad \textbf{Equation 2.28}$$

No comparison with field data was presented, but the author stated that the values evaluated from the holding tests were in agreement with the values back-calculated from the settlement of a structure in the U.K..

Robertson et al. (1992) proposed an empirical correlation between the horizontal coefficient of permeability and t_{50} observed in dissipation tests in clay soils. The correlation was based on the values of t_{50} obtained with a Type 2 piezocone because that location for measuring pore pressure

gave the most consistent results; however, the relationship showed a significant amount of scatter (Figure 2.21).

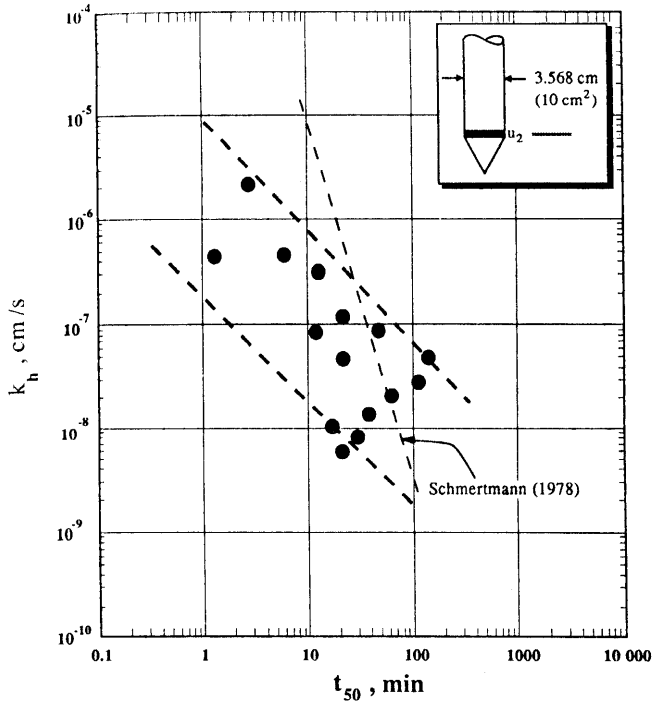

Figure 2.21. Empirical Permeability Correlation Robertson et al. (1992)

Manassero (1994) performed piezocone tests in a cement-bentonite slurry wall in order to assess the construction quality and to evaluate the hydraulic conductivity of the barrier. However, the data gathered with the piezocone were not reliable because the pore pressure transducer used was limited to 2 MPa, and the data collected showed obvious truncation. The cone data were classified according to the method of Robertson et al. (1986) by choosing an equivalent soil type from that classification, for example clay to clayey silt. The coefficient of consolidation was assessed from piezocone dissipation tests using the method of Teh and Houlsby (1991), and the permeability was calculated using Equation 2.24 which the author stated gave good agreement with laboratory measured values. A procedure was proposed which assigned hydraulic conductivity values on the basis of the equivalent soil type from the piezocone classification method.

Gaberc et al. (1995) used piezocone dissipation tests to predict the permeability of organic marshland soils. The coefficient of consolidation was predicted according to the methods of Levadoux and Baligh (1986), Tumay et al. (1985), Houlsby and Teh (1988), and Gupta and Davidson (1986) with the results from Gupta and Davidson (1986) giving the results in closest agreement with the laboratory measured values. The permeability was then evaluated according to the method proposed by Baligh and Levadoux (1986) for normally consolidated Boston Blue Clay. The predicted results were approximately one order of magnitude higher than the laboratory measured values.

Parez and Fauriel (1988) presented a method for evaluation of the permeability of a soil deposit based on correlation with t_{50} measured from Type 2 dissipation tests [referenced in Leroueil

and Jamiolkowski (1991)]. The relationship was developed for soils ranging from gravel to clay (Figure 2.22) and the mean trend is approximately given as follows:

$$k = (251 \cdot t_{50})^{-1.25} \qquad \textbf{Equation 2.29}$$

where k is in cm/s and t_{50} is in seconds.

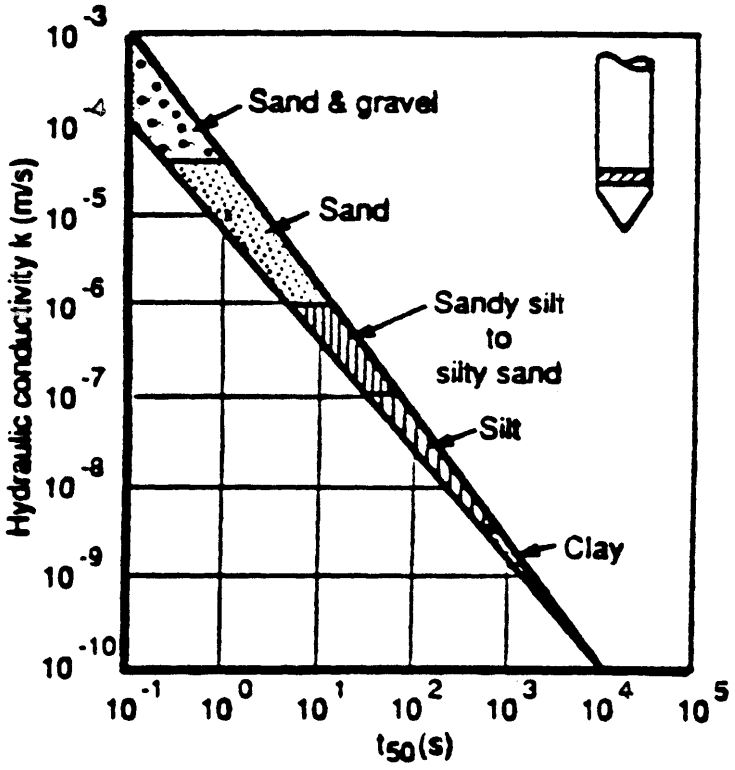

Figure 2.22. Permeability - t_{50} Correlation (Parez and Fauriel, 1988)

Summary

In summary, multiple methods exist to evaluate the permeability of a soil deposit, either in a laboratory or field setting. Laboratory methods offer the advantages of controlled boundary conditions, control of permeating fluid, control of applied stresses, and control of fluid gradient, while in-situ testing offers the advantages of minimal soil disturbance, constant geochemical regimes, field temperature, and large volumes of representative soil being tested.

Comparative studies (Leroueil et al., 1992) in a uniform clay with silt and sand lenses showed that in-situ methods of testing of the soil permeability measured consistently lower values than those obtained in the laboratory, most likely due to the influence of high-permeability lenses in the lab specimens. However, many environmental applications, including the transport of contaminants through a soil profile, are not suited to full-scale in-situ testing, and must be confined to laboratory measurements. In all testing methodologies, the experimental setup will affect the

measured values; consequently, care should be taken to guarantee that the boundary and initial conditions are representative of the actual problem, and that the proper data are being measured, for example, measurement of horizontal permeability versus vertical permeability. Field permeability tests are the most common method for evaluating the permeability in-situ; however, the data gathered during piezocone dissipation testing yield information about the flow of pore fluid through a soil deposit and can be interpreted to assess field-measured values of the soil permeability.

CHAPTER 3

INTEGRATED OPTO-ELECTRONIC CHEMICAL SENSOR FOR BTEX DETECTION IN CONE PENETRATION TESTING

Introduction

Inclusion of an integrated optic (IO) chemical sensor, capable of quantitatively measuring chemical concentration, within a cone penetrometer offers many advantages over the more traditional methods of groundwater sampling and analysis. Because the IO sensor operation is fast and reversible, contaminant concentration with depth can be mapped essentially continuously, during the cone push. In addition, there is no exposure of the groundwater to the atmosphere during sampling, and there is no need for transportation of the sample to a laboratory for analysis. While the integrated optic chemical sensor will not eliminate the use of monitoring wells, it can help optimize placement of these expensive wells and also reduce the number of wells required for adequate coverage of a site.

This chapter details the operation of the newly developed integrated opto-electronic sensor used for the detection of benzene, toluene, ethylbenzene, and xylene (BTEX chemicals). During this study, the sensor was miniaturized for inclusion within a trailing cone penetrometer module. While the sensor used in this series of experiments was developed for the detection of the BTEX chemicals, the design can be readily adapted to detect a wide variety of other chemicals as well, including chlorinated hydrocarbons and dissolved metals.

In this study, a series of bench-top experiments were performed, under laboratory conditions, as a proof-of-concept for the operation of the sensor in a soil environment. This chapter outlines the operating principle of the sensor and gives the details of the initial experimental performance in its miniaturized form.

Sensor Operation

The Hartman interferometer used in the testing program was originally developed at the Georgia Tech Research Institute (GTRI) for the detection of gaseous ammonia, NH_3 (Hartman et al., 1988; Hartman, 1990; Ross et al., 1991; Hartman et al., 1992). More recent versions of the interferometer are used for the measurement of pH (hydrogen ion concentration) and for the detection of the BTEX chemicals. Sponsorship for the integration of the sensor into a cone penetrometer was provided by the Army Research Office (ARO) in Raleigh, North Carolina. Phase I, which was a proof-of-concept stage was completed in June, 1997; Phase II is a joint venture between ARO and the US Army Corps of Engineers Waterways Experiment Station (WES), and includes the complete integration of the sensor into a trailing module of a cone penetrometer. Phase II is scheduled for completion in February, 1999.

The basic operation of the sensor relies on the use of a chemically-selective polymeric coating placed on an optically transparent waveguide (Figure 3.1) to interact with the chemical of interest either through adsorption, absorption, or a chemical reaction. The measuring device includes the glass waveguide (12 mm by 25 mm by 2 mm), polymeric coating (0.14 μm thick), a small commercial laser light source (12.7 mm diameter by 16.5 mm length), and a data processing electronics circuit board (127 mm long by 27 mm wide). The sensor, laser, and processing electronics are packaged within a stainless steel casing, which is 35 mm in diameter and 100 mm long.

When the specific chemical of interest interacts with the polymer, the effective index of refraction is altered, and the velocity of an optical beam which is passed through the waveguide

changes, and becomes either slower or faster. The optical beam produces electric fields which decay into the cover film; when the speed of this beam is altered, the electric field from the optical beam is altered, which creates a different decay into the cover film (Figure 3.2 and Figure 3.3). The changed optical beam from the chemically-reactive channel is then combined with an unaltered reference channel light beam which produces an interference pattern between the two beams. This pattern can then be correlated to the concentration of the chemical being measured. The sensor can be configured to measure both gaseous and aqueous phases; however, the sensor used in this study was limited to aqueous measurements of the BTEX chemicals. Additionally, the chemically-reactive coating can be changed in order to detect different, or multiple chemicals or to optimize the detection of specific contaminants. The original IO system was a large bench-top configuration using lasers, mirrors, and a table array for setup. During this study, Photonic Sensor Systems and GTRI miniaturized the layout into a compact size for incorporation into a cone penetrometer module.

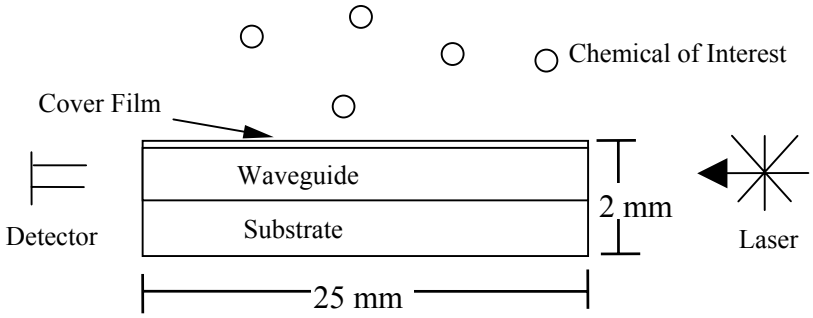

Figure 3.1. Integrated Optic Sensor Schematic (not to scale)

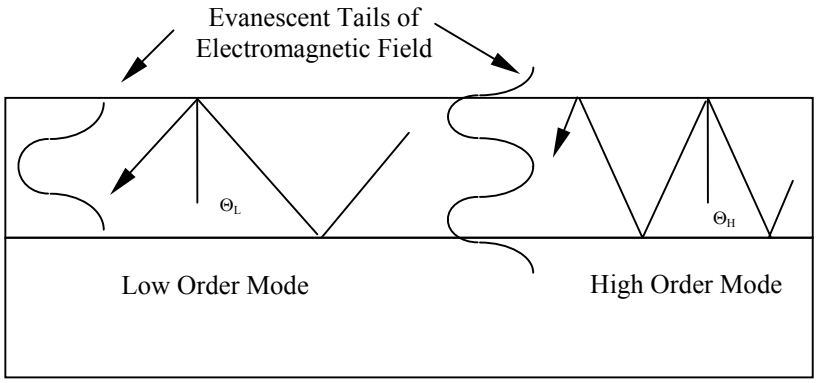

Figure 3.2. Principle of Waveguide (not to scale)

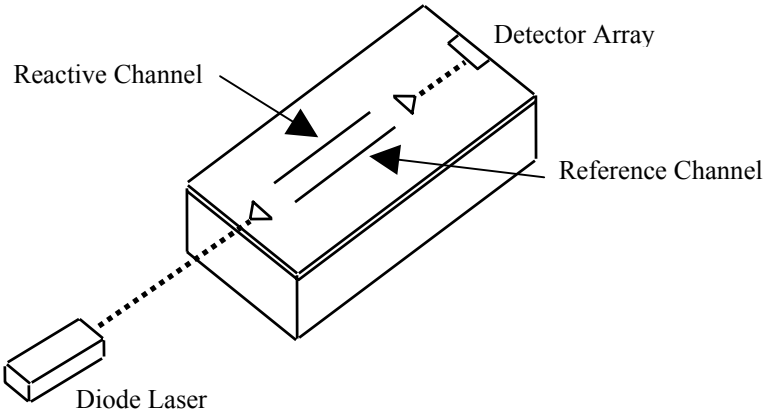

Figure 3.3. Sensor Configuration (not to scale)

Sensor Housing

One of the key aspects to the integration of the BTEX sensor into a cone penetrometer is the development of an adequate casing to carry the device into the subsurface. The following section reviews the design aspects which are involved in the Phase II inclusion of the sensor as an integral part of the cone penetrometer. Because the integrated optic sensing chip cannot withstand the abrasion of direct soil contact during a cone sounding, it must be housed within an internal chamber inside the cone module. Small groundwater samples (approximately 0.5 cc) will be drawn into the chamber and into contact with the sensor. The key elements in the design of the system are the fluid delivery (generation of flow) and the filtration of the fluid entering the chamber to prevent the influx of soil particles across the waveguide.

Fluid Sampling System

Fluid can be drawn into the sensing chamber either by pumping or by the gradients flow caused by cone motion. A moving penetrometer causes significant gradients in the vicinity of the cone tip. Robertson et al. (1986) show that the relative pore pressure gradients decrease from the cone tip/face to the cone shaft for different soil types (Figure 3.4). All measured penetration pore pressures shown in the figure are normalized by the hydrostatic value established by the groundwater table. The effect is much more dramatic for stiff to hard clays than it is for loose sands. In fact, for very hard overconsolidated and fissured clays, the gradients are extremely large (Mayne et al., 1990). The gradients generated during cone penetration testing may be used to provide movement of fluids into a small cavity in the penetrometer, where exposure to the integrated optic sensor can occur. Only small volumes are required (≈ 0.5 cm^3) because of the miniature sensor size. In typical soil deposits, the void ratio (e_o) is on the order of 1.0, indicating that half the volume is occupied by solid particles and half by void space. Voids are filled with either vapor, fluids, or both. In saturated soils all pore space is filled with fluid; consequently, a 15 cm^2 cone penetrometer (44 mm diameter) with length of 60 cm will displace a volume of soil equal to 900 cm^3, of which 450 cm^3 are incompressible solids and 450 cm^3 are fluids and vapors (assuming $e_o = 1$). Under these circumstances, a normal cone penetration rate should provide adequate fluid flow for chemical testing, without the aid of artificial pumping.

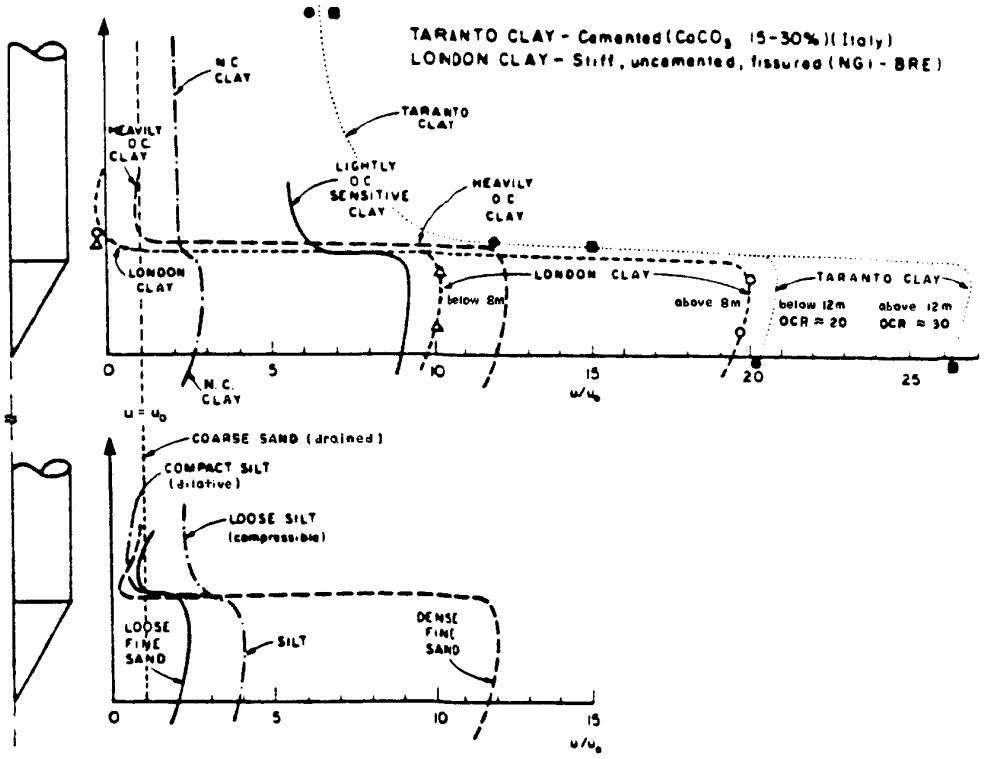

Figure 3.4. Distribution of Normalized Porewater Pressures During Penetration in Different Soil Types (Robertson et al., 1986)

In a static condition, sampling of pore fluid will require a miniaturized pump to draw the sample into the sensor flow cell. EPA guidelines permit the use positive displacement, peristaltic, and gas-drive pumps for sampling of inorganic materials like dissolved metals or for non-volatile organics; however, only positive displacement bladder, helical rotor, and gear-drive pumps are recommended for the sampling of volatile organic compounds (EPA, 1993). Two currently available miniaturized pump designs for groundwater sampling include a piston pump which uses hydraulic pressure to draw the sample in and to expel the sample out of the chamber and another device known as the Cone Sipper™ which uses check valves in combination with vacuum and pressure lines in order to sample the groundwater (Lightner and Purdy, 1995).

Future work in this ongoing study will evaluate the use of a miniaturized positive displacement bladder pump and the Cone Sipper™ operating under a variety of physical and chemical conditions. Physical conditions will include the simulation of variable groundwater flowrates and variable hydrostatic pressures in order to monitor pump operation. In addition, the study will examine the effect of pumping samples into a chamber on the measured chemical concentrations, through comparison of sensor-measured values with known reference concentrations. The influence of pumping is expected to be most significant in terms of the monitoring of volatile organic chemicals.

Geochemical Behavior of the BTEX Chemicals

The BTEX chemicals belong to the group of aromatic hydrocarbons (Figure 3.5) and are constituents of fuel products. Aromatic hydrocarbons are composed of a benzene ring with additional functional groups attached in the ortho-, meta-, and para-positions. The chemicals are classified as light non-aqueous phase liquids (LNAPLs) because they are less dense than water and are not miscible with water; however, they are slightly soluble (Table 3.1). Because they are the most soluble components of gasoline, the BTEX chemicals are commonly used as diagnostics of gasoline spills, either from leaking underground storage tanks or from surficial spills. Sampling of the BTEX chemicals is difficult due to their volatility; consequently, in-place measurements of BTEX concentrations, which do not expose the chemicals to atmospheric oxygen are desirable.

Laboratory Testing Program

A preliminary laboratory testing program was undertaken in order to demonstrate the viability of the BTEX sensor in a soil environment. Initial experiments were performed in aqueous solutions and subsequent experiments were performed with the sensor in a soil/water matrix. The soil used in all testing was Ottawa 20/30 sand which is a relatively unreactive sand soil composed of

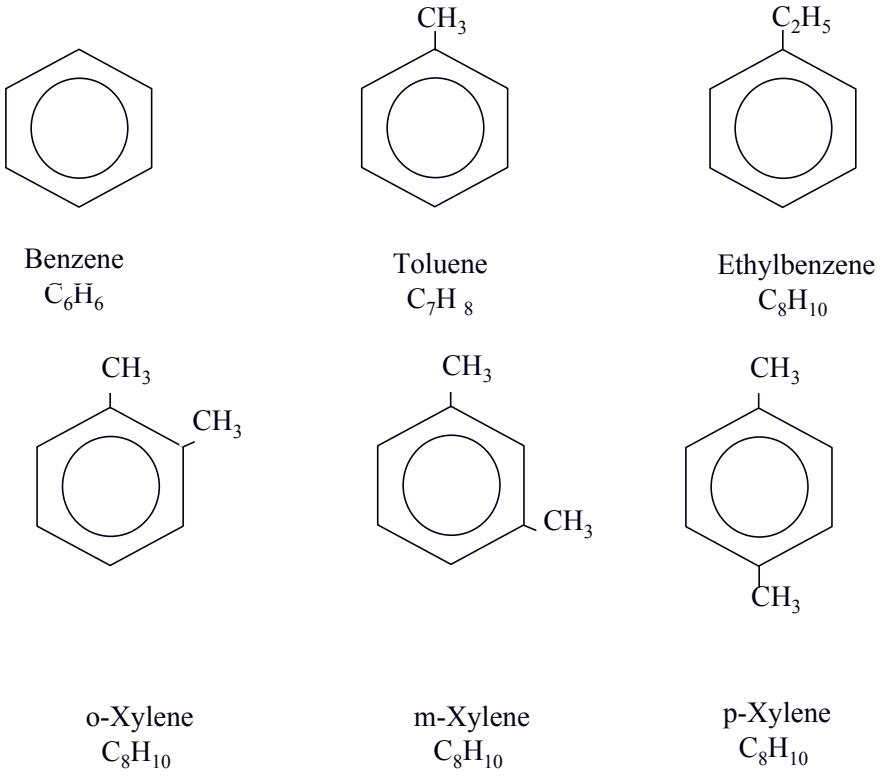

Figure 3.5. Structure of the BTEX Chemicals

Table 3.1. BTEX Chemical Characteristics (CRC, 1993)

Chemical	Molecular Weight (g)	Solubility in Water (mg/L)	Soil Water Partition Coefficient	Vapor Pressure (mm Hg)	Henry's Constant (atm-m^3/mol)	Log K_{ow}	Boiling Point (^oC)	Melting Point (^oC)
Benzene	78.11	1780	97	95.2	5.53	2.12	80.1	5.5
Ethylbenzene	92.10	500	242	22.0	5.13	2.73	110.6	-95.0
Toluene	106.17	150	622	7.0	6.10	3.15	136.2	-95.0
o-Xylene	106.17	170	363	10.0	7.04	3.26	144.4	-25.3

essentially pure silica (Lambe and Whitman, 1969; Mitchell, 1993). Ottawa sand was chosen as the soil matrix because it is a well-characterized soil and provides relatively little chemical interference during the testing.

All tests were performed in a laboratory setting using a triaxial calibration chamber (14 cm diameter; 61 cm height) constructed out of BTEX resistant materials: Pyrex glass, stainless steel, and Viton o-rings (Figure 3.6). The IO sensor was enclosed in a stainless steel tube which was the approximate diameter of a 10 cm^2 cone penetrometer (35.7 mm diameter) and 400 mm length. Inflow and outflow tubes made of Teflon® were connected to the flow cell over the waveguide in order to draw the sample into the probe and into contact with the waveguide and the tubing was changed between each experiment. Polyethylene filters (2 μm) were attached to the inflow section of tubing in order to limit the migration of fines into the waveguide. Additionally, a stainless steel filter was purchased for its better compatibility with the organic chemicals and testing conditions; however, it was not available during the initial phase of testing. Flow through the cell was initiated by suction using a syringe. The inflow tubing was buried approximately six to seven inches below the sand surface, and the outflow was directed to a container outside of the testing chamber. Calibration of the sensor was performed by preparing solutions of known concentration and measuring the sensor response. In addition, calibration of the sensor response to toluene was performed using a Hewlett Packard 5890 Series II Gas Chromatograph (Figure 3.7); however, calibrations were not performed for benzene or xylene due to sensor malfunctioning which is discussed in more detail later. For the concentration ranges tested, the sensor response was essentially linear. All tests were performed in a static system; the IO sensor was not moved once it was placed within the calibration chamber. A schematic of the testing setup is shown in Figure 3.8. A series of tests were performed using benzene, toluene, and xylene as the contaminating chemicals. Data acquisition was performed using a Pentium notebook computer (Figure 3.9) which was used to monitor 8 channels from the waveguide. Figure 3.10 shows a picture of the miniaturized sensor supported by an external clamp on a laboratory bench-top. The processing electronics are to the left of the clamp, and the sensor, flow cell, and inflow and outflow tubing are to the right of the clamp. Note also that a glass waveguide is shown at the right mid-center.

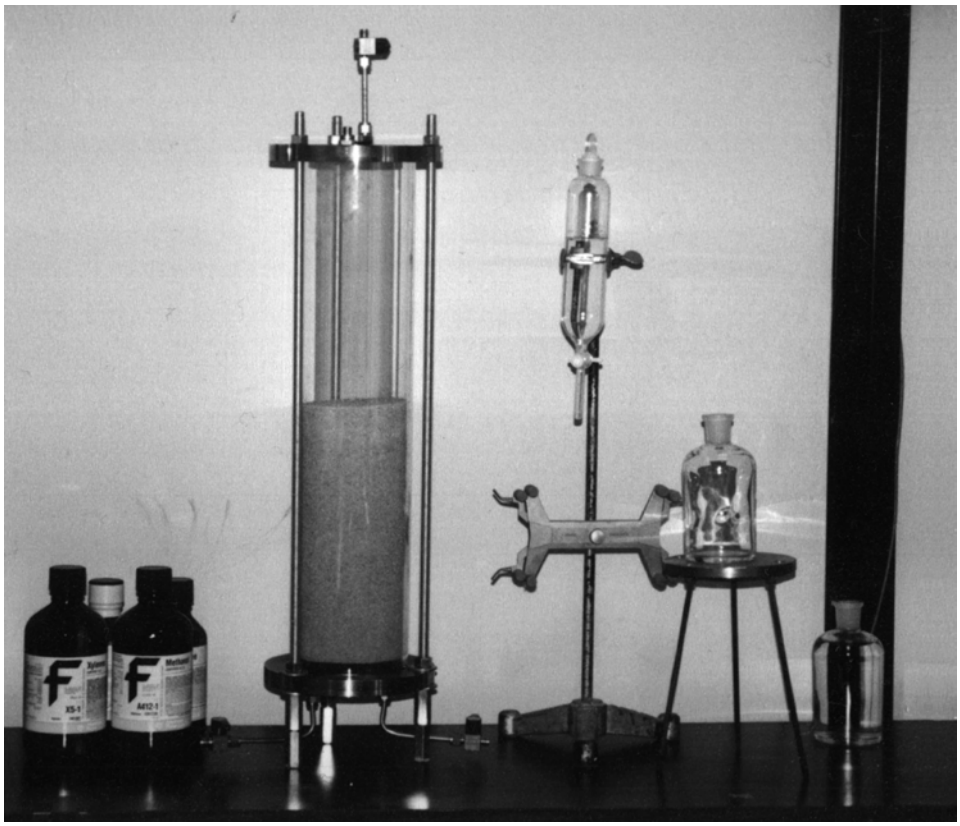

Figure 3.6. BTEX Testing Chamber for IO Sensor Experiments

Figure 3.7. Gas Chromatograph Used for Reference Chemical Concentrations

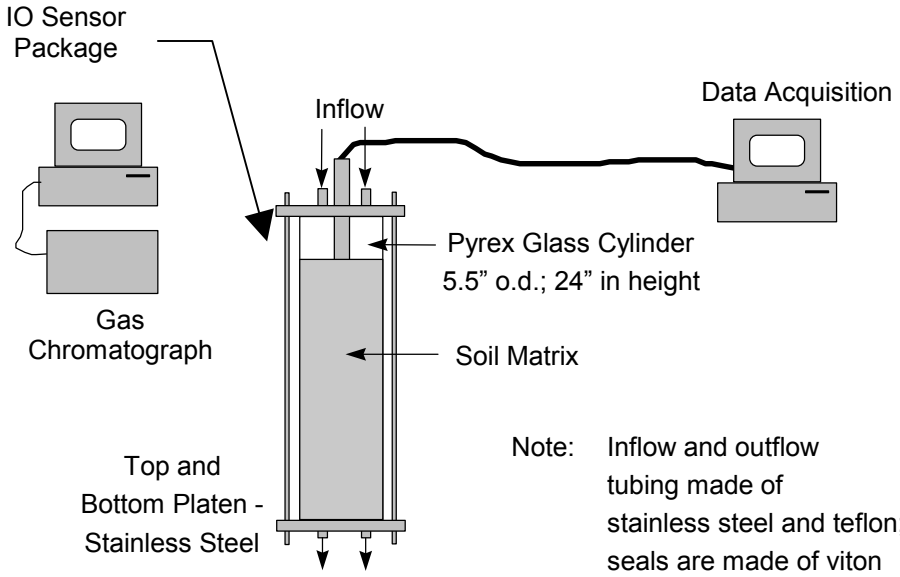

Figure 3.8. Testing Schematic for BTEX Detection by IO Sensor

Figure 3.9. Miniaturized Optic Sensor Configuration and Data Acquisition

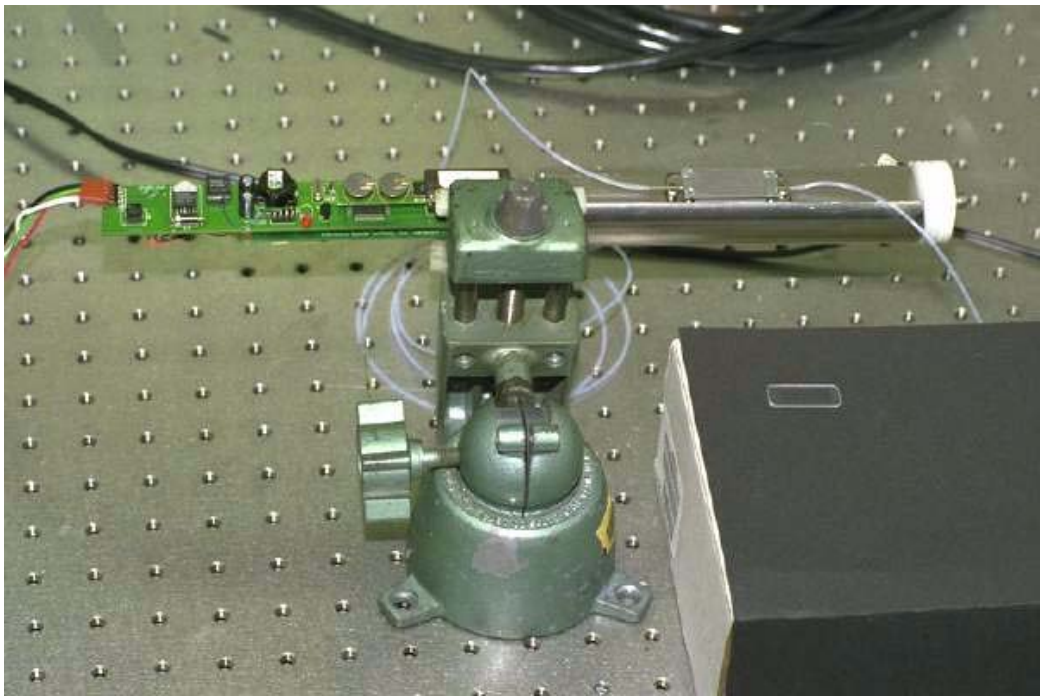

Figure 3.10. Complete Integrated Optics Sensor Package Configuration

Experimental Results

Seven experiments were performed with the sensor in aqueous and/or saturated sand matrices (Table 3.2). The experiments performed were initial proof-of-concept tests done to verify the proper operation of the miniaturized sensor in a soil matrix. The initial tests were successful; however, malfunctioning of the prototype sensor operation prevented further experimentation. Consequently, only the results of the initial testing program are presented.

Table 3.2. Test Series of Preliminary Experimental Program With IO Sensor

Exp No.	Chemical	Concentration (ppm)	Matrix	Waveguide Coating
1	Benzene	250	Aqueous	PBIBMA*
2	Benzene	190-380	Aqueous/Sand	PBIBMA*
3	Toluene	25	Aqueous	Teflon-A
4	Toluene	18	Aqueous/Sand	Teflon-A
5	Xylene	6	Aqueous	Teflon-A
6	Xylene	9.5	Aqueous/Sand	Teflon-A
7	Xylene	7	Aqueous/Sand	Teflon-A

*polybutylisobutylmethacralate (PBIBMA)

The results from the seven experiments are shown in Figure 3.11 through Figure 3.17 in both aqueous and soil environments. Figure 3.11 shows the sensor response [chemically reactive coating polybutylisobutylmethacralate (PBIBMA)] in de-ionized water with benzene added after nine minutes of operation at a stable baseline. The addition of benzene produced an immediate response which measured increasing concentration up to a concentration of 250 ppm. After four minutes of operation at a constant concentration, de-ionized water was added to the test cell in order to dilute the concentration of benzene, and the sensor measured a decrease in concentration. Figure 3.12 shows the results of a test performed with the sensor operating in a soil/aqueous environment. This figure shows the continuation of a previous test where the concentration in the test cell was initially 190 ppm. Additional benzene was added in order to raise the concentration in the test cell to 380 ppm. One notable difference in the response of the sensor in a soil matrix as opposed to a pure aqueous environment is the rate at which the concentration changes. The soil matrix, as would be expected, slows the movement of the contaminant to the inflow tubing of the sensor, producing slower changes in concentration than are seen in pure aqueous solutions. This behavior is consistent throughout the tests performed.

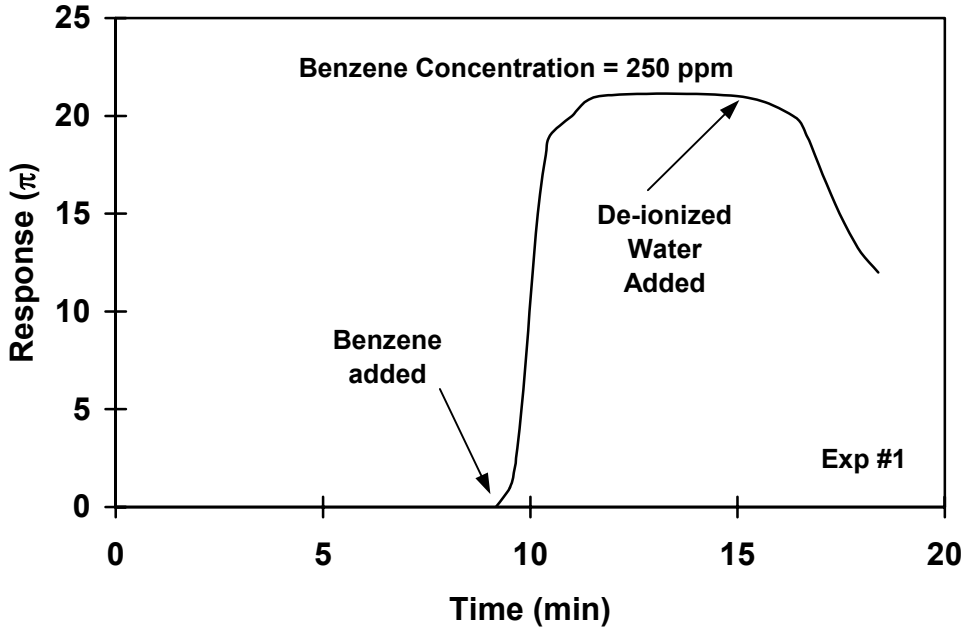

Figure 3.11. Sensor Response to Benzene in Aqueous Solution

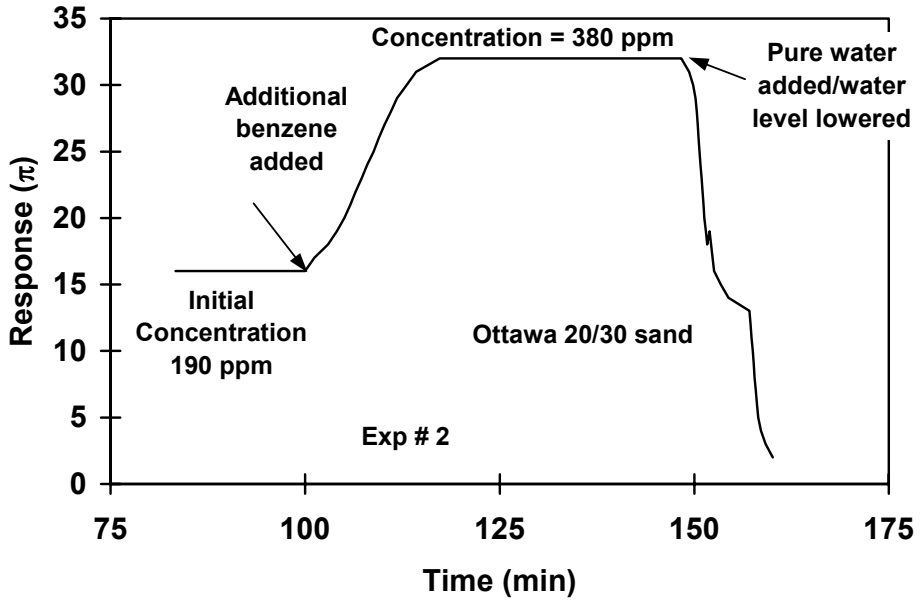

Figure 3.12. Sensor Response to Benzene in Soil Matrix

Figure 3.13 and Figure 3.14 show the response of a different chemically reactive coating, Teflon-A, to toluene. The Teflon-A was used as the reactive coating in these experiments because the response was much more definitive than the response seen with the PBIBMA coating. In fact, the sensor response time was so rapid that the data acquisition electronics could not record data fast enough to monitor the concentration change of benzene, the smallest molecule. Consequently, these tests were performed using toluene and xylene which are larger molecules and have slower response time due to mass transfer effects into the coating. The toluene behavior recorded again shows rapid response and concentration change in aqueous solutions while the response in the soil/aqueous matrix demonstrates a significantly slower response (Figure 3.13 and Figure 3.14).

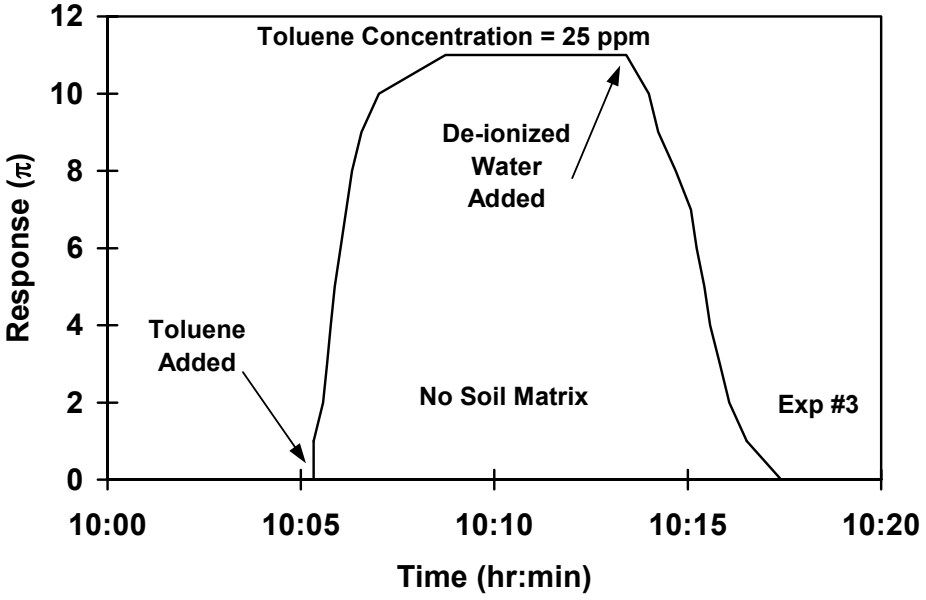

Figure 3.13. Sensor Response to Toluene in Aqueous Solution

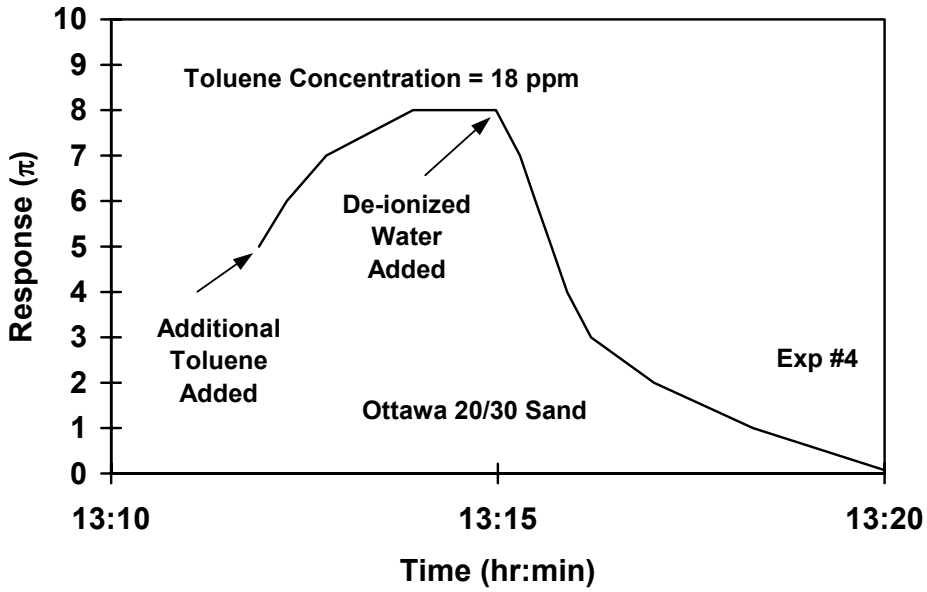

Figure 3.14. Sensor Response to Toluene in Soil Matrix

The final set of experiments were performed using the Teflon-A reactive coating in both aqueous and soil environments. Xylene, which is a larger molecule than toluene, shows a slower response time than the smaller molecules, even in aqueous solution. Figure 3.15 shows the sensor's response to xylene (concentration = 6 ppm) in an aqueous solution and Figure 3.16 and Figure 3.17 show the sensor's response in a soil matrix (concentration = 9.5 ppm and 7 ppm). The same patterns

are evident in the sensor response to xylene in a soil matrix as were seen with benzene and toluene: the soil matrix slows the transport and diffusion of the chemical through the soil and into contact with the sensor.

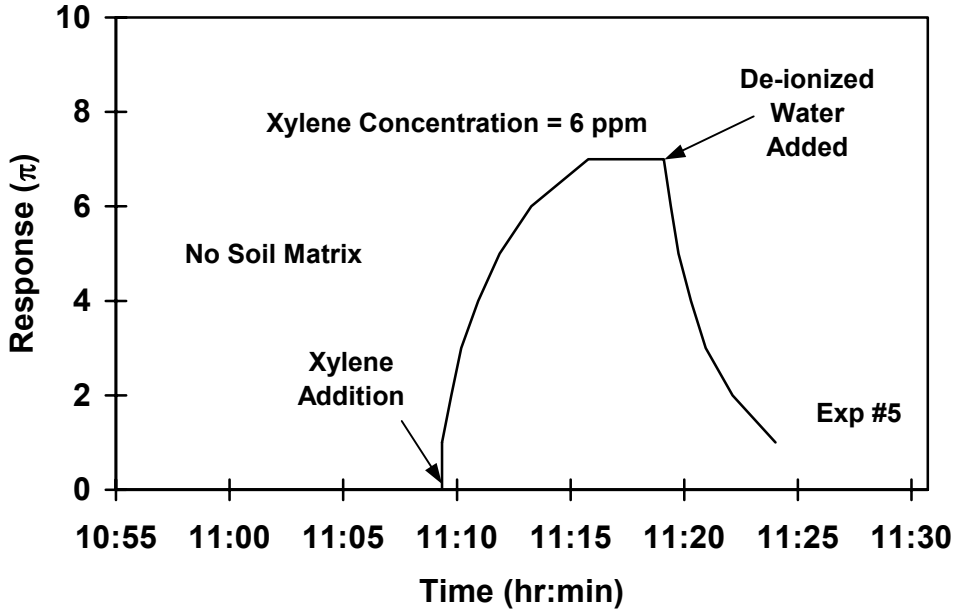

Figure 3.15. Sensor Response to Xylene in Aqueous Solution

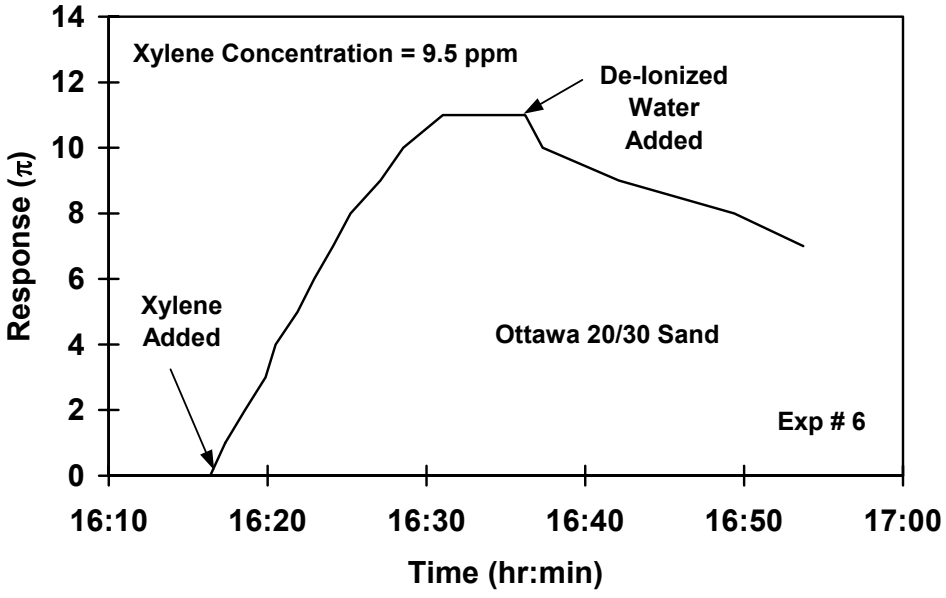

Figure 3.16. Sensor Response to Xylene in Soil Matrix (9.5 ppm)

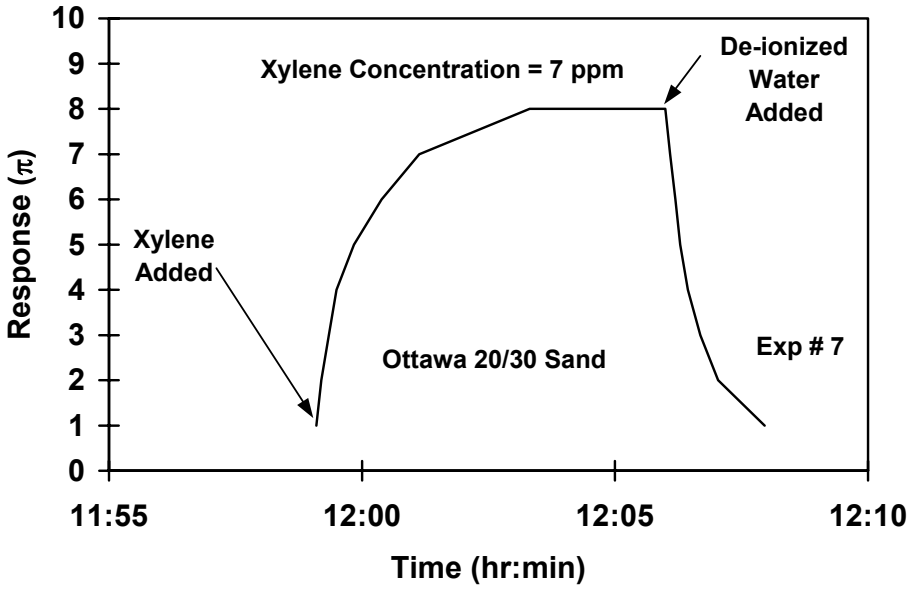

Figure 3.17. Sensor Response to Xylene in Soil Matrix (7 ppm)

Discussion

Two serious complications with the prototype sensor hardware prevented further experimental testing during this phase: the waveguide mount was not machined to a sufficient tolerance and broke the glass waveguide when it was tightened into place. Fracturing of the waveguide occurred on three separate occasions, which required approximately two months for repair in each instance. Additionally, there was an incompatibility of communication protocols between the waveguide hardware and the data acquisition electronics which prevented the rapid data transfer needed for measurement of some chemicals. The sensor development was performed at GTRI, independently of the electronics development which was performed by General Atomics in Florida. Ongoing work in Phase II is underway to re-design the communication systems in order to obtain sensor-electronics compatibility. Additionally, the electronics processing hardware is being developed under the Environmental Systems Management, Analysis, and Reporting Network (E-SMART) in order to provide a standard for connection of environmental monitoring sensors used by the U.S. Department of Defense.

While a complete evaluation of the sensor behavior in a variety of soil environments was not possible due to the above reasons, enough data was gathered to demonstrate that the sensor can measure BTEX chemical concentrations in an Ottawa sand soil matrix. A range of concentrations were measured, from a high of 380 ppm benzene to a low of 6 ppm xylene, which demonstrates the sensor versatility in terms of detection limits. Additionally, the only limits on the measurement response time were imposed by the data acquisition software and hardware which is currently being upgraded in order to improve processing time. Another key factor in the sensor performance was the question of reversibility. In repeated experiments, the sensor demonstrated that increases as well as decreases in chemical concentration could be measured.

Experimental work with the next version of the IO sensor is currently being planned in order to verify its field applicability, including a study of sensor response to a mixture of chemicals, the effect of soil grain size on sensor measurements, sensor response at extremes of pH, sensor response in high ionic strength environments, the interaction of naturally occurring soil acids with the sensor's measurement, the influence of sampling procedure including sampling and filtering materials and pump configurations, and the influence of dynamic penetration on the sensor readings.

Conclusions

The integrated optic sensor was miniaturized during this study and has demonstrated viability for the detection of the BTEX chemicals in soil environments under laboratory conditions. While the robustness of the device must be improved in order to withstand the rigors of cone penetration testing, the BTEX sensor is clearly a promising tool in terms of providing quantitative measurement of chemical concentrations in-situ. Of particular interest to other applications is the fact that the waveguide and electronics packaging would be the same for sister sensors because only the polymeric coating is changed for detecting other chemistries.

CHAPTER 4

PIEZOCONE MODEL FOR EVALUATING THE COEFFICIENT OF CONSOLIDATION IN SOFT TO HARD CLAYS

Introduction

In addition to the measurement of soil properties and contaminant concentrations, data gathered from piezocone soundings can be used for the interpretation of soil and pore fluid characteristics. This chapter develops a model for the interpretation of pore pressure dissipation data measured in the Type 2 location using a hybrid model based on cavity expansion theory (Vesic, 1972) and critical-state soil mechanics (Wroth, 1984). Extending beyond prior interpretative methods, the approach can represent the dilatory dissipation behavior observed in heavily-overconsolidated clays, as well as the common monotonically decreasing decay of pore pressures in soft to firm clays and silts. While it is known that the cavity expansion model for cone penetration is a simplification in that it assumes isotropic soil and one-dimensional behavior, it offers a straightforward and reasonable approach to the analysis of dissipation behavior in clays. Similarly, the adopted isotropic constitutive soil model (Modified Cam Clay) is also over simplistic, yet conveys the general nature of soil behavior. The goal of this chapter is to represent the porewater pressure dissipation behavior of normally-consolidated to heavily-overconsolidated clays using the hybrid formulation in combination with an analytical closed-form solution to the radial consolidation equation.

Components of Porewater Pressure

During cone penetration, excess pore pressures develop due to changes in both normal and shear stresses. Compression-induced pore pressures from increasing normal stresses are always positive; however, shear-induced porewater pressure may be either positive (contractive) or negative (dilatant). Under the cone tip, the shear stress component is derived from stress path analysis and always has positive values (Chen and Mayne, 1994) and the magnitude of the normal-induced response is often much larger than that of the shear-induced response. However, along the shaft, the normal- and shear-induced components can be comparable in magnitude. While the normal component will always remain positive, the shear-induced component can be positive at low OCRs, or negative at high OCRs.

The zone of influence of the octahedral normal stress is a function of the rigidity index of the soil and is large (approximately 10 to 20 diameters across), in comparison to the zone of influence of the shear stress. The rigidity index is defined as $I_r = G/s_u$, where G = the undrained shear modulus and s_u = the undrained shear strength. The shear modulus is defined as $G = \tau/\gamma$, the ratio of shear stress to shear strain. It can be related to an equivalent Young's modulus by $E = 2G(1+\nu)$, where E = Young's modulus and ν = Poisson's ratio. In undrained loading, $\nu = 0.5$ and typically, E might be taken as E_{50}, the secant modulus at one-half the undrained shear strength. This yields: $G = E_{50}/3$.

In contrast, the zone affected by interface shear stresses is limited to a thin annulus next to the body of the cone penetrometer (say 1 to 10 mm). Because the volume affected by the normal stress is much larger than that affected by the shear stress, the dissipation of the shear-induced pressures will occur more rapidly than will the dissipation of the normal-induced pore pressures.

The measured porewater pressures (u_m) are the combined magnitudes of the normal- and shear-induced components at any given time, t, plus hydrostatic pressure. Consequently, a dissipation test with measured u_m will reflect the overall summation of the individual components with time. Figure 4.1 shows the conceptual behavior of the individual components: note that the octahedral normal-induced pore pressures are large in magnitude and decay over a long time span,

while the shear-induced pore pressures are lower in magnitude and decay much more rapidly. The hydrostatic water pressure remains essentially constant in most environments; notable exceptions to this condition are tidally influenced areas. Figure 4.2 shows the measured behavior with the contributions summed. The total magnitude of measured pore pressure is represented as follows:

$$u_m = \Delta u_{oct} + \Delta u_{shear} + u_o \qquad \textbf{Equation 4.1}$$

Shoulder Position Dissipation Model

The core of the model presented uses cavity expansion theory to represent the octahedral normal component of excess pore pressure combined with Modified Cam Clay to quantify the shear-induced component of excess pore pressure and the variation of the undrained shear strength as a function of OCR. The hybrid cavity expansion/critical-state formulation has successfully represented penetration porewater pressures in a variety of clays with consistencies ranging from soft to stiff to hard (Mayne, 1991). The initial piezocone dissipation model based in this approach used a finite-difference scheme to decay these components with time (Burns and Mayne, 1995a); however, the solution required considerable computer time and was conditionally stable at early stages. Consequently, the latest version of the model relies on an analytical solution to the consolidation equation which is rapid and not subject to instability. The procedure to model both lightly- and heavily-overconsolidated clay dissipation behavior with time is outlined below with a brief review of the concepts of Cavity Expansion, Modified Cam Clay, and the derivation of the analytical solution to the one-dimensional consolidation equation.

Normal-Induced Pore Pressures From Cavity Expansion Theory

Cavity expansion theory was originally developed for application to the expansion of either a spherical or cylindrical cavity indentation in metals (Bishop et al., 1945). Vesic (1972) developed solutions to the expansion of spherical and cylindrical cavities in a soil with Mohr-Coulomb frictional parameters, and Torstensson (1977) applied the solution to cone penetration testing. The solution was able to estimate ultimate stresses (bearing capacity) and the generated pore water pressures due to normal stress changes in the case of undrained cavity expansion in a soil medium and is often used as a model for cone penetration testing. A review of the solution as applicable to the model used in this chapter is given below.

During the expansion of a cavity in a soil medium, a plastic zone develops surrounding the cavity and the equations of equilibrium for an element within that zone are written as:

Spherical Cavity: $$\frac{\partial \sigma_r}{\partial r} + 2\frac{\sigma_r - \sigma_\theta}{r} = 0 \qquad \textbf{Equation 4.2}$$

Cylindrical Cavity: $$\frac{\partial \sigma_r}{\partial r} + \frac{\sigma_r - \sigma_\theta}{r} = 0 \qquad \textbf{Equation 4.3}$$

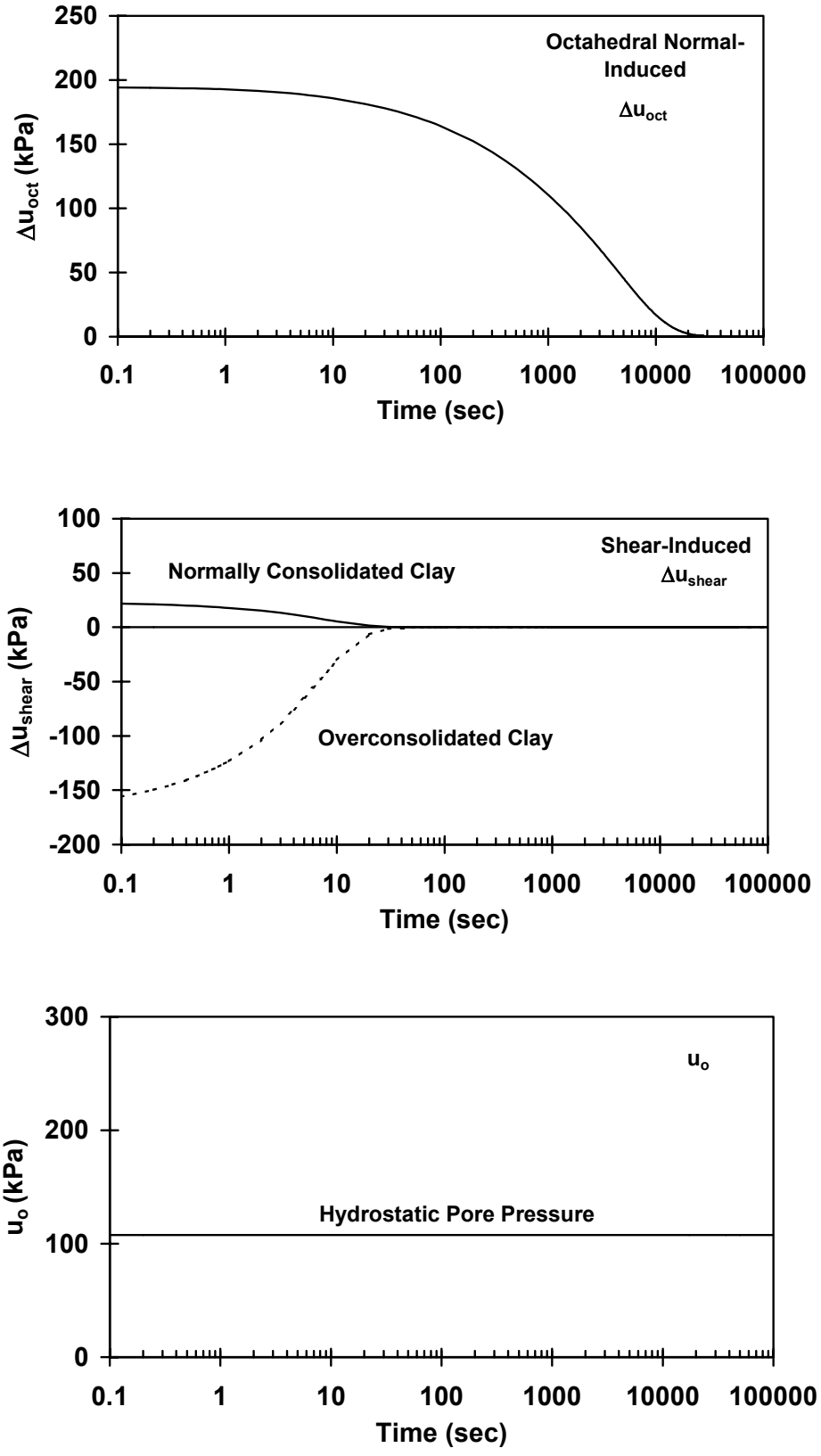

Figure 4.1. Dissipation Behavior of Components of Measured Pore Pressure

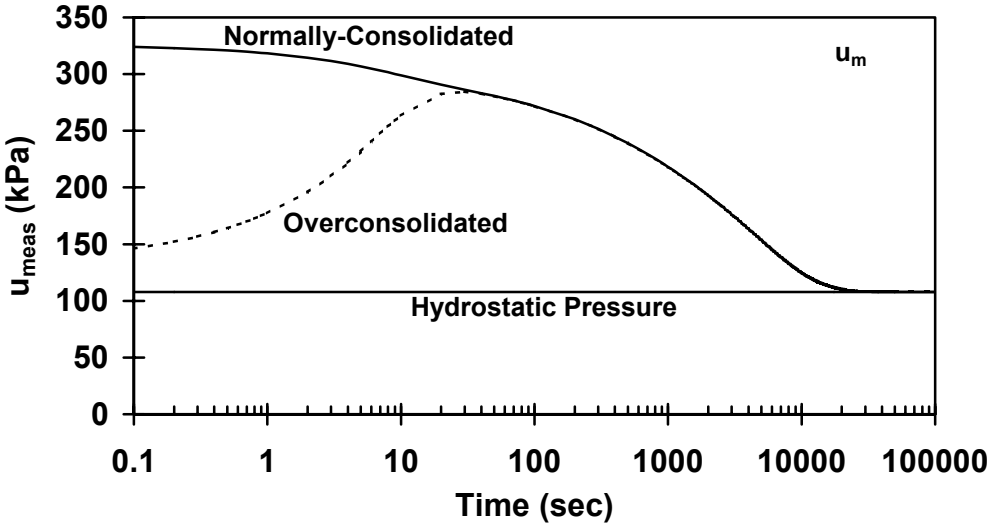

Figure 4.2. Dissipation Behavior with Summation of Components

where σ_r = radial normal stress, σ_Θ = circumferential normal stress, and r = distance to the center of the cavity. A diagram of the soil elements is shown in Figure 4.3.

The failure condition for soils in undrained shear is given by Mohr:

$$\sigma_r - \sigma_\theta = 2s_u \qquad \textbf{Equation 4.4}$$

where s_u = the undrained shear strength.

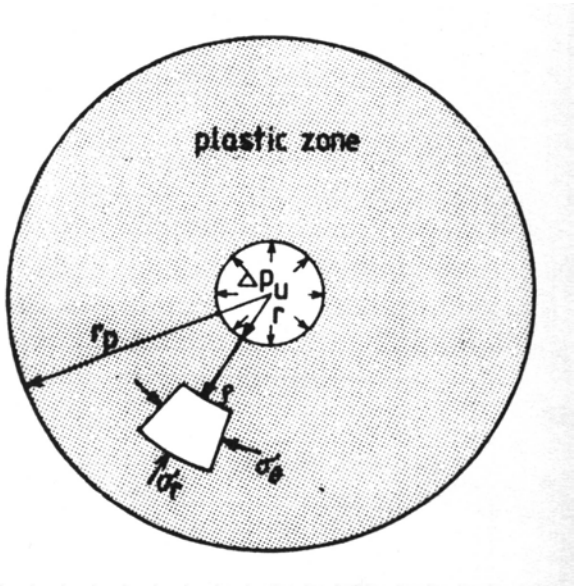

Figure 4.3. Soil Elements in Cavity Expansion (Torstensson, 1977)

The solution used by Torstensson (1977) assumed that the soil was an ideal elastic-plastic material and that there were no volume changes within the plastic zone, which led to the following formulation for the width of the induced plastic zone:

Spherical Cavity $$\frac{r_p}{r_o} = \sqrt[3]{\frac{E}{2(1+\nu)s_u}}$$ **Equation 4.5**

Cylindrical Cavity $$\frac{r_p}{r_o} = \sqrt{\frac{E}{2(1+\nu)s_u}}$$ **Equation 4.6**

where r_p = radius of the plastic zone and r_o = radius of the cone.

From the preceeding equations, the ultimate cavity pressure (Δp_u) was derived to be:

Spherical Cavity $$\Delta p_u = \frac{4}{3} s_u \ln \frac{E}{2s_u(1+\nu)}$$ **Equation 4.7**

Cylindrical Cavity $$\Delta p_u = s_u \ln \frac{E}{2s_u(1+\nu)}$$ **Equation 4.8**

Finally, for the calculation of pore pressure, it was assumed that the change in pore pressure, Δu, was equal to the change in the mean stress:

$$\Delta u = \Delta\sigma_m = \frac{1}{3}(\Delta\sigma_r + \Delta\sigma_\theta + \Delta\sigma_z) \qquad \textbf{Equation 4.9}$$

where $\Delta\sigma_m$ = change in the mean stress. This yielded the following equations for the generated pore pressure:

Spherical Cavity $$\Delta u = \frac{4}{3} s_u \ln \frac{E}{2s_u(1+\nu)} \qquad \textbf{Equation 4.10}$$

Cylindrical Cavity $$\Delta u = s_u \ln \frac{E}{2s_u(1+\nu)} \qquad \textbf{Equation 4.11}$$

In summary, in the present formulation, cavity expansion theory is used to represent the pore pressures generated due to changes in the octahedral normal-induced stresses during cone penetration testing.

Shear-Induced Pore Pressures From Modified Cam Clay

Development of shear-induced pore pressures in undrained loading is evaluated using a constant p stress path for isotropically consolidated soil in Cambridge q-p space (Wroth, 1984). The shear-induced pore stress can then be expressed as the difference between the initial and final effective mean stresses:

$$\Delta u_{shear} = \sigma_o' - \sigma_f' \qquad \textbf{Equation 4.12}$$

where σ_o' = the initial effective normal stress and σ_f' = mean effective stress at failure. The stress path representation is shown in Figure 4.4.

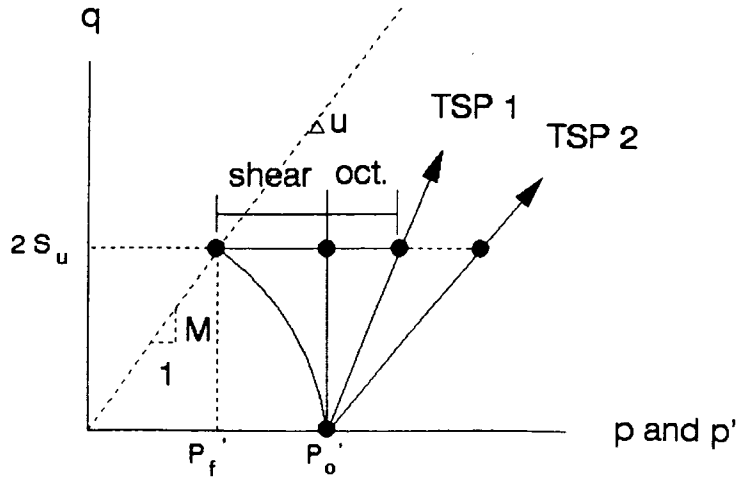

Figure 4.4. Stress Path Representation for Shear-Induced Pore Pressures (Chen and Mayne, 1994)

According to Modified Cam Clay, the final mean effective stress can be represented by the following:

$$\sigma_f' = \sigma_o' \left(\frac{OCR}{2}\right)^{\Lambda} \qquad \textbf{Equation 4.13}$$

where Λ = the plastic volumetric strain ratio = $1 - C_s/C_c$ where C_s = the swelling index and C_c = the compression index. Data compiled by Mayne (1988) indicated that $\Lambda = 0.80$ is sufficient for many clays. For estimation of the shear-induced pore pressures along the cone shaft at the Type 2 position, a value of $\Lambda = 0.80$ is used in this representation.

Derivation of the Analytical Solution to the Consolidation Equation

The linear partial differential equation which controls radial consolidation surrounding a piezocone was solved in order to obtain an analytical solution for use in the model. Previous researchers have dealt with similar problems in relation to heat flow and consolidation surrounding driven piles (Carslaw and Jaeger, 1959; Randolph and Wroth, 1979b). The consolidation equation was given in Equation 2.9:

$$\frac{\partial u}{\partial t} = c_h \frac{\partial^2 u}{\partial r^2} + \frac{c_h}{r}\frac{\partial u}{\partial r} \qquad \textbf{Equation 4.14}$$

for $a < r < b$ where $a = r_{cone}$ and $b = r_{plastic}$. Assume a solution of the form:

$$u = ve^{-c\alpha^2 t} \qquad \textbf{Equation 4.15}$$

where $v = f(r)$ only. Then:

$$\frac{\partial u}{\partial t} = -c\alpha^2 v e^{-c\alpha^2 t} \qquad \textbf{Equation 4.16}$$

$$\frac{\partial u}{\partial r} = e^{-c\alpha^2 t}\frac{dv}{dr} \qquad \textbf{Equation 4.17}$$

$$\frac{\partial^2 u}{\partial r^2} = e^{-c\alpha^2 t}\frac{d^2 v}{dr^2} \qquad \textbf{Equation 4.18}$$

Substitute:

$$-c\alpha^2 v e^{-c\alpha^2 t} = c e^{-c\alpha^2 t}\frac{d^2 v}{dr^2} + \frac{c}{r}e^{-c\alpha^2 t}\frac{dv}{dr} \qquad \textbf{Equation 4.19}$$

Divide by $ce^{-c\alpha^2 t}$:

$$\frac{d^2 v}{dr^2} + \frac{1}{r}\frac{dv}{dr} + \alpha^2 v = 0 \qquad \textbf{Equation 4.20}$$

which is Bessel's Equation of zero order. The solution is of the form (Abramowitz and Stegun, 1964):

$$v(r) = AJ0(\alpha r) + BY0(\alpha r) \qquad \textbf{Equation 4.21}$$

where *J0* and *Y0* are Bessel functions of the first and second kind, respectively and *A* and *B* are constants. Now, use the first boundary condition which states that there is no excess pore pressure generated outside the plasticized zone ($r_{plastic} = r_{cone}\, I_r^{0.333}$) to evaluate the constants *A* and *B* (at $r = r_{plastic}$, $u = 0$):

$$v(r_{plastic}) = AJ0(\alpha r_{plastic})BY0(\alpha r_{plastic}) = 0 \qquad \textbf{Equation 4.22}$$

Solve for A:

$$A = \frac{-BY0(\alpha r_{plastic})}{J0(\alpha r_{plastic})} \qquad \textbf{Equation 4.23}$$

Substitute:

$$\frac{-BY0(\alpha r_{plastic})}{J0(\alpha r_{plastic})}J0(\alpha r) + BY0(\alpha r) = 0 \qquad \textbf{Equation 4.24}$$

Divide by *B*:

$$-Y0(\alpha r_{plastic})J0(\alpha r) + J0(\alpha r_{plastic})Y0(\alpha r) = 0 \qquad \textbf{Equation 4.25}$$

Substitute into solution to yield:

$$v(r) = -J0(\alpha r_{plastic})Y0(\alpha r) + Y0(\alpha r_{plastic})J0(\alpha r) \qquad \textbf{Equation 4.26}$$

Use the second boundary condition which states that the cone is an impermeable boundary (at $r = r_{cone}$, $\frac{\partial v}{\partial r} = 0$):

Note: $J0' = -J1$ and $Y0' = -Y1$ **Equation 4.27**

$$\frac{\partial v}{\partial r} = \alpha J0(\alpha r_{plastic})Y1(\alpha r) - \alpha Y0(\alpha r_{plastic})J1(\alpha r_{cone}) = 0 \qquad \textbf{Equation 4.28}$$

Divide by α:

$$J0(\alpha r_{plastic})Y1(\alpha r_{cone}) - Y0(\alpha r_{plastic})J1(\alpha r_{cone}) = 0 \qquad \textbf{Equation 4.29}$$

In order to evaluate α, the root of the previous equation must be taken; however, this equation has an infinite number of roots. The solution will be the sum of all possible solutions; however, evaluation of the first 50 roots yields sufficient accuracy.

$$u = \sum_{n=1}^{\infty} B_n[-Y0(\alpha_n r)J0(\alpha_n r_{plastic}) + Y0(\alpha_n r_{plastic})J0(\alpha_n r)] \qquad \textbf{Equation 4.30}$$

Using the initial condition imposed by spherical cavity expansion to calculate the pore pressures due to octahedral normal stress (at *t=0*):

$$u = 4s_u \ln(\frac{r_{cone} I_r^{0.333}}{r}) \qquad \textbf{Equation 4.31}$$

Substitute:

$$4s_u \ln(\frac{r_{cone} I_r^{0.333}}{r}) = \sum_{n=1}^{\infty} B_n [Y0(\alpha_n r_{plastic}) J0(\alpha_n r) - J0(\alpha_n r_{plastic}) Y0(\alpha_n r)] \quad \textbf{Equation 4.32}$$

Set $\alpha_n = \alpha_1$ and multiply both sides by $r[Y0(\alpha_1 r_{plastic})J0(\alpha_1 r) - J0(\alpha_1 r_{plastic})Y0(\alpha_1 r)]$:

$$r4s_u \ln(\frac{r_{cone} I_r^{0.333}}{r})[Y0(\alpha_1 r_{plastic}) J0(\alpha_1 r) - J0(\alpha_1 r_{plastic}) Y0(\alpha_1 r)] =$$
$$\sum_{n=1}^{\infty} B_n r[Y0(\alpha_n r_{plastic}) J0(\alpha_n r) - J0(\alpha_n r_{plastic}) Y0(\alpha_n r)] \cdot \quad \textbf{Equation 4.33}$$
$$[Y0(\alpha_1 r_{plastic}) J0(\alpha_1 r) - J0(\alpha_1 r_{plastic}) Y0(\alpha_1 r)]$$

Integrate from a to b:

$$4s_u \int_a^b r \ln(\frac{r_{cone} I_r^{0.333}}{r})[Y0(\alpha_1 r_{plastic}) J0(\alpha_1 r) - J0(\alpha_1 r_{plastic}) Y0(\alpha_1 r)] dr =$$
$$\int_a^b r \sum_{n=1}^{\infty} B_n [Y0(\alpha_n r_{plastic}) J0(\alpha_n r) - J0(\alpha_n r_{plastic}) Y0(\alpha_n r)] \cdot \quad \textbf{Equation 4.34}$$
$$[Y0(\alpha_1 r_{plastic}) J0(\alpha_1 r) - J0(\alpha_1 r_{plastic}) Y0(\alpha_1 r)] dr$$

By the properties of cylinder functions, the right hand side of the equation will vanish in all cases except where $\alpha_n = 1$:

$$4s_u \int_a^b r \ln(\frac{r_{cone} I_r^{0.333}}{r})[Y0(\alpha_1 r_{plastic}) J0(\alpha_1 r) - J0(\alpha_1 r_{plastic}) Y0(\alpha_1 r)] dr = \quad \textbf{Equation 4.35}$$
$$B_1 \int_a^b r[Y0(\alpha_1 r_{plastic}) J0(\alpha_1 r) - J0(\alpha_1 r_{plastic}) Y0(\alpha_1 r)]^2 dr$$

Solve for B_1 to B_n:

$$B_1 = \frac{4s_u \int_a^b r \ln(\frac{r_{cone} I_r^{0.333}}{r})[Y0(\alpha_1 r_{plastic}) J0(\alpha_1 r) - J0(\alpha_1 r_{plastic}) Y0(\alpha_1 r)] dr}{\int_a^b r[Y0(\alpha_1 r_{plastic}) J0(\alpha_1 r) - J0(\alpha_1 r_{plastic}) Y0(\alpha_1 r)]^2 dr} \quad \textbf{Equation 4.36}$$

Now all unknowns are known and the solution for *u = f(r and t)* is:

$$u = \sum_{n=1}^{\infty} B_n e^{-c\alpha_n^2 t}[-Y0(\alpha_n r)J0(\alpha_n r_{plastic}) + Y0(\alpha_n r_{plastic})J0(\alpha_n r)] \qquad \textbf{Equation 4.37}$$

This equation accounts for the pore pressure increase due to spherical cavity expansion. Because the original equation is a linear equation, the solutions for all sets of initial conditions and boundary conditions can be summed.

Consequently, the equation is again solved using the boundary and initial conditions for the shear-induced pore pressure. Assuming a shear zone of radius $r = r_{shear}$ and by the same reasoning as before with the following boundary conditions (at $r = r_{shear}$, $u = 0$ and at $r = r_{cone}$, $\frac{\partial v}{\partial r} = 0$):

$$u = \sum_{n=1}^{\infty} A_n[-Y0(\beta_n r)J0(\beta_n r_{shear}) + Y0(\beta_n r_{shear})J0(\beta_n r)] \qquad \textbf{Equation 4.38}$$

Using the initial condition (at *t=0)*:

$$u = \frac{\sigma_{vo}'(1-(0.5OCR)^{0.8})r - \sigma_{vo}'(1-(0.5OCR)^{0.8})r_{shear}}{(r_{cone} - r_{shear})} \qquad \textbf{Equation 4.39}$$

Solve for A_1 to A_n:

$$A_1 = \frac{\int_a^b r[\frac{(\sigma_{vo}'[(1-(0.5OCR)^{0.8})r - \sigma_{vo}'[(1-(0.5OCR)^{0.8})r_{shear}}{(r_{cone} - r_{shear})}][Y0(\beta_1 r_{shear})J0(\beta_1 r) - J0(\beta_1 r_{shear})Y0(\beta_1 r)]dr}{\int_a^b r[Y0(\beta_1 r_{shear})J0(\beta_1 r) - J0(\beta_1 r_{shear})Y0(\beta_1 r)]^2 dr}$$

Equation 4.40

The solution for shear-induced pore pressures is then:

$$u = \sum_{n=1}^{\infty} A_n e^{-c\beta_n^2 t}[-Y0(\beta_n r)J0(\beta_n r_{shear}) + Y0(\beta_n r_{shear})J0(\beta_n r)] \qquad \textbf{Equation 4.41}$$

The individual solutions can then be summed and solved for a summation of n = 1 to 50 to yield the complete solution:

$$u = \sum_{n=1}^{\infty} B_n e^{-c\alpha_n{}^2 t}[-Y0(\alpha_n r)J0(\alpha_n r_{plastic}) + Y0(\alpha_n r_{plastic})J0(\alpha_n r)] + \sum_{n=1}^{\infty} A_n e^{-c\beta_n{}^2 t}[-Y0(\beta_n r)J0(\beta_n r_{shear}) + Y0(\beta_n r_{shear})J0(\beta_n r)]$$ **Equation 4.42**

Equation 4.41 represents the analytical solution which governs the radial consolidation of porewater surrounding an impermeable probe. This is the form of the equation which will be used in the evaluation of the coefficient of consolidation.

Model Parameters

In its most simple form, the dissipation model requires input values for the effective vertical stress (σ_{vo}'), the hydrostatic pore water pressure (u_o), the radius of the cone used (r), the rigidity index (I_r), the OCR, and the effective stress friction angle (ϕ'). The actual OCR was reported in the published literature for all the sites modeled in this study; however, in a situation where the OCR is not known, it could be calculated from the following approximate equation (Chen and Mayne, 1994; 1995; 1996):

$$OCR \cong 0.46\frac{(q_T - u_2)}{\sigma_{vo}'}$$ **Equation 4.43**

where q_T = corrected cone tip resistance, u_2 = pore pressure measured at the cone shoulder, and σ_{vo}' = effective vertical stress. The undrained shear strength was calculated from the critical-state Modified Cam Clay model and corresponds to triaxial compression loading in terms of effective stresses (Wroth and Houlsby, 1985):

$$\frac{s_u}{\sigma_{vo}'} = \frac{M}{2}\left(\frac{OCR}{2}\right)^{\Lambda}$$ **Equation 4.44**

where Λ = plastic volumetric strain ratio = $1\text{-}C_s/C_c$ and M = the slope of the critical state line in triaxial compression:

$$M = \frac{6\sin\phi'}{3 - \sin\phi'}$$ **Equation 4.45**

In all the experimental case studies evaluated, the actual value of ϕ' was known for each clay; however, it is interesting to note that for the case when the effective stress friction angle is equal to 30^o (assumed value if ϕ' is unavailable), the equation for undrained shear strength reduces to:

$$\frac{s_u}{\sigma_{vo}'} = 0.345OCR^{0.8}$$ **Equation 4.46**

which is approximately the same result as the empirical trend given by Jamiolkowski et al. (1985).

The undrained shear strength ratio is a function of overconsolidation and will increase as the overconsolidation increases. This is consistent except in cases where the clay becomes fissured. Fissures are defined cracks and planes of weakness in a soil, commonly the result of passive failure due to unloading or desiccation effects, which decrease the ultimate shear strength the clay is capable of achieving (Marsland and Quarterman, 1982). Fissures can occur at many scales within the soil, each of which will affect the measurement of properties differently (Figure 4.5). The effects of fissures and joints in clay reduce the undrained strength of the soil mass. Based on experimental work by Bishop (1972) and Skempton et al. (1969), a strength reduction factor of 0.5 was chosen as appropriate for the very heavily fissured clays. Additional work in quantifying the strength reduction factor is warranted.

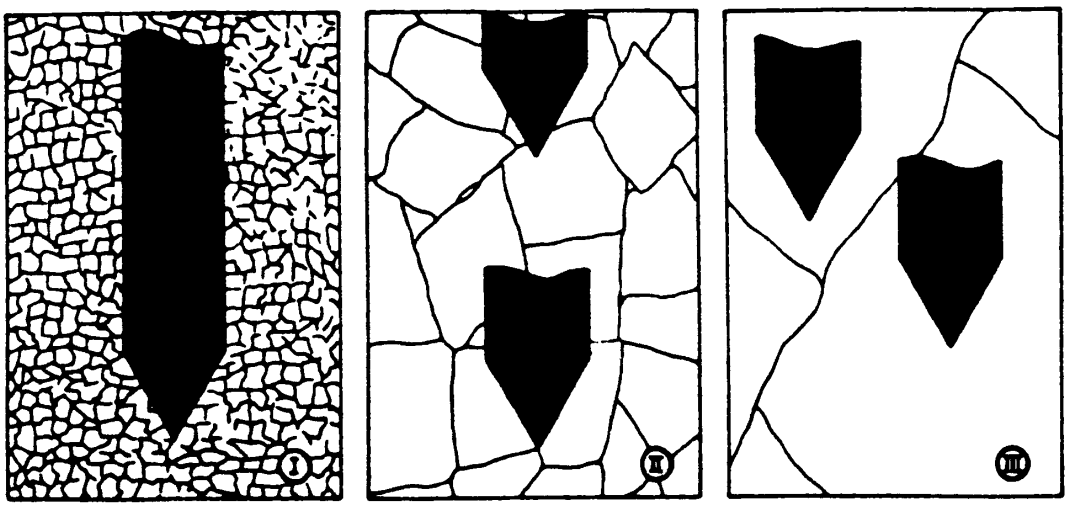

Figure 4.5. Scale Effects of Fissuring as Related to Cone Penetration (Marsland and Quarterman, 1982)

The size of the induced plasticized zone generated by the cone sounding was calculated according to spherical cavity expansion using Equation 4.5. Note that:

$$I_r = \frac{E}{2(1+\nu)s_u} = \frac{G}{s_u} \qquad \textbf{Equation 4.47}$$

where E = equivalent elastic Young's modulus = $2G(1+\nu)$, G = shear modulus, ν = Poisson's ratio (= 0.5 for undrained conditions), and s_u = undrained shear strength. The rigidity index affects both the size of the plasticized zone as well as the increase in excess pore stress due to changes in octahedral normal stresses. However, the appropriate value of the rigidity index is ill-defined and generally quite difficult to assess for a given soil (Mayne, 1995). Consequently, the rigidity index was taken as an input parameter and multiple dissipation curves are presented based on chosen values for the rigidity index. Alternately, when the initial generated pore pressure is measured, the rigidity index can be calculated because all other parameters (u_{meas}, σ_{vo}', ϕ', OCR, and u_o) are known.

The next step in the model was to calculate the excess pore pressure generated due to cone penetration. The octahedral normal component of the pore pressure was calculated using spherical cavity expansion (Equation 4.10). Pore pressure was assumed to increase only within the plastic zone; excess pore pressure outside the plastic zone was set equal to zero.

Finally, the magnitude of shear-induced pore pressures for a Type 2 cone was calculated using the concepts of Cam Clay (Mayne and Bachus, 1988):

$$\Delta u_{shear} = \sigma_{vo}'[1-(\frac{OCR}{2})^{\Lambda}] \qquad \textbf{Equation 4.48}$$

where Δu_{shear} = excess pore pressure generated due to shear stress changes.

The determination of the width of the zone which is affected by the shear stresses is not as straight-forward as is the determination for the octahedral normal stresses. In the analysis of shear stresses developed during the driving of piles, Randolph and Wroth (1978, 1979a) show that shear stress decreases as a function of radial distance away from the pile. Consequently, the increase in excess pore pressure due to changes in shear stress were assumed to decrease linearly with distance away from the cone body. The thickness of the shear zone was set at 2 mm; however, the error surfaces were plotted in order to asses the effect of the width of the shear zone (from 1 mm to 10 mm) on the calculated pore pressure dissipation. The error surfaces will be discussed later in the chapter.

The final form of the equation for calculating the generated excess pore pressure is as follows:

at $t = 0$ $$u_m = \frac{4}{3}[\sigma_{vo}' \cdot \frac{M}{2}(\frac{OCR}{2})^{\Lambda}]\ln I_r + \sigma_{vo}'[1-(\frac{OCR}{2})^{\Lambda}] + u_o \qquad \textbf{Equation 4.49}$$

at $t = t_{100}$ $$u_m = u_o \qquad \textbf{Equation 4.50}$$

The initial distribution of the excess pore pressure within the plastic zone was used as the initial condition to solve the one-dimensional, uncoupled partial differential consolidation equation for radial drainage as derived previously (Equation 2.9). Boundary conditions assume that there is no increase in excess pore pressure outside the spherical cavity plastic zone ($\Delta u = 0$) and that the cone body was an impermeable boundary. After the excess pore pressure dissipation was calculated, the values were added to the hydrostatic pore pressure value at that depth. This was done because the piezocone measures total pore pressures (hydrostatic plus excess).

The final version of the model used an analytical solution to the consolidation equation to predict pore pressure as a function of time (Carslaw and Jaeger, 1959; Randolph and Wroth, 1979b). All calculations were performed using the software package MathCad. The analytical solution was an improvement over the originally used finite difference scheme for many reasons. First of all, the forward finite difference solution is severely limited by the stability criterion which requires that $c_h \Delta t/\Delta r^2 < 0.5$. This forces small times steps which require excessive computer time. The analytical solution is not limited by stability concerns, is rapid because pore pressure can be calculated at any radius and any time, and requires less memory and less time. A typical solution using the finite

difference approximation required one hour using a pentium 75 MHz processor, while the analytical solution required fifteen seconds on the same computer.

The model was run interatively with an input value of c_h chosen for the initial run. Based on the results of the first iteration, a new value for c_h was chosen until the deviation of the predicted dissipation curve was at a minimum from the actual measured dissipation curve as determined using the sum of the squared errors.

Evaluated Results From Test Sites

Documented porewater pressure dissipation measurements from piezocone soundings and instrumented driven pile test sites in both normally-consolidated to lightly-overconsolidated and heavily-overconsolidated clays were chosen for comparison with the prediction of the model. Six soft clay sites which exhibited normal monotonically-decreasing dissipation curves and nine stiff to hard clays (3 crustal) which exhibited dilatory pore pressure behavior were chosen.

A listing of the fifteen sites used for evaluation is given in Table 4.1. All model predictions of the value of the coefficient of consolidation were performed without prior knowledge of either the laboratory measured values or of previously predicted field values. Table 4.1 shows a compilation of the relevant soil parameters for each site evaluated by the method including the input data [hydrostatic pressure (u_o), effective overburden stress (σ_{vo}'), overconsolidation ratio (OCR), and effective friction angle (ϕ')], the cone data [corrected tip resistance (q_T), measured pore pressure (u_2), and depth of dissipation test or piezometer measurements (d)], and the clay characteristics [natural water content (w_n), liquid limit (LL), and plasticity index (PI)]. References for the data are also listed.

Reference Values of the Coefficient of Consolidation

The most common method to obtain a representative value of the coefficient of consolidation is from the one-dimensional consolidation test. The procedure is a fitting method, based on either a logarithmic time or Taylor square root of time plot of the rate of compression data for a clay in an oedometer test. The measured value is the vertical coefficient of consolidation because drainage in the consolidation test is limited to the vertical direction. In reality, the value of c_v obtained from consolidation testing is somewhat arbitrary due to the empirical steps in the fitting, to the dependence on load increment, to the small sample size, and due to the one-dimensional limitations imposed on the test. While measurements of the coefficient of consolidation are useful for estimating rate of settlement and for correlating with the hydraulic conductivity, the values are only approximate.

In an extensive study on the permeability characteristics of soft clays, Tavenas et al. (1983a; 1983b) noted that the assumptions of constant permeability, compressibility, and coefficient of consolidation in Terzaghi's one-dimensional consolidation theory are not accurate for a soil exhibiting a changing void ratio. Numerical modeling which accounted for the changes in permeability and compressibility during a consolidation step showed a value of c_v which was 4.4 times larger at the beginning of the load step than it was at the end of the step (Tavenas et al., 1983a; 1983b). The study results call into question the reliability of the values for the coefficient of consolidation obtained from empirical construction techniques on one-dimensional consolidation curves. Several researchers have shown that the measured laboratory values of the coefficient of consolidation can vary by several orders of magnitude from the field values which were determined from back-calculation of settlement data (Rowe and Barden, 1966; Rowe, 1972; Grisak, 1975; Grisak and Cherry, 1975).

Table 4.1. Clay Sites Used For Dissipation Modeling

Test Site	Depth (m)	u_o (kPa)	σ_{vo}' (kPa)	OCR	w_n	LL	PI	ϕ'	s_u (kPa)	q_T (kPa)	u_2 (kPa)	Reference
Bothkennar, U.K.	12.0	107.8	96.2	1.4	55	72	50	33	48	898	499	Jacobs and Coutts 1992
Drammen, Norway	19.5	179.0	121.0	1.1	30	20	10	34	52	890	450	Lacasse and Lunne 1982
McDonald Farm, B.C.	20.0	181.5	178.5	1.1	36	35	10	35	78	1036	600	Sully, 1991; Robertson et al., 1988a
Onsøy, Norway	18.5	159.4	114.5	1.4	60	75	36	34	49	754	450	Lacasse and Lunne 1982
Porto Tolle, Italy*	9.3	81.4	90.6	1.2	36	52	30	30	36	580	250	Battaglio et al. 1981
St. Alban, Quebec	4.6	40.2	42.6	1.2	54	38	18	27	15	300	160	Roy et al. 1981; Roy et al. 1982
Amherst, MA	3.0	16.7	38.2	7.0 (crust)	40	38	11	30.5	64	1369	80	Lutenegger 1995; Lally 1993
Brent Cross, U.K.	12.0	115.0	117.8	31.0	29	75	51	20	204	2200	100	Lunne et al. 1985 Lunne et al. 1986b
Canon's Park, U.K.**	5.7	46.1	67.9	14.0	30	75	50	22.5	141	2590	436	Jardine and Bond 1989
Cowden, U.K.	17.2	95.0	283.4	3.4	15	32	16	24	140	898	575	Lunne et al. 1985; Lehane and Jardine 1994
Madingley, U.K.**	5.8	37.2	72.8	35.0	31	78	48	26	125	2000	200	Coop and Wroth, 1989; Lunne et al. 1986b
Raquette River, NY	3.0	22.7	44.0	8.0 (crust)	46	68	48	25	66	1447	317	Lutenegger and Kabir 1987
St Lawrence Seaway, NY	6.1	53.0	63.0	3.5 (crust)	60	50	30	30	59	976	382	Lutenegger and Kabir 1987
Strong Pit, B.C.	6.7	0.0	146.3	4.4	15	26	11	35	195	2174	1200	Sully 1991; Sully and Campanella, 1994
Taranto, Italy***	9.0	78.5	101.5	26.0	23	60	27	28	532	5451	1818	Pane et al. 1995; Battaglio et al. 1986

*Piezoprobe
**Pile
***Cemented

It is also of interest to note that additional studies regarding the ratio of the horizontal permeability of clays to the vertical permeability showed that for the natural clays tested, the ratio ranged from 0.81 to 1.16 with an average value of 1.03 (Tavenas et al., 1983a; 1983b). The authors and others found significant anisotropy in permeability behavior restricted to a small group of atypical clays including varved clays and highly stratified deposits (Leroueil and Jamiolkowski, 1991).

Dissipation Sites

The model results for the clay sites are discussed below; summary data for all sites modeled (normally-consolidated and overconsolidated) are listed in Table 4.1 and Table 4.2. Table 4.2 lists the output information generated by the c_h evaluation. While the method was developed for the estimation of the coefficient of consolidation, it is also useful to obtain an approximate value of the rigidity index through magnitude of the initial generated pore pressures. Table 4.2 compares laboratory data with the method-estimated data as well. In general, the piezocone-evaluated

numbers are similar to the laboratory reported numbers measured in the one-dimensional consolidation test.

Table 4.2. Comparison of Model Predictions and Laboratory Values

Site	Depth (m)	I_r	Piezo Element Data (This study) c_h (mm^2/s)	Lab Measured c_v (mm^2/s)	Comment	Reference
Bothkennar, U.K.	12.0	100	0.2	0.32 0.08 - 0.13*		Nash et al. (1992) Jacobs and Coutts (1992)
Drammen, Norway	19.5	100	0.2	0.53 - 1.52		Lacasse and Lunne (1982)
McDonald Farm, B.C.	20.0	200	1.9	1.8 - 5.5*		Sully (1991) Robertson et al. (1988a)
Onsøy, Norway	18.5	100	0.05	0.44 - 0.79** 0.10 - 0.22*		Lacasse and Lunne (1982)
Porto Tolle, Italy	9.3	50	0.2	0.29 - 0.54 0.20 - 0.35*	15 mm Piezo Probe	Battaglio et al. (1981) Battaglio et al. (1986)
Saint Alban, Quebec	4.6	200	0.6	0.30 0.10 - 0.20*		Roy et al. (1981); Roy et al. (1982)
Amherst, MA	3.0	15	0.4	0.07 - 0.10*	Crust	DeGroot and Lutenegger (1994) Lally (1993)
Brent Cross, U.K.	12.0	~10	0.0005	0.008 - 0.03*		Lunne et al. (1985) Lunne et al. (1986b)
Canon's Park, U.K.	5.7	100	0.25	0.01 - 0.03*	102 mm Pile	Jardine and Bond (1989)
Cowden, U.K.	17.2	200	0.2	0.05 - 0.19*		Lunne et al. (1985) Lehane and Jardine (1994)
Madingley, U.K.	5.8	~10	0.05	0.03 - 0.08*	80 mm Pile	Coop and Wroth (1989) Lunne et al. (1986b)
Raquette River, NY	3.0	50	0.5	0.035 - 0.70	Crust	Lutenegger and Kabir (1987)
St Lawrence Seaway, NY	6.1	50	0.3	0.25 - 0.80 0.07 - 0.10*	Crust	Lutenegger and Kabir (1987)
Strong Pit, B.C.	6.7	200	0.2	0.06 - 0.30*		Sully (1991); Sully and Campanella (1994)
Taranto, Italy	9.0	200	0.4	0.10 - 0.25	Cemented Clay	Battaglio et al. (1986) Bruzzi and Battaglio (1987)

*Data collected by Robertson et al. (1992) in a review of methods of coefficient of consolidation prediction from dissipation testing.
**Results from horizontal oedometer test.

Soft Clay Sites

Six soft clay sites were chosen from the literature for dissipation modeling. The sites examined included Bothkennar, Drammen, McDonald Farm, Onsøy, Porto Tolle, and St. Alban. Results from the evaluation are shown in Figure 4.6 through Figure 4.11. For the most part, the estimated value of the coefficient of consolidation reasonably approximated the laboratory measured value, and are typically within one-half to two times the laboratory measured value of c_v. An interesting feature to note in the evaluation of the dissipation curves is the good agreement in the fit of the estimated and the measured dissipation curves.

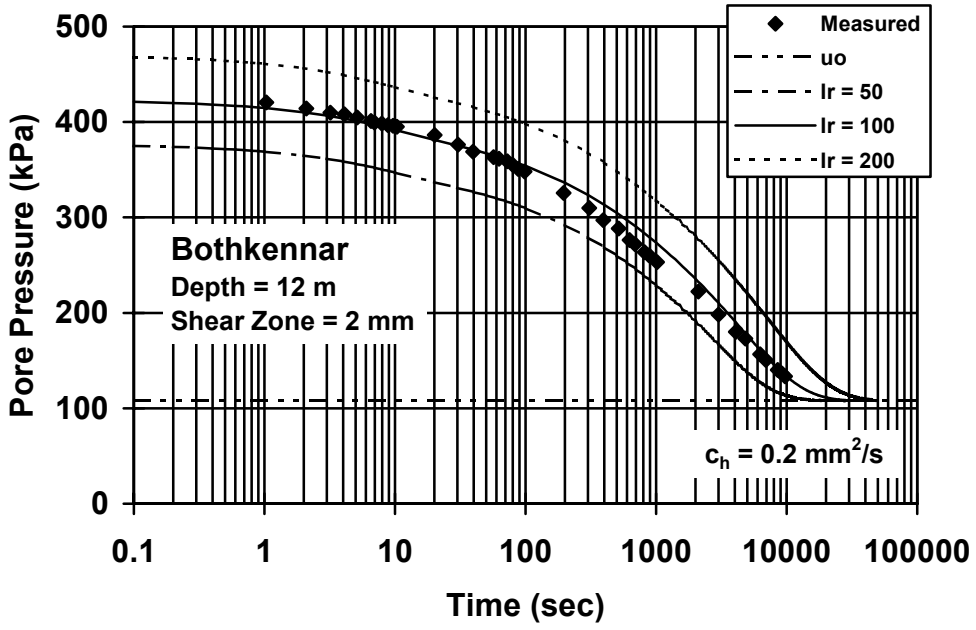

Figure 4.6. Model Predictions at Bothkennar, U.K.
(Data from Jacobs and Coutts, 1992)

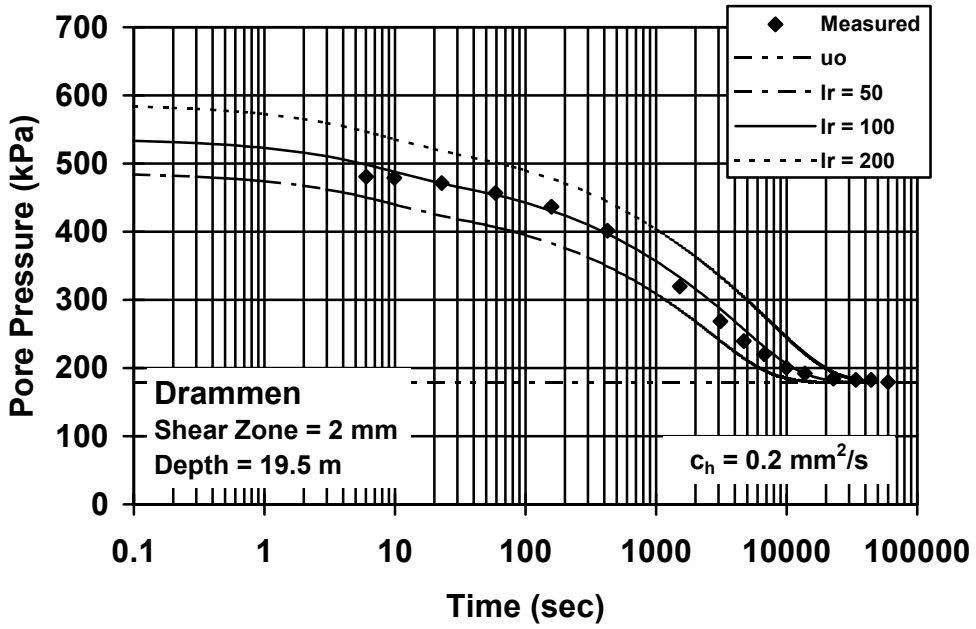

Figure 4.7. Model Predictions at Drammen, Norway
(Data from Lacasse and Lunne, 1982)

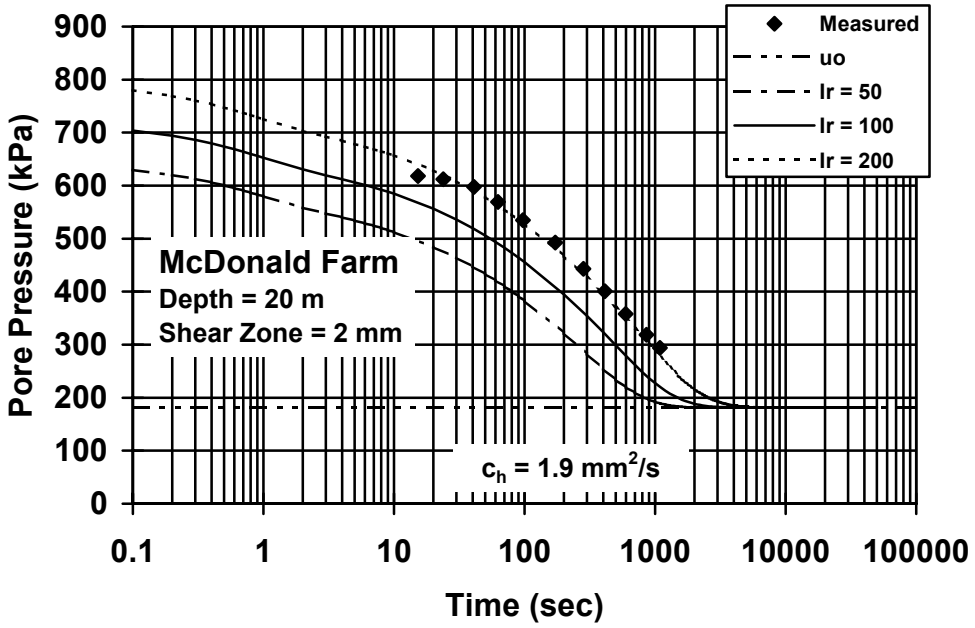

Figure 4.8. Model Predictions at McDonald Farm, B.C.
(Data from Sully, 1991)

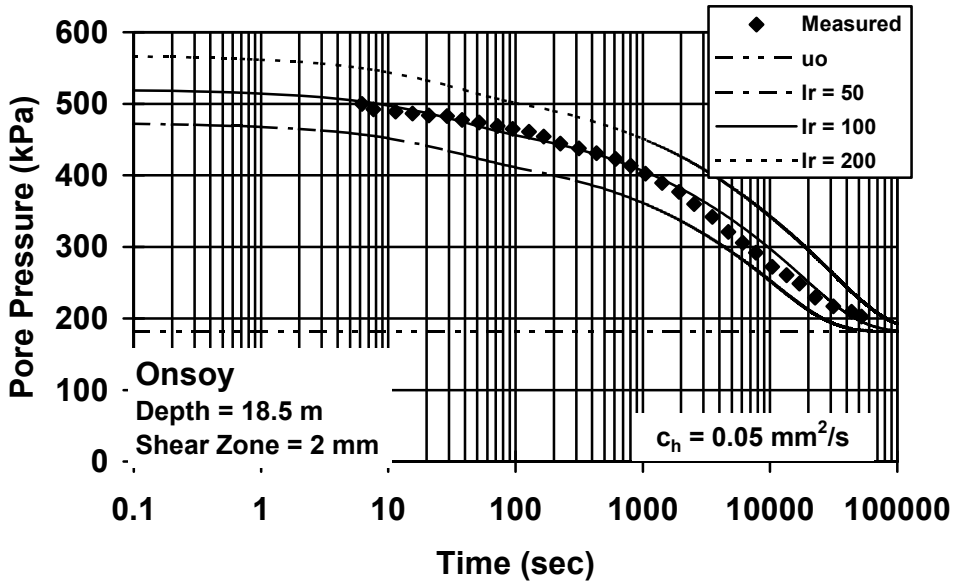

Figure 4.9. Model Predictions at Onsoy, Norway
(Data from Lacasse and Lunne, 1982)

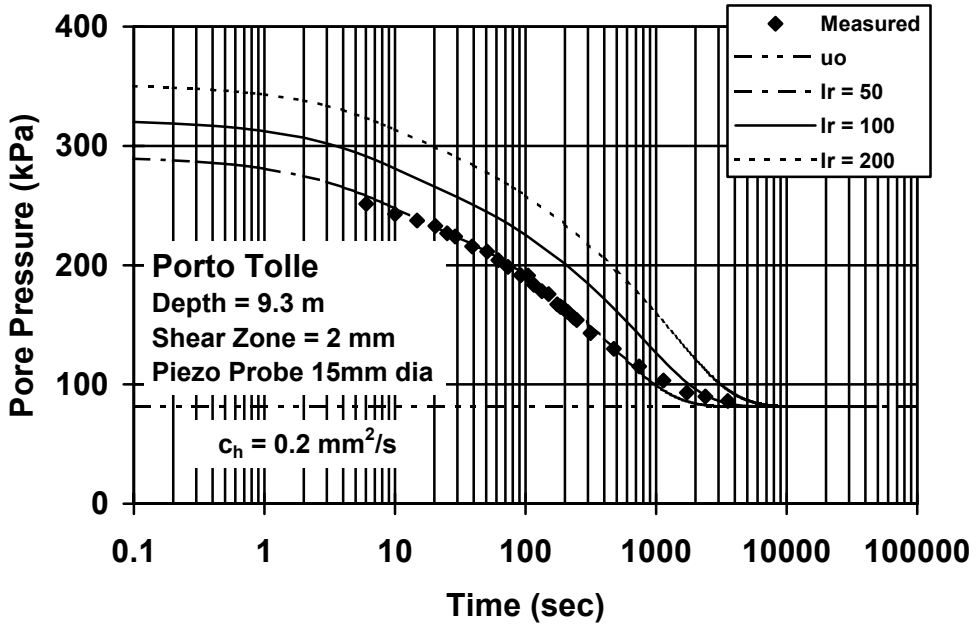

Figure 4.10. Model Predictions at Porto Tolle, Italy (Piezoprobe Data from Battaglio et al., 1981)

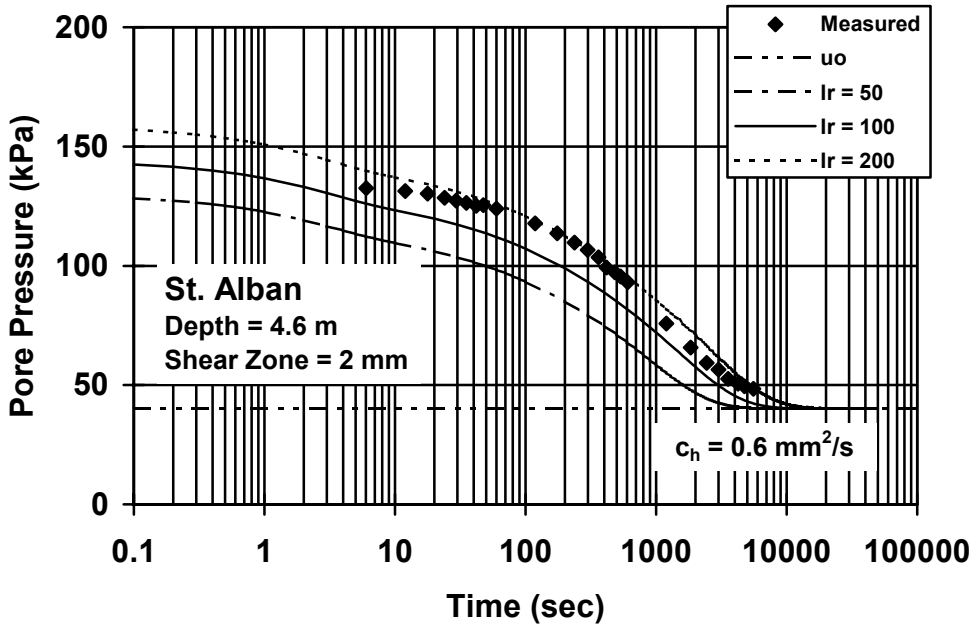

Figure 4.11. Model Predictions at Saint Alban (Data from Roy et al., 1982)

Stiff Clay Sites

Nine hard to stiff clay sites were chosen from the literature for dissipation modeling in cases where the pore pressures values demonstrated the dilatory behavior as a function of time in either piezocone dissipation records or instrumented pile pore pressure transducer records. The sites evaluated included Brent Cross, Canon's Park, Cowden, Madingley, Taranto and the crustal layers at Amherst, Raquette River, and St. Lawrence Seaway. For dissipation in stiff clays, the model input parameters were the same as in the soft clay sites.

In the case of overconsolidated clays (OCR > ~3), the shear-induced pore pressures can go negative and force a draw-down in the value of pore pressure close to the cone body; however, the shear-induced pore pressures are limited to a thin zone adjacent to the cone body. Because this creates a large gradient, these pore pressures can dissipate more rapidly, allowing the pore pressure to return to the value induced by octahedral normal stresses. In the field, this phenomenon is observed when testing with a dual-element piezocone in overconsolidated clays. The recorded Type 1 pore pressures begin positive and decay, while the Type 2 pore pressures begin negative, then increase, and then decay monotonically along the same line as the Type 1 pore pressures (Chen and Mayne, 1994).

Results from the evaluation at the stiff clay sites are shown in Figure 4.12 through Figure 4.20. While the estimated values of the coefficient of consolidation at the sites are reasonable with respect to the laboratory values, there is a bias toward estimating a faster rate of dissipation, or a higher value of c_v, in the heavily-overconsolidated clays than was measured in laboratory testing. Additionally, the shape of the dissipation curves is also an important factor, especially for the transient-increasing behavior. Several of the sites have dissipation curves which match the predicted shape very well; however, some of the sites have significant variations, especially in the initial portion of the curves, which indicates that there are other additional factors which influence the dissipation process . Nonetheless, the results are promising and are worthy of further exploration.

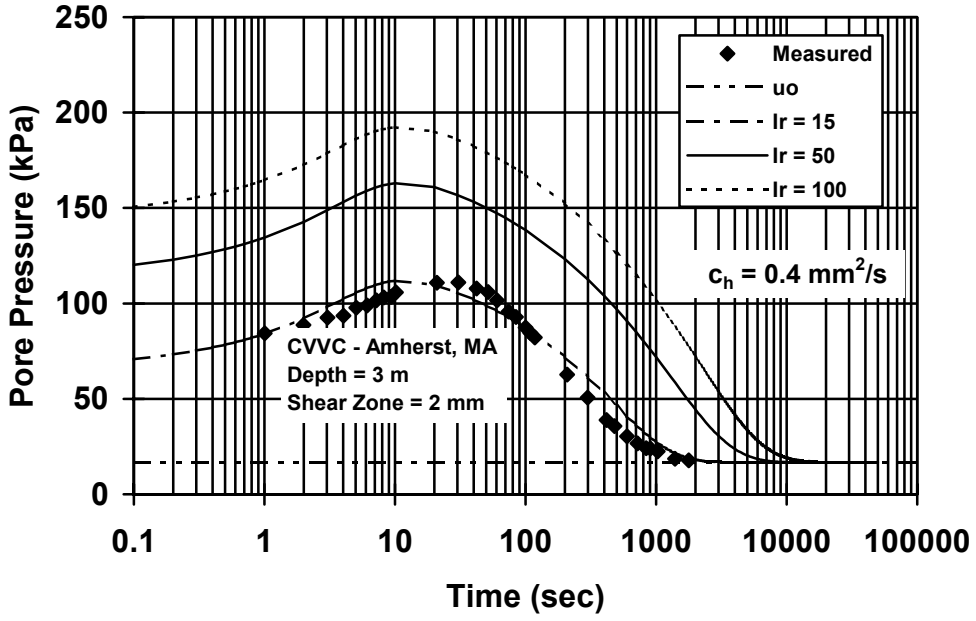

Figure 4.12. Model Prediction in OC Crust at Amherst, MA (Data from Lally, 1993)

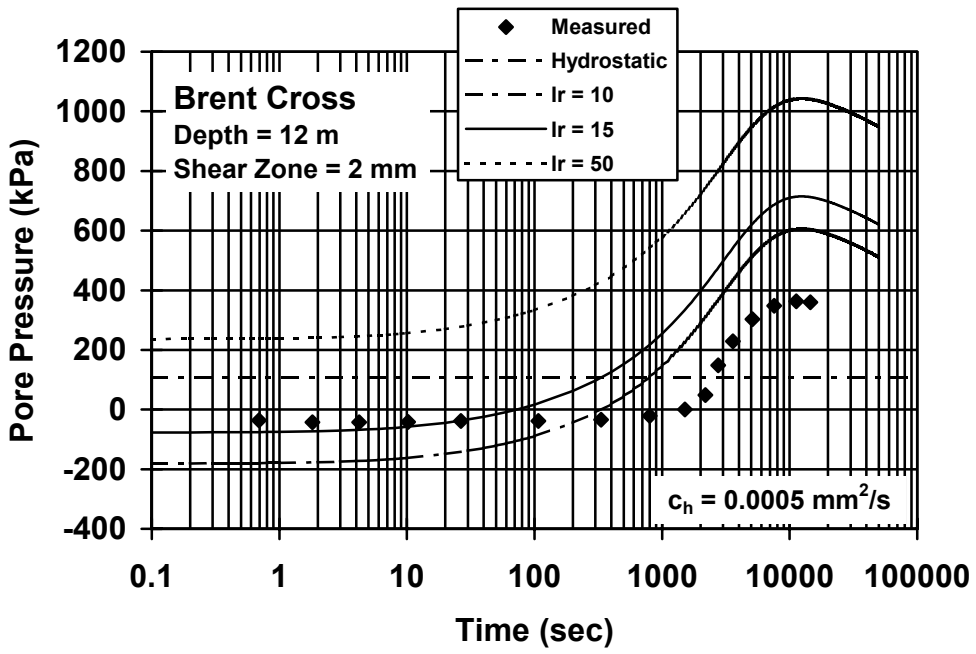

Figure 4.13. Model Prediction at Brent Cross, U.K.
(Data from Lunne et al., 1985)

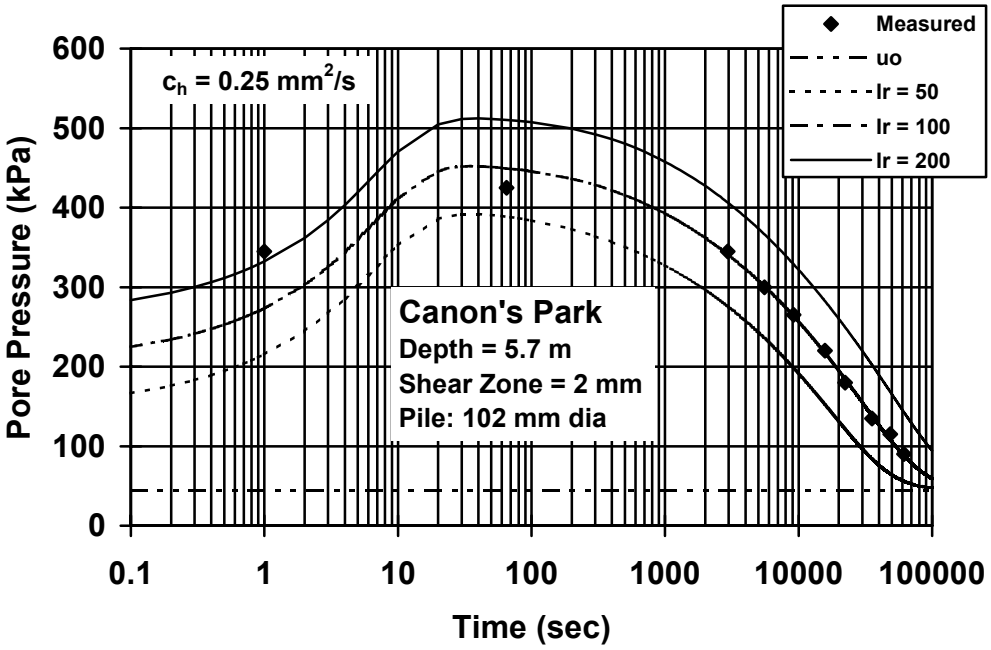

Figure 4.14. Model Prediction at Canon's Park, U.K.
(Instrumented Pile Data from Bond and Jardine, 1991)

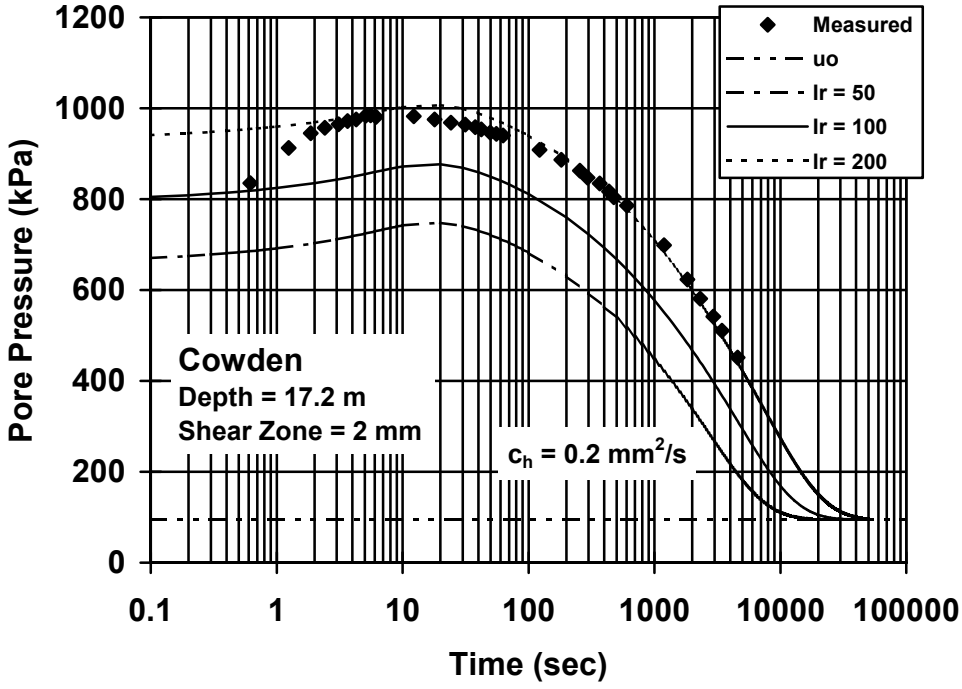

Figure 4.15. Model Predictions at Cowden, U.K.
(Data from Lunne et al., 1985)

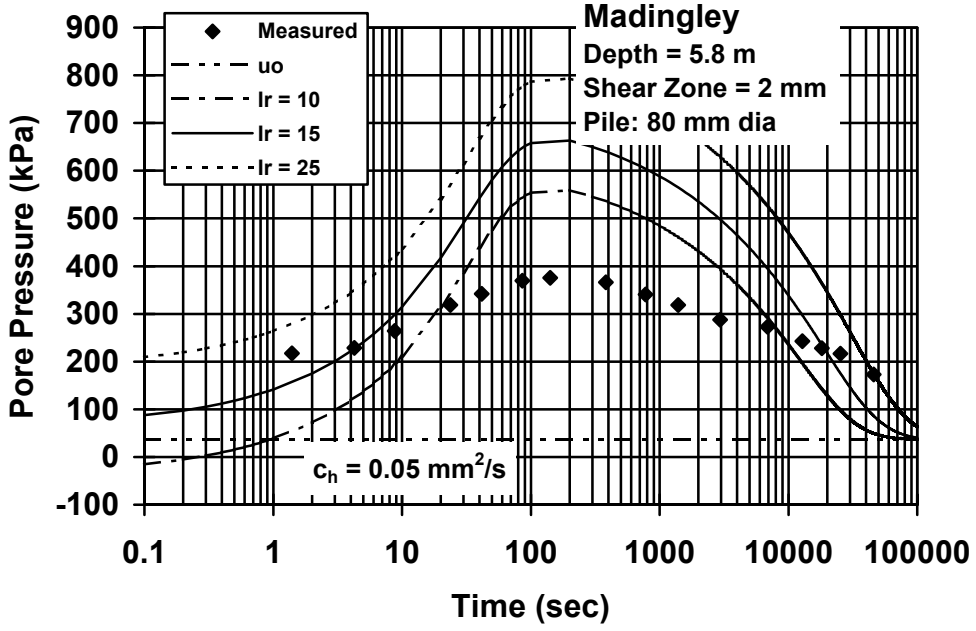

Figure 4.16. Model Predictions at Madingley, U.K.
(Instrumented Pile Data from Coop and Wroth, 1989)

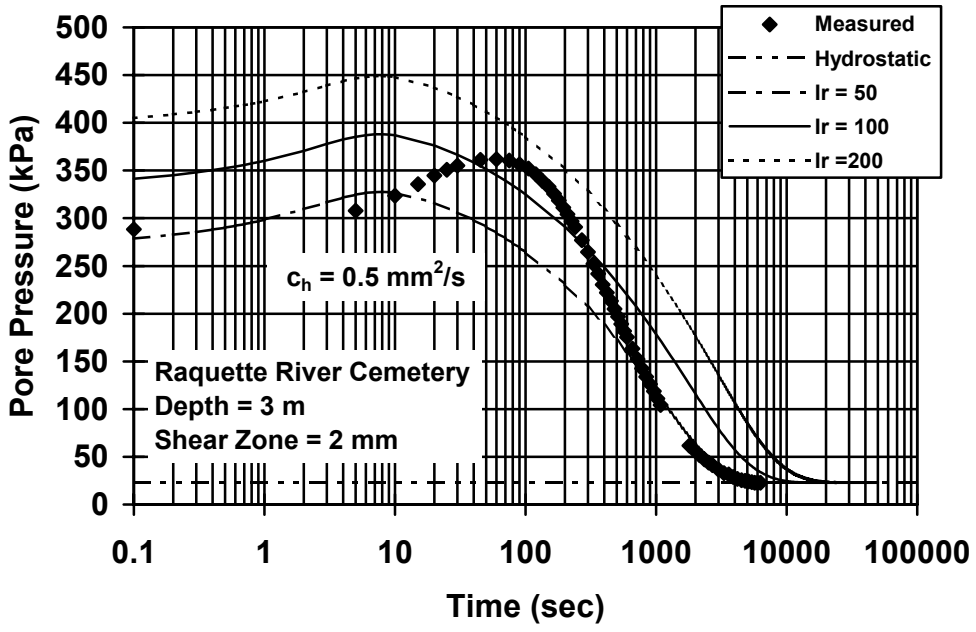

Figure 4.17. Model Prediction in Crustal Clay at Raquette River Cemetery, NY
(Data from Lutenegger, 1997)

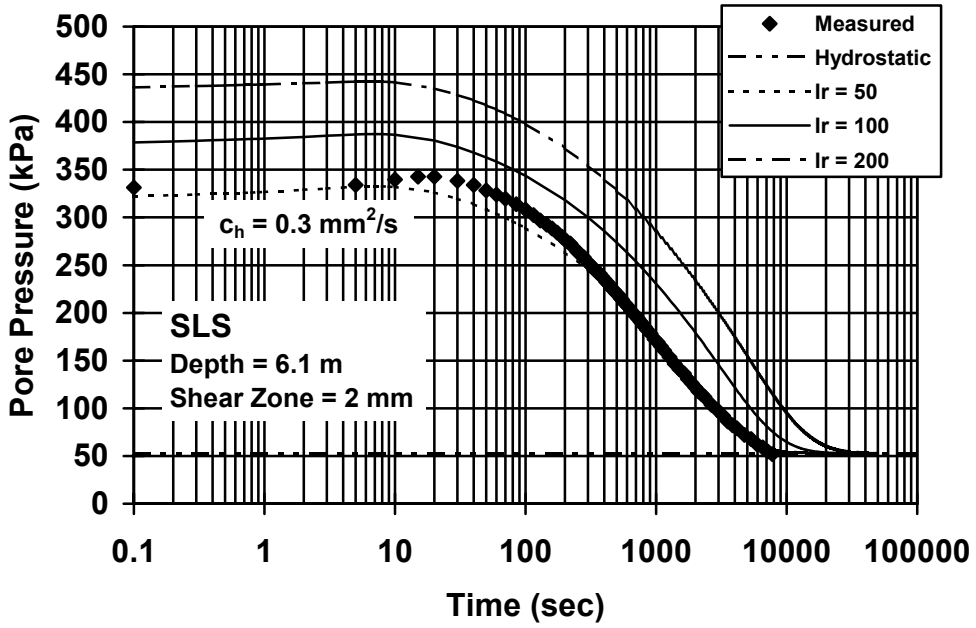

Figure 4.18. Model Prediction in Crustal Clay at Saint Lawrence Seaway, NY (Data from Lutenegger, 1997)

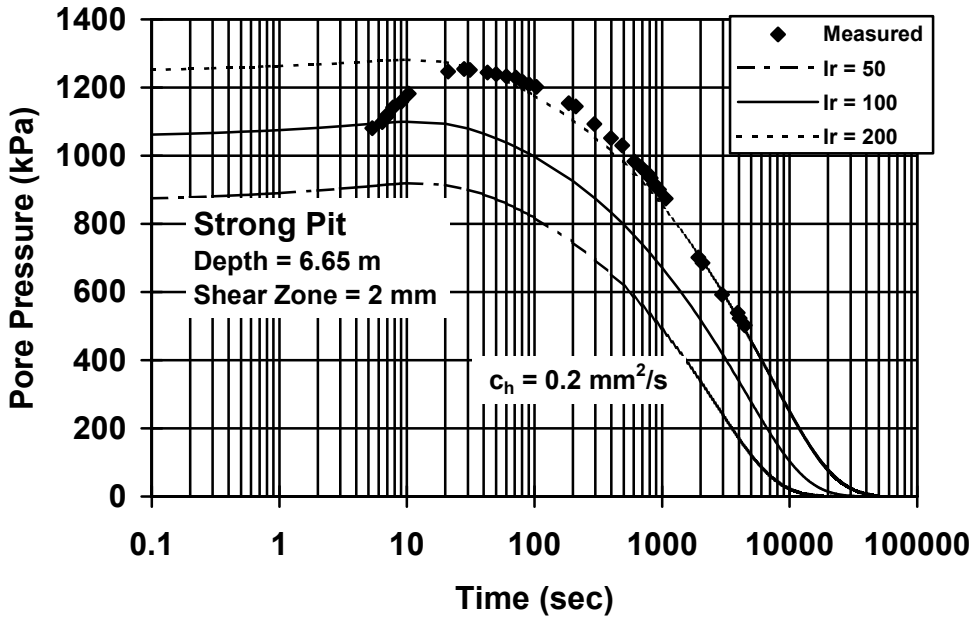

Figure 4.19. Model Prediction at Strong Pit, Canada (Data from Sully, 1991)

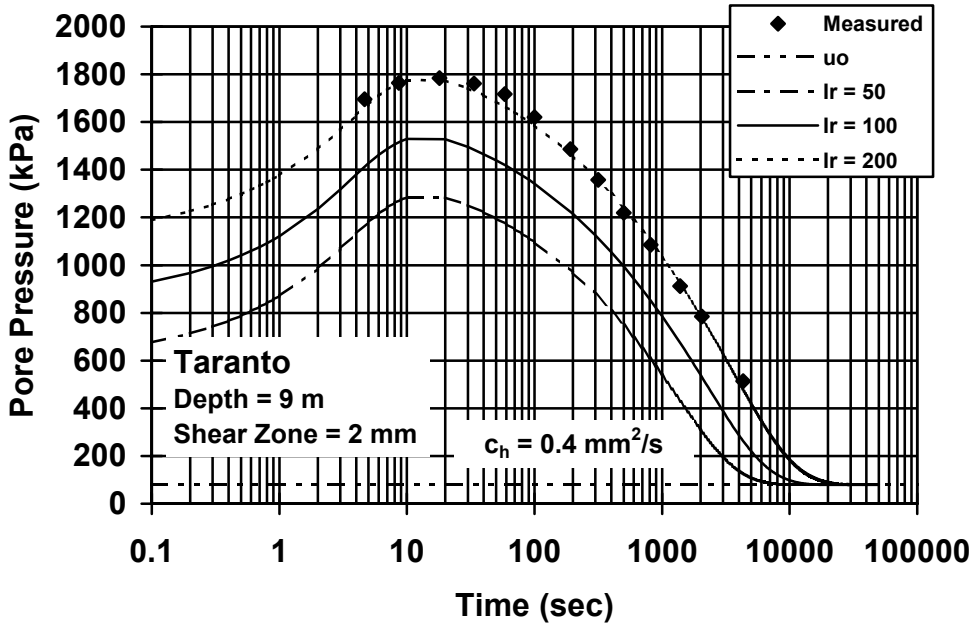

Figure 4.20. Model Prediction in Cemented Clay at Taranto, Italy (Data from Bruzzi and Battaglio, 1987)

Error Surfaces for Model Parameters

A study was performed in order to identify the effect of the model input parameters on the predicted results. Specifically, the error, or the residual, was calculated between each predicted and actual measurement by the following (Santamarina and Fratta, 1997):

$$e_i = y_i^{(meas)} - y_i^{(pred)} \qquad \textbf{Equation 4.51}$$

where e_i = the error, $y_i^{(meas)}$ = the measured value, and $y_i^{(pred)}$ = the model predicted value. The error norm was then calculated as the sum of the squared errors using the following equations:

$$L_n = \left[\sum_i \left| e_i \right|^n \right]^{\frac{1}{n}} \qquad \textbf{Equation 4.52}$$

$$L_2 = \left[\sum_i \left| e_i \right|^2 \right]^{\frac{1}{2}} \qquad \textbf{Equation 4.53}$$

where L_2 = error norm with n = 2. The best fit for the model parameters was then achieved by varying one parameter until the error converged to a minimum. The L_2 error norm uses a least squares minimization, and assumes that the measured data follow a Gaussian distribution. The input parameters which were varied included the width of the shear zone, the coefficient of consolidation,

the rigidity index, the effective friction angle, and the OCR. The error norms are plotted versus a reasonable operating range in engineering practice for the parameters investigated.

Figure 4.21 and Figure 4.22 show the resulting error norms from changing the width of the zone of soil affected by the shearing action due to the soil and penetrometer interaction in a soft clay (Bothkennar) and in a hard clay (Taranto), respectively. Each point on the graphs represents a different run of the model. The results show clearly that the width of the shear zone has little effect in the soft clay where the contribution of shear stresses are less significant than in the stiff clay. In the soft clay, the sum of the squared errors remained essentially constant. However, the width of the shear zone in the hard clay had a more significant effect, especially as the width of the shear zone was increased over 2 mm. The calculated error norm reached a minimum at 2 mm, and increased as the width of the shear zone was increased.

Variation of the shear zone width has several physical implications for the dissipation of excess pore pressure. First, the width of the shear zone will affect the magnitude and distribution of shear-induced excess pore pressures as a function of distance from the cone. Pile foundation studies show that the shear-induced pore pressures decrease as a function of distance from the penetrometer (Randolph and Wroth, 1979a); therefore, a narrow shear zone will concentrate the increase in pore pressures due to shear stresses adjacent to the cone body. Changing the width of the shear zone also affects the dissipation behavior surrounding a penetrometer. Figure 4.23 illustrates the zones of soil surrounding the penetrometer which are affected by the soil/probe interaction. A narrow shear zone will have a large increase in total pore pressure adjacent to the cone body which will drop significantly outside the zone of shear-induced pore pressures. Consequently, a narrow shear zone will differ from a wider one in dissipation behavior due to the initial distribution of pore pressures. In the more narrow zone, the shear-induced pore pressures are concentrated in a small band which creates a larger gradient (same magnitude of shear-induced pore pressure over a shorter

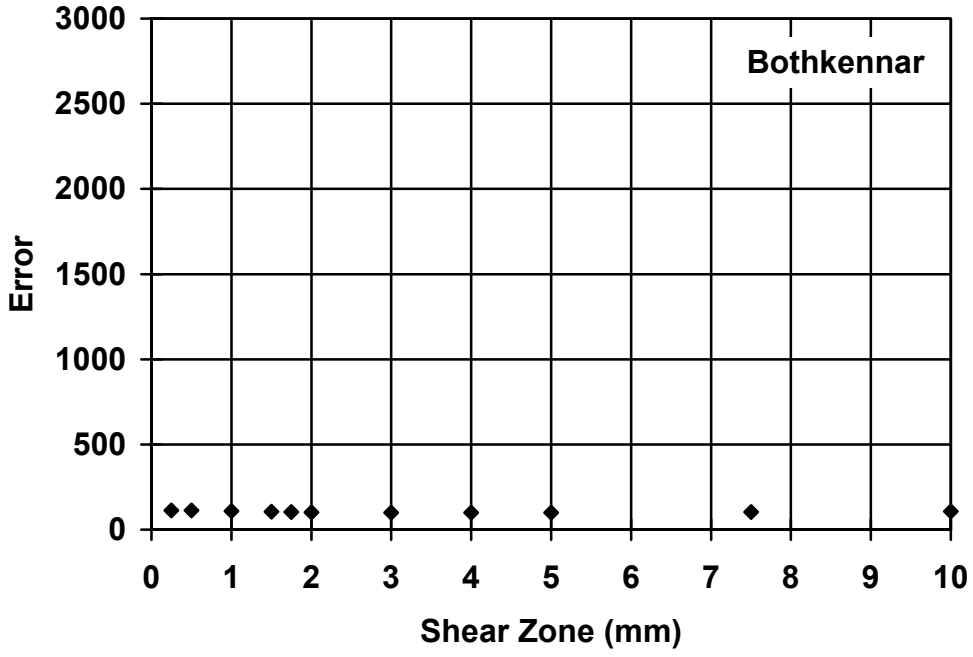

Figure 4.21. Error Norm for the Width of Shear Zone in a Soft Clay

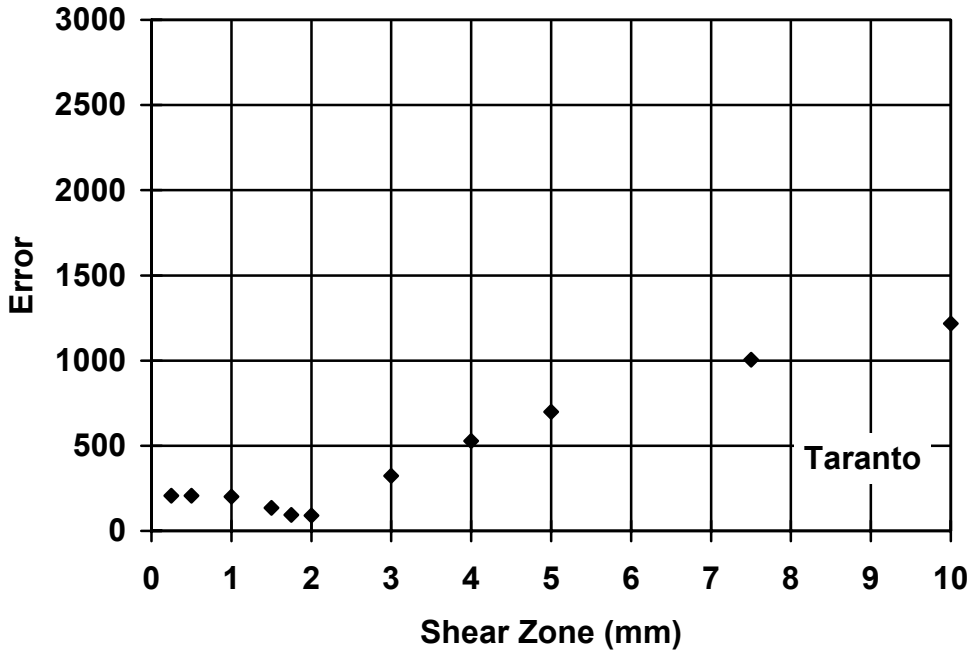

Figure 4.22. Error Norm for the Width of Shear Zone in a Hard Clay

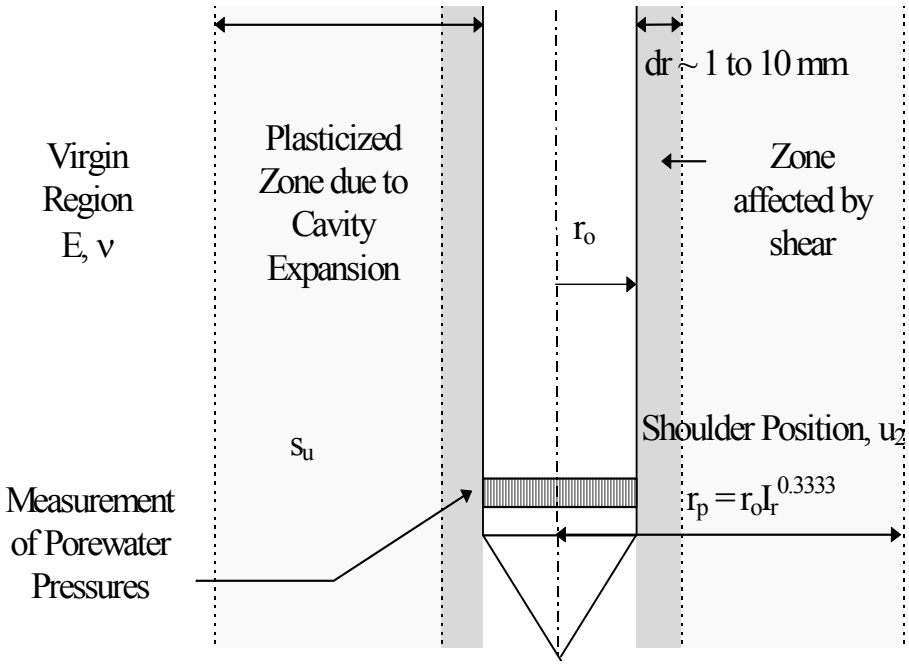

Figure 4.23. Zones Affected By Cone Penetration

distance) and allows for more rapid dissipation of pore pressures. After the initial rapid dissipation of the shear-induced pore pressures, the dissipation curves all follow essentially the same pattern.

Based on the results of the parametric study for the sites evaluated in this study, a shear zone with a width of 2 mm was chosen as the value which best estimated the experimental data. However, the width of shear is probably variable and affected by test strain rate, which would produce a different width zone for a cone penetration sounding versus a jacked pile.

The error norms which resulted from variation of the value of the coefficient of consolidation were also plotted. Figure 4.24 shows the effect of varying c_h over approximately two orders of magnitude in the Bothkennar clay and Figure 4.25 shows the same for the Taranto clay. In both cases, the value of the coefficient of consolidation was easily identified; however, in the Taranto case, steep gradients of approach of the error from both the lower and higher values of the parameter were observed. For the same level of error, the range in the value of the coefficient of consolidation is much larger for the soft clay than it is for the hard clay, indicating that the model is more sensitive to variation in the parameter in the case of the hard clay.

The error norms for the rigidity index in both the soft and hard clay deposits are shown in Figure 4.26 and Figure 4.27. In both cases, variation of the value of the rigidity index significantly affected to calculated error norm for magnitudes less than the minimum error, but had a less significant effect at values larger than the minimum error. Again, as was the case for the coefficient of consolidation, the hard clay site was more sensitive to variation in the parameter than was the soft clay site.

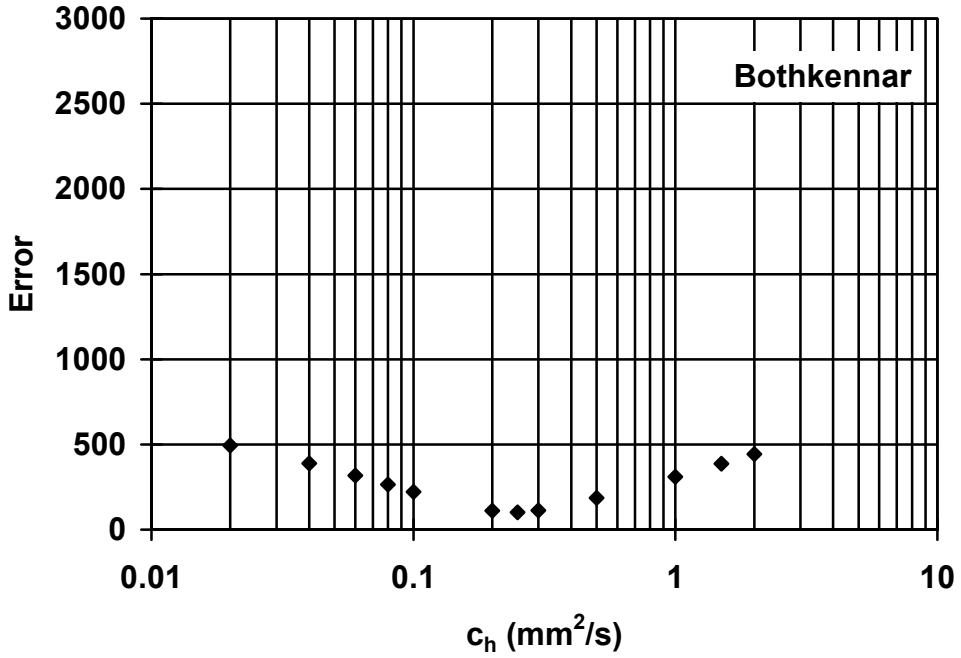

Figure 4.24. Error Norm for the Coefficient of Consolidation in a Soft Clay

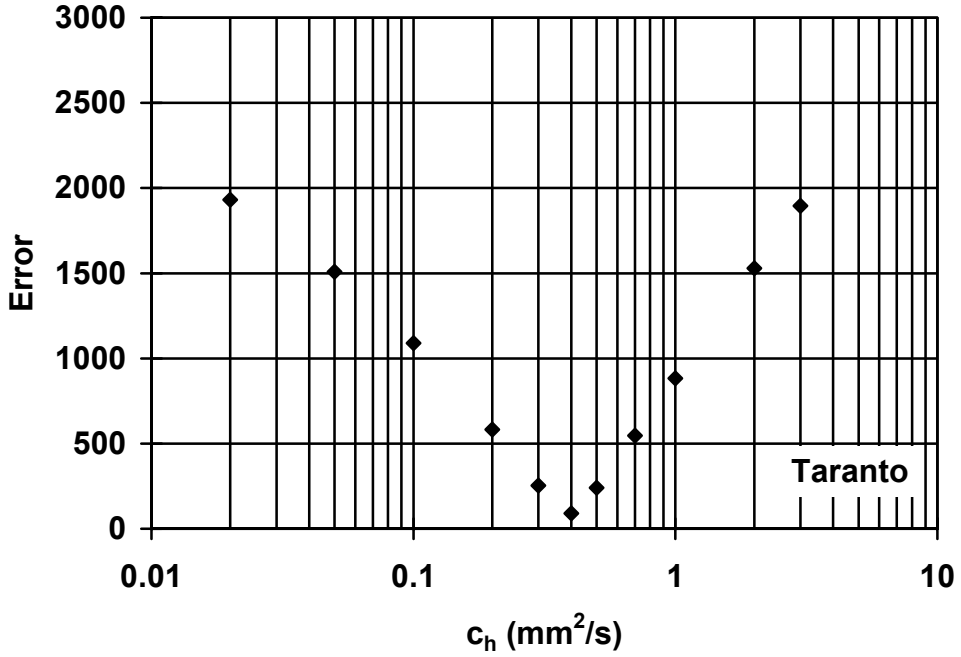

Figure 4.25. Error Norm for the Coefficient of Consolidation in a Hard Clay

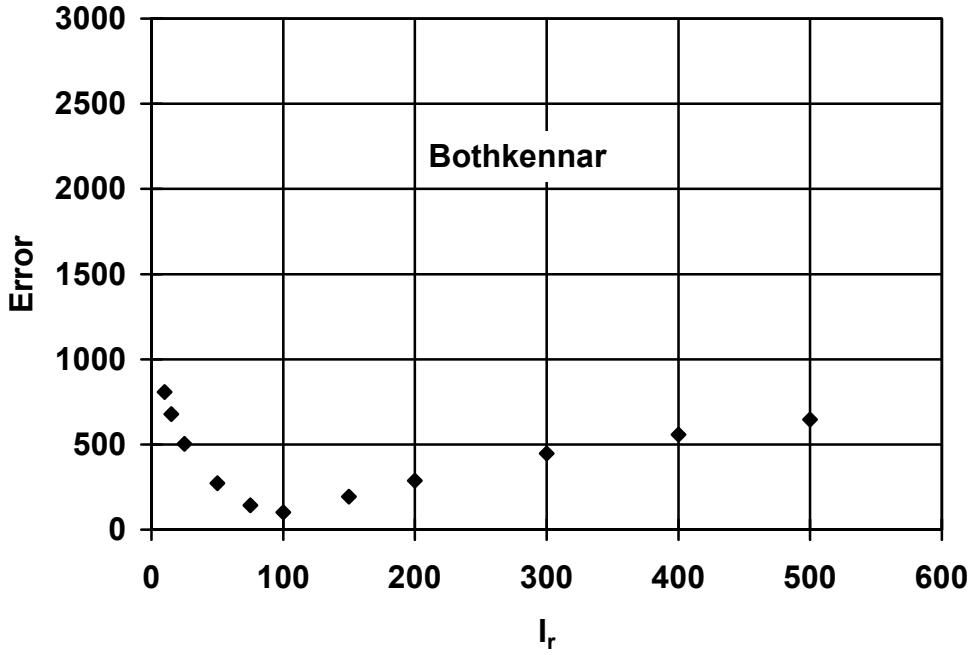

Figure 4.26. Error Norm for the Rigidity Index in a Soft Clay

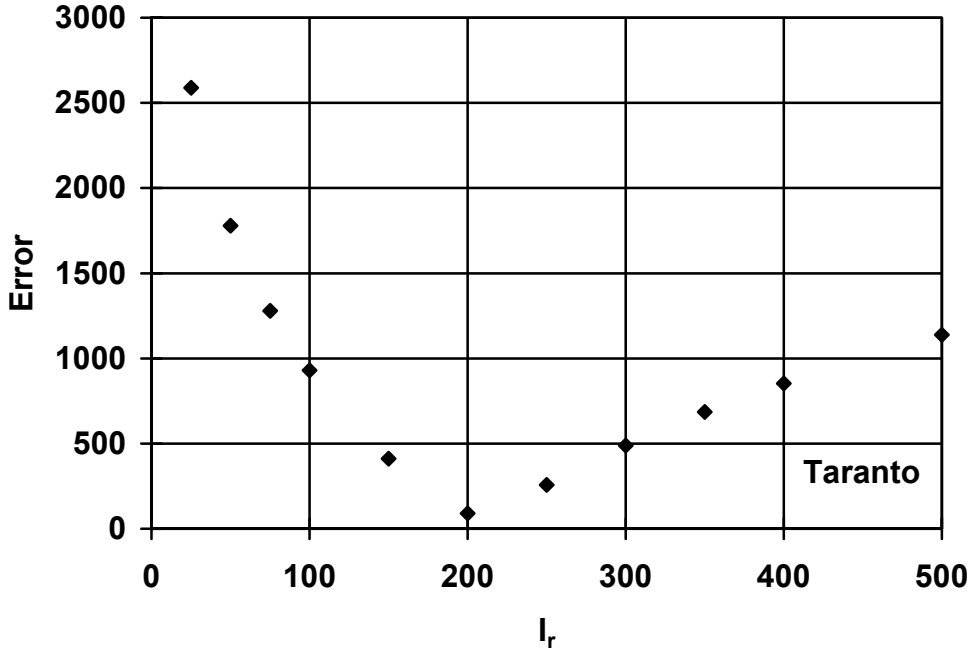

Figure 4.27. Error Norm for the Rigidity Index in a Hard Clay

The error norms for the effective friction angle and OCR are shown in Figure 4.28 through Figure 4.31. Again, the data from the Bothkennar and Taranto sites were used for comparison. Of all the parameters examined for the hard clays, the changes produced by these two parameters were the most significant. The error norms for the friction angle and OCR in the hard clay show steep gradients moving away from the error minimum, showing that the model is sensitive to the input value of these parameters. Similar to the trends seen previously, the variation of the effective stress angle and OCR are less significant for the soft clay, producing a smaller level of error for the same variation, than was seen in the hard clay. The significant effect on the prediction of the effective stress friction angle and OCR makes the initial evaluation of these parameters of critical importance in the estimation of the coefficient of consolidation, primarily because they represent the undrained strength and initial penetration porewater pressure regime used in the evaluation.

Comparison With Existing Solutions

A comparison between the model estimated values and the solution proposed by Teh and Houlsby (1988) was performed in order to evaluate the method. The soft clay sites were used as the basis of comparison because due to the difficulty in assessing t_{50} for the dilatory response in hard clays. The method of Teh and Houlsby was chosen for comparison because it appears to be the most widely-used solution for piezocone dissipation at present (Robertson et al., 1992). The results of the comparison are shown in Figure 4.32; it is interesting to note that the new method predicts lower values in each instance. In general, neither method appears to have a distinct advantage in the prediction of c_h, however.

Normalized Dissipation Data

The evaluated dissipation results can also be presented as a series of normalized curves, similar to those given by Teh and Houlsby (1991). Figure 4.33 through Figure 4.35 show the normalized dissipation curves estimated for values of ϕ' equal to 20^o, 30^o, and 40^o. As seen in the figures, the lower value of ϕ' leads to more significant differences in behavior for different values of OCR. This is because the lower value of the friction angle leads to a smaller initial magnitude of pore pressure, and a more rapid decay of the pressures when the values are normalized to the initial value.

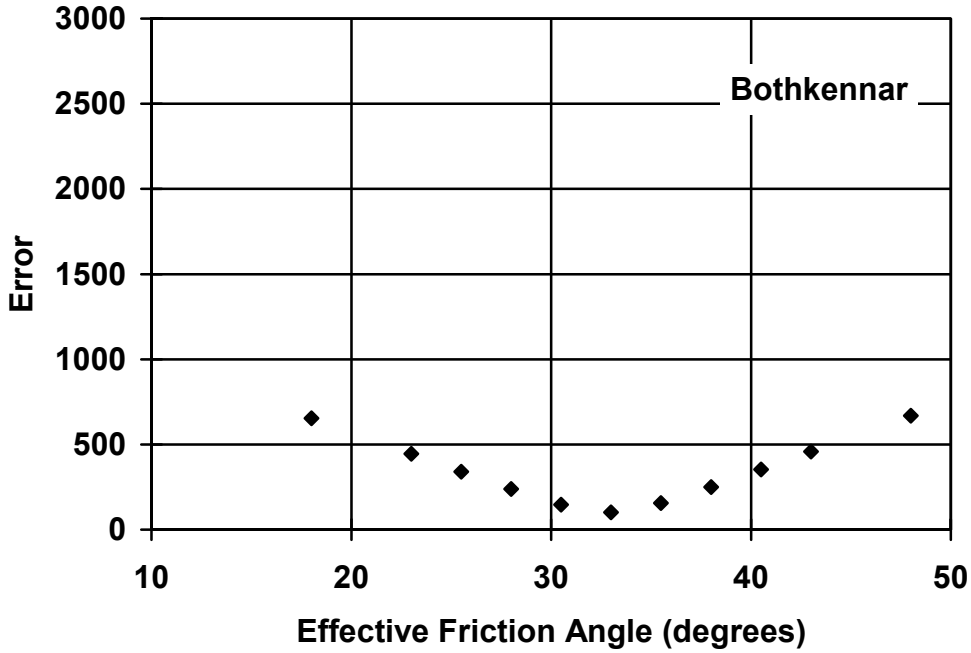

Figure 4.28. Error Norm for the Effective Stress Friction Angle in a Soft Clay

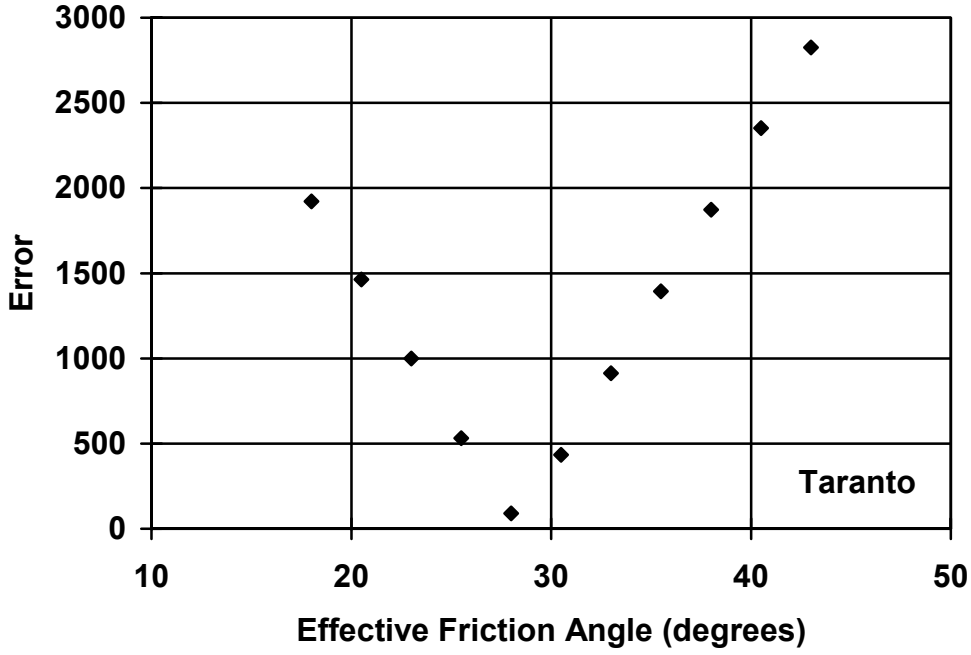

Figure 4.29. Error Norm for the Effective Stress Friction Angle in a Hard Clay

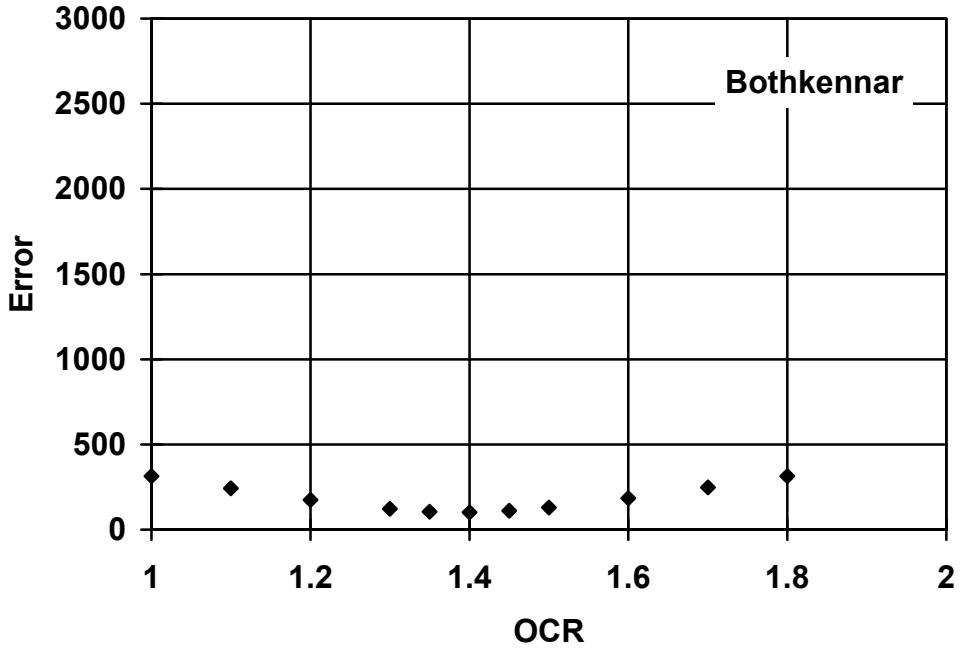

Figure 4.30. Error Norm for the OCR in a Soft Clay

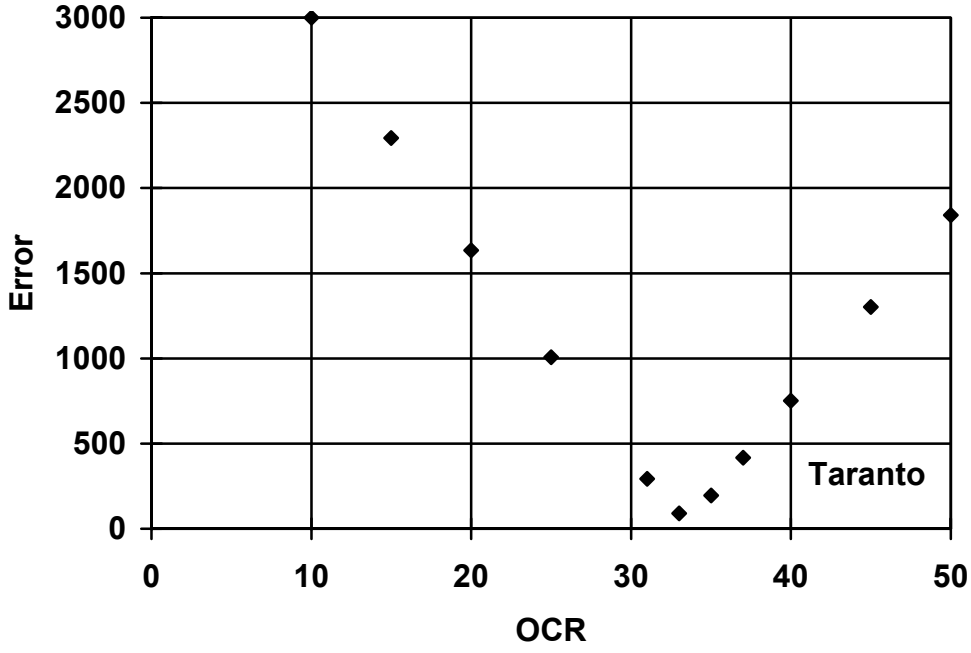

Figure 4.31. Error Norm for the OCR in a Hard Clay

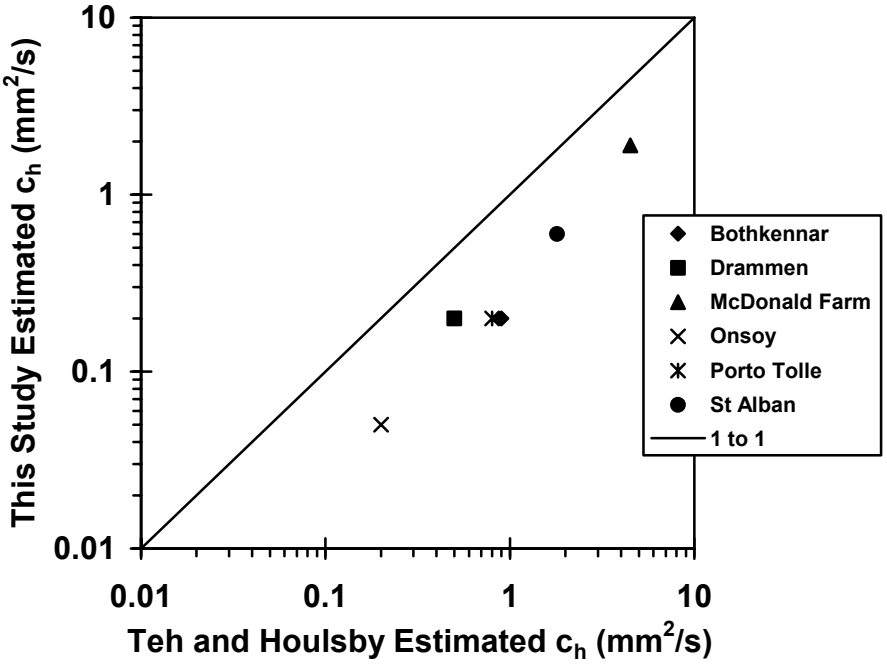

Figure 4.32. Model Comparison with Existing Methods

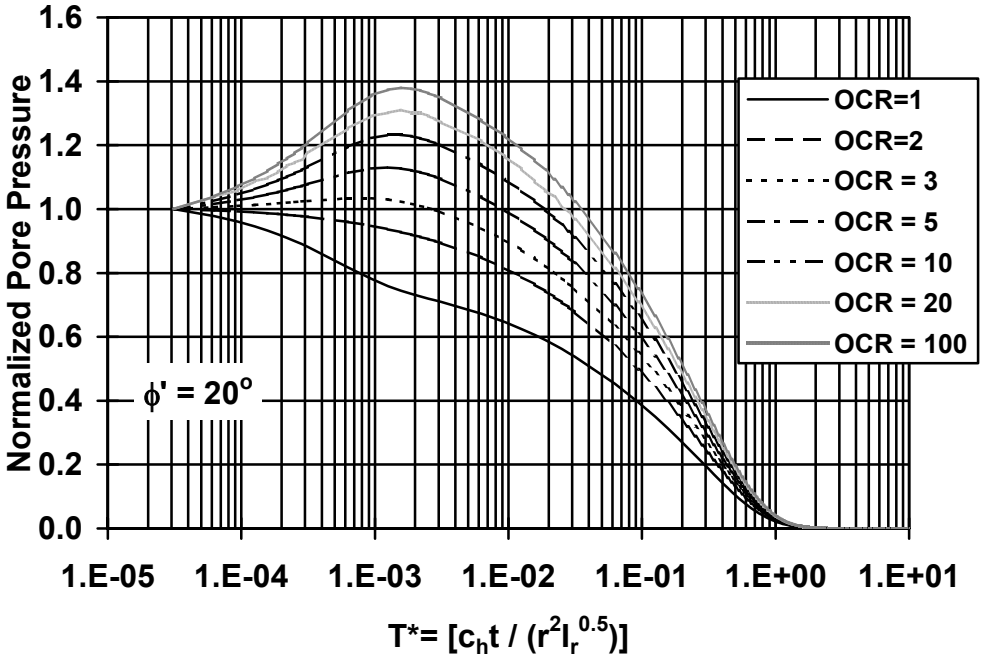

Figure 4.33. Normalized Dissipation Curves for $\phi' = 20^o$

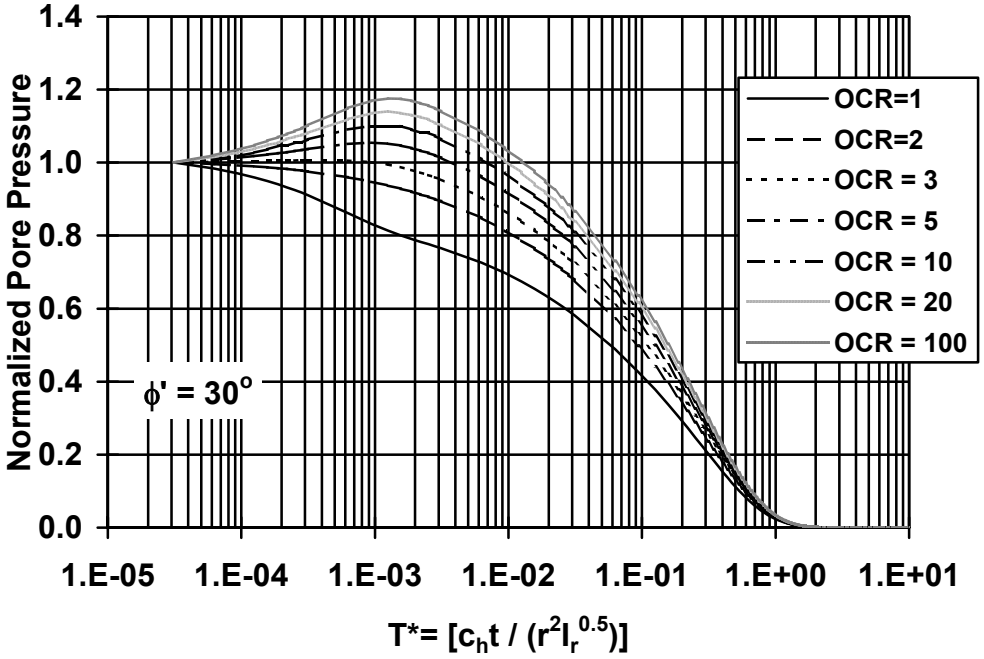

Figure 4.34. Normalized Dissipation Curves for $\phi' = 30^o$

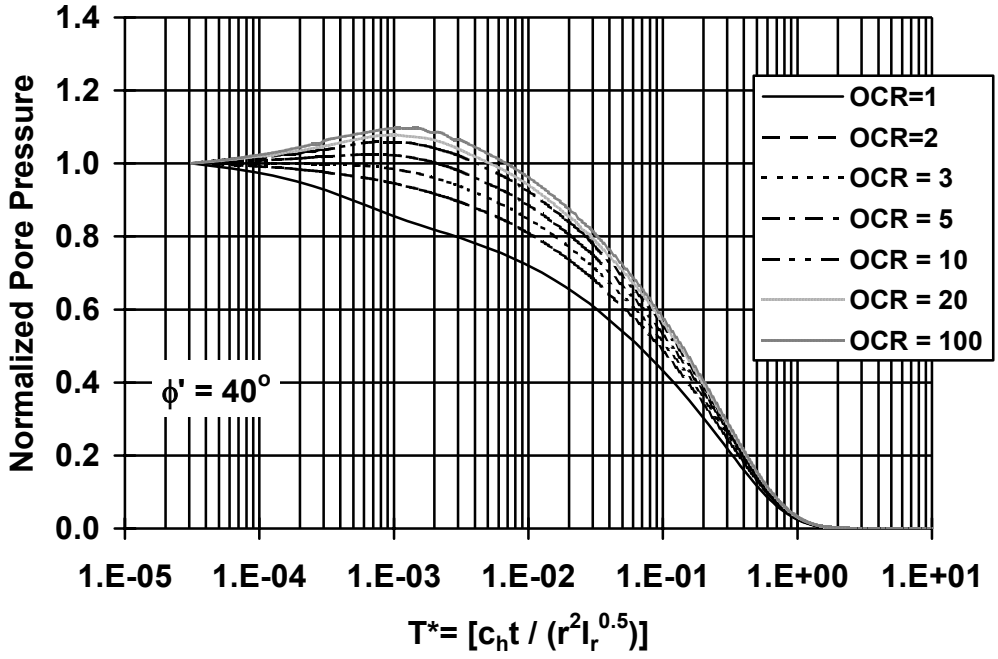

Figure 4.35. Normalized Dissipation Curves for $\phi' = 40^o$

Discussion

A hybrid cavity expansion model was chosen for the evaluation of the coefficient of consolidation. Extensive experimental evidence suggests that the dissipation of pore pressures surrounding a Type 2 piezocone is controlled by horizontal drainage; consequently, the consolidation equation was solved assuming only radial drainage, or a cylindrical cavity expansion model. However, the most reliable evaluation of the coefficient of consolidation was achieved by assuming spherical cavity expansion for the initial generated magnitude of pore pressure and for the radius of the zone of disturbance. In actuality, the Type 2 location of the pore pressure element, just behind the cone tip, is controlled by large stress gradients which are not modeled exactly by either spherical or cylindrical cavity expansion.

The interesting feature of this model's approach is that pore pressures can be either positive or negative. Negative penetration pore pressures are seen in heavily-overconsolidated clays when the pore pressure is measured with the filter in the Type 2 position. Previous models have either failed to provide a coherent reason for why the pore pressure might dissipate in this atypical manner, or have chosen to neglect the phenomenon completely.

Conclusions

A cavity expansion and critical-state model was introduced for evaluating the horizontal coefficient of consolidation in clays ranging from soft to stiff to hard clays. The scheme is able to predict standard monotonic dissipation characteristic of soft to firm normally- to lightly-overconsolidated clays, as well as the dilatory dissipation behavior observed in heavily-overconsolidated clays. The formulation incorporates a component of shear-induced pore pressure which can be either positive at low OCRs or negative at higher values of OCR. A comparison between the predicted and lab-measured values of the coefficient was shown in Table 4.2. The fit is within range of measured values, especially considering the approximate nature of the laboratory estimated values of coefficient of consolidation. While the prediction of the shape of the dissipation curve is often quite good, there still remain cases where the dissipation behavior deviates from the predicted behavior. This indicates that there still may be some physical phenomena occurring which the model does not take into account. These effects can include smear, soil fabric, sensitivity, fissures, and hydraulic fracturing; consequently, future development should investigate these aspects.

Additional complicating aspects to the prediction include the fact that reference measurements for the coefficient of consolidation are typically obtained in the one-dimensional consolidation test which is a measure of the vertical value, rather than the horizontal value of coefficient of consolidation. Also, saturation of the pore pressure filter element and pore pressure transducer chamber should be performed meticulously in order to eliminate the trapping of air bubbles. Poorly saturated filter elements can produce pore pressure dissipation curves which mimic the dilatory behavior of pore pressure seen in heavily-overconsolidated clays, so data integrity must be ascertained before predictions can be considered valid.

An interesting facet is that the rigidity index (I_r) of the clay is evaluated by the analytical method. The rigidity index was taken as an input value for the model and varied in order to yield a series of curves for each dissipation test. At low values of OCR, the value for rigidity index which most closely models the dissipation curve is approximately 100, while at higher OCRs (7 to 26), the most appropriate value for rigidity index is on the order of 50 or less. This is consistent with existing laboratory triaxial data which show I_r decreasing as a function of increasing OCR and increasing plasticity index (Keaveny and Mitchell, 1986; Kulhawy and Mayne, 1990). For uncemented clays, a graph of rigidity index (curves from Keaveny and Mitchell, 1986) with the model-evaluated values superimposed is shown in Figure 4.36.

It is also important to note that the model prediction is sensitive to the input values of ϕ' and OCR. In this formulation, the initial magnitude of pore pressure was calculated assuming the triaxial compression mode of failure. However, failure modes surrounding a cone penetrometer are probably a hybrid value between triaxial compression under the tip and direct simple shear along the sides. Nonetheless, the use of triaxial compression mode of failure is a reasonable approximation for the test conditions. Notably, the additional influences of anisotropic stress state, stress rotation effects, and strain rate have not been addressed here, but may influence the results. These issues should be addresses in future studies.

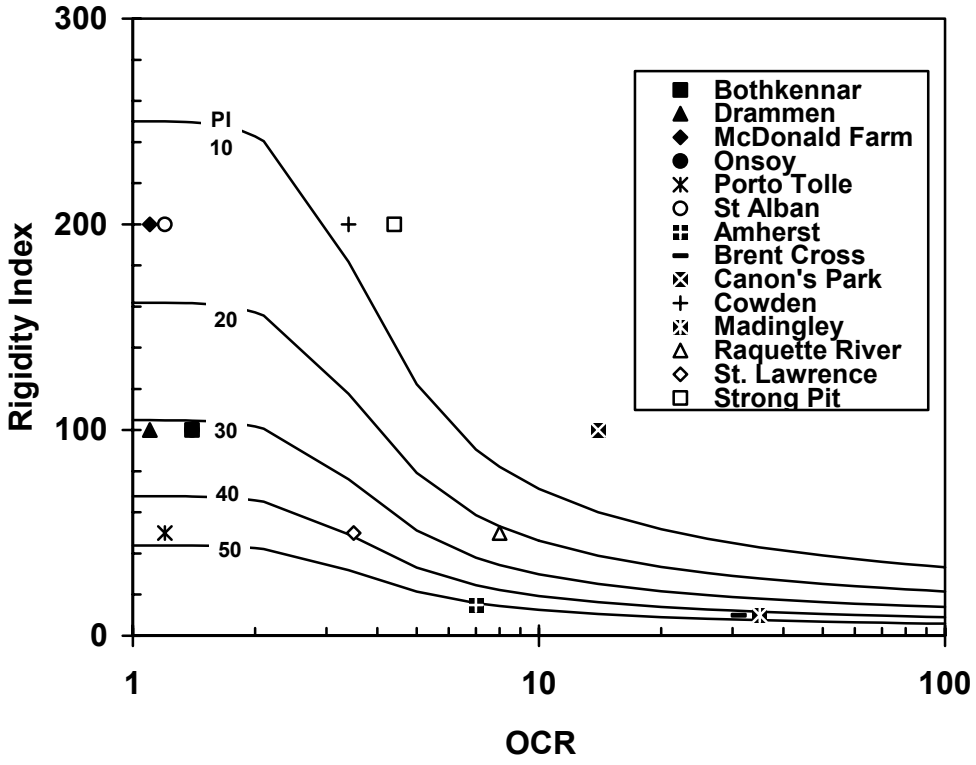

Figure 4.36. Model Evaluation of Rigidity Index in Non-Cemented Clays
Note: Plasticity Index Curves from Keaveny and Mitchell (1986)

The final predictive form for obtaining the coefficient of consolidation from piezocone dissipation test data is:

$$c_h = \frac{T^* r^2 I_r^{0.5}}{t} \qquad \textbf{Equation 4.54}$$

where the modified time factor T* is given as a function of both ϕ' and OCR (Figures 4.33 through 4.35).

CHAPTER 5

INTERPRETATION OF SEISMIC PIEZOCONE RESULTS FOR THE EVALUATION OF SOIL PERMEABILITY IN CLAYS

Introduction

One of the most critical parameters for soil characterization in geoenvironmental engineering is the permeability of a soil deposit. Permeability controls the flow of groundwater through the subsurface, and consequently, the advective transport of contaminating chemicals. However, quantification of the soil permeability is a most difficult task because its value can change orders of magnitude as a function of grain size (Mitchell, 1993). This section seeks to develop a methodology to evaluate the in-situ soil permeability based solely on seismic piezocone test data.

The addition of an accelerometer or geophone to a cone penetrometer enables the direct measurement of the soil shear wave velocity (V_s) with depth during a seismic piezocone sounding. Conventional applications of shear wave velocity data include the evaluation of dynamic stiffness (low-strain shear modulus, $G_{max} = G_o = \rho V_s^2$, where ρ = mass density) for dealing with foundation vibration problems and the evaluation of site-specific amplification response spectra for earthquake events. Figure 5.1 shows seismic piezocone tests being performed for the Missouri Department of Transportation in an evaluation of bridge stability in the event of an earthquake.

In a different application of the shear wave velocity, this section seeks to use the measurements obtained during a seismic piezocone test to develop predictive relationships between V_s and the mass density and constrained modulus of a soil deposit. Using these correlations in combination with the value of the coefficient of consolidation estimated in Chapter 4, a methodology is developed to evaluate the permeability of a soil deposit using data gathered solely from the seismic piezocone test.

Seismic Cone Penetration Test

The seismic cone penetration test is a rapid and economical method for obtaining shear wave velocity profiles in a downhole manner at a given site. Seismic cone penetrometers are instrumented with either one or multiple accelerometers or geophones in the cone body to measure shear wave arrival times emanating from a distant source.

The geophysical portion of the seismic cone test is typically performed as a downhole test with the wave source generated at the surface (Campanella, 1994). A typical test setup is shown in Figure 5.2. Surveys via the crosshole testing method (ASTM D-4428) are also possible (Baldi et al., 1989). The seismic source and trigger used in the downhole surveys performed by Georgia Tech consists of an instrumented sledge hammer which is struck against the side of a plank that is firmly coupled to the ground by the weight of a truck. Leads from the geophone and the hammer are connected to a Hewlett Packard Model 54601-A oscilloscope.

During the pause in cone penetration while each successive rod is added, the hammer is struck and the travel time response is monitored on the oscilloscope. The incremental distance over incremental time is used to calculate shear wave velocity, $V_s = \Delta x/\Delta t$, providing a pseudo-interval approach (Sully and Campanella, 1995). A true-interval approach can be obtained if two accelerometers are located a fixed distance apart within the cone penetrometer (Burghignoli et al., 1991). Several tests, taking only about 15 seconds each for trigger and register, are made at each depth for the pseudo-interval approach in order to verify repeatability of the measurements. A reverse strike may also be used for comparing polarized wave time records.

Figure 5.1. Seismic Piezocone Testing for Missouri DOT in New Madrid Earthquake Region

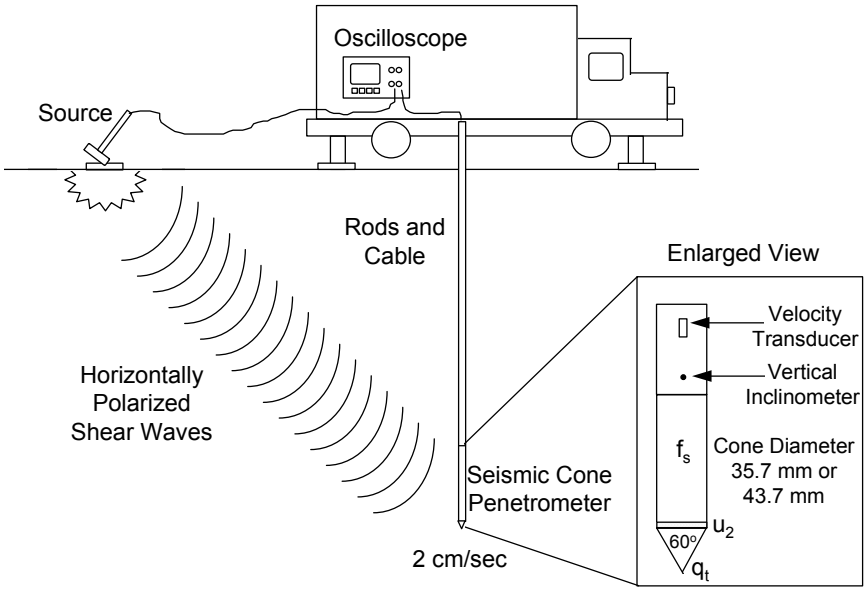

Figure 5.2. Configuration For Seismic Cone Test

Seismic cone penetration tests were performed at a variety of locations throughout the country (Burns and Mayne, 1994; Burns et al., 1994; Burns and Mayne, 1995b; Mayne et al., 1996). Figure 5.3 and Figure 5.4 show seismic cone test results obtained near San Manuel, Arizona. The sounding was performed in mine tailings built from the spoils of a copper mining operation. These tailings consist of approximately 20-60% fines ("rock flour") forming silty sands and sandy silts. The tailings are deposited in large cycloned dams for dewatering and disposal purposes. As would

be anticipated in these heterogeneous mining materials where the depositional process was turbulent, the shear wave velocity profiles for the dam are somewhat variable, as are the related profiles of q_c, f_s, and u_2.

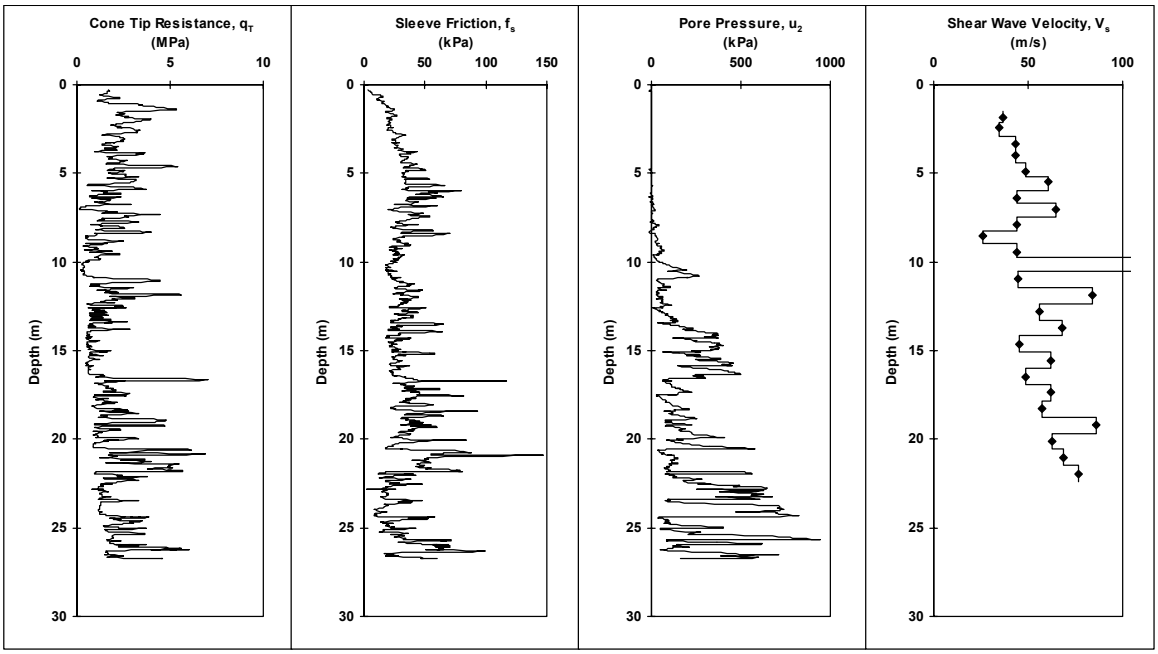

Figure 5.3. Seismic Cone Test in Copper Mine Tailings at San Manuel, Arizona (Burns and Mayne, 1994)

Figure 5.4. Seismic Cone Testing at San Manuel, AZ

Figure 5.5 and Figure 5.6 show the derived shear wave velocity profile obtained on Hutchinson Island in Savannah, Georgia (Burns and Mayne, 1995b). The soil overburden consists of Atlantic coastal plain sediments with interbedded layers of soft plastic clay and loose clayey sand. A rather uniform profile of shear wave velocity measurements was obtained at this site which is indicative of the slow sedimentation process that formed these marine deposits.

Measurement of shear wave velocity using the seismic piezocone also enables the calculation of the low-amplitude shear modulus, G_{max}, if the unit weight is known:

$$G_{\max} = \rho V_s^{\,2} \qquad \textbf{Equation 5.1}$$

where ρ = mass density = γ_t/g, γ_t = total unit weight, and g = gravitational acceleration constant (= 9.8 m/sec^2; = 32.2 ft/sec^2). Values of unit weight for real and natural soils are quite varied and may range anywhere from as low as 10 kN/m^3 (64 pcf) for very soft peats and organic plastic clays to as high as 21 kN/m^3 (134 pcf) for dense glacial tills. With clean sands, it may be possible to infer the unit weight through an evaluation of relative density (D_r) from the cone tip resistance (Robertson and Campanella, 1983; Kulhawy and Mayne, 1990; Lunne et al., 1992). However, in clays and silts, the dependence of q_c on void ratio is very small (Mayne and Rix, 1993) and therefore not directly applicable to evaluating either unit weight or mass density of these materials. Consequently, more systematic approaches other than estimating ρ for soils are desirable and explored in this chapter. For this purpose, a database from all types of geomaterials (clays to sands to rocks) has been created and a global correlation between mass density and shear wave velocity was developed.

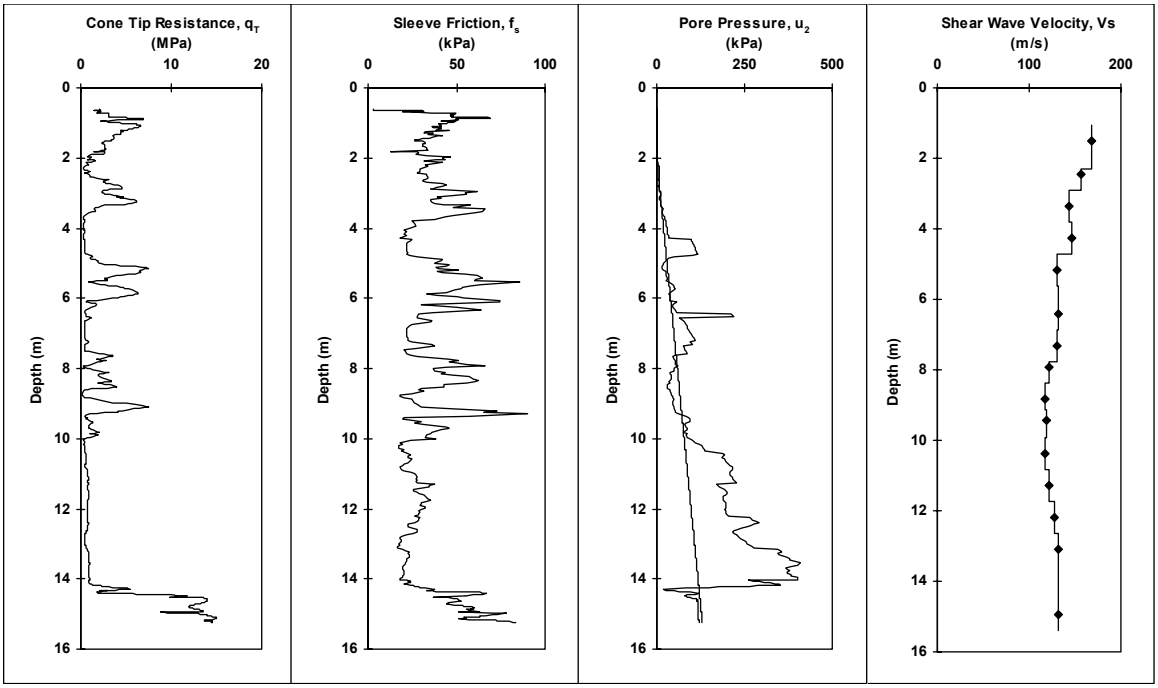

Figure 5.5. Seismic Cone Test in Atlantic Coastal Plain Sediments at Hutchinson Island, Georgia (Burns and Mayne, 1995b)

Figure 5.6. Seismic Cone Testing at Hutchinson Island, GA

V_s-q_T Relationships in Soils

Because both the cone tip resistance and shear wave velocity depend on the effective geostatic state of stress, it is possible to correlate the two parameters; however, the relationship is soil type dependent. For instance, Baldi et al. (1989) showed the existence of a V_s-q_T correlation for clean quartz sands is given by the following:

$$V_s = 277(q_T)^{0.13}(\sigma_{vo}')^{0.27} \qquad \textbf{Equation 5.2}$$

q_T and V_s from SCPT tests can be used to evaluate e_o in intact clays:
where V_s is in m/s, q_T is in MPa, and σ_{vo}' = effective overburden stress in MPa.

Mayne and Rix (1995) compiled a database of 31 different clay sites including intact and fissured clays with varied plasticity characteristics (8 < PI < 300), sensitivities (2 < S_t< 200+), and overconsolidation stress states (1 < OCR < 100+). Approximate estimates of V_s solely as a function of q_T can be made; however, the correlation is very much improved when the void ratio is also included as a correlative parameter. Using data from intact clays only, the following correlation between V_s, q_T, and e_o was developed (n = 339, r^2 = 0.832):

$$V_s = 9.44 \frac{q_T^{0.435}}{e_o^{0.532}} \qquad \textbf{Equation 5.3}$$

where q_T is in kPa and V_s is in m/s. Figure 5.7 shows the multiple regression relationship with data superimposed for comparison. Through inversion of this equation, the independent measurements of

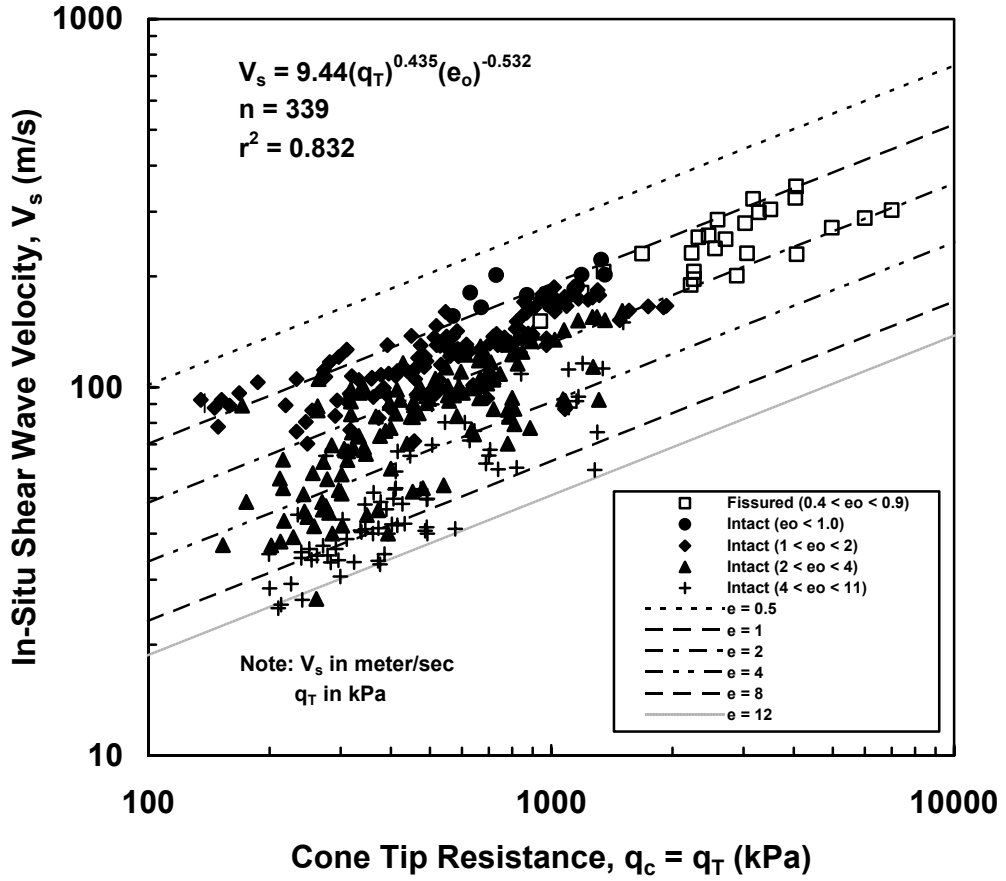

Figure 5.7. Shear Wave Velocity-Cone Tip Resistance Correlations in Clay (After Mayne and Rix, 1995)

$$e_o = 68\frac{q_T^{0.818}}{V_s^{1.88}} \qquad \textbf{Equation 5.4}$$

where q_T is in kPa and V_s is in m/s. This equation provides an approximate and immediate estimation of e_o in clays where values are not normally known a priori. Furthermore, in saturated clays, $\gamma_{sat} = [(G_s+e)/(1+e)]\gamma_w$, and a systematic assessment of total unit weight is obtained for calculating the low-strain shear modulus, $G_{max} = (\gamma_t/g)V_s^2$.

Two case studies not included in the original clay database were examined in order to verify the applicability of the void ratio estimations. The first site was St. Alban, Quebec (Lefebvre et al., 1994), which is underlain by sensitive marine clays that have a relatively high void ratio profile with values varying between 1 and 3. The groundwater table is approximately 1.2 m deep. Figure 5.8 shows the estimated e_o values from the equation and, although the prediction varies from the actual values somewhat, the increase and subsequent decrease in the e_o trend with depth is evident.

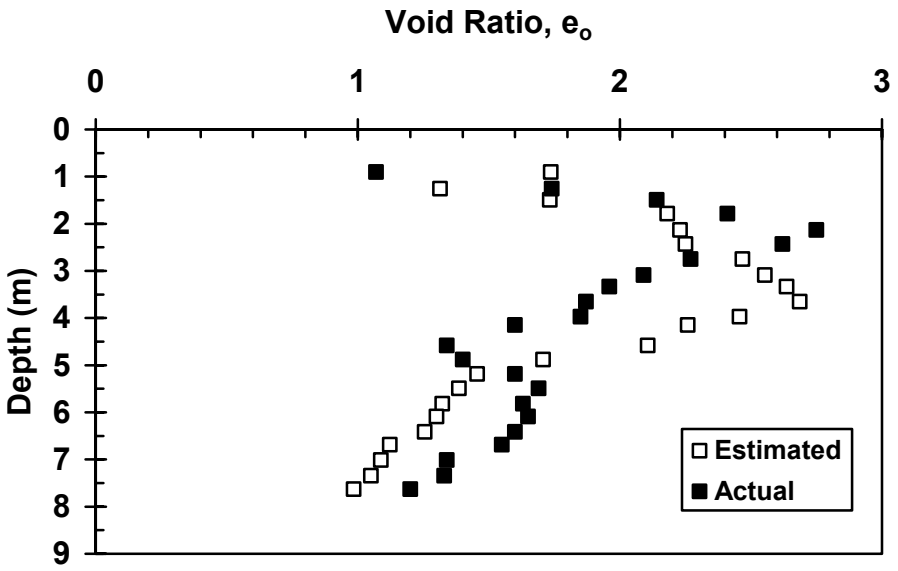

Figure 5.8. Void Ratio Prediction at St. Alban Site (Lefebvre et al., 1994)

Void ratio estimations for a site tested with the Georgia Tech seismic cone system are shown in Figure 5.9 (Burns and Mayne, 1995). The site is located on Hutchinson Island in Savannah, Georgia and is comprised of Atlantic coastal plain sediments consisting of interbedded layers of plastic clay and sand (shown previously in Figure 5.5). The groundwater table is approximately 2 meters deep at this site. Again, the void ratio predictions are very approximate, but the general trend in the prediction is in agreement.

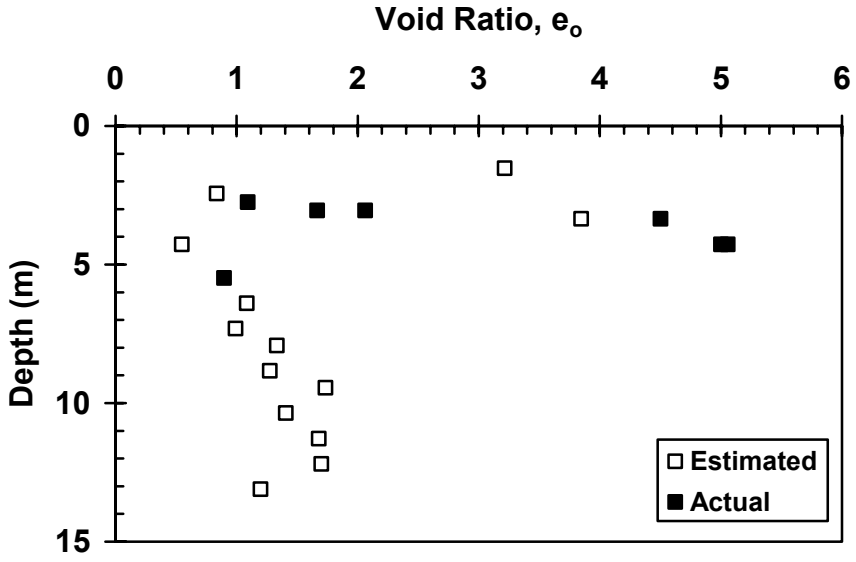

Figure 5.9. Void Ratio Predictions for Hutchinson Island, Savannah, GA (Burns and Mayne, 1995)

Geotechnical Estimation of Mass Density

Often in geotechnical analyses, the magnitude of γ_t is merely estimated. A more rigorous approach requires the direct measurement of γ_t from undisturbed thin-wall samples taken in adjacent borings; however, this is neither feasible nor practical when using cone penetration tests for exploration.

A more generalized approach to the ρ estimation problem was sought by compiling data from a wide variety of geomaterials including: intact rocks, gravels, sands, silts, and clays (Burns and Mayne, 1996). Table 5.1 summarizes the list of soils and rocks where both shear wave velocity measurements and mass densities of these materials were known. Seismic wave velocities for soils were determined from in-situ methods (seismic cone, crosshole, spectral analysis of surface waves, or suspension logging techniques). The unit weights and mass densities ($\rho = \gamma/g$) of these materials were determined from thin-wall tube, piston, or core samples taken in either the same or adjacent boreholes. Data for clays were summarized by Mayne and Rix (1995) and data for sands were compiled by Hegazy and Mayne (1995). For the rock materials, the data were obtained generally from laboratory testing on small specimens, usually with ultrasonic techniques applied to determine V_s.

A correlation was observed between the mass density of the geomaterial and the measured shear wave velocity. Figure 5.10 shows the trend and resulting statistics from a regression analysis of the data (n = 438; $r^2 = 0.765$; S.E. = 0.126):

$$\rho = 0.277 + 0.648 \log V_s \qquad \textbf{Equation 5.5}$$

where ρ = mass density (g/cc), V_s = shear wave velocity (m/s), n = number of data sets, r^2 = coefficient of determination, and S.E. = standard error of the independent variable (same units as ρ). Since V_s is recognized to increase with increasing effective overburden stress, a multiple regression analysis was also investigated with two independent variables; the results are summarized in Figure 5.11. The statistical results showed an improved trend (n = 438; $r^2 = 0.820$; S.E. = 0.118):

$$\rho = 0.701 \frac{V_s^{\,0.227}}{(\sigma_{vo}')^{0.057}} \qquad \textbf{Equation 5.6}$$

where σ_{vo}' = effective vertical overburden stress (kN/m^2). However, an iterative approach is required for this equation since σ_{vo}' depends upon a knowledge of the mass density profile with depth before calculation. As a consequence, the aforementioned equation may be of more practical usage in routine explorations involving the need to convert V_s to G_{max}. The correlation will also be of immediate value to V_s surveys conducted using the spectral analysis of surface waves (SASW) since no other information may be available before this test is conducted.

Table 5.1. Geomaterials Database - Known Mass Density and Shear Wave Velocity

Site/Location	Geomaterial Type	Test Method	Reference Sources of Data
Atlanta, GA	residual silty sand	SASW	Mayne and Harris (1993)
Bäckebol, Sweden	soft postglacial clay	SCPT	Larsson and Mulabdic (1991)
Bagdad, AZ	mine tailings	SCPT	Burns et al. (1994)
Berea sandstone, CA	sandstone	Lab	Hilbert et al. (1994)
Bothkennar, UK	soft organic clay	SCPT	Hepton (1988)
Brent Cross, UK	fissured London clay	SASW	Lunne et al. (1986b)
Chase Group C, KS	siltstone	Lab	Yale and Jamieson (1994)
Chase Group A, KS	dolostone	Lab	Yale and Jamieson (1994)
Chase Group B, KS	limestone	Lab	Yale and Jamieson (1994)
DOE site, SC	clayey sand	SCPT	Bratton et al. (1993)
Drammen, Norway	sensitive clay	SCPT	Campanella et al. (1986b)
Fucino, Italy	soft cemented clay	SCPT, CHT	Burghignoli et al. (1991)
Holmen, Norway	clean sand	SCPT	Lunne et al. (1986b)
Houston, TX	stiff Beaumont clay	CHT	Mahar and O'Neill (1983)
Langley, BC	soft glacio-marine clay	SCPT	Grieg et al. (1988)
Lilla Mellösa, Sweden	soft organic clay	SCPT	Larsson and Mulabdic (1991a)
Long Beach A, CA	clean sand & gravel	CHT	McLamore et al. (1978)
Long Beach B, CA	clean sand & gravel	CHT	McLamore et al. (1978)
Long Beach C, CA	stiff lean clay	CHT	McLamore et al. (1978)
Long Beach C, CA	silty sand	CHT	McLamore et al. (1978)
Long Beach D, CA	stiff plastic clay	CHT	McLamore et al. (1978)
Long Beach D, CA	clean & silty sands	CHT	McLamore et al. (1978)
Long Beach E, CA	limestone	CHT	McLamore et al. (1978)
Lower 232nd St., BC	NC sensitive glacial clay	SCPT	Campanella et al. (1988, 1989)
Madingley, UK	fissured Gault clay	SASW	Lunne et al. (1986b)
McDonald's Farm, BC	soft clayey silt	SCPT	Campanella et al. (1986b)
McDonald's Farm, BC	clean sand	SCPT	Robertson et al. (1986)
Munkedal, Sweden	sensitive clay	SCPT	Larsson and Mulabdic (1991)
Norrköping, Sweden	soft varved clay	SCPT	Larsson and Mulabdic (1991)
Onsöy, Sweden	soft marine clay	SCPT	Lacasse and Lunne (1983)
Po River, Italy	clean sand	SCPT	Baldi et al. (1988)
Såro Rd. 7/600, Sweden	organic clay & gyttja	SCPT	Larsson and Mulabdic (1991)
Såro Rd. 6/900, Sweden	soft organic clay	SCPT	Larsson and Mulabdic (1991)
Skå-Edeby, Sweden	soft plastic clay	SCPT	Larsson and Mulabdic (1991)
Texcoco CAO, Mexico	NC very plastic clay	SPSL	Jaime and Romo (1988)
Texcoco SCT, Mexico	LOC very plastic clay	SPSL	Jaime and Romo (1988)
Tuve, Sweden	organic marine clay	SCPT	Larsson and Mulabdic (1991)
Vålen, Sweden	soft organic clay	SCPT	Larsson and Mulabdic (1991)
Xochimilco, Mexico	soft very plastic clay	SPSL	Jaime and Romo (1988)
Yucca Mt., NV	Paintbrush tuff	Lab	Price et al. (1994)

Notes: NC = normally consolidated
LOC = lightly overconsolidated
CHT = crosshole test
SCPT = seismic cone penetration test.
SPSL = suspension P & S-wave logging.
SASW = spectral analysis of surface waves.

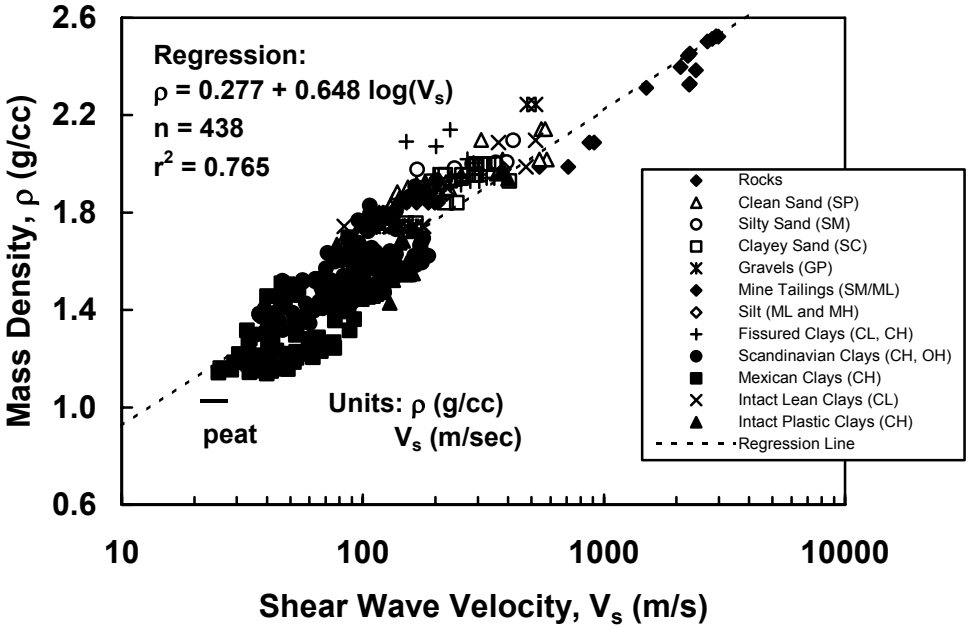

Figure 5.10. Mass Density-Shear Wave Velocity Correlations in Geomaterials

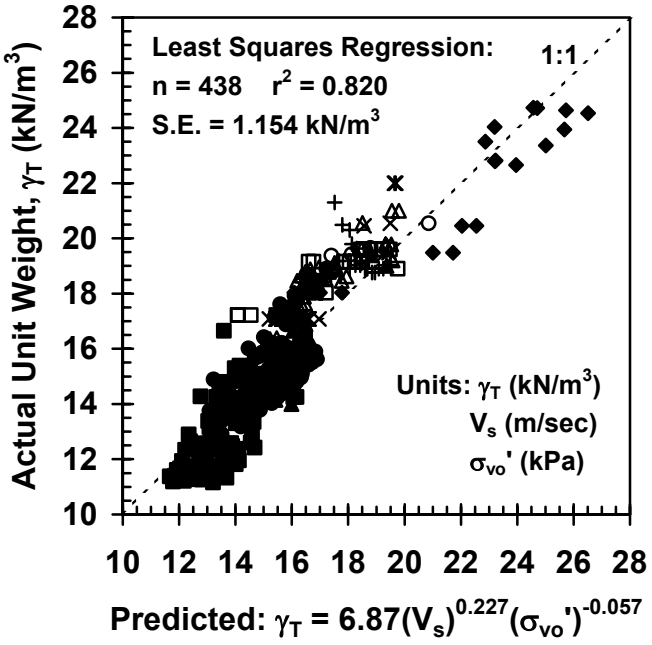

Figure 5.11. Multiple Regression Evaluation for Total Unit Weight

Methodologies for Evaluating Permeability from Piezocone Data

Data gathered from seismic cone penetration tests yield information about the soil mass density and porosity and this information can be combined with the estimated values of the

coefficient of consolidation (Chapter 4) in order to evaluate the permeability. In this section, three alternate methodologies are developed to evaluate the permeability from seismic piezocone dissipation tests. The first approach relies only on standard piezocone measurements of tip resistance and pore pressure. In two other related schemes, readings from seismic piezocone soundings are utilized and the independent V_s measurement is employed in the estimation of D. The methodologies will be evaluated using the database listed in Table 5.2.

Table 5.2. Input and Reference Database for Permeability Evaluation

Site	Depth (m)	c_h ** (mm^2/s)	q_T (kPa)	σ_{vo} (kPa)	σ_{vo}' (kPa)	V_s (m/s)	Lab k (cm/s)	Reference
Bothkennar, U.K.	12.0	0.20	898	204	96	130	6.0×10^{-8}	Jacobs and Coutts (1992)
Drammen, Norway	19.5	0.20	1000	300	121	200	1.0×10^{-8}	Lacasse and Lunne (1982)
McDonald Farm, B.C.	20.0	1.90	1036	360	179	180	4.0×10^{-7}	Sully (1991)
Onsoy, Norway	18.5	0.05	754	296	115	130	1.3×10^{-7}	Lacasse and Lunne (1982)
St. Alban, Quebec	4.6	0.60	300	137	43	100	3.0×10^{-7}	Roy et al. (1981)
Amherst, MA (crust)	3.0	0.40	1369	55	100*	175	2.0×10^{-7}	DeGroot and Lutenegger (1994)
Madingley, U.K.	5.8	0.05	2000	110	100*	256	1.4×10^{-9}	Coop and Wroth (1989)

*σ_a = 100 for OC clay
**from piezocone dissipation

Evaluation of the Constrained Modulus from Piezocone Data

For one-dimensional drainage in oedometer tests, the permeability of a soil deposit is defined as:

$$k = \frac{c_v \gamma_w}{D} \qquad \textbf{Equation 5.7}$$

where D = the constrained modulus = $\Delta\sigma_z/\Delta\varepsilon_z$ for confined compression. Using this formulation in combination with the estimated value of c_h rather than c_v developed in Chapter 4, the only unknown remaining for the determination of the permeability is the constrained modulus. Three different methods for the estimation of the constrained modulus using piezocone data are presented and evaluated.

Cone Tip Resistance Correlation

A common correlation found in the literature relates the constrained modulus with cone tip resistance in the form:

$$D = \alpha q_c$$ **Equation 5.8**

where α = an empirical correlation coefficient and q_c = the measured cone tip resistance. Mitchell and Gardner (1975) compiled various relationships from the literature and found that the value of α ranged from 0.4 to 8 for clay soils; the large scatter was in part due to the fact that the data were not collected using standardized cones and testing procedures, and q_c was not corrected for pore pressure effects (Lunne et al., 1986a). Kulhawy and Mayne (1990) compiled a piezocone database of 12 clay sites with corrected tip resistances and constrained modulus data and developed the following correlation (n = 42, r^2 = 0.795, S.D. = 67 p_a):

$$D = 8.25(q_T - \sigma_{vo})$$ **Equation 5.9**

or, the constrained modulus is equal to 8.25 times the net cone resistance (Figure 5.12). Note M = to the constrained modulus in the figure.

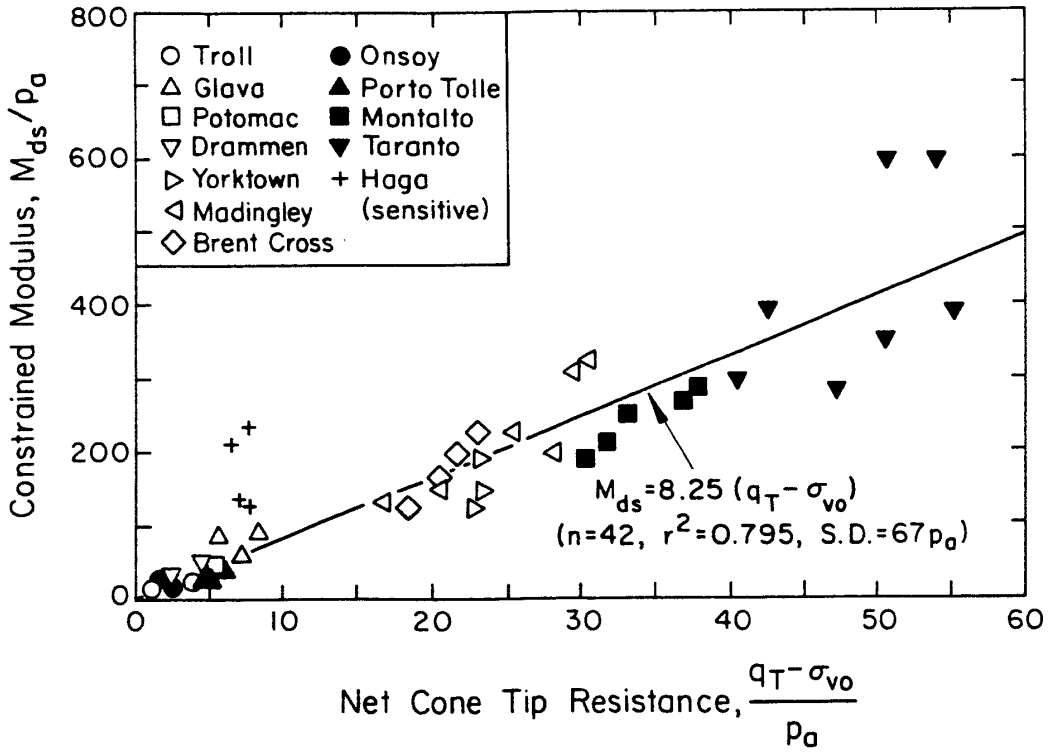

Figure 5.12. Constrained Modulus as a Function of Net Cone Tip Resistance (Kulhawy and Mayne, 1990)

While the empirical correlation of tip resistance with constrained modulus yields a reasonable approximation, there are fundamental reasons which make the relationship questionable. The constrained modulus is a parameter assessed in a drained environment but the corrected tip resistance in clays is an undrained parameter, which means that the two parameters are evaluated

under completely different effective stress conditions. Additionally, tip resistance in the cone penetration test is essentially a measurement of soil strength, while the modulus is a measurement of soil deformability. Correlations between the two are empirical at best. Due to these limitations, two additional methodologies for evaluating the constrained modulus are examined.

Janbu's Method

Janbu (1963, 1985) presented a universal trend relating the constrained modulus of different soils and rocks to the porosity (n), or alternately, the in-situ void ratio (e). The in-situ void ratio at each clay site was evaluated using the method based on seismic cone data presented earlier in this chapter and the constrained modulus was evaluated using Janbu's method. In most cases, seismic piezocone data were available to provide all the necessary relevant data from a single sounding. However, in the case of St. Alban, the shear wave velocities were gathered using surface geophysical techniques at the same location. The formulation for the estimation of in-situ void ratio was presented in Equation 5.4:

$$e_o = \frac{68 q_T^{0.818}}{V_s^{1.88}} \qquad \textbf{Equation 5.10}$$

In a soil system, the in-situ void ratio can be related to the porosity by the following formulation:

$$n = \frac{e_o}{1 + e_o} \qquad \textbf{Equation 5.11}$$

where n = porosity. Janbu's method presents the evaluation of the modulus of clays as a function of porosity and effective overburden stress through the following relationship:

normally consolidated clays $D = m\sigma_{vo}'$ **Equation 5.12**

overconsolidated clays $D = m\sigma_a'$ **Equation 5.13**

where $m = [(1+e_o)/C_c]ln10$ = the modulus number, C_c = the compression index, and σ_a' = 100 kPa. Reference values of m for all materials are presented in Figure 5.13; values of m for normally consolidated clays are presented in Figure 5.14. For clays, the data are presented in terms of in-situ water content which can be related to the void ratio through the following formulation:

$$w_n = \frac{S}{G_s} e_o \qquad \textbf{Equation 5.14}$$

where w_n = the water content, S = the saturation, and G_s = the specific gravity of the solids. In saturated media with $S = 1$, the water content is a function of the void ratio and the specific gravity.

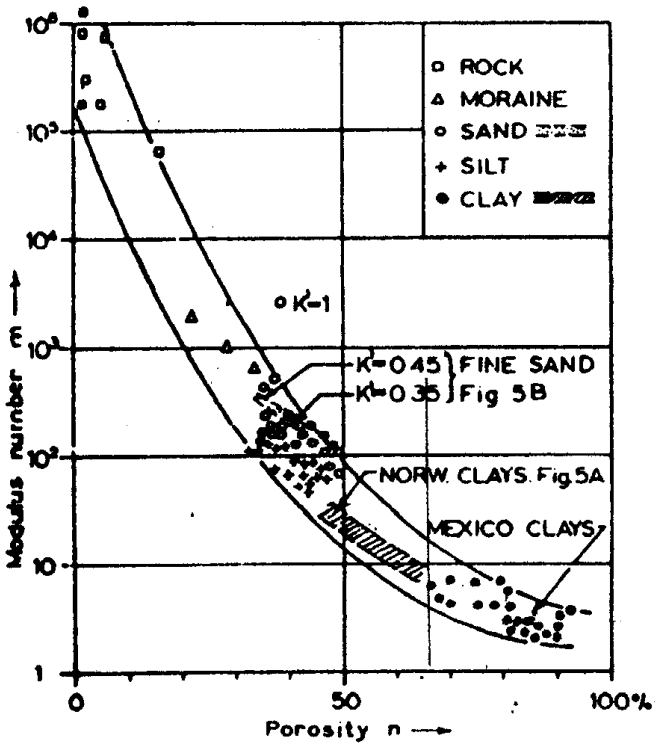

Figure 5.13. Constrained Modulus for All Materials

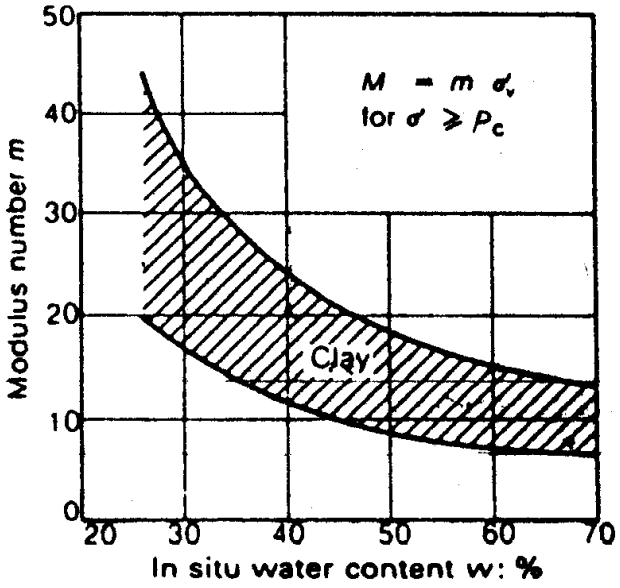

Figure 5.14. Constrained Modulus for Normally-Consolidated Clays

The Janbu method presents a range for the value of the modulus; consequently, the data estimated by this method are presented as a range of values, corresponding to the lower and upper bounds for the modulus. After the void ratio is evaluated using the shear wave velocity and cone tip resistance data, it is converted to a value of porosity or void ratio. The modulus number, *m*, is then estimated and the lower and upper values for the constrained modulus are evaluated from the Janbu method.

Shear Wave Velocity Correlation

This methodology relies on a correlation between the seismic cone measured values of shear wave velocity and laboratory measured values of constrained modulus. A database of clay soils with known shear wave velocity and constrained modulus was compiled in order to form the correlation. The database for fourteen different sites, with a brief site description, is shown in Table 5.3.

Table 5.3. Shear Wave Velocity - Constrained Modulus Database

Site	Site Description	V_S (m/s)	D (kPa)	Reference
Bothkennar	NC organic clay/silt	89	490	Nash et al. (1992)
		96	630	
		103	1050	
		105	811	
		111	690	
		117	1050	
		121	1135	
		127	1460	
		130	1230	
		137	1585	
		142	1460	
		147	1725	
		160	2040	
Brent Cross	HOC London Clay	206	8410	Powell and Uglow (1988)
		231	8180	
		258	9150	
		285	10300	
Drammen	Sensitive aged NC	96	2490	Lacasse and Lunne (1982)
		118	2575	
		121	2760	
		130	2450	
		130	3350	
		156	250	
Fucino	Soft cemented clay	89	1250	Brignoli et al. (1995)
		155	2880	
Hutchinson Island	Soft silty clay	142	1880	Burns and Mayne (1995)
		146	980	
		135	1880	
		158	582	
Lilla Mellosa	Soft organic clay	38	200	Larsson (1986)
		43	200	
		51	190	
		59	200	
		67	200	
		75	200	

		83 91 99 105 113	200 200 260 260 320	
Madingley	HOC Gault Clay	231 256 279 304 327 351	6570 7070 8370 9170 11450 12430	Powell and Uglow (1988)
Montalto	Stiff plastic clay	300 326 316 378 347	18000 21000 25000 26000 28000	Holtz et al. (1985) Jamiolkowski et al. (1995)
Onsoy	Soft NC aged	76 86 92 94 114 134	1600 1100 700 1000 2150 1500	Lacasse and Lunne (1982)
Pentre	Stiff silty clay	462 549 592 627 779 777 803 821 844	5925 5925 9143 6214 6660 14545 17297 12308 8767	Lambson et al. (1993)
Pisa	Soft LOC clay	158 186 161 264	780 1400 1325 5375	Mitchell et al. (1977) Jamiolkowski et al. (1995)
Saint Alban	Sensitive soft aged	66	472	Leroueil (1996)
Ska Edeby	Soft plastic clay	49 57 64 70 77 83 88 95 105	250 240 250 250 310 310 400 400 500	Larsson (1986)
Tilbrook	Stiff fissured clay	1159 959	62500 62500	Lambson et al. (1993)

Note: NC = normally consolidated, OC = overconsolidated, LOC = lightly overconsolidated, HOC = heavily overconsolidated

The following correlation was observed between the shear wave velocity and constrained modulus (n = 82, $r^2 = 0.7844$, S.E. = 0.162):

$$D = 0.265 \cdot V_s^{1.74} \qquad \textbf{Equation 5.15}$$

where D is in kPa and V_s is in m/s. The compiled database is shown in Figure 5.15:

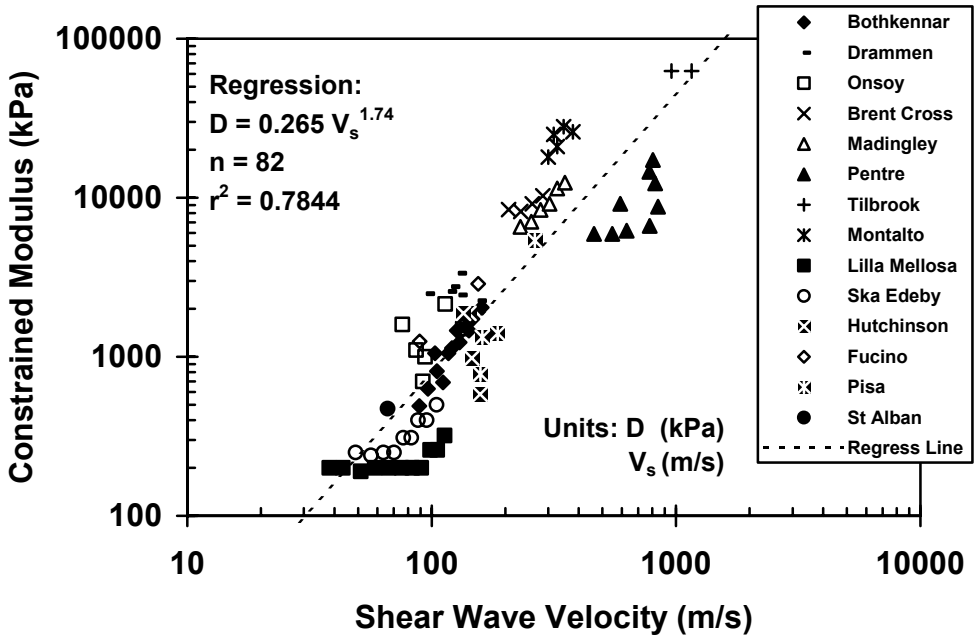

Figure 5.15. Constrained Modulus - Shear Wave Velocity Correlation in Clays

While the loading mechanisms to measure constrained modulus and shear wave velocity, or shear modulus, are very different, the same material parameters influence both moduli, making the relation between the two reasonable. Based on elastic theory, the constrained modulus can be related to the elastic parameters E and ν (Equation 2.27 and Equation 2.28). Additionally, both the constrained modulus and shear wave velocity are strong functions of the void ratio and effective overburden stress in a soil deposit. Consequently, the correlation between the two relies on the fact that the parameters are both dependent on the same soil properties.

Evaluation of Permeability

Using the three methods for the evaluation of the constrained modulus leads to the following three formulations for the soil permeability:

Cone Tip Resistance Correlation $\quad k_h = \dfrac{c_h \gamma_w}{8.25(q_T - \sigma_{vo})}$ **Equation 5.16**

Janbu's Method (Lower)* $$k_h = \frac{c_h \gamma_w}{1.112 \cdot \left[\frac{\frac{68 \cdot q_T^{0.818}}{V_s^{1.88}}}{1 + \frac{68 \cdot q_T^{0.818}}{V_s^{1.88}}} \right]^{-4.12} \cdot \sigma_{vo}'}$$ **(Equation 5.17)**

(Upper)* $$k_h = \frac{c_h \gamma_w}{2.503 \cdot \left[\frac{\frac{68 \cdot q_T^{0.818}}{V_s^{1.88}}}{1 + \frac{68 \cdot q_T^{0.818}}{V_s^{1.88}}} \right]^{-5.66} \cdot \sigma_{vo}'}$$ **(Equation 5.18)**

Shear Wave Velocity Correlation $$k_h = \frac{c_h \gamma_w}{0.265 \cdot V_s^{1.74}}$$ **(Equation 5.19)**

*(Note for Janbu's method: σ_{vo}' used for normally consolidated clays, σ_a' used for overconsolidated clays).

Input data used for the evaluation of permeability are shown in Table 5.2. The results of the three prediction methods are shown graphically in Figure 5.16, Figure 5.17, and Figure 5.18. Additionally, the results are shown numerically in Table 5.4.

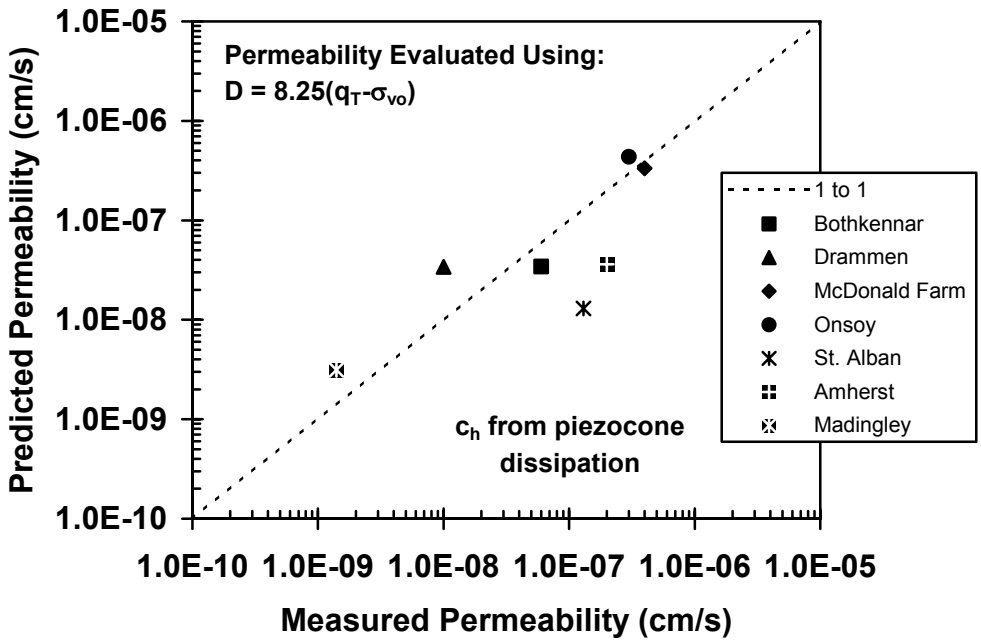

Figure 5.16. Permeability Evaluation Using Constrained Modulus Estimated from Net Cone Resistance

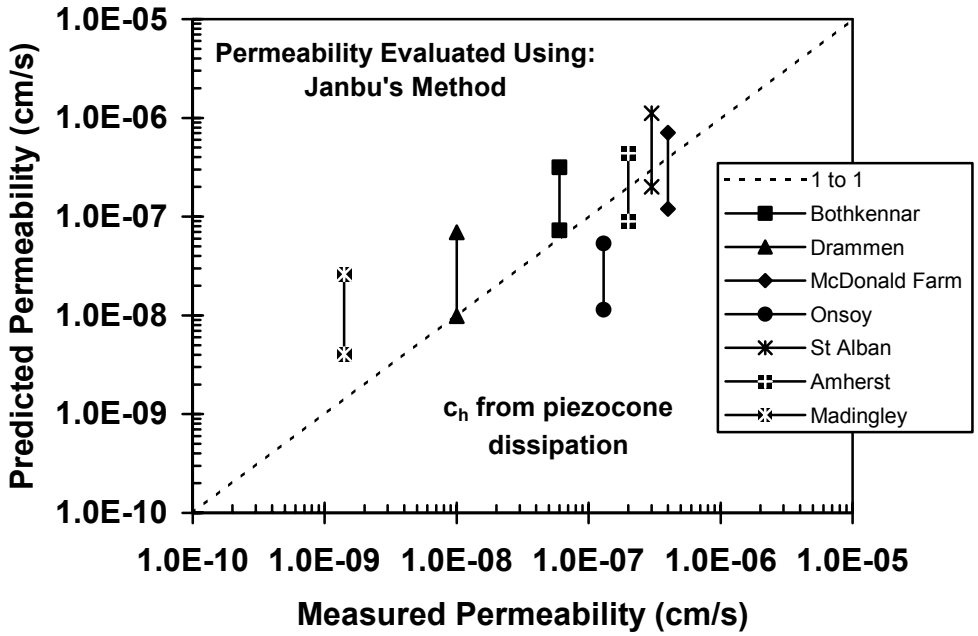

Figure 5.17. Permeability Evaluated Using Janbu's Method of Modulus Determination

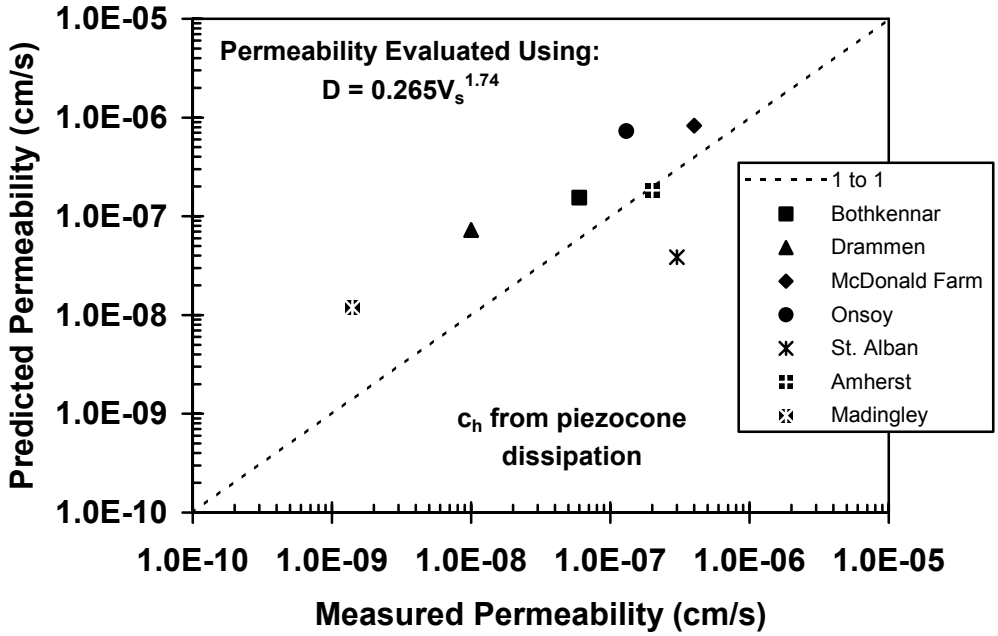

Figure 5.18. Permeability Evaluation Using Seismic Piezocone Data

Table 5.4. Estimated Values of Permeability Using Seismic Cone Data

Site	Predicted k (cm/s) Method 1*	Predicted k (cm/s) Method 2* (low)	Predicted k (cm/s) Method 2* (high)	Predicted k (cm/s) Method 3*	Lab k (cm/s)	Reference
Bothkennar, U.K.	3.4×10^{-8}	7.3×10^{-8}	3.2×10^{-7}	1.5×10^{-7}	6.0×10^{-8}	Jacobs and Coutts (1992)
Drammen, Norway	3.4×10^{-8}	9.8×10^{-9}	6.9×10^{-8}	7.3×10^{-8}	1.0×10^{-8}	Lacasse and Lunne (1982)
McDonald Farm, B.C.	3.3×10^{-7}	1.2×10^{-7}	7.1×10^{-7}	8.3×10^{-7}	4.0×10^{-7}	Sully (1991)
Onsoy, Norway	1.3×10^{-8}	2.3×10^{-8}	1.1×10^{-7}	3.9×10^{-8}	1.3×10^{-7}	Lacasse and Lunne (1982)
St. Alban, Quebec	4.4×10^{-7}	1.3×10^{-7}	7.4×10^{-7}	7.3×10^{-7}	3.0×10^{-7}	Roy et al. (1981)
Amherst, MA (crust)	3.6×10^{-8}	1.1×10^{-8}	5.5×10^{-8}	1.8×10^{-7}	2.0×10^{-7}	DeGroot and Lutenegger (1994)
Madingley, U.K.	3.1×10^{-9}	8.1×10^{-10}	5.2×10^{-9}	1.2×10^{-8}	1.4×10^{-9}	Coop and Wroth (1989)

* Method 1 = Evaluation of constrained modulus using net cone tip resistance correlation (Figure 5.12)
Method 2 = Evaluation of constrained modulus using Janbu's method (Figure 5.14)
Method 3 = Evaluation of constrained modulus using shear wave velocity correlation (Figure 5.15)

For the most part, the methods tend to overpredict the laboratory measured values of permeability. However, the laboratory values themselves are not without fault and suffer from problems of sample disturbance, smearing, stress relief, and variability. Also, it is important to note that the reference values used for comparison are average values for the sites, not values specific to the location of the dissipation tests.

Estimated Permeability Comparison with Existing Methods

In order to further validate the approach, a comparison was made between the empirical method proposed by Parez and Fauriel (1988) and the permeability predicted using the direct shear wave velocity - constrained modulus correlation. The results of the comparison for the soft clays sites is shown in Figure 5.19. Only the soft clay sites were used for comparison due to the ambiguity in defining a value of t_{50} in dissipation tests which exhibit the dilatory behavior. While the two methods are based on very different approaches to evaluating the permeability, similar results are produced, with neither method showing a distinct advantage in the prediction.

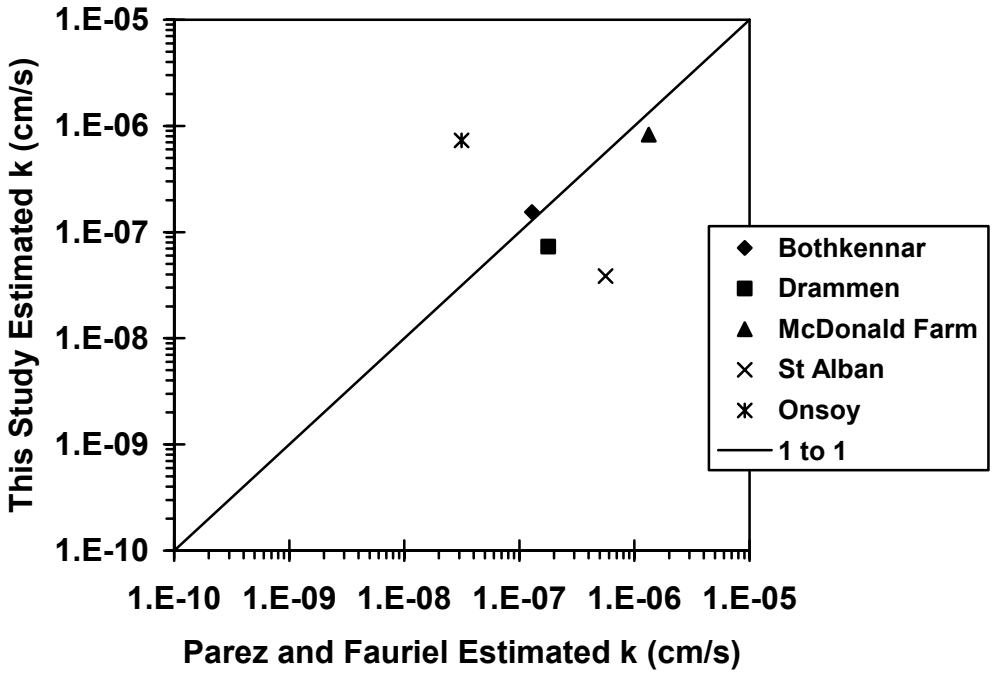

Figure 5.19. Comparison of V_s - D Correlation with the Method of Parez and Fauriel (1988)

Conclusions

A general methodology has been presented for the evaluation of the permeability (*k*) based on seismic cone penetration data, with three alternate approaches given in estimating the constrained modulus (*D*). While all three methods yielded results which were in reasonable agreement with laboratory measured values of permeability, two of the latter methods were based on a separate and independent measurement of soil stiffness because the evaluation of the constrained modulus using the method presented by Janbu (1963) and by the correlation with shear wave velocity introduces another independent measurement into the procedure.

A summary outline of the three alternate methodologies is presented in Table 5.5. In Method 1, the constrained modulus is empirically related to the net cone resistance; in Method 2, the void ratio is related to the shear wave velocity and the constrained modulus is evaluated using Janbu's relationship between void ratio and modulus; and in Method 3, the constrained modulus is related to the shear wave velocity directly. Finally in all methods, the permeability is calculated according to one-dimensional consolidation theory.

Table 5.5. Flowchart For Evaluating Permeability From Seismic Piezocone Data

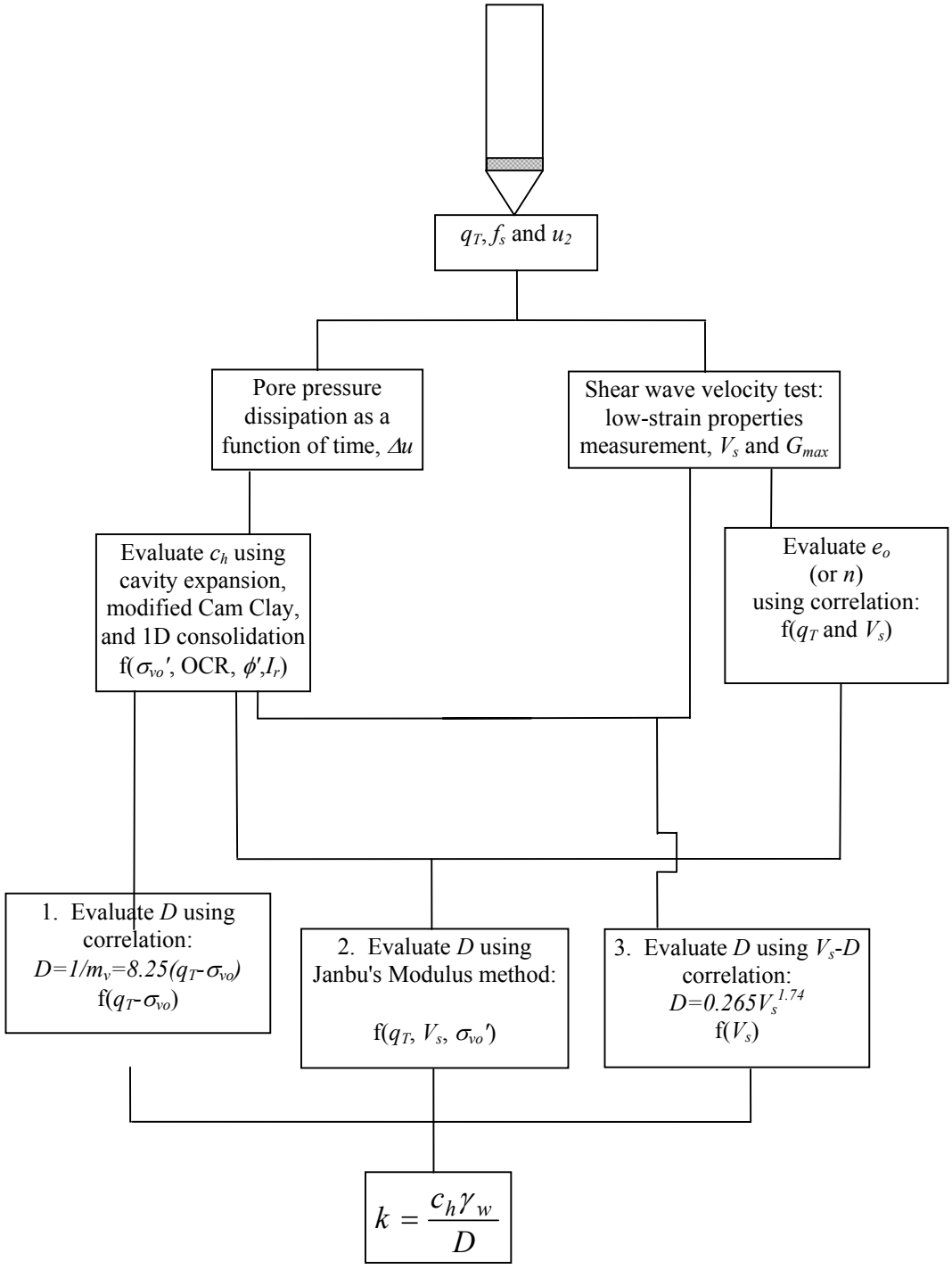

CHAPTER 6

CONCLUSIONS AND RECOMMENDATIONS

Conclusions

Developments related to the usefulness of piezocone penetrometers for geoenvironmental site characterization have been addressed in this study. These include preliminary experimentation on the detection of the BTEX chemicals using an integrated optic sensor miniaturized for inclusion in a cone penetrometer, and improved procedures for the determination of the coefficient of consolidation c_h, the permeability k, and the constrained modulus D, especially in heavily-overconsolidated clays. The focus of this study concentrated on the optimization of the methods of subsurface characterization using piezocone penetrometers.

A set of initial experiments was performed to evaluate the behavior of an integrated opto-electronic BTEX sensor in an Ottawa sand/aqueous environment. The sensor had been miniaturized from a bench-scale apparatus in order to fit inside a trailing module of a cone penetrometer. The tests were performed as proof-of-concept experiments in order to demonstrate the sensor's viability in a soil environment. Seven exploratory experiments were performed in which concentrations as low as 6 ppm (xylene) and as high as 380 ppm (benzene) were detected by the sensor while operating in a sand/water matrix. Malfunctioning of the sensor prevented further testing of its operating characteristics; however, the initial tests demonstrated the sensor's viability in a soil environment and a new version of the sensor is currently under development in order to facilitate future testing.

The radial coefficient of consolidation (c_h) was evaluated using a methodology based on critical state soil mechanics and cavity expansion theory, in combination with an analytical solution to the one-dimensional consolidation equation. The method was able to evaluate the standard monotonic porewater pressure dissipation behavior in lightly-overconsolidated clays, as well as the dilatory pore pressure behavior observed in heavily-overconsolidated clays. Because the pore pressures which are induced by the shearing action of a cone penetrometer can be negative in heavily-overconsolidated clays and affect only a thin zone beside the cone penetrometer, the pore pressure dissipation profile can drawdown to magnitudes lower than hydrostatic. However, because these shear-induced pore pressures dissipate rapidly, the effect is limited to a short period of time.

In this evaluation, the dissipation of the octahedral normal stress-induced pore pressures was handled separately from the shear-induced pore pressures and then summed in order to achieve the complete profile. Estimation of the coefficient of consolidation was achieved through matching of the field-measured curve with the method-evaluated curve. The values of the coefficient of consolidation generally agreed in soft clays and in most cases for the hard clays; however, there were several overconsolidated clay pore pressure profiles not accurately represented by the procedure. In these cases, there appear to be additional factors influencing the consolidation behavior surrounding the cone. The model accounted for the effects of the width of shear zone, the rigidity index, the OCR, and the effective friction angle. Additional parameters which should be investigated include the influence of rate of penetration, possible smearing effects, the degree of fissuring, the effect of possible hydraulic fracturing, and the effect of drainage along the side of the cone penetrometer.

In order to perform an in-situ evaluation of the soil permeability, a methodology was developed using the aforementioned coefficient of consolidation in combination with three alternate estimates of the constrained modulus based on cone data. The proposed methods for the evaluation of permeability ($k = c_h\gamma_w/D$) tended to over-estimate the lab-measured values for the seven case studies examined.

Recommendations

Recommendations for future research in the detection of chemicals using integrated optic sensors in cone penetrometers includes a series of calibration chamber tests, which are currently in progress with the BTEX sensor, for the evaluation of the sensor behavior in a variety of geochemical environments including extremes of pH and concentrated as well as dilute BTEX solutions. The effects of natural organic matter, effects of high temperature induced by cone penetration, and penetration rate effects from the cone sounding should also be studied. Incorporation of the sensor behind a cone penetrometer and upgrade of the sensor's communication electronics are also in progress. New variations on the sensor coating will also enable detection of additional chemicals ranging from chlorinated hydrocarbons to dissolved metals. In addition to its incorporation in a cone penetrometer, the IO sensor shows promise as a push-in place detector which could be left to monitor long-term concentrations of chemicals at a contaminated site.

Regarding the evaluation of the coefficient of consolidation from piezocone dissipation tests, recommendations include the assurance of proper test procedures, especially complete saturation of the pore pressure filter element which can produce dilatory dissipation behavior similar to that seen in heavily-overconsolidated clays if not done properly. An important parameter is the width of shear zone induced around the cone penetrometer during a sounding. Little experimental evidence exists which quantifies the size of this zone or the effect of penetration rate on the width of the zone. Because the width of the shear zone is important in the evaluation of the dissipation behavior of the shear-induced pore pressures, further study of this parameter is needed.

In the methodology to evaluate the in-situ permeability of a soil, additional well-controlled lab tests data should be performed for calibration and verification of improved numerical schemes. The reference values used for comparison of the estimated permeability were average values reported at the sites. Because permeability can vary significantly in soil deposits, more site- and depth-specific data would provide a more reliable comparison.

Figure 6.1 illustrates a conceptual environmental seismic piezocone penetrometer which includes the traditional cone measurement capabilities of tip resistance, sleeve friction, and pore pressure, combined with an accelerometer to measure shear wave velocity, and a chemical detection module. While the seismic piezocone penetrometer is currently available commercially, the incorporation of the chemical detection module is still in development.

A listing of the measured and derived parameters used throughout this thesis is also presented in Figure 6.1. On the left side of the figure are shown the parameters which can be measured using the geoenvironmental cone, while the right side shows the parameters which can be derived from those measurements. The chemical module allows for the detection and measurement of concentration as a function of depth and of time, which is useful not only for site characterization, but also for mass transport studies. The seismic module can measure both compression and shear wave velocities, which can be used to detect the water table, and also to measure the stiffness of a soil deposit, which can be correlated with soil density. The traditional cone sensors include tip resistance, sleeve friction, and pore pressure, and are used for identification of soil type. In this study, the pore pressure sensor was used to monitor pressure as a function of time in order to evaluate the coefficient of consolidation in a soil deposit. As shown, an in-situ estimation of the permeability of a soil deposit can be made through the combination of readings from the pore pressure transducer and seismic velocity transducer. The soil permeability is a fundamental element in the advective transport of groundwater and contaminating chemicals. The conceptual cone penetrometer can provide significantly improved site characterization in the investigation of geoenvironmental parameters.

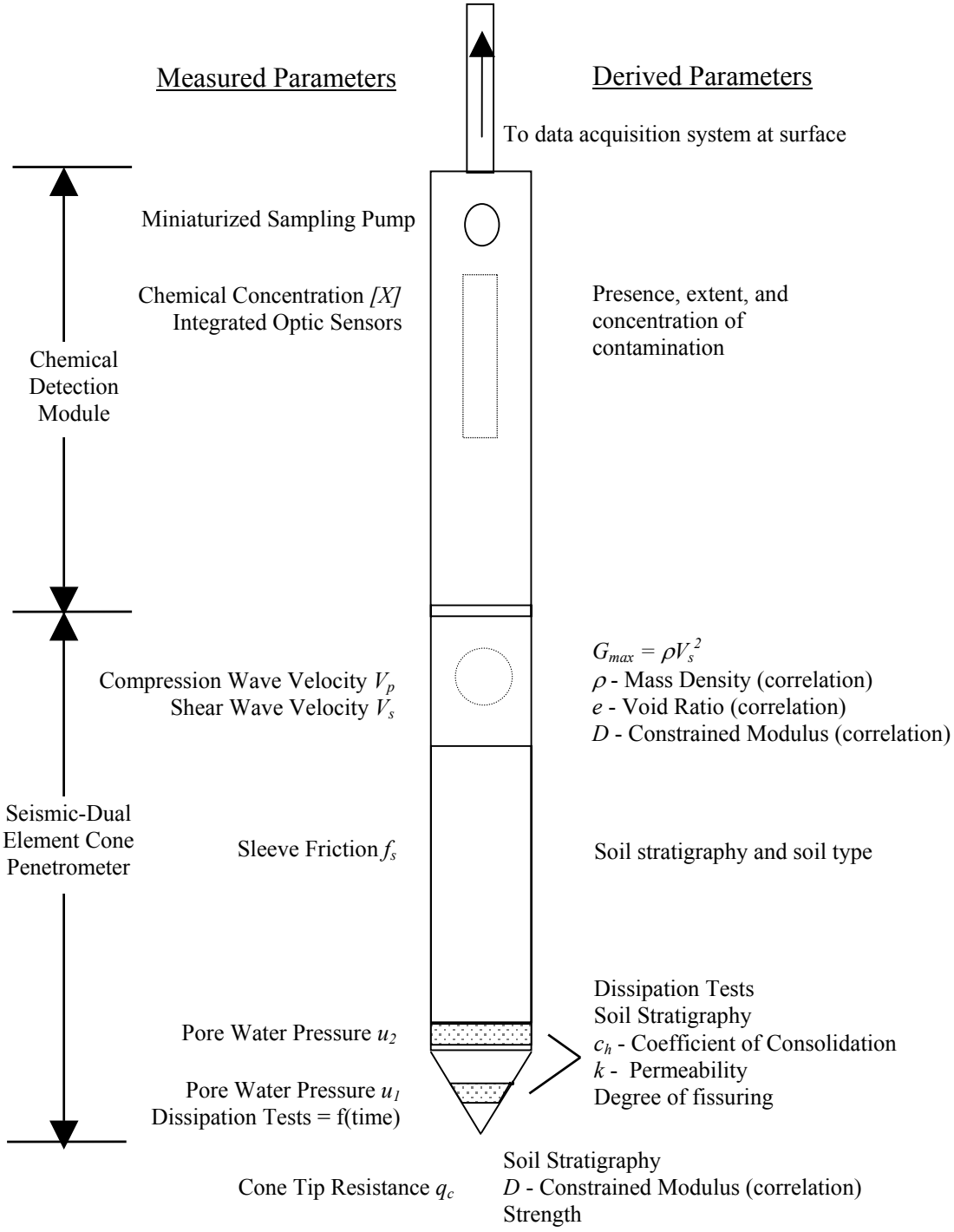

Figure 6.1. Environmental Seismic Piezocone Penetrometer Schematic

BIBLIOGRAPHY

Abramowitz, M. and Stegun, I. (1964). Handbook of Mathematical Functions, U.S. Government Printing Office, Washington, D.C., 1046 pp.

Acar, Y.B. and Tumay, M.T. (1986). Strain Fields Around Cones in Steady Penetration, *Journal of Geotechnical Engineering*, ASCE, Vol. 112, No. 2, pp. 207-213.

American Society for Testing and Materials. (1996). Standard Test Methods for Crosshole Seismic Testing (D4428), Annual Book of Standards, Vol. 4.08, Section 4, West Conshohocken, PA, pp. 636-645..

American Society for Testing and Materials. (1996). Standard Method for Performing Electronic Friction Cone and Piezocone Penetration Testing of Soils (D5778-95), Annual Book of Standards, Vol. 4.08, West Conshohocken, PA.

Apitz, S.E., Theriault, G.A., and Lieberman, S.H. (1992a). Optimization of the Optical Characteristics of a Fiber-Optic Guided Laser Fluorescence Technique for the In-Situ Evaluation of Fuels in Soils, *Proceedings*, Environmental Process and Treatment Technologies, Los Angeles, The International Society for Optical Engineering, January.

Apitz, S.E., Borbridge, L.M., Theriault, G.A., and Lieberman, S.H. (1992b). Remote In-Situ Determination of Fuel Products in Soils: Field Results and Laboratory Investigations, *Analusis*, Vol. 20, Elsevier, Paris, pp. 461-474.

Arulmoli, K. (1994). Users' Perspective - In Situ Sampling Systems, *Summary Report*, Workshop on Advancing Technologies for Cone Penetration Testing for Geotechnical and Geoenvironmental Site Characterization, Engineering and Environmental Sciences Division, US Army Research Office, Research Triangle Park, June.

Aubeny, C.P. (1992). Rational Interpretation of In Situ Tests in Cohesive Soils, *Ph.D. Thesis*, Massachusetts Institute of Technology, Cambridge, MA.

Auxt, J.A. and Wright, D. (1995). Environmental Site Characterization in the United States Using the Cone Penetrometer, *Proceedings*, International Symposium on Cone Penetration Testing, Vol. 2, Linköping, Sweden, pp. 387-392.

Baldi, G., Bellotti, R., Ghionna, V., Jamiolkowski, M., and LoPresti, D.C. (1989). Modulus of sands from CPTs and DMTs, *Proceedings*, 12th International Conference on Soil Mechanics and Foundation Engineering, Vol. 1, Rio de Janeiro, pp. 165-170.

Baldi, G., Bruzzi, D., Superbo, S., Battaglio, M., and Jamiolkowski, M. (1988). Seismic Cone in Po River Sand, *Proceedings*, International Symposium on Penetration Testing, J.D. Ruiter (ed), A.A. Balkema, Rotterdam, The Netherlands, Vol. 1, pp. 643-650.

Baligh, M.M. (1985). Strain Path Method, *Journal of Geotechnical Engineering*, ASCE Vol. 111, No. 9, pp. 1108-1136.

Baligh, M.M. (1986). Undrained Deep Penetration, II: Pore Pressures, *Geotechnique*, Vol. 36, No. 4, pp. 487-501.

Baligh, M.M. and Levadoux, J.N. (1980). Pore Pressure Dissipation After Cone Penetration, *Research Report R80-11*, Department of Civil Engineering, Massachusetts Institute of Technology, Cambridge, MA, 367 pp.

Baligh, M.M. and Levadoux, J.-N. (1986). Consolidation After Undrained Piezocone Penetration. II: Interpretation, *Journal of Geotechnical Engineering*, ASCE, Vol. 112, No. 7, pp. 727-745.

Baligh, M.M. et al. (1981). The Piezocone Penetrometer, *Proceedings*, Cone Penetration Testing and Experience, G.M. Norris and R.D. Holtz, Ed., American Society of Civil Engineers, New York, pp. 247-263.

Battaglio, M., Bruzzi, D., Jamiolkowski, M., and Lancellotta, R. (1986). Interpretation of CPT's and CPTU's: Undrained Penetration of Saturated Clays, *Fourth International Geotechnical Seminar, Field Instrumentation and In-Situ Measurements*, Singapore, pp. 129-156.

Battaglio, M., Jamiolkowski, M., Lancellotta, R., and Maniscalco, R. (1981). Piezometer Probe Test in Cohesive Deposits, *Proceedings*, Cone Penetration Testing and Experience, G.M. Norris and R.D. Holtz, Ed., American Society of Civil Engineers, New York, pp. 264- 302.

Bellotti, R., Benoit, J., and Morabito, P. (1994). A Self-Boring Electrical Resistivity Probe for Sands, *Proceedings*, 13th International Conference on Soil Mechanics and Foundation Engineering, New Dehli.

Bishop, A.W. (1972). Shear Strength Parameters for Undisturbed and Remolded Soil Specimens, *Proceedings*, Roscoe Memorial Symposium, Cambridge University, Foulis & Co., pp. 3-139.

Bishop, R.F., Hill, R., and Mott, N.F. (1945). The Theory of Indentation and Hardness Tests, *Proceedings of the Physical Society*, London, Vol. 57, No. 3, pp. 147-159.

Bjerrum, L. and Johannessen, I. (1961). Pore Pressure Resulting from Driving Piles in Soft Clay, *Pore Pressure and Suction in Soil*, Butterworth, London, pp. 108-111.

Bond, A.J. and Jardine, R.J. (1991). Effects of Installing Displacement Piles in a High OCR Clay, *Geotechnique*, Vol. 41, No. 3, pp. 341-363.

Bond, A.J. and Jardine, R.J. (1995). Shaft Capacity of Displacement Piles in a High OCR Clay, *Geotechnique*, Vol. 45, No. 1, pp. 3-23.

Bowders, J. and Daniel, D.E. (1994). Cone Penetration Technology for Subsurface Characterization, *Geotechnical News*, Vol. 12, No. 3, September.

Bratton, J.L. and Timian, D.A. (1995). Environmental Site Applications of the Environmental CPT, *Proceedings*, International Symposium on Cone Penetration Testing, Vol. 2, Linköping, Sweden, pp. 429-434.

Bratton, W.L., Bratton, J.L., and Shinn, J.D. (1995). Direct Penetration Technology for Geotechnical and Environmental Site Characterization, *Proceedings*, Geoenvironment 2000 (GSP No. 46), Vol. 1, American Society of Civil Engineers, New Orleans, pp. 105-122.

Bratton, W.L., Timian, S.M., and Fisk, B.E. (1993). Piezoseismic-Cone-Penetration Tests at the In-Tank Precipitation Facility, Savannah River Site, Aiken, S.C., Applied Research Associates, South Royalton, Vermont.

Brignoli, E., Burghignoli, A., and Faiella, D. (1995). Performance of a Silo Founded on a Lacustrine Deposit: A Case History, *Proceedings*, Compression and Consolidation of Clay Soils, Yoshikuni, H. and Kusakabe, O. (eds), Balkema, Rotterdam, Vol. 1, pp. 617-622.

Brodzinski, R.L. (1995). Cone Penetrometer Deployment Demonstration for Radiation Detection Instrumentation, Draft Copy.

Brown, D.N. (1993). Determination of Stress State of Clays by Piezocone, *M.S. Thesis*, School of Civil and Environmental Engineering, Georgia Institute of Technology, Atlanta, GA, 168 pp.

Bruzzi, D. and Battaglio, M. (1987). Pore Pressure Measurements During Cone Penetration Tests, *I quaderni dell'ISMES*, No. 229, Milan, Italy, 246 pp.

Brylawski, E. (1994). AP Van den Berg Inc, Milford, PA, 18337.

Burghignoli, A., Cavalera, L., and Chieppa, V. (1991). Geotechnical Characterization of Fucino Clay, *Proceedings*, 10th European Conference on Soil Mechanics and Foundation Engineering, Firenze, Vol. 1, pp. 27-40.

Burns, S.E., Hegazy, Y., and Mayne, P.W. (1994). Seismic Piezocone Penetration Tests, Bagdad Copper Mines - Bagdad, AZ, *Geotechnical Report*, Georgia Institute of Technology, Atlanta, GA.

Burns, S.E. and Mayne, P.W. (1994). Seismic Piezocone Penetration Tests, San Manuel Copper Mine Tailings - Tucson, AZ, *Geotechnical Report*, Georgia Institute of Technology, Atlanta, GA.

Burns, S.E. and Mayne, P.W. (1995a). Coefficient of Consolidation (c_h) from Type 2 Piezocone Dissipation in Overconsolidated Clays, *Proceedings*, International Symposium on Cone Penetration Testing (CPT '95), Linköping, Sweden, Vol. 2, pp. 137-142.

Burns, S.E. and Mayne, P.W. (1995b). Seismic Piezocone Penetration Tests, Georgia International Maritime Facility - Hutchinson Island, Georgia, *Geotechnical Report*, Georgia Institute of Technology, Atlanta.

Burns, S.E. and Mayne, P.W. (1996). Small- and High-Strain Measurements of In-Situ Soil Properties Using the Seismic Cone Penetrometer, *Transportation Research Record*, National Research Council, Washington D.C., No. 1548, pp. 81-88.

Campanella, R.G. (1994). Field Methods for Dynamic Geotechnical Testing, *Dynamic Geotechnical Testing II*, Special Technical Publication 1213, American Society for Testing and Materials, Philadelphia, pp. 3-23.

Campanella, R.G., Baziw, E.J., and Sully, J.P. (1989). Interpretation of Seismic Cone Data Using Digital Filtering Techniques, *Proceedings*, 12th International Conference on Soil Mechanics and Foundation Engineering, Vol. 1, Rio de Janeiro, Balkema, Rotterdam, pp. 195-198.

Campanella, R.G. and Robertson, P.K. (1988). Current Status of the Piezocone, *Proceedings*, International Symposium on Penetration Testing, J.D. Ruiter (ed), A.A. Balkema, Rotterdam, Vol. 1, pp. 93-116.

Campanella, R.G., Robertson, P.K., and Gillespie, D. (1986a). Factors Affecting the Pore Water Pressure and Its Measurement Around a Penetrating Cone, *Proceedings*, 39th Canadian Geotechnical Conference, Ottawa, pp. 291-299.

Campanella, R.G., Robertson, P.K., and Gillespie, D. (1986b). Seismic Cone Penetration Test, *Use of In-Situ Tests in Geotechnical Engineering*, Geotechnical Special Publication No.6, ASCE, New York, 116-130.

Campanella, R.G., Sully, J.P., and Robertson, P.K. (1988). Interpretation of Piezocone Soundings in Clay - A Case History, *Penetration Testing in the U.K.*, Thomas Telford, London, pp. 203-208.

Campanella, R.G. and Weemees, I.A. (1989). Development and Use of an Electrical Resistivity Cone for Groundwater Contamination Studies, *Proceedings*, 42nd Annual Canadian Geotechnical Conference, Winnipeg, pp. 1-11.

Carrabba, M.M. (1995). Phase I Topical Report: Field Raman Spectrograph for Environmental Analysis, *DOE Contract DE-AC21-92MC29108*.

Carslaw, H.D. and Jaeger, J.C. (1959). *Conduction of Heat in Solids*, 2nd Edition, Oxford University Press, London, 510 pp.

Chen, B.S.Y. and Mayne, P.W. (1994). Profiling the Overconsolidation Ratio of Clays by Piezocone Tests, *Georgia Institute of Technology Internal Report*, No. GIT-CEEGEO-94-1, Atlanta, 279 pp.

Chen, B.S.Y. and Mayne, P.W. (1995). Type 1 and 2 Piezocone Evaluations of Overconsolidation Ratio in Clays, *Proceedings*, International Symposium on Cone Penetration Testing (CPT '95), Vol. 2, Linköping, Sweden, pp. 143-148.

Chen, B.S.Y. and Mayne, P.W. (1996). Statistical Relationships Between Piezocone Measurements and Stress History of Clays, *Canadian Geotechnical Journal*, Vol. 33, No. 3, pp. 488-498.

Coop, M.R. and Wroth, C.P. (1989). Field Studies of an Instrumented Model Pile in Clay, *Geotechnique*, Vol. 39, No. 4, pp. 679-696.

CRC. (1993). Handbook of Chemistry and Physics, 74th Edition, D.R. Lide, Ed., CRC Press, Boca Rato.

Daniel, D.E. (1989). In-Situ Hydraulic Conductivity Tests for Compacted Clay, *Journal of Geotechnical Engineering*, ASCE, Vol. 115, No. 9, pp. 1205-1226.

Daniel, D.E. (1994). State-of-the-Art: Laboratory Hydraulic Conductivity Tests for Saturated Soils, *Hydraulic Conductivity and Waste Containment Transport in Soils*, ASTM STP 1142, Daniel, D.E. and Trautwein, S.J., Eds., American Society for Testing and Materials, Philadelphia, pp. 30-78.

Daniel, D.E., Anderson, D.C., and Boynton, S.S. (1985). Fixed-Wall Versus Flexible-Wall Permeameters, *Hydraulic Barriers in Soil and Rock*, ASTM STP 874, A.I. Johnson, R.K. Frobel, N.J. Cavalli, and C.B. Pettersson, eds., American Society for Testing and Materials, Philadelphia, pp. 107-126.

Davidson, J.L. (1985). Pore Pressures Generated During Cone Penetration Testing in Heavily Overconsolidated Clays, *Proceedings*, 11th International Conference on Soil Mechanics and Foundation Engineering, San Francisco, Vol. 5, pp. 2699.

Degroot, D.J. and Lutenegger, A.J. (1994). A Comparison Between Field and Laboratory Measurements of Hydraulic Conductivity in a Varved Clay, *Hydraulic Conductivity and Waste Contaminant Transport in Soil, ASTM STP 1142*, D.E. Daniel and S.J. Trautwein, eds, American Society for Testing and Materials, Philadelphia, pp. 300-317.

Du, J. and Wu, T.H. (1992). *Proceedings*, US-China Workshop on Cooperative Research in Geotechnical Engineering, Tongji University, Shanghai (NSF and NNSF/PRC), 215 pp.

Elsworth, D. (1990). Theory of Partially Drained Piezometer Insertion, *Journal of Geotechnical Engineering*, ASCE, Vol. 116, No. 6, pp. 899-912.

Elsworth, D. (1993). Analysis of Piezocone Dissipation Data Using Dislocation Methods, *Journal of Geotechnical Engineering*, ASCE, Vol. 119, No. 10, pp. 1601-1623.

Environmental Protection Agency. (1993). Subsurface Characterization and Monitoring Techniques, *EPA/625/R-93/003a*, Office of Research and Development, Washington D.C.

Gaberc, A., Ajdiç, I., and Majes, B. (1995). Vertical and Horizontal Permeability of Marshland Subsoils, *Proceedings*, 11th European Conference on Soil Mechanics and Foundation Engineering, Copenhagen, Vol. 1, pp. 127-132.

Ghionna, V. et al. (1995). Cone Pressuremeter Tests in Po River Sand, *The Pressuremeter and Its New Avenues*, Balkema, Rotterdam, pp. 471-480.

Gillespie, D. and Campanella, R.G. (1981). Consolidation Characteristics from Pore Pressure Dissipation After Piezometer Cone Penetration, Soil Mechanics Series 47, Department of Civil Engineering, The University of British Columbia, Vancouver, 17 pp.

Gillespie, D., Lunne, T., and Eidsmoen, T. (1985). Cone Penetration Tests in Onsøy Clay, *Internal Report - In Situ Site Investigation Techniques and Interpretation for Offshore Practice*, No. 40019-7, Norwegian Geotechnical Institute, Oslo.

Greig, J.W., Campanella, R.G., and Robertson, P.K. (1988). Comparison of Field Vane Results with Other In-Situ Test Results, *Vane Shear Strength Testing in Soils: Field and Laboratory Studies*, ASTM STP 1014, pp. 247-263.

Grisak, G.E. (1975). The Fracture and Porosity of Glacial Till, *Canadian Journal of Earth Science*, Vol. 12, No. 3, pp. 513-515.

Grisak, G.E. and Cherry, J.A. (1975). Hydrologic Characteristics and Response of Fractured Till and Clay Confining a Shallow Aquifer, *Canadian Geotechnical Journal*, Vol. 12, No. 1, pp. 23-43.

Gupta, R.C. (1983). Determination of the Insitu Coefficient of Consolidation and Permeability of Submerged Soils Using Electrical Piezoprobe Soundings, *Ph.D. Thesis*, University of Florida, Gainesville, 303 pp.

Gupta, R.C. and Davidson, J.L. (1986). Piezoprobe Determined Coefficient of Consolidation, *Soils and Foundations*, Vol. 26, No. 3, pp. 12-22.

Hansbo, S., Jamiolkowski, M., and Kok, L. (1981). Consolidation by Vertical Drains, *Geotechnique*, Vol. 31, No. 1, pp. 45-66.

Hartman, N.F. (1990). Optical Sensing Apparatus and Method, *U.S. Patent No. 4,940,3228*, Washington, D.C., July.

Hartman, N.F., Campbell, D.L., and Gross, M. (1988). Waveguide Interferometer Configurations, *Proceedings*, Leos Annual Meeting Conference, Santa Clara, November.

Hartman, N.F., Walsh, J.L., Ross, C.C., and Campbell, D.P. (1992). An Integrated Optic Gaseous Ammonia Sensor, *Proceedings*, Sensors Expo, Chicago, September.

Hegazy, Y.A. and Mayne, P.W. (1995). Statistical Correlations Between V_s and Cone Penetration Data for Different Soil Types. *Proceedings*, International Symposium on Cone Penetration Testing (CPT'95), Linköping, Sweden, Vol. 2, pp. 173-178.

Henkel, D.J. (1959). The Relationships Between the Strength, Pore Water Pressure, and Volume Change Characteristics of Saturated Clays, *Geotechnique*, Vol. 9, pp. 119-135.

Hepton, P. (1988). Shear Wave Velocity Measurements During Penetration Testing, *Proceedings*, Penetration Testing in the U.K., Thomas Telford LTD, London, pp. 275-278.

Hilbert, L.B., Hwong, T.K., Cook, N.G.W., Nihei, K.T., Myer, L.R. (1994). Effects of Strain Amplitude on Static and Dynamic Nonlinear Deformation of Berea Sandstone, *Rock Mechanics: Models and Measurements*, (P.P. Nelson and S.E. Laubach, eds.), Balkema Publishers, Rotterdam, Netherlands, pp. 463-471.

Hill, R. (1950). The Mathematical Theory of Plasticity, Oxford University Press, London.

Hird, C.C., Powell, J.J.M., and Yung, P.C.Y. (1991). Investigations of the Stiffness of a Glacial Clay Till, *Proceedings*, 10th International Conference on Soil Mechanics and Foundation Engineering, Florence, Vol. 1, pp. 107-110.

Holtz, R.D., Jamiolkowski, M.B., and Lancellotta, R. (1985). Lessons from Oedometer Tests on High Quality Samples, *Journal of Geotechnical Engineering*, ASCE, Vol. 112, No. 8, pp. 768-776.

Horsnell, M.R. (1988). The Use of Cone Penetration Testing to Obtain Environmental Data, *Proceedings*, Penetration Testing in the U.K., Thomas Telford, London, pp. 289-295.

Houlsby, G.T. and Hitchman, R. (1988). Calibration Chamber Tests of a Cone Pressuremeter in Sands, *Geotechnique*, Vol. 38, No. 1, pp. 39-44.

Houlsby, G.T. and Teh, C.I. (1988). Analysis of the Piezocone in Clay, *Proceedings*, International Symposium on Penetration Testing, J.D. Ruiter (ed), A.A. Balkema, Rotterdam, The Netherlands, Vol. 1, pp. 777-783.

Houlsby, G.T. and Withers, N.J. (1988). Analysis of the Cone Pressuremeter in Clay, *Geotechnique*, Vol. 38, No. 4, pp. 575-587.

Hryciw, R.D. and Raschke, S.A. (1996). Development of Computer Vision Technique for In-Situ Soil Characterization, *Transportation Research Record*, National Research Council, Washington D.C., No. 1526, pp. 86-97.

Jacobs, P.A. and Coutts, J.S. (1992). A Comparison of Electric Piezocone Tips at the Bothkennar Test Site, *Geotechnique*, Vol. 42, No. 2, pp. 369-375.

Jaime, A. and Romo, M.P. (1988). The Mexico Earthquake of September 19, 1985 - Correlations Between Dynamic and Static Properties of Mexico City Clay, *Earthquake Spectra*, Vol. 4, No. 4, pp. 787-804.

Jamiolkowski, M. (1995). Opening Address, *Proceedings*, International Symposium on Cone Penetration Testing (CPT '95), Linköping, Sweden, Vol. 3, pp. 7-15.

Jamiolkowski, M., Ladd, C.C., Germaine, J., and Lancelotta, R. (1985). New Developments in Field and Lab Testing of Soil, *Proceedings*, 11th International Conference on Soil Mechanics and Foundation Engineering, San Francisco, Vol. 1, pp. 57-154.

Jamiolkowski, M., Lancellotta, R., and Lo Presti, D.C.F. (1995). Remarks on the Stiffness at Small Strains of Six Italian Clays, *Proceedings*, International Symposium on Pre-Failure Deformation Characteristics of Geomaterials (Sappro), Balkema Press Rotterdam, Vol. 2, pp. 817-836.

Jamiolkowski, M. and Robertson, P.K. (1988). Future Trends for Penetration Testing, *Proceedings*, Penetration Testing in the U.K., Thomas Telford, London, pp. 321-342.

Janbu, N. (1963). Soil Compressibility as Determined by Oedometer and Triaxial Tests, *Proceedings*, 3rd European Conference on Soil Mechanics, Wiesbaden, Vol. 1, pp. 19-25.

Janbu, N. (1985). Soil Models in Offshore Engineering, *Geotechnique*, Vol. 35, No. 3, pp. 241-281.

Janbu, N. and Sennesset (1974). Effective Stress Interpretation of In Situ Static Cone Penetration Tests, *Proceedings*, European Symposium on Penetration Testing I, Stockholm, Vol. 2, pp. 181-195.

Jardine, R.J. and Bond, A.J. (1989). Behaviour of Displacement Piles in a Heavily Overconsolidated Clay, *Proceedings*, 12th International Conference on Soil Mechanics and Foundation Engineering, Rio de Janeiro, Vol. 2, pp. 1147-1151.

Jones, G.A. and Van Zyl, D.J.A. (1981). The Piezometer Probe - A Useful Investigation Tool, *Proceedings*, 10th International Conference on Soil Mechanics and Foundation Engineering, Stockholm, Vol. 3, pp. 489-495.

Kabir, M.G. and Lutenegger, A.J. (1987). Discussion on Piezoprobe Determined Coefficient of Consolidation, *Soils and Foundations*, Vol. 27, No. 2, pp. 70-72.

Kabir, M.G. and Lutenegger, A.J. (1990). In Situ Estimation of the Coefficient of Consolidation in Clays, *Canadian Geotechnical Journal*, Vol. 27, No. 1 , pp. 58-67.

Kavvadas, M. (1982). Non-linear Consolidation Around Driven Piles in Clay, *Ph.D. Thesis*, Massachusetts Institute of Technology, Cambridge, MA.

Keaveny, J.M. and Mitchell, J.K. (1986). Strength of Fine-Grained Soils Using the Piezocone, *Proceedings*, Use of In-Situ Tests in Geotechnical Engineering (In-Situ 86), ASCE, Geotechnical Special Publication No. 6,New York, pp. 668-685.

Koga, Y., Sasaki, Y., Itoh, Y., and Matsuo, O. (1986). Field Investigation of Seismically Damaged Sites By Use of Vibratory Cone Penetrometer, *Proceedings*, 18th Joint Meeting US-Japan Panel on Wind and Seismic Effects, Washington, D.C.

Koizumi, Y. and Ito, K. (1967). Field Tests With Regard to Pile Driving and Bearing Capacity of Piled Foundations, *Soils and Foundations*, Vol. 7, No. 3.

Konrad, J.-M. and Frechette, P. (1995). The Piezocone-Permeameter Probe: A Promising Tool?, *Proceedings*, Geoenvironment 2000 (GSP No. 46), American Society of Civil Engineers, Vol. 1, New Orleans, pp. 93-104.

Kulhawy, F.H. and Mayne, P.W. (1990). Soil Properties Manual, *Report EL-6800*, Electric Power Research Institute, Palo Alto, 306 p.

Lacasse, S., Ladd, C.C., and Baligh, M.M.. (1978). Evaluation of Field Vane, Dutch Cone Penetrometer, and Piezometer Probe Testing Devices, *Final Reports*, prepared for U.S. Department of Transportation, Federal Highway Administration, Washington, DC.

Lacasse, S., and Lunne, T. (1982). Penetration Tests in Two Norwegian Clays, *Proceedings*, 2nd European Symposium on Penetration Testing, Vol. 2, Amsterdam, pp. 661-669.

Lacasse, S. and Lunne, T. (1983). Dilatometer Tests in Two Soft Marine Clays, Report No. 146, Norwegian Geotechnical Institute, Oslo, Norway.

Lally, M.J. (1993). A Field and Laboratory Investigation of Geotechnical Properties for Design of a Seasonal Heat Storage Facility, *Master of Science Thesis*, Civil Engineering Department, University of Massachusetts at Amherst, 224 pp.

Lambe, T.W. (1951). Soil Testing for Engineers, John Wiley and Sons, New York, 165 pp.

Lambe, T.W. and Whitman, R.V. (1969). Soil Mechanics, John Wiley and Sons, New York, 553 pp.

Lambrechts, J.R., and Leonards, G.A. (1978). Effects of Stress History on Deformation of Sand, *Journal of Geotechnical Engineering*, ASCE, Vol. 104, No. GT11, pp. 1371-1388.

Lambson, M.D., Clare, D.G., Senner, D.W.F., and Semple, R.M. (1993). Investigation and Interpretation of Pentre and Tilbrook Grange Soil Conditions, *Large Scale Pile Tests in Clay*, Thomas Telford, London, pp. 134-196.

Lambson, M. and Jacobs, P. (1995). The Use of Laser Induced Fluorescence Cone for Environmental Investigations, *Proceedings*, International Symposium on Cone Penetration Testing (CPT '95), Linköping, Sweden, Vol. 2, pp. 29-34.

Larsson, R. (1986). Consolidation of Soft Soils, *Report 29*, Swedish Geotechnical Institute, Linköping, Sweden, 174 pp.

Larsson, R., and Mulabdic, M. (1991). Shear Moduli in Scandinavian Clays: Measurement of Initial Shear Modulus with Seismic Cones, *Report 40*, Swedish Geotechnical Institute, Linköping, Sweden, 127 pp.

Larsson, R. and Mulabdic, M. (1993). *Report 42*, Swedish Geotechnical Institute, Linköping, Sweden, 240 pp.

Lefebvre, G. Leboeuf, D., Rahhal, M., Lacroix, A., and Warde, J. (1994). Laboratory and Field Determination of Small-Strain Shear Modulus for a Structured Champlain Clay, *Canadian Geotechnical Journal*, Vol. 31, No. 1, pp. 61-70.

Lehane, B.M. and Jardine, R.J. (1994). Displacement Pile Behavior in Glacial Clay, *Canadian Geotechnical Journal*, Vol. 31, No. 1, pp. 79-90.

Leroueil, S. (1996). Compressibility of Clays: Fundamental and Practical Aspects, *Journal of Geotechnical Engineering*, ASCE, Vol. 122, No. 7, pp. 534-543.

Leroueil, S. and Jamiolkowski, M. (1991). General Report on Exploration of Soft Soil and Determination of Design Parameters, *Proceedings*, Geo-Coast '91, Yokohama, 29 pp.

Leroueil, S., Lerat, P., Hight, D.W., and Powell, J.J.M. (1992). Hydraulic Conductivity of a Recent Estuarine Silty Clay at Bothkennar, *Geotechnique*, Vol. 42, No. 2, pp. 275-288.

Levadoux, J.N. (1980). Pore Pressures in Clays Due to Cone Penetration, *Ph.D. Thesis*, Civil Engineering Department, Massachusetts Institute of Technology, Cambridge, MA, Vol. 1, 386 pp.

Levadoux, J.N. and Baligh, M.M. (1980). Pore Pressure During Cone Penetration, *Research Report*, R80-15, Department of Civil Engineering, Massachusetts Institute of Technology, Cambridge, MA, 310 pp.

Levadoux, J.-N. and Baligh, M.M. (1986). Consolidation After Undrained Piezocone Penetration. I: Prediction, *Journal of Geotechnical Engineering*, ASCE, Vol. 112, No. 7, pp. 707-726.

Lieberman, S.H., Theriault, G.A., Cooper, S.S., Malone, P.G., Olsen, R.S., and Lurk, P.W. (1991). Rapid, Subsurface, In-Situ Field Screening of Petroleum Hydrocarbon Contamination Using Laser Induced Fluorescence Over Optical Fibers, *Proceedings*, 2nd International Symposium for Field Screening Methods for Hazardous Wastes and Toxic Chemicals, Las Vegas, pp. 57-63.

Lightner, E.M. and Purdy, C.B. (1995). Cone Penetrometer Development and Testing for Environmental Applications, *Proceedings*, International Symposium on Cone Penetration Testing, Vol. 2, Linköping, Sweden, pp. 41-48.

Lo, K.Y. and Stermac, A.G. (1965). Induced Pore Pressures During Pile Driving Operations, *Proceedings*, 6th International Conference on Soil Mechanics and Foundation Engineering, Montreal, Vol. 2.

Lunne, T., Eidsmoen, T.E., Gillespie, D., and Howland, J. (1986a). Laboratory and Field Calibration of Cone Penetrometers, *Use of In-Situ Tests in Geotechnical Engineering*, Geotechnical Special Publication No. 6, American Society of Civil Engineers, New York, pp. 714-729.

Lunne, T. Eidsmoen, T.E., Powell, J.J.M., and Quarterman, R.S.T. (1986b). Piezocone Testing in Overconsolidated Clays, *Proceedings*, 39th Canadian Geotechnical Conference, Ottawa, pp. 209-218.

Lunne, T., Lacasse, S., and Rad, N. S. (1992). General Report: Recent Developments in In-Situ Testing, *Proceedings*, 12th International Conference on Soil Mechanics and Foundation Engineering, Rio de Janiero, Vol. 4, pp. 2339-2403.

Lunne, T., Powell, J., Eidsmoen, T., and Quarterman, R. (1985). Comparison of Piezocones in Overconsolidated Clays, *Contract Report No. 84223-1*, Norwegian Geotechnical Institute, Oslo, 53 pp.

Lutenegger, A.J. (1995). Geotechnical Behavior of Overconsolidated Surficial Clay Crusts, *Transportation Research Record*, No. 1479, National Academy Press, Washington D.C., pp. 61-74.

Lutenegger, A.J. (1997). Personal Communication.

Lutenegger, A.J. and Kabir, M.G. (1987). Pore Pressures Generated by Two Penetrometers in Clays, *Report No. 87-2*, Department of Civil and Environmental Engineering, Clarkson University, Potsdam, 45 pp.

Lutenegger, A.J. and Kabir, M.G. (1988). Interpretation of Piezocone Results in Overconsolidated Clays, *Proceedings*, Penetration Testing in the U.K., Thomas Telford, London, pp. 147-150.

Lutenegger, A.J., Kabir, M.G., and Saye, S.R. (1988).Use of Penetration Tests to Predict Wick Drain Performance in a Soft Clay, *Proceedings*, International Symposium on Penetration Testing, J.D. Ruiter (ed), A.A. Balkema, Rotterdam, The Netherlands, Vol. 2, pp. 843-848.

Lutenegger, A.J. and Timian, D.A. (1986a). Flat-Plate Penetrometer Tests in Marine Clays, *Proceedings*, 39th Canadian Geotechnical Conference, Ottawa, 9 pp.

Lutenegger, A.J. and Timian, D.A. (1986b). In-situ Tests with K_o Stepped Blade, *Proceedings*, Use of In-Situ Tests in Geotechnical Engineering (In-Situ 86), ASCE, Geotechnical Special Publication No. 6,New York, pp. 730- 751.

Mahar, .J. and O'Neill, M.W. (1983). Geotechnical Characteristics of Desiccated Clay, *Journal of Geotechnical Engineering*, ASCE, Vol. 109, No. 1, pp. 56-71.

Malone, P.G., Comes, G.D., Chrestman, A.M., Cooper, S.S., and Franklin, A.G. (1992). Cone Penetrometer Surveys of Soil Contamination, *Environmental Technology*, Usmen and Acar, eds, Balkema, Rotterdam, pp. 251-257.

Manassero, M. (1994). Hydraulic Conductivity Assessment of Slurry Wall Using Piezocone, *Journal of Geotechnical Engineering*, ASCE, Vol. 120, No. 10, pp. 1725-1746.

Marsland, A. (1974). Comparison of the Results from Static Penetration Tests and Large In-situ Plate Tests in London Clay, *Proceedings*, European Symposium on Penetration Testing, ESOPT, Stockholm, Vol. 2:1, pp. 245-252.

Marsland, A. and Quarterman, R.S.T. (1982). Factors Affecting the Measurements and Interpretation of Quasi Static Penetration Tests in Clay, *Proceedings*, Second European Symposium on Penetration Testing, Vol. 2, Amsterdam, pp. 697-702.

Marton, R., Taylor, L., and Wilson, K. (1988). Development of an In-Situ Subsurface Radioactivity Detection System - the Radcone, *Proceedings*, Waste Management '88, University of Arizona, Tucson.

Massarsch, R. (1986). Acoustic Penetration Testing, Fourth International Geotechnical Seminar on Field Instrumentation and In Situ Measurements, Singapore, pp. 71-76.

Mayne, P.W. (1988). Determining OCR of Clays from Laboratory Strengths, *Journal of Geotechnical Engineering*, ASCE, Vol. 114, No. GT1.

Mayne, P.W. (1991). Determination of OCR in Clays by Piezocone Tests Using Cavity Expansion and Critical State Concepts, *Soils and Foundations*, Vol. 31, No. 2, pp. 65-76.

Mayne, P.W. (1995). Undrained Plastic Modulus from Original Cam Clay, *Journal of Geotechnical Engineering*, ASCE, Vol. 121, No. 5, pp. 448-451.

Mayne, P.W. and Bachus, R.C. (1988). Profiling OCR in Clays by Piezocone Soundings, *Proceedings*, International Symposium on Penetration Testing, J.D. Ruiter (ed), A.A. Balkema, Rotterdam, The Netherlands, Vol. 2, pp. 857-864.

Mayne, P.W., Burns, S.E., Hegazy, Y., and Kates, G. (1996). Report of Seismic Piezocone and Flat Dilatometer Tests in Pemiscot and Dunklin Counties, *Geotechnical Report*, Georgia Institute of Technology, Atlanta, GA.

Mayne, P.W. and Harris, D.E. (1993). Axial Load-Displacement Behavior of Drilled Shaft Foundations in Piedmont Residuum, *Technical Report to*: Federal Highway Administration, Turner-Fairbanks Highway Lab, McLean, Virginia, FHWA Reference No. 41-30-2175, Georgia Tech.

Mayne, P.W., Kulhawy, F., and Kay, J.N. (1990). Observations on the Development of Pore-Water Stresses During Piezocone Penetration in Clays, *Canadian Geotechnical Journal*, Vol. 27, No. 4, pp. 418-428.

Mayne, P.W., Mitchell, J.K., Auxt, J.A., and Yilmaz, R. (1995). U.S. National Report on CPT, *Proceedings*, International Symposium on Cone Penetration Testing (CPT '95), Linköping, Sweden, Vol. 1, pp. 263-276.

Mayne, P.W. and Rix, G. J. (1993). G_{max}-q_c Relationships for Clays, *ASTM Geotechnical Testing Journal*, Vol. 16, No. 1, pp. 54-60.

Mayne, P.W. and Rix, G.J. (1995). Correlations Between Shear Wave Velocity and Cone Tip Resistance in Natural Clays, *Soils and Foundations*, Vol. 35, No. 2, pp. 107-110.

Mayne, P.W. and Stewart, H. E. (1988). Pore Pressure Behavior of K_o-Consolidated Clays, *Journal of Geotechnical Engineering*, ASCE, Vol. 114, No. 11, pp. 1340-1346.

McLamore, V.R., Anderson, D.G., and Espana, C. (1978). Cross Hole Testing Using Explosive and Mechanical Energy Sources, *Dynamic Geotechnical Testing*, STP 654, ASTM, Philadelphia, PA, pp. 30-55.

Menge, P. and Van Impe, W. (1995). The Application of Acoustic Emission Testing With Penetration Testing, *Proceedings*, International Symposium on Cone Penetration Testing (CPT '95), Linköping, Sweden, Vol. 2, pp. 49-54.

Mimura, M., Shrivastava, A.K., Shibata, T., and Nobuyama, M. (1995). Performance of RI Cone Penetrometers in Sand Deposits, *Proceedings*, International Symposium on Cone Penetration Testing (CPT '95), Linköping, Sweden, Vol. 2, pp. 55-60.

Mitchell, J.K. (1988). New Developments in Penetration Tests and Equipment, *Proceedings*, International Symposium on Penetration Testing, J.D. Ruiter (ed), A.A. Balkema, Rotterdam, The Netherlands, Vol. 1, pp. 245-261.

Mitchell, J.K. (1993). Fundamentals of Soil Behavior, 2nd Edition, John Wiley and Sons, New York, 437 pp.

Mitchell, J.K. and Gardner, W.S. (1975). In-Situ Measurement of Volume Change Characteristics, *Proceedings*, ASCE Specialty Conference on In-Situ Measurement of Soil Properties, Vol. 2, Raleigh, pp. 279-345.

Mitchell, J.K., Vivatrat, V., and Lambe, T.W. (1977). Foundation Performance of Tower of Pisa, *Journal of Geotechnical Engineering*, ASCE, Vol. 103, No. GT3, pp. 227-249.

Nash, D.F.T., Powell, J.J.M., and Lloyd, I.M. (1992). Initial Investigations of the Soft Clay Test Site at Bothkennar, *Geotechnique*, Vol. 42, No. 2, pp. 163-181.

Naval Command. (1995). Laser Induced Fluorometry / Cone Penetrometer Technology Demonstration Plan at the Hydrocarbon National Test Site, *Report*, prepared by Naval Command, Control and Ocean Surveillance Center, San Diego.

Olie, J.J., Van Ree, C.C.D.F., and Bremmer, C. (1992). In-Situ Measurement by Chemoprobe of Groundwater from In-Situ sanitation of Versatic Acid Spill, *Geotechnique*, Vol. 42, No. 1, pp. 13-21.

Olsen, R.S. (1994). Normalization and Prediction of Geotechnical Properties Using the CPT, *Technical Report GL-94-29*, U.S. Army Waterways Experiment Station, Vicksburg, 323 p.

O'Neill, D.A., Baldi, G., and Della Torre, A. (1996). The Multifunctional Envirocone Test, *Proceedings*, Advances in Site Investigation Practice, Thomas Telford, London, pp. 420-437.

Pane, V., Brignoli, E., Manassero, M., and Soccodato, C. (1995). Cone Penetration Testing in Italy, *Proceedings,* International Symposium on Cone Penetration Testing, Vol. 1, Swedish Geotechnical Society, Linkoping, pp. 101-114.

Parez and Fauriel (1988). Le Piézocône Améliorations Apportées à la Reconnaissance de Sols, *Revue Française de Géotech*, Vol. 44, pp. 13-27.

Parker, L.V. (1992). Suggested Guidelines for the Use of PTFE, PVC, and Stainless Steel in Samplers and Well Casings, *Current Practices in Ground Water and Vadose Zone Investigations*, (ASTM STP 1118), D. M. Nielson and M. N. Sara, Eds., American Society for Testing and Materials, pp. 217-229.

Piccoli, S. and Benoit, J. (1995). Geo-environmental Testing Using the Environmental Cone, *Proceedings*, Geoenvironment 2000 (GSP 46), New Orleans, American Society of Civil Engineers, New York, Vol. 1, pp. 93-104.

Pluimgraaf, D., Hilhorst, M, and Bratton, W.L. (1995). CPT Sensors for Bio-Characterization of Contaminated Sites, *Proceedings*, International Symposium on Cone Penetration Testing, Vol. 2, Linköping, Sweden, pp. 569-575.

Powell, J.J.M. (1997). Personal Communication.

Powell, J.J.M., Quarterman, R.S.T., and Lunne, T. (1988). Interpretation and Use of the Piezocone Test in U.K. Clays, *Proceedings*, Penetration Testing in the U.K., Thomas Telford, London, pp. 151-156.

Powell, J.J.M. and Uglow, M. (1988). The Interpretation of the Marchetti Dilatometer Test in UK Clays, *Proceedings*, Penetration Testing in the U.K., Thomas Telford, London, pp. 269-273.

Price, R.H., Boyd, P.J.., Noel, J.S., and Martin, R.J. (1994). Relationship Between Static and Dynamic Rock Properties in Welded and Non-welded Tuff, *Rock Mechanics: Models and Measurements*, (P.P. Nelson and S.E. Laubach, eds.), Balkema Publishers, Rotterdam, Netherlands, pp. 505-512.

Randolph, M.F. and Wroth, C.P. (1978). Analysis of Deformation of Vertically Loaded Piles, *Journal of the Geotechnical Engineering*, ASCE Vol. 104, No. GT12, pp. 1465-1488.

Randolph, M.F. and Wroth, C.P. (1979 a). A Simple Approach to Pile Design and the Evaluation of Pile Tests, *Behavior of Deep Foundations, ASTM STP 670*, Raymond Lundgren, Ed., American Society for Testing and Materials, Philadelphia, pp. 484-499.

Randolph M.F. and Wroth, C.P. (1979 b). An Analytical Solution for the Consolidation Around a Driven Pile, *International Journal for Numerical and Analytical Methods in Geomechanics*, Vol. 3, pp. 217-229.

Raschke, S.A. and Hryciw, R.D. (1997). Vision Cone Penetrometer (VisCPT) for Direct Subsurface Soil Observation, *Journal of Geotechnical and Geoenvironmental Engineering*, Vol. 123, No. 11, *in press*.

Robertson, P.K. (1990). Soil Classification Using the Cone Penetration Test, *Canadian Geotechnical Journal*, Vol. 27, No. 1, pp. 151-158.

Robertson, P.K. and Campanella, R.G. (1983). Interpretations of Cone Penetration Tests, *Canadian Geotechnical Journal*, Vol. 20, No. 4, pp. 718-745.

Robertson, P.K., Campanella, R.G., Brown, P.T., and Robinson, K.E. (1988a). Prediction of Wick Drain Performance Using Piezometer Cone Data, *Canadian Geotechnical Journal*, Vol. 25, pp. 56-61.

Robertson, P.K., Campanella, R.G., Gillespie, D., and By, T. (1988b). Excess Pore Pressures and the Flat Dilatometer Test, *Proceedings*, International Symposium on Penetration Testing, J.D. Ruiter (ed), A.A. Balkema, Rotterdam, The Netherlands, Vol. 2, pp. 567-576.

Robertson, P.K., Campanella, R.G., Gillespie, D., and Grieg, J. (1986). Use of Piezometer Cone Data, *Proceedings*, Use of In-Situ Tests in Geotechnical Engineering (In-Situ '86), GSP No. 6, American Society of Civil Engineers, New York.

Robertson, P.K., Lunne, T., and Powell, J. (1996). Applications of Penetration Tests for Geo-Environmental Purposes, *Proceedings*, Advances in Site Investigation Practice, Thomas Telford, London, pp. 407-420.

Robertson, P.K., Sully, J.P., Woeller, D.J., Lunne, T., Powell, J.J.M., and Gillespie, D.G. (1992). Estimating Coefficient of Consolidation From Piezocone Tests, *Canadian Geotechnical Journal*, Vol. 29, No. 4, pp. 539-550.

Ross, C.W., Walsh, J.W., Hartman, N.F., and Boswell, F.C. (1991). Development of a Field Worthy Sensor System to Monitor Gaseous Nitrogen Transfer from Agricultural Cropland, *Phase I Final Report*, DE-FC07-89ID12905, U.S. DOE Office of Industrial Technologies, September.

Rowe, P.W. (1972). The Relevance of Soil Fabric to Site Investigation Practice, 12th Rankine Lecture, *Geotechnique*, Vol. 22, No. 2, pp. 195-300.

Rowe, P.W. and Barden, L. (1966). A New Consolidation Cell, *Geotechnique*, Vol. 16, No. 2, pp. 162-170.

Roy, M., Blanchet, R., Tavenas, F., and La Rochelle, P. (1981). Behavior of a Sensitive Clay During Pile Driving, *Canadian Geotechnical Journal*, Vol. 18, No. 1, pp. 67-85.

Roy et al. (1979). Behavior of a Sensitive Clay During Pile Driving, *Proceedings*, 32nd Canadian Geotechnical Conference, Quebec, pp. 4.28-4.49.

Roy, M., Tremblay, M., Tavenas, F., and La Rochelle, P. (1982). Development of Pore Pressures in Quasi-static Penetration Tests in Sensitive Clay, *Canadian Geotechnical Journal*, Vol. 19, No. 1, pp. 124-138.

Santamarina, J.C and Fratta, D. (1997). Discrete Signals and Inverse Problems in Civil Engineering, American Society of Civil Engineers Press, *in press*.

Sasaki, Y. and Koga, Y. (1982). Vibratory Cone Penetrometer to Assess the Liquefaction Potential of the Ground, *Proceedings*, 14th Panel on US-Japan Panel on Wind and Seismic Effects, Washington, D.C.

Sasaki, Y., Koga, Y., Itoh, Y., Shimazu, T., and Kondo, M. (1985). In Situ Tests for Assessing Liquefaction Potential Using Vibratory Cone Penetrometer, *Proceedings*, 17th Joint Meeting US-Japan Panel on Wind and Seismic Effects, Tsukuba, Japan.

Schmertmann, J.H. (1978). Guidelines for Cone Penetration Tests: Performance and Design, *Report FHWA-TS-78-209*, Federal Highway Administration, Washington, D.C.

Schnaid, F., Sills, G.C., Soares, J.M., and Nyirenda, Z. (1997). Predictions of the Coefficient of Consolidation from Piezocone Tests, *Canadian Journal of Geotechnical Engineering*, Vol. 34, pp. 315-327.

Senneset, K., Janbu, N., and Svanφ, G. (1982). Strength and Deformation Parameters from Cone Penetration Tests, *Proceedings*, Second European Symposium on Penetration Testing, Vol. 2, (ESOPT-2, Amsterdam), Balkema, Rotterdam, pp. 863-870.

Senneset, K., Sandven, R., and Janbu, N. (1989). Evaluation of Soil Parameters from Piezocone Tests, *Transportation Research Record 1235*, Washington, D.C., pp. 24-37.

Shibata, T., Mimura, M., Shrivastava, A.K., and Nobuyama, M. (1992). Moisture Measurement by Neutron Moisture Cone Penetrometer: Design and Application, *Soils and Foundations*, Vol. 32, No. 4, pp. 58-67.

Sills, G.C., Almeida, M.S.S., and Danziger, F.A.B. (1988). Coefficient of Consolidation From Piezocone Dissipation Tests in a Very Soft Clay, *Proceedings*, International Symposium on Penetration Testing, J.D. Ruiter (ed), A.A. Balkema, Rotterdam, The Netherlands, Vol. 2, pp. 967-974.

Skempton, A.W., Schuster, R.L., and Petley, D.J. (1969). Joints and Fissures in the London Clay at Wraysbury and Edgware, *Geotechnique*, Vol. 19, pp. 205-217.

Smits, F.P. (1982). Penetration Pore Pressure Measured With Piezometer Cones, *Proceedings*, Second European Symposium on Penetration Testing, Vol. 2, Amsterdam, pp. 871-876.

Soares, M.M., Lunne, T., and Lacasse, S. (1987). In-Situ Site Investigation Techniques and Interpretation for Offshore Practice. Interpretation of Dissipation Tests in Onsφy Clay, *Internal Report 40019-15*, Norwegian Geotechnical Institute, Oslo, November, 45 pp.

Soderburg, L.O. (1962). Consolidation Theory Applied to Foundation Pile Time Effects, *Geotechnique*, Vol. 12, pp. 217-225.

Stienstra, P. and van Deen, J.K. (1994). Field Data Collection Techniques - Unconventional Sounding and Sampling Methods, *Proceedings*, 20 Year Jubilee Symposium of the Ingeokring 1994, Delft, the Netherlands, Balkema, Rotterdam, pp. 41-56.

Strutynsky, A.I. and Sainey, T.J. (1992). Use of Piezometric Cone Penetration Testing and Penetrometer Ground Water Sampling for Volatile Organic Contaminant Plume Detection, *Current Practices in Ground Water and Vadose Zone Investigations*, (ASTM STP 1118), David M. Neilson and Martin N. Sara, Eds., American Society for Testing and Materials, pp. 199-214.

Strutynsky, A.I., Sandiford, R.E., and Cavaliere, D. (1991). Use of Piezometer Cone Penetration Testing with Electrical Conductivity Measurements for the Detection of Hydrocarbon Contamination in Saturated Granular Soils, *Current Practices in Ground Water and Vadose Zone Investigations*, (ASTM STP 1118), David M. Neilson and Martin N. Sara, Eds., American Society for Testing and Materials.

Sully, J.P. (1991). Measurement of In Situ Lateral Stress During Full-Displacement Penetration Tests, *Ph.D. Thesis*, Department of Civil Engineering, University of British Columbia, 470 pp.

Sully, J.P. and Campanella, R.G. (1994). Evaluation of Field CPTU Dissipation Data in Overconsolidated Fine-Grained Soils, *Proceedings*, 13th International Conference on Soil Mechanics and Foundation Engineering, Vol. 1, New Delhi, pp. 201-204.

Sully, J. P. and Campanella. R.G. (1995). Evaluation of In-situ Anisotropy from Crosshole and Downhole Shear Wave Velocity Measurements, *Geotechnique*, Vol. 45, No. 2, pp. 267-282.

Sully, J.P. and Echezuria, H.J. (1988). In-Situ Density Measurement with Nuclear Cone Penetrometer, *Proceedings*, International Symposium on Penetration Testing, J.D. Ruiter (ed), A.A. Balkema, Rotterdam, The Netherlands, Vol. 2.

Tavenas, F., Leblond, P., Jean, P., Leroueil, S. (1983a). The Permeability of Natural Soft Clays. Part I: Methods of Laboratory Measurement, *Canadian Geotechnical Journal*, Vol. 20, No. 3, pp. 629-644.

Tavenas, F., Leblond, P., Jean, P., Leroueil, S. (1983b). The Permeability of Natural Soft Clays. Part II: Permeability Characteristics, *Canadian Geotechnical Journal*, Vol. 20, No. 3, pp. 645-660.

Tavenas, F. Leroueil, S., and Roy, M. (1982). The Piezocone Test in Clays: Use and Limitations, *Proceedings*, 2nd European Symposium on Penetration Testing, Amsterdam, Vol. 2, pp. 889-894.

Teh, C.I. (1987). An Analytical Study of the Cone Penetration Test, D.Phil. Thesis, Department of Civil Engineering, Oxford University, UK.

Teh, C.I. and Houlsby, G.T. (1989). An Analytical Study of the Cone Penetration Test in Clay, *Soil Mechanics Report No. SM099/89*, University of Oxford, Oxford, U.K., 47 pp.

Teh, C.I. and Houlsby, G.T. (1991). An Analytical Study of the Cone Penetration Test in Clay, *Geotechnique*, Vol. 41, No. 1, pp. 17-34.

Teparaksa, W. (1987). Use and Application of Penetration Tests to Assess Liquefaction Potential of Soils, *PhD Thesis*, Department of Civil Engineering, Kyoto University, Kyoto, Japan.

Teparaksa, W. (1990). Cone Penetration Resistance of Sandy Soil and Triaxial Liquefaction Strength, *Proceedings*, 22nd Annual Meeting of the Japanese Society of Soil Mechanics and Foundation Engineering, pp. 587-590.

Theriault, G.A., Newbery, R., Andrews, J.M., Apitz, S.E., and Lieberman, S.H. (1992). Fiber Optic Fluorometer Based on a Dual Wavelength Laser Excitation Source, *Proceedings*, OE/Fibers '92, Boston, September.

Tokimatsu, K. (1988). Penetration Tests for Dynamic Problems, *Proceedings*, International Symposium on Penetration Testing, J.D. Ruiter (ed), A.A. Balkema, Rotterdam, The Netherlands, Vol. 1, pp. 117-136.

Torstensson, B.-A. (1975). Pore Pressure Sounding Instrument, *Proceedings*, ASCE Specialty Conference on In Situ Measurement of Soil Properties (ISMOSP), Raleigh, N.C., Vol. 2, pp. 48-54.

Torstensson, B.-A. (1977). The Pore Pressure Probe, Nordiske Geotekniske Møte, Oslo, Paper No. 34, pp. 34.1 to 34.15.

Torstensson, B.-A. (1984). A New System for Ground Water Monitoring, *Ground Water Monitoring Review*, Vol. 4, No. 4, pp. 131-138.

Tringale, P.T. and Mitchell, J.K. (1982). An Acoustic Cone for Site Investigations, *Proceedings*, Second European Symposium on Penetration Testing, Amsterdam, pp. 909-914.

Tumay, M.T. and Acar, Y.B. (1985). Piezocone Penetration Testing in Soft Cohesive Soils, *Strength and Testing of Marine Sediments: Laboratory and In Situ Measurements*, American Society for Testing and Materials, Special Technical Publication 883, Philadelphia, pp. 72-82.

Tumay, M.T., Acar, Y.B., Cekirge, M.H., and Ramesh, N. (1985). Flow Field Around Cones in Steady Penetration, *Journal of Geotechnical Engineering*, ASCE, Vol. 111, No. 2, pp. 193-204.

Tumay, M.T., Acar, Y., and Deseze, E. (1982). Soil Exploration in Soft Clays with the Quasi-Static Electric Cone Penetrometer, *Proceedings*, 2nd European Symposium on Penetration Testing, Amsterdam.

Vesic, A.S. (1972). Expansion of Cavities in Infinite Soil Mass, *Journal of the Soil Mechanics and Foundation Division*, American Society of Civil Engineers, Vol. 98, No. SM3, pp. 265-290.

Vesic, A.S. (1975). Bearing Capacity of Shallow Foundations, *Chapter 3*, Foundation Engineering Handbook, H, Winterkorn and H.Y. Fang, eds., Van Nostrand Reinhold Company, New York, pp. 121-147.

Villet, W.C.B., Mitchell, J.K., and Tringale, P.T. (1981). Acoustic Emission Generated During the Quasi-Static Cone Penetration of Soils, *Acoustic Emission in Geotechnical Engineering Practice*, Drnevich, V.P. and Gray, R.E., eds, ASTM STP 750, pp. 174-193.

Whittle, A.J. (1987). A Constitutive Model for Overconsolidated Clays with Application to the Cyclic Loading of Friction Piles, *Sc.D. Thesis*, Department of Civil Engineering, Massachusetts Institute of Technology.

Wissa, A.E., Martin, R.E., and Garlanger, J.E. (1975). The Piezometer Probe, *Proceedings*, ASCE Specialty Conference on In-Situ Measurement of Soil Properties, Vol. 1, Raleigh, NC, pp. 536-545.

Woeller, D.J., Weemees, I., Kohan, M., Jolly, G., and Robertson, P.K. (1991a). Penetration Testing for Groundwater Contaminants, *Proceedings*, Geotechnical Engineering Congress, ASCE, Boulder, CO, pp. 76-83.

Woeller, D.J., Weemees, I., Kurfurst, P.J., and Robertson, P.K. (1991b). Penetration Testing for Arctic Soil and Permafrost Conditions, *Proceedings*, 44th Canadian Geotechnical Conference, Vol. 1, Calgary, pp. 44-1 to 44-7.

Wroth, C.P. (1984). The Interpretation of In-Situ Soil Tests (24th Rankine Lecture), *Geotechnique*, Vol. 34, No. 4, pp. 449-489.

Wroth, C.P. and Houlsby, G.T. (1985). Soil Mechanics - Property Characterization and Analysis Procedures, *Proceedings*, 11th International Conference on Soil Mechanics and Foundation Engineering, San Francisco, Vol. 1, pp. 1-54.

Yale, D.P. and Jamieson, W.H. (1994). Static and Dynamic Mechanical Properties of Carbonates, *Rock Mechanics: Models and Measurements*, (P.P. Nelson and S.E. Laubach, eds.), Balkema Publishers, Rotterdam, Netherlands, pp.463-471.